UNIVERSITAT DE BARCELONA

Departament de Geologia Dinàmica, Geofísica i Paleontologia

Rifting and seafloor spreading in backarcs: The Bransfield and North Fiji Basins (NW Antarctica and SW Pacific)

"Rifting" i acreció oceànica de rere-arc: les conques de Bransfield i Nord Fijiana (Antàrtida i Pacífic Sudoest)

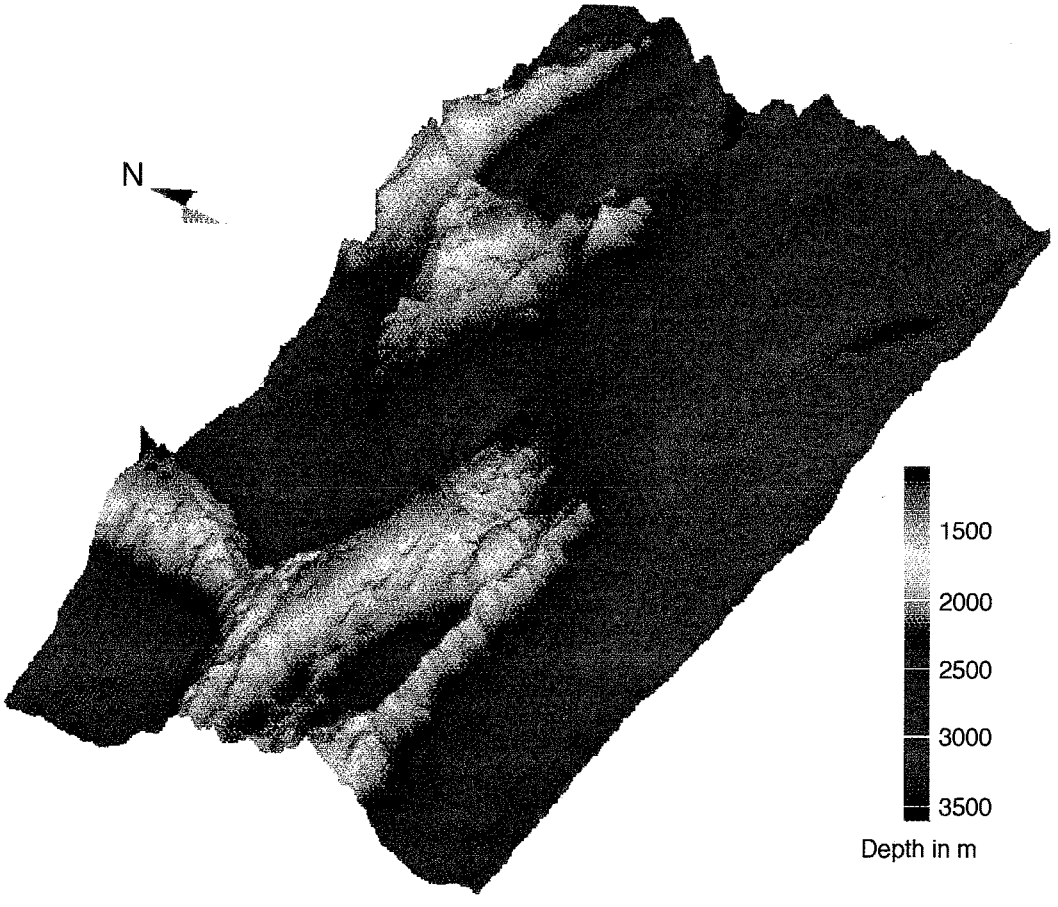

Eulàlia Gràcia i Mont

Tesi Doctoral

Barcelona, Gener de 1996

Cover: 3-D block of the 173°50'E Overlapping Spreading Centre (O.S.C.) between the SPR1 and SPR0 second-order segments of the South Pandora Ridge (Northern North Fiji Basin) (see Chapter 8). Image produced at the IFREMER-Brest centre using data from the NOFI cruise.

Portada: *Bloc 3-D del Centre d'Expansió Sobreposat (C.E.S.) de 173°50'E entre els segments de segon ordre SPR1 i SPR0 de la Dorsal de Sud Pandora (nord de la Conca Nord Fijiana) (veure Capítol 8). La imatge ha estat produïda al centre IFREMER de Brest a partir de les dades de la campanya oceanogràfica NOFI.*

UNIVERSITAT DE BARCELONA

Departament de Geologia Dinàmica, Geofísica i Paleontologia
UNIVERSITAT DE BARCELONA

Menció de Doctor Europeu

Rifting and seafloor spreading in backarcs: The Bransfield and North Fiji Basins (NW Antarctica and SW Pacific)

"Rifting" i acreció oceànica de rere-arc: les conques de Bransfield i Nord Fijiana (Antàrtida i Pacífic Sudoest)

Realitzada per:

EULÀLIA GRÀCIA i MONT

en el Departament de Geologia Dinàmica, Geofísica, i Paleontologia de la Universitat de Barcelona sota la direcció del Dr. Miquel Canals i Artigas i del Dr. Jean-Marie Auzende per optar al grau de Doctor en Geologia.

Barcelona, Gener de 1996

La Doctoranda,
Eulàlia Gràcia

Els Directors,
Jean Marie Auzende Miquel Canals

Aquest treball ha estat finançat per la beca de Formació de Professorat Universitari (FPU) AP-91 46338255 del Ministeri de Educació i Ciència enmmarcada dintre del projectes ANT-93-1008-C03-01 (CICYT) i STARMER.

El mar no calla,
però ningú no comprèn el llenguatge
que amaga aquesta dimensió.
Lliscar de vaixells tan perplexos
com qui més, davant de tants camins.

Feliu Formosa
"Poques vegades he esmentat el mar"

Agraïments

Als meus tres "Reis d'Orient":

En Jean-Marie Auzende, co-director de Tesi, que amb el seu bon humor em va "enredar" en tot això del programa STARMER quan feia el DEA a Brest l'any 1991. Gràcies a ell vaig embarcar en les campanyes Yokosuka 90 i Yokosuka 91, en què vaig poder veure "en directe" la dorsal central de les Fiji amb el submergible Shinkai 6500. M'ha ajudat a trobar bones estades a l'estranger, i tot i que des del 1993 s'ha exiliat a Nouméa, hem pogut salvar els 20.000 km que ens separen gràcies a Internet.

En Miquel Canals, co-director de Tesi, per acollir-me al Departament l'estiu de 1991 per fer la Tesina. Després sempre m'ha ajudat moltíssim a trobar beques, sense les quals aquesta Tesi no hauria estat possible. Per comptar amb mi i convidar-me a participar en projectes i en dues campanyes a l'Antàrtida. La seva ajuda i sentit crític en les correccions d'aquest treball han estat d'un gran valor.

En Yves Lagabrielle, que ha estat el meu co-director a Brest després de la marxa d'en JMA cap al Pacífic Sud. Ha posat confiança en mi tot convidant-me a participar a la campanya NOFI i al *workshop* de Nouméa. M'ha ajudat molt a tenir un punt de vista més global i a fer el *brain-storming* de les discussions de la Tesi.

Als qui m'han acollit i m'han ensenyat tantes coses en les estades que he fet en altres centres durant aquests anys: Philippe Huchon de *l'École Normale Supérieure de Paris,* Martin Sinha dels *Bullard Laboratories-University of Cambridge,* Lindsay Parson de l'*Institute of Oceanographic Sciences-Deacon Laboratory* i Ken Macdonald, de la *University of California-Santa Barbara* .

A la Hélène Ondréas del DRO/GM (IFREMER) per la nostra estreta amistat, per tanta feina que hem fent totes dues juntes, pels cops de mà i les injeccions de moral que m'ha donat tots aquests anys i per passar-nos-ho sempre bé tant sigui a Brest sota la pluja com a les platges de Fiji sota d'un cocoter! Ella i la Cathy Satra em van ajudar a fer els blocs batimètrics 3-D.

A en Jordi Sorribas i en Marcel.lí Farran per fer el mapa 1:250000 del Bransfield, passar-me els fitxers x,y,z de la batimetria de la Conca de Bransfield i per ajudar-me en questions informàtiques quan ha calgut. A en Manabu Tanahashi per passar-me els fitxers x,y,z de la batimetria de la Centre d'Expansió Central. A l'Eric Hardy per trobar sempre un lloc per a mi i els meus fitxers a la UBO.

A la gent que m'he anat trobant a través de *reviews* de papers, congressos, cursos, o xerrades de passadís i que m'han ajudat a veure el camí una mica més clar. Alguns d'ells són: John Madsen, Brian Taylor, Pascal Gente, Rodey Batiza, Cesc Sábat, Amotz Agnon, Jean-Louis Olivet, Shu-Khun Shu, Javi Escartin, Rob Bird, Jean-Philippe Eissen, Etienne Ruellan, Doug Wilson, Bramley Murton, Louis Géli, Mathilde Cannat, Fernando Martinez...

Als companys "marins", especialment a la Maria José Prieto per les xerrades que hem tingut sobre la sísmica del Bransfield i també sobre la gent que allà hi treballa, la Isa, la Mireia, la Judit, en José Luis, l'Alejandro, en Toni, en Jordi S., en Paulino, la Bárbara, en Roger i en Joan; i de la resta del Departament, en Jordi "Corbi", la Glòria F., en Jordip, en Miguelillo, l'Eula, en Bernat, la Françoise, en Ramon, que són o han passat per aquí i que m'han ajudat a fer aquesta feina més agradable.

A la gent amb qui també he treballat a la UBO de Brest, la Chantal Tisseau, la Marcia Maia, i en Thierry Tonnerre, co-autors del paper *Mar. Geophys. Res.* Als companys que eren allà o al DRO/GM, la Valérie, en Vassilios, en Save, l'Ann, en José, en Remy, la Cécile... i especialment a la Laure, per les corregudes al Bois de Kerhual després de les escapades nocturnes a "La Soute".

No puc oblidar els companys i amics que durant tot aquest temps m'han ajudat tant en qüestions logístiques per tal que no em quedés sota un pont: a Brest, el Dr. Pepone (en incomptables ocasions!); en Benoit; en Momo, l'An, en Bernard, i... en Giovanni (per no ser-hi!). A París, la Glòria, en Pierre i la Lara; l'Eduardillo; i en Philippe i família. A Cambridge, en Dave L., en Dave C., la Louise, i en "Hamish". A Santa Barbara, l'Ann, la Leslie, la Julie, en Lex, i la "Bear".

A en Robin Rycroft del Servei d'Assesorament Lingüístic de la UB per les correccions de l'anglès, i a en Lluís Pallàs per les correccions del català.

Als membres del tribunal que han acceptat de jutjar aquest treball.

A en Raimon per passar-nos-ho tan bé a les "verdes" i a les "madures" durant aquests anys de Tesi. A la meva Família, que sempre m'ha recolzat i animat suportant tan bé les llargues absències.

Dedico aquest treball a en Jordi, la Fina i la Pilar.

Contents

PART III: DATA AND RESULTS

Abstract

This Thesis deals with the study of the rifting and seafloor spreading processes in backarc basins using swath-bathymetry and geophysical data. The geophysical methods used are mainly magnetism and gravimetry, although other methods, such as seismic reflection and submersible data are also presented in some chapters. Three areas are selected for this study: The Central and Eastern Bransfield Basins, northwest Antarctic Peninsula, and the Central Spreading Ridge and the South Pandora-Tripartite Ridges in the North Fiji Basin, southwest Pacific.

The Bransfield Basin is a narrow and elongated active backarc basin located between the Antarctic Peninsula and the South Shetland Islands, at the southwestern edge of the Scotia Arc. The Bransfield Basin is composed of three small basins, Western, Central and Eastern, separated respectively by Deception and Bridgeman Islands. The last two were surveyed by the GEBRA 93 cruise during which full swath-bathymetric coverage, single-channel seismic reflection and magnetic profiles were acquired.

The Central Bransfield Basin is 60 km wide, 230 km long and 1950 m deep and the structures mainly trend N55-60. The basin morphology is dominated by six large seamounts (labelled A to F) that outcrop from the sedimented seafloor of the Central Bransfield Basin and align with the basin axis. The seamounts present circular, semi-circular and elongated morphologies. Moreover, the Eastern Bransfield Basin is 42 km wide, 150 km long, deeper than 2700 m and trends N40-45. The basin is characterised by four deep *en échelon* troughs having a lozenge shape, and small, scattered volcanic cones mainly located in the southwestern half basin. A total of 119 submarine volcanoes are observed in these two basins, with a predominance of higher edifices (over 150 m high) in the Central Basin. Magnetic anomalies are difficult to identify in the Bransfield Basin, although a positive alignment well correlated with the submarine volcanic edifices of the Central Bransfield Basin was recognized and named the Bransfield Rift Anomaly. When this anomaly is tentatively interpreted as Anomaly 1, the maximum age of spreading in the Central Bransfield Basin would be 0.71 Ma and the resulting maximum full rate 0.83 mm/yr. The free-air gravity anomalies are well correlated with the bathymetric maps.

The North Fiji Basin is a mature backarc basin located between two active subduction zones of opposite polarity: the New Hebrides and the Tonga-Kermadec trenches. Several extensional features and spreading centres have been identified within the North Fiji Basin. Two of these features are studied in detail here: the Central Spreading Ridge and the South Pandora-Tripartite Ridges.

The Central Spreading Ridge is the most widely explored and best known of all the spreading centres identified in the basin, and has been intensively explored during the cruises of the French-Japanese STARMER project (1987-1991). Six cruises were undertaken in the area during this project: 4 surface cruises (swath-bathymetry, geophysics and sampling) and 2 diving cruises. The Central Spreading Ridge is more than 800 km long and 50-60 km wide, and is segmented into three first order segments labelled, from north to south, N160, N15 and N-S according to their orientation. The N160 segment is 210 km long and is composed of three second-order segments (CSR1 to CSR3), which are a succession of long *en échelon* grabens, similar to that of the Mid Atlantic Ridge. The N15 segment is 165 km long and comprises two segments, CSR4 and CSR5. The axial morphology is characterized by a double ridge, split by an axial graben. The N-S segment is 255 km long and divided into three second-order segments (CSR6 to CSR8). The segment morphology shows a central flat and rectangular high, like in the East Pacific Rise. Magnetic anomalies up to Anomaly 2A (3.5 Ma) are recognized along the N-S segment, whereas only Anomalies J and 1 (0.97 and 0.7 Ma, respectively) are clearly identified along the other two segments. The calculated spreading rate is intermediate,

decreasing northwards from 80 to 50 mm/yr. In addition, there is a change in the axial gravity structure along the Central Spreading Ridge. The mantle Bouguer anomalies obtained on the northern part of the Central Spreading Ridge (N160/N15 segments) show "bull's eye" structures interpreted as the result of mantle upwelling at the middle of the segments. In contrast, the mantle Bouguer anomalies of the southern part of the ridge (N-S segment) are more homogeneous and consistent with the observed smooth topography.

The South Pandora-Tripartite Ridges are located in the northern part of the North Fiji Basin, one of the less explored areas of the basin. The area was surveyed by the NOFI cruise during which swath-bathymetry, geophysical and geological data were acquired. The South Pandora-Tripartite system extends over more than 800 km, and three first-order segments are distinguished according to their orientation: N75 and E-W (South Pandora Ridge) and N110 (Tripartite Ridge). The N75 segment is 170 km long and is composed of two second-order segments, SPR4 and SPR3. Its axial morphology is dominated by an axial graben disturbed only by an abrupt central seamount in the middle of segment SPR3. The E-W segment is 300 km long and composed of three segments, SPR2, SPR1 and SPR0, from west to east respectively. This segment also shows a contrasting longitudinal morphology. The N110 segment is 280 km long and composed by TR3, TR2 and TR1 second-order segments. Bathymetric maps show axial seamounts and deep troughs alternating along-axis. Preliminary interpretations of magnetic anomalies are presented, and Anomalies 1 to 3A (7 Ma) are identified along the South Pandora Ridge. The calculated spreading rate is ultra-slow at 16 mm/yr. In contrast, only Anomaly 1 is clearly identified along the Tripartite Ridge, with a full spreading rate decreasing from 8.5 to 0 mm/yr towards the southeast. The gravity structure also shows "bull's eye" lows associated with the contrasting volcanic highs.

Several points are discussed concerning backarc evolution, the comparison between backarc and mid-ocean ridge spreading, the role of seamount volcanism, differences in thermal regimes along the Central Spreading Ridge, and models of backarc accretion. The main conclusions are:

1) The three areas studied have been classified in terms of backarc evolutionary stages, from incipient and pre-spreading rifting stages (Central and Eastern Bransfield Basins, respectively) to well organized seafloor spreading, and from young (Tripartite Ridge) to mature (Central Spreading Ridge and South Pandora Ridge).

2) The present-day opening seems to be related to the rollback of the subduction hinge in the Bransfield Basin. In contrast in the North Fiji Basin the opening seems to be linked to a regional thermal anomaly instead of a subduction zone.

3) The initial rifting of the arc may pre-determine the future segmentation of the basin. Even if the accretionary processes are similar in backarc and mid-ocean ridge settings, differences appear concerning ridge segmentation and axial discontinuities. First-order backarc segmentation is short-lived and about half the length of that in mid-ocean ridges. The fundamental difference between backarc and mid-ocean ridges is the lack of large fracture zones and transform faults separating the backarc segments.

4) Large seamount volcanism may play a fundamental role in backarc axial construction, and may be a common characteristic of slow and ultra-slow mature spreading ridges and incipient spreading centres, as observed along the South Pandora-Tripartite Ridges and the Central Bransfield Basin, respectively.

5) The variability of the axial morphology and gravity structure observed along the Central Spreading Ridge is explained in terms of differences in thermal regime. The limits between "cold" and "hot" segments are propagating rifts, which may be interpreted as thermal boundaries.

6) Two end-member models of backarc crustal accretion and mantle upwelling are presented: focused-type and continuous-type accretion. The focused-type would show an extremely contrasted morphology and deep structure along the segments, with punctiform upwellings. The continuous-type accretion would be homogeneous and uninterrupted along the ridge, with a persistent magma chamber. Internal (ridge evolution, spreading rate, thermal regime) and external factors (nature of the surrounding lithosphere, proximity of mantle plumes and subduction zones) may control the type of accretion.

Resum

Aquesta Tesi estudia els processos de *rifting* i acreció oceànica en les conques de rere-arc utilitzant dades de batimetria multifeix i dades geofísiques. Els mètodes geofísics emprats han estat, principalment, magnetisme i gravimetria. En alguns capítols també es presenten dades de sísmica de reflexió i dades de submergible. Per a aquest treball s'han seleccionat tres àrees: les conques Central i Oriental de Bransfield, a l'Antàrtida Occidental, el Centre d'Expansió Central i les Dorsals de Sud Pandora-Tripartita, a la Conca Nord-Fijiana, Pacífic Sudoest.

La Conca de Bransfield és una conca de rere-arc activa que es troba entre la Península Antàrtica i les Illes Shetland del Sud, a la vora sudoest de l'Arc de Scotia. La Conca de Bransfield està formada per les conques Occidental, Central i Oriental, separades per les Illes Deception i Bridgeman. Les conques Central i Oriental van ser estudiades durant la campanya oceanogràfica GEBRA 93, en la qual es van adquirir dades de batimetria multifeix, magnetisme i sísmica de reflexió monocanal.

La Conca Central de Bransfield té 60 km d'amplada, 230 km de longitud, una profunditat màxima de 1950 m i la majoria d'estructures estan orientades N55-N60. La morfologia de la conca està dominada per sis *seamounts* alineats seguint l'eix de la conca (anomenats A a F), que afloren entre el fons recobert de sediments de la Conca Central de Bransfield. Els *seamounts* es caracteritzen per diferents morfologies: circular, semi-circular i allargades. Per altra part, la Conca Oriental té 42 km d'amplada, 150 km de longitud, una profunditat máxima de 2700 m i la majoria d'estructures estan orientades N40-N45. La conca es caracteritza per quatre depressions profundes de forma romboïdal i disposades *en échelon* i per cons volcànics petits i dispersos principalment localitzats a la meitat sudoest de la conca. Entre les dues conques s'ha observat un total de 119 volcans submarins, amb predomini dels edificis grans (de més de 150 m d'alçada) en la Conca Central. Les anomalies magnètiques són difícils d'identificar en la Conca de Bransfield, però així i tot s'ha observat un alineament magnètic positiu, anomenat Anomalia del Rift de Bransfield, ben correlacionat amb els volcans submarins de la Conca Central. Si interpretem aquesta anomalia com l'Anomalia 1, l'edat màxima de la conca seria de 0.71 Ma i la taxa d'expansió resultant de 0.83 mm/a. Les anomalies gravimètriques a l'aire lliure estan ben correlacionades amb les estructures batimètriques.

La Conca Nord Fijiana és una conca de rere-arc madura que es troba entre dues zones de subducció actives i de polaritat oposada: les fosses de les Noves Hèbrides i de Tonga-Kermadec. En la Conca Nord Fijiana s'han identificat diverses estructures extensives i centres d'expansió. Dues d'aquestes estructures s'han estudiat en detall en el present treball: el Centre d'Expansió Central i les Dorsals de Sud Pandora-Tripartita.

El Centre d'Expansió Central és el més conegut de tots els centres d'expansió de la conca i ha estat intensament explorat durant les campanyes del projecte franco-japonés STARMER (1987-1991). S'hi han realitzat sis campanyes oceanogràfiques, quatre de superfície (batimetria multifeix, geofísica i mostreig) i dues d'immersió. El Centre d'Expansió Central té més de 800 km de longitud, 50-60 km d'amplada i està dividit en tres segments de primer ordre, anomenats segons les seves direccions predominants, N160, N15 i N-S. El segment N160 té 210 km de longitud i está format per tres segments de segon ordre (CSR1 to CSR3), els quals són una successió de llargs grabens *en échelon* , similars als que es troben a la Dorsal Mèdio-Atlántica. El segment N15 té 165 km de longitud i comprèn dos segments, CSR4 i CSR5. La morfologia axial es caracteritza per una doble cresta partida per un graben axial. El segment N-S té 255 km llargada i está dividit en tres segments de segon ordre (CSR6 to CSR8). La morfologia es caracteritza per una cresta elevada i plana, anàloga a la Dorsal del Pacífic Est. En el segment N-S s'han identificat fins a l'Anomalia 2A (3.5 Ma), mentre que en els altres dos segments s'han identificat només les Anomalies J i 1 (0.97 and 0.71 Ma, respectivament).

L'índex d'expansió calculat és intermedi i disminueix de 80 a 50 mm/a. A més, s'ha observat un canvi en l'estructura gravimètrica axial al llarg del Centre d'Expansió Central. Les anomalies de Bouguer del mantell obtingudes en la part nord del Centre d'Expansió Central mostren estructures en *bull's eye* que s'interpreten com resultat d'un *upwelling* mantèlic a la part central dels segments. En canvi, les anomalies de Bouguer del mantell observades en la part sud de la dorsal són molt més homogènies i compatibles amb les morfologies observades.

Les Dorsals de Sud Pandora-Tripartita es troben en la part nord de la Conca Nord Fijiana, una de les zones menys explorades de tota la conca. Aquesta àrea ha estat estudiada durant la campanya NOFI, en la qual es van adquirir dades de batimetria multifeix, geofísiques i geològiques. El sistema Sud Pandora-Tripartita s'estén al llarg de més de 800 km de llargada i s'hi han distingit tres segments de primer ordre segons la seva orientació: N75, E-W (Dorsal de Sud Pandora) i N110 (Dorsal Tripartita). El segment N75 té 170 km de longitud i es compon de dos segments de segon ordre, anomenats SPR4 i SPR3. La morfologia axial està dominada per grabens intruïts al centre del segment per *seamounts*. El segment E-W té 300 km de longitud i, d'oest a est, està format per tres segments, SPR2, SPR1 i SPR0. El segment E-W també es caracteritza per una morfologia longitudinal molt contrastada. El segment N110 té 280 km de longitud i està format per tres segments de segon ordre anomenats TR3, TR2 i TR1. Els mapes batimètrics mostren una alternança entre *seamounts* axials i profundes depressions al llarg del segment N110. En les interpretacions preliminars de les anomalies magnètiques s'han identificat les Anomalies 1 fins a la 3A (7 Ma) en la Dorsal de Sud Pandora. L'índex d'expansió calculat és ultra-lent, de 16 mm/a. En canvi, en la Dorsal Tripartita només s'ha identificat l'Anomalia 1, amb un índex d'expansió que disminueix cap al sudest entre 8.5 a 0 mm/a. L'estructura gravimètrica mostra anomalies negatives tipus *bull's eye* associades als alts volcànics.

Es discuteixen diversos punts, referents sobretot a l'evolució de rere-arc, la comparació entre l'expansió de rere-arc i mèdio-oceànica, el paper del vulcanisme corresponent als *seamounts*, les diferències en els règims tèrmics al llarg del Centre d'Expansió Central i models d'acreció de rere-arc. Les principals conclusions són les següents:

1) Les tres àrees estudiades han estat classificades en estadis evolutius de rere-arc, des d'estadis incipient i de pre-expansió (Conques Central i Oriental de Bransfield, respectivament) fins a expansió oceànica ben organitzada de jove (Dorsal Tripartita) a madura (Centre d'Expansió Central i Dorsal Sud Pandora).

2) L'obertura actual de la Conca de Bransfield sembla estar relacionada amb el retrocés de la zona de subducció. En canvi, en la Conca Nord Fijiana, l'obertura sembla relacionada amb una anomalia tèrmica regional.

3) El *rifting* inicial de l'arc pot pre-determinar la futura segmentació de la conca. Els processos d'acreció de rere-arc i mèdio-oceànics són força similars, però s'observen algunes diferències relacionades amb la segmentació i les discontinuïtats axials. La segmentació de rere-arc de primer ordre es de curta durada i té la meitat de longitud que en les dorsals mèdio-oceàniques. La diferència fonamental entre les dorsals de rere-arc i les mèdio-oceàniques és la manca de zones de fractura que separin els segments de rere-arc.

4) El vulcanisme de grans *seamounts* pot tenir un paper fonamental en la construcció de les dorsals de rere-arc. Proposem que deuen ser una característica comuna en les dorsals lentes i ultra-lentes així com en els centres d'expansió incipients, tal com ha estat observat al llarg de la Dorsal de Sud Pandora-Tripartita i el Centre d'Expansió Central, respectivament.

5) La variabilitat de la morfologia axial i l'estructura gravimètrica observada al llarg del centre d'expansió central pot explicar-se mitjançant diferències en el règim tèrmic. Els límits entre els segments "freds" i calents" son *rifts* que es propaguen, els quals poden ser interpretats com a fronteres tèrmiques.

6) Es presenten dos models extrems d'acreció crustal i *upwelling* mantèlic de rere-arc: Acreció focalitzada i acreció contínua. L'acreció focalitzada es caracteritza per una morfologia i estructura profunda molt contrastada al llarg dels segments, amb *upwellings* de distribució puntual. L'acreció contínua es més homogènia i ininterrumpuda al llarg de la dorsal, amb una cambra magmàtica persistent. Els tipus d'acreció poden ser controlats per factors interns (evolució de la dorsal, índex d'expansió, règim tèrmic) i factors externs (tipus de litosfera, plomes mantèliques i zones de subducció).

Foreword

Most deep-sea, plate tectonics-related marine geology and geophysics was initially devoted to the study of mid-ocean ridges, such as the East Pacific Rise and the Mid-Atlantic Ridge. It was not until ten to fifteen years ago that the scientific community began focusing on backarc basins, on their dynamics and on their poorly known accretionary systems. At present, the exploration of the general structure of backarc basins has made notable progress, research projects address detailed studies of their spreading centres by means of swath-bathymetry and imagery, state-of-the-art marine geophysics, satellite-derived data, submersible observations and sampling and *in situ* monitoring.

This Thesis aims to contribute to this international effort for the understanding of extensional and accretionary processes in backarc basins. To this purpose, we follow the theoretical and methodological approaches commonly used in the exploration and analysis of mid-ocean ridges, thus involving most of the techniques described in the former paragraph. Three areas have been selected (Fig. i): The Central and Eastern Bransfield Basin (northwest Antarctica), the Central Spreading Ridge, in the central North Fiji Basin, and the South Pandora-Tripartite Ridges in the northern North Fiji Basin (southwest Pacific).

The data from the Bransfield Basin (Table I.i) come from the Spanish *Programa Nacional de Investigación en la Antártida,* project ANT-93-1008-C03-01, funded by the *Comisión Interministerial de Ciencia Y Tecnología* (CICYT) in 1993-94. The project entitled: *"Evolución geológica de la Cuenca de Bransfield y de la Dorsal Sur del Mar de Scotia (GEBRA)"* was leaded by the *Grup de Recerca en Geociències Marines* from the *Universitat de Barcelona,* although other institutions have also participated, as the *Institut de Ciències del Mar-Consejo Superior de Investigaciones Cientificas* (CSIC) of Barcelona, *Instituto Español de Oceanografía* (IEO) of Madrid, and the Renard Centre for Marine Geology (RCMG) of Gent, Belgium.

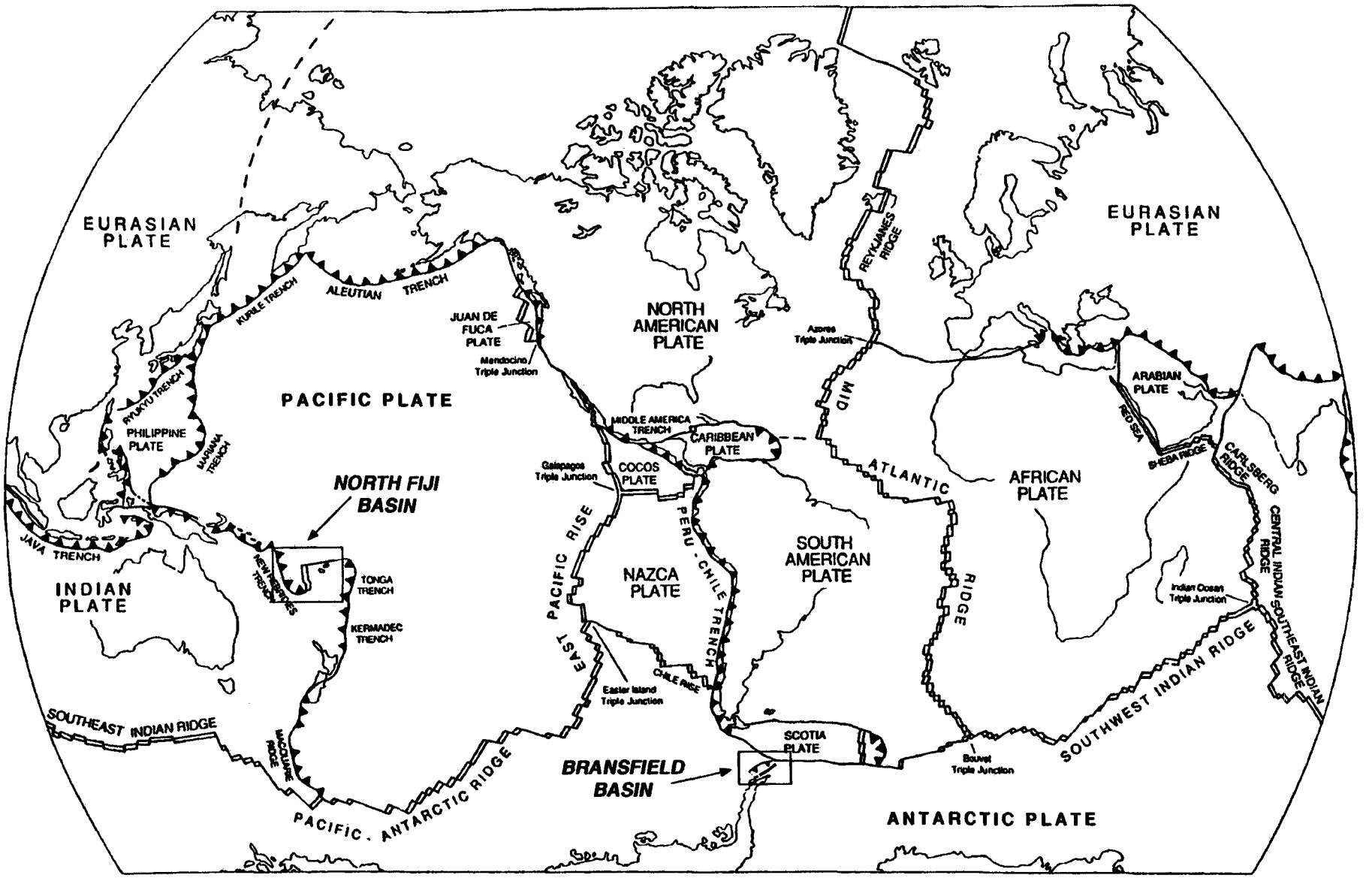

Fig. i. Sketch of the major tectonic plates, mid-ocean ridges and transform faults and trenches. The two backarc basins studied in this Thesis, Bransfield Basin and North-Fiji Basin, are located within boxes.

Moreover, the data of the central and northern North Fiji Basin mainly come from the French-Japanese STARMER (1987-1992) and New STARMER (1994-1999) projects, respectively (Table I.i), devoted to the study of the accretionary processes (tectonics, magmatism and hydrothermalism) in marginal basins of the southwest Pacific, and particularly the North Fiji Basin. The projects were coordinated by the Science and Technology Agency of Japan, and the *Institut Français pour la Recherche et Exploitation de la Mer*, IFREMER (France), with the cooperation of other institutions (Table I.i).

Areas	**CBB-EBB** **Central - Eastern Bransfield Basin**	**CSR** **Central Spreading Ridge**	**SPR-TR** **South Pandora - Tripartite Ridges**
Locations	Bransfield Strait (NW Antarctic Peninsula)	Central North Fiji Basin (SW Pacific)	Northern North Fiji Basin (SW Pacific)
Projects	*Prog. Nacional Inv. Antártida* (1992-1994)	STARMER (1987-1991)	New STARMER (1994-1999)
Organizations	UB (Spain) ICM (Spain) IEO (Spain) RCMG (Belgium)	IFREMER (France) INSU (France) STA (Japan) JAMSTEC (Japan) SOPAC (SW Pac)	INSU (France) IFREMER (France) STA (Japan) JAMSTEC (Japan) SOPAC (SW Pac)
Cruises	GEBRA 93	KAIYO 87-88-89 YOKOSUKA 90-91 STARMER	NOFI 94
Res. Vessels	Hesperides	Kaiyo Yokosuka Nadir	L'Atalante
Data	Swath-bathymetry Bot. Parametric Source Magnetics Seismics Sediment sampling	Swath-bathymetry Magnetics Seismics Submersible dives Rock/water sampling	Swath-bathymetry Acoustic imagery Magnetics Gravity Seismics Rock sampling

Table I.i. Summary of the locations, projects, organizations involved, cruises, research vessels and data acquired in the three study areas.

My personal participation in the above mentioned projects started in 1990, with a fellowship of *"la Caixa"*. Then, I attended the cruise Yokosuka

90, a surface-ship survey in the frame of the STARMER project. This first cruise, was followed in 1991 by a diving cruise, the Yokosuka 91, with the submersible Shinkai 6500. Also in 1991, I completed the D.E.A. *"Géosciences Marines"* at the UBO-Brest (France). Since 1992, I benefited from the fellowship AP-91-46338255 of *Formación de Profesorado Universitario* from the *Ministerio de Educación y Ciencia,* and I completed my Master Thesis at the University of Barcelona. Moreover, I participated in the *Programa Nacional de Investigación en la Antártida* with the cruise GEBRA 93. The recently started New-STARMER program allowed me to take part in the NOFI 94 cruise. Along these five years, I have had open access to all the data from STARMER and GEBRA projects

This Thesis is composed of the following parts:

• Part I. Introduction to the geophysical methods used in ocean ridge surveys, new insights into ocean ridges and some general aspects of backarc basins.

• Part II. Geological setting of the Bransfield Basin and North Fiji Basin, focusing on their regional geodynamic setting imaged from GEOSAT satellite data, as well as some hypotheses about the origin and evolution of these basins.

• Part III. Data and main results obtained in the study of the Central and Eastern Bransfield Basin, the Central Spreading Ridge and the South Pandora-Tripartite Ridges. The results are obtained principally from the study and interpretation of swath-bathymetry, magnetics and gravity data, although seismic reflection and submersible data are also presented in some chapters.

• Part IV. The essential points discussed in this part are the evolution from backarc rifting to mature spreading, the similarities and differences between backarc and mid-ocean spreading, the role of seamount volcanism in accretionary processes, and the variability between the superficial and deep structure along a backarc spreading ridge. Finally, we propose two end-member models of backarc accretion.

And now, sit-down comfortably, relax and...enjoy your reading!

PART I:
INTRODUCTION

Over the past 15 years our understanding of the evolution of the mid-ocean ridge system, and the processes associated with the creation of new oceanic crust has changed significantly. This new thinking has been stimulated in part by the availability of new surveying instruments, such as high-resolution swath mapping and side-scan systems, satellite altimetry, geophysical methods, and submersible exploration. All this has allowed researchers to map the seafloor with an unprecedented level of resolution. In part, this changing view recognizes a complex dynamic system within which magmatic, tectonic and hydrothermal processes are intimately linked (Detrick and Humphris, 1992).

Three different aspects will be covered in the next three chapters, which form the introductory part of this Thesis. The three are fundamental for a better understanding of Parts III and IV. In Chapter 1 we present the various geophysical tools commonly used in the survey of ocean ridges. Chapter 2 is based on the new approaches in ocean ridge analysis in terms of its surface and deep structure, leading to the concept of ridge segmentation. Finally, Chapter 3 deals with the main characteristics of backarc basins, which constitute the geodynamic setting in which the studied areas are located.

Chapter 1

GEOPHYSICAL METHODS IN OCEAN RIDGE SURVEYS

Geophysical methods are essential tools for the survey and study of oceanic areas, such as mid-ocean ridges and spreading centres. In this chapter we summarize some of the methods most commonly used in marine geology and geophysics. These methods provide the basis for this Thesis. A basic explanation about the data processing is also presented. Each method results in specialized and unique data sets which, at the same time, are complementary with others. We consider two different working scales in marine geology and geophysics: macro- and meso-scale.

- Macro-scale. This is mainly based on satellite data. These data give accurate information on the marine gravity field at a large scale, for example a whole ocean basin. Satellite data are essential to assess the main features of poorly surveyed areas, such as southern hemisphere oceans and circum-polar seas.

- Meso-scale. Two approaches are considered: Shipborne and submersible data.
  - Shipborne data comprise all the different types of geophysical data acquired during oceanographic cruises. This is the approach most generally used to survey and map an oceanic area. Some of the most common methods are bathymetry, imagery, magnetic, gravity, seismic reflection, and seismic refraction. In this chapter we describe only the methods used for this study.

  - Submersible data. Once one area has been completely mapped using satellite and shipborne data, manned submersibles and remote operated vehicles (ROV) are essential to geological observations *in situ* and detailed sampling of the deep-ocean bottom.

1.1. Satellite data

Satellite altimetry is used to study the marine gravity field over the world's oceans (Sandwell, 1984; Haxby and Weissel, 1986; McAdoo and Marks, 1992). Satellites such as Geos-3, Seasat, and Geosat use pulse-limited radar to measure the topography of the ocean surface, which is a good approximation to the marine geoid. For marine geology and geophysics it is desirable to compute the gravity anomaly from the geoid height. At short wavelengths (<200 km) the gravity anomaly mimics the seafloor topography, and thus provides essential information over vast areas of uncharted seafloor, such as southern oceans and Antarctic margins (Sandwell, 1992).

In this section we present, first, the basic principles of the altimetric method based on a synthesis made by Gilg-Capar (1994), and, second, the main characteristics of the Geosat satellite data.

1.1.1. THE ALTIMETRIC MEASUREMENT

The principle of altimetry is based on the height of the geoid (N), which is obtained after some corrections from the measurement of the variations in the height of the ocean surface (geoid) above a reference ellipsoid (Gilg-Capar, 1994) (Fig. 1.1).

The satellite carries an altimeter that emits pulses of a particular frequency, and records the reflected signal from the ocean surface at the vertical of the satellite position. The two-way travel time propagation of this wave gives the distance H, which is the distance between the satellite and the ocean surface (Fig. 1.1). Nevertheless, there are some dynamic phenomena that introduce a difference between the geoid and the ocean instantaneous surface. Some of these events correspond to tides, currents, and sea-level variations caused by changes in the atmospheric pressure. All these events are referred to as "oceanographic component", and are labelled h_c (Fig. 1.1). Data from on-land stations allow scientists to calculate the distance (h) between the satellite position and the reference ellipsoid. This distance h comprises the height (N) of the geoid above the reference ellipsoid, the oceanographic component (h_c), and the distance (H) between the satellite and the ocean surface (Fig. 1.1).

The height of the geoid (N) (Fig. 1.1), which is defined as the geoid variations in respect to the reference ellipsoid, is represented in the following formula (Tapley et al., 1982):

$$N = h - (H + h_c)$$

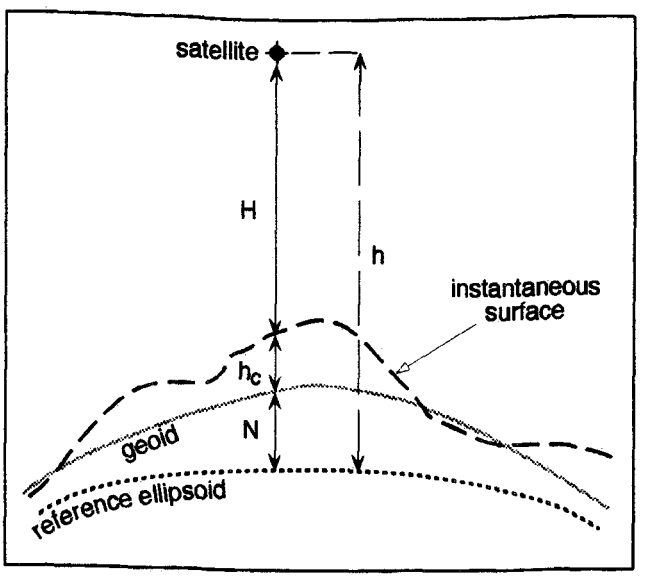

Fig. 1.1. Scheme of the principle of satellite altimetry modified from Tapley et al. (1982) and Gilg-Capar (1994). N is the geoid height, h is the height of the satellite, H is the distance between the satellite and the ocean surface, and h_C is the oceanographic component.

1.1.2. THE GEOSAT DATA

The Geodetic Satellite (Geosat) was launched in March 1985 by the United States Navy. Its primary (and classified) Geodetic Mission (GM) was to map the marine gravity field at a high spatial resolution on a global basis (Sandwell, 1992). In September 1986 Geosat started its first scientific mission: The Geosat/Exact Repeat Mission (ERM). Examples of marine gravity field or geoid mappings from Seasat (satellite launched in 1978) or Geosat/ERM data are given by several authors as Sandwell (1984), Haxby and Weissel (1986), and Sandwell and McAdoo (1988).

Sandwell (1992) summarized the measurement capabilities for satellite altimeter missions (Table 1.I). Measurement precision is evaluated in terms of vertical deflection (sea surface slope) along individual satellite altimeter profiles, and 1 μrad of vertical deflection error translates into 0.98 mGal of gravity anomaly error. The along-track resolution of the altimeter profiles is estimated by calculating the spectral coherence between independent

repeated profiles (e.g. Sandwell and McAdoo, 1990). The cross-track resolution is twice the characteristic spacing of the profiles (Sandwell, 1992).

Satellite	Precision	Along-track resolution	Cross-track resolution	Year of launching
Geos-3	30 μrad	80 km	20-400 km	1975
Seasat	10 μrad	50 km	80-120 km	1978
Geosat/GM	6 μrad	30 km	4 km	1985
Geosat/ERM	<1 μrad	20 km	160 km	1987

Table 1.I. *Altimeter capabilities (Sandwell, 1992).*

The profiles from the Geos-3 altimeter are "noisy" (30 μrad) in comparison with latter missions. This low precision limits the along-track resolution to 80 km (Table 1.I). The Seasat altimeter collected a data set having a precision of 10 μrad with an along-track resolution of 50 km (Marks and Sailor, 1986). However, the short lifetime of the mission resulted in a poor cross-track resolution of 80-120 km. The precision of the Geosat/ERM is generally better than 1 μrad and the full-wavelength resolution is 20-24 km, whereas the cross-track resolution is poorly resolved (160 km). High density Geosat/GM profiles have a precision of about 6 μrad and along-track resolution of about 30 km. The close spacing of the profiles supports a cross-track resolution of 4 km (Table 1.I). At present-day, the Geosat/GM profiles are declassified only south of 30°S.

Global marine gravity field data base

Sea surface height data from multiple high resolution satellites, such as Geosat/GM, ERS-1/GM, Seasat, and Topex, have recently been combined to produce a new global marine gravity field data base (Sandwell et al., 1994). The accuracy and resolution of this global field approaches the best fields derived from declassified Geosat/GM data south of 30°S (3 km of cross-track resolution at 30°S). A new free-air anomaly map has been established by Sandwell et al. (1994) revealing many structures not visible in the previously published map (Sandwell and Smith, 1992). The new map clearly reflects details of the bathymetric structures, such as fracture zones, active and fossil ocean ridge axes, and differences in roughness relied to specific structures, such as propagating rifts, triple junctions, microplates, and seamounts. Thus, the Sandwell et al. (1994) free-air anomaly map can be directly interpreted as a sort of morphological map.

The original gridded data of the Sandwell et al. (1994) map are available by ftp through Internet. We have extracted parts of this grid in order to produce satellite-derived free-air gravity maps that are presented in Parts II and III of the Thesis.

1.2. Shipborne data

Shipborne data are the most common data used in Marine Geology and Geophysics, and they comprise a wide range of tools and methods. In this section we focus on the three main methods of ocean ridge exploration used in this Thesis: bathymetry, magnetism and gravimetry. In the Bransfield Basin, where there is a significant sedimentary cover, single-channel seismic reflection data were also acquired. Although some of the main results of seismic reflection data are presented in Chapter 6, we will not describe this method here because it is not essential to ocean ridge surveys.

1.2.1. BATHYMETRY

Bathymetric techniques reveal the shape and structure of the ocean floor. Macdonald et al. (1992b) and Smith (1992) explained the evolution of mapping tools in oceanography, which we summarize in the next paragraphs.

The first soundings of the deep ocean floor were made in the 1800's with ropes and later with wire ropes. In the late 1920's, a major advance was made with the development of the echo-sounder, an instrument that measures the time it takes a sound pulse generated at the sea surface to return to the surface after reflecting off the seafloor. The travel time is converted to water depth using a velocity-depth curve for sound in the water column.

Since the 1960's, three major advances were made:

- **Echo-sounders.** They were developed with narrower beams and towed closer to the seafloor (Spiess and Tyce, 1973). A limitation was the ship speed (about 1.6 knots) and, in consequence, only small areas, less than a few hundred square kilometres, were mapped in this way.

- **Side-scan sonar.** In this new system the amplitude of the echo is recorded as a function of time. The strength of the echo is a measure of backscatter (bottom roughness) and slope. In general, there is an inverse relationship between the width of the side-scan swath and the resolution (Davis et al., 1986). Some examples of side-scan sonars are

SeaMARC II and HMR-1 (USA), GLORIA and TOBI (United Kingdom), and SAR (France).

• **Multibeam echo-sounder** (Fig. 1.2). This was the most critical advance in terms of mapping large areas of the seafloor with high resolution. The multibeam echo-sounder produces an array of 16 to 120 beams which are very narrow (1-3°). The array of beams constitutes a wide "swath" beneath the ship up to 7.5 times the water depth in the Simrad EM-1000 and EM-12D. Resolution varies from approximately 5 m for near-vertical beams to ≈50 m for echoes 60° from vertical and water depths of 2-6 km (Renard et al., 1991). Different systems have been developed. Thus for deep areas, from 100 to 10,000 m, we mention Seabeam 2000 (USA), Hydrosweep (Germany), Echos-XDM (Finland), Simrad EM-12 (Norway), and Furuno HS-10 (Japan). For shallow areas, from 5 to 800 m, the most important systems are the Simrad EM-100, EM-950, and EM-1000 (Norway).

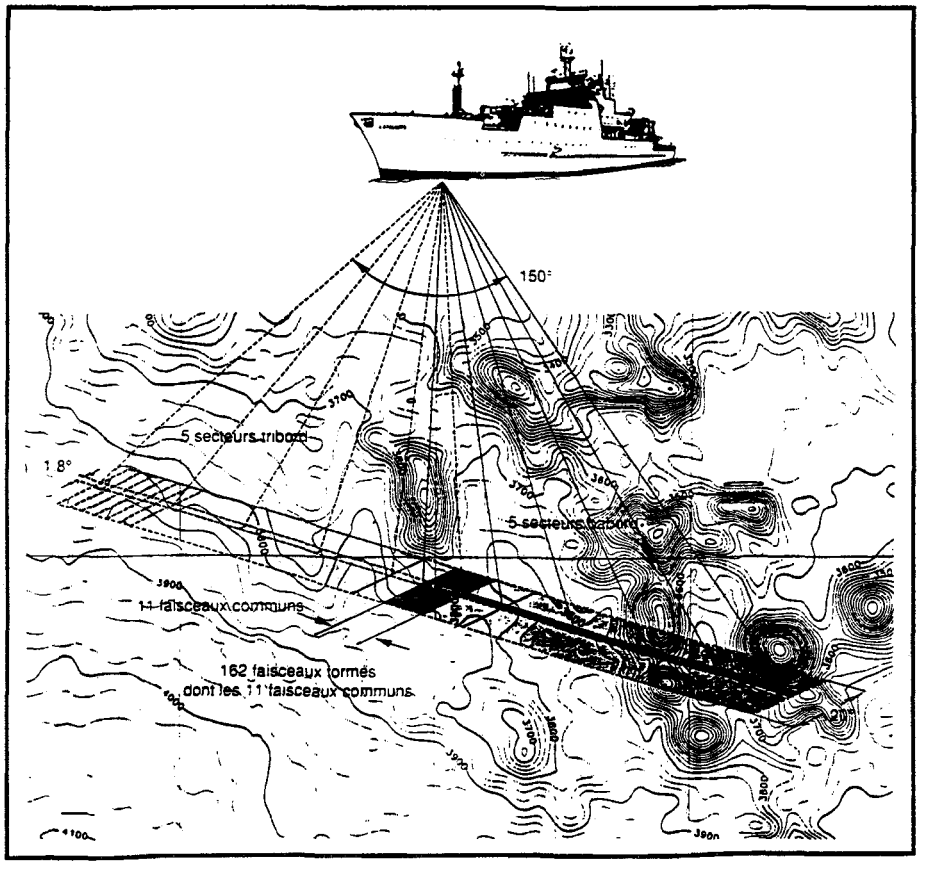

Fig. 1.2. Sketch of the Simrad EM-12 Dual, the multibeam echo-sounder installed on board the French RV L'Atalante, used during the NOFI survey of the northern North Fiji Basin (see Chapter 8).

The relative lack of erosion in many places of the deep ocean floor, and its relatively simple history, means that high resolution bathymetric maps together with side-scan mosaics may be translated directly into a map of structure, tectonics, and volcanism. This tool is particularly powerful in mid-ocean ridge regions which are relatively free of sediment burial, and are the birthplace of ≈60% of the Earth's crust and lithosphere (Macdonald et al., 1992b).

Swath bathymetry data processing

The raw bathymetric data are processed using programs specially developed for multibeam echo-sounders. We used Neptune and TRISMUS processing system, and all the colour bathymetric maps presented in Chapters 6, 7 and 8 (Part III) were obtained using the latter. In the next paragraphs we summarize its principal characteristics.

TRISMUS, which means, in French, *TRaitement Interactif des donnéeS MUltifaiSceaux*, is an interactive program developed at the Department of Computing of the IFREMER-Brest Centre (France). This program helps to process and represent graphically swath-bathymetry data. The main objective of TRISMUS is to create a bathymetric map issued from a Digital Terrain Model calculated from the multibeam echo-sounder. Although it was specially made for processing Simrad EM-12 Dual data, this program now also accepts the most common formats of swath-bathymetric systems, like those cited above.

Once having the (x,y,z) files containing latitude, longitude and depth, the successive processing steps are as follows:

- Data gridding. The first step is to grid the (x,y,z) data to create the Digital Terrain Model (DTM). In order to obtain the best results, the DTM grid must be proportional to the scale of the final plot (Sorribas et al., 1995). For example, for a bathymetric map at 1:200,000 scale, the right DTM should have a 200 m grid; for a 1:1,000,000 map, the DTM should be of 1 km grid. Two gridding methods are available.

- DTM operations. These comprise a succession of arithmetical and geometrical operations (e.g. interpolation, smoothing, reduction) that allow the user to modify or combine two or more DTM's.

• Data filtering. The raw (x,y,z) data are compared to a reference DTM in order to eliminate erroneous values (spikes).

• Plots. The final DTM can be represented graphically as along-track bathymetric profiles, isobath contour maps, colour contour maps, isobath and colour contour maps, or 3-D view block diagrams.

All the colour bathymetric maps presented in Part III have the same colour code. That is: reds for the shallow areas, orange, yellows and greens for the intermediate values from shallow to deep areas respectively, and blues for the deepest. Bathymetric contours with labels every 5 lines are superimposed on the colour images. Shaded relief maps derived from bathymetric gradients are also presented in Chapters 7 and 8. They are useful for illustrating the degree of topographic roughness along the ridge.

1.2.2. MAGNETISM

The magnetic method is based in measuring the strength of the Earth's magnetic field. Over the oceans, magnetic field measurements are made by towing in a sensor (usually a proton magnetometer) at a distance equal to at least 2.5 times the length of the vessel to remove its magnetic effects. Magnetic surveying is normally carried out in conjunction with other marine geophysical methods, such as bathymetry, gravity, and seismic reflection.

In order to obtain information about crust magnetization, it is necessary to subtract the International Geomagnetic Reference Field (IGRF) from the magnetic field measured, and the magnetic anomalies are then obtained. The magnetometer measures the magnitude but not the direction of the total magnetic field (only three-component magnetometers measure this, e.g. Isezaki, 1986). Thus, marine magnetic anomalies are anomalies in the magnitude (or total intensity) of the Earth's magnetic field (Fowler, 1990).

Magnetic anomaly maps of oceanic regions show alternate strips of high and low values of the magnetic field. Magnetic anomalies are positive when the magnetization is normal, and negative when they are magnetized following a reversed magnetic field. These magnetic strips, which are tens of km wide, offset by fracture zones and typically ± 500 nT in magnitude (Pitman and Heirtzler, 1966), run parallel to and are symmetric about the

spreading axes. In consequence, magnetic anomaly maps are very useful in delineating ridge axes and fracture zones (Fowler, 1990).

The origin of these magnetic stripes was firstly interpreted by Vine-Matthews in 1963. The Vine-Matthews hypothesis led directly to the theory of seafloor spreading and the establishment of a time scale for polarity transitions of the geomagnetic field (Heirtzler et al., 1968). Marine magnetic anomaly patterns may be used to date oceanic lithosphere back to mid-Jurassic time with an accuracy of a few million years (Kearey and Vine, 1990) (Fig. 1.3), and also to obtain spreading rates, which are intermediate values for the relative motion between two diverging plates (Vine, 1966).

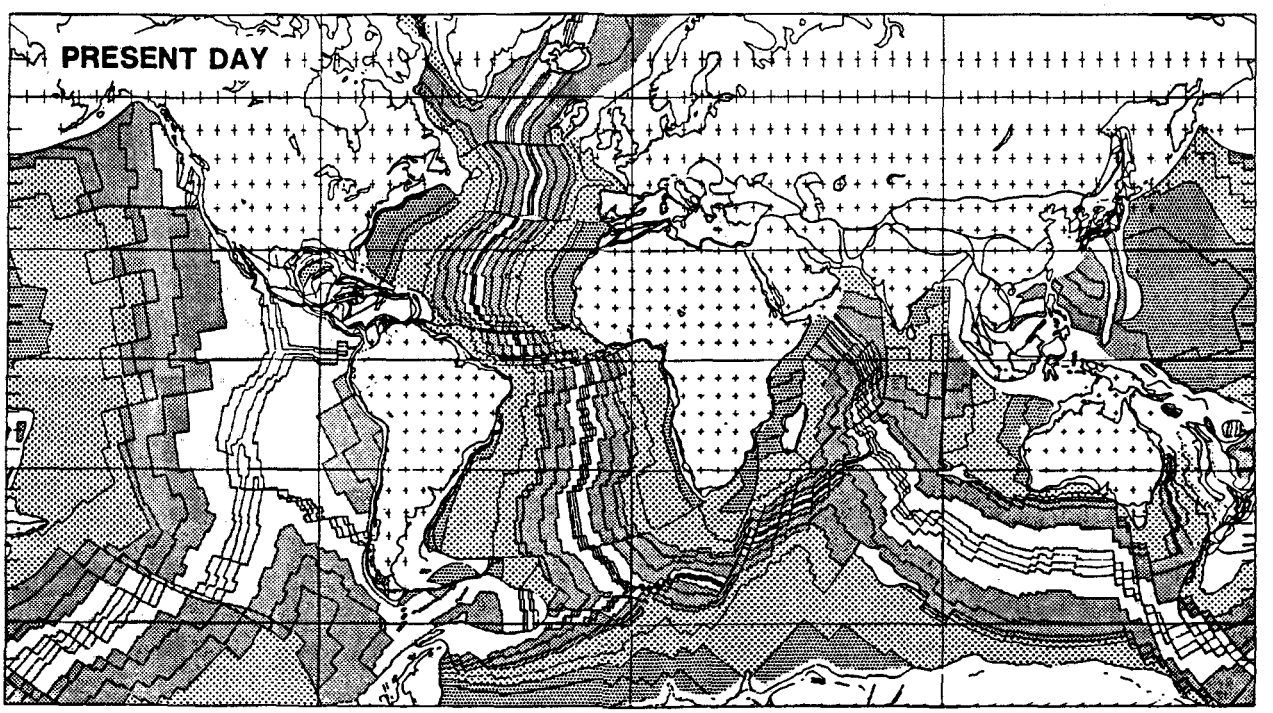

Fig. 1.3. The age of the ocean floor determined by using magnetic anomaly data, basement ages from deep sea drilling anomaly time scale and rotation poles and angles. White indicates the youngest ocean floor, light grey: 2-23 Ma, dark grey: 23-59 Ma; coarse light stipple: 59-84 Ma, and coarse dark stipple: 84-144 Ma (Scotese et al., 1988).

A high magnetization zone is sometimes found within the Central Anomaly, located over the axial zone. This magnetic high, named Central Anomaly Magnetic High (Tivey and Johnson, 1987), bisects the Brunhes Anomaly exactly where the present-day accretion is produced, and thus gives information about the precise location of the spreading axis (Klitgord, 1976; Tivey and Johnson, 1987).

Magnetic data processing

An example of the processing of magnetic data is presented by Huchon et al. (1994) for the Central Spreading Ridge (North Fiji Basin) (Fig. 1.4). Here we summarize the main parts of the magnetic data processing.

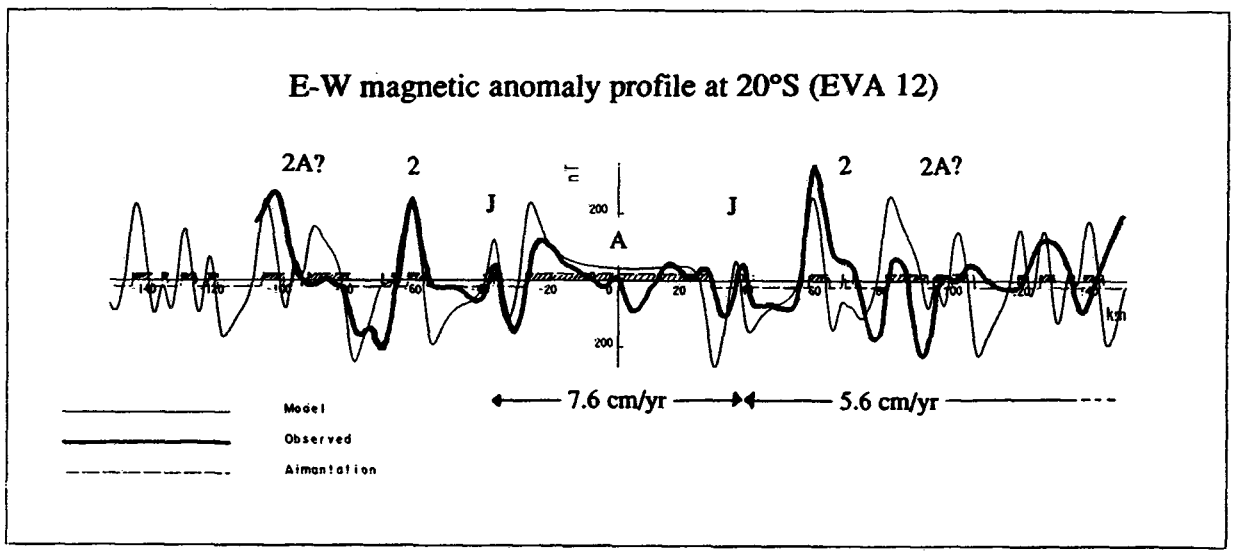

Fig. 1.4. Example of a magnetic anomaly profile located in the Central Spreading Ridge (North Fiji Basin) at 20°S (Huchon et al., 1994). Anomalies 1 to 2A are clearly identified. An increase in the spreading rate from 5.6 cm/yr to 7.6 cm/yr is deduced from the width of the anomalies. Bold line: Observed magnetic profile; Thin line: Synthetic magnetic profile.

The first step is to remove all anomalous data points, such as spikes and noise, by the radial amplitude-slope rejection method of Neff and Wyatt (1986). Other errors, such as cross track errors, are mostly due to the diurnal variation of the magnetic field and to differences between IGRF's used for computing the magnetic anomalies. To remove some of these errors, Huchon et al. (1994) applied a band-pass filter using a Fast Fourier Transform (Schouten and McCamy, 1972). This processing includes:

- Identification of profiles of sufficient length (at least 10 km) and proper orientation (not oblique to the axis by more than 45°);
- Projection of each profile on the selected direction;
- Interpolation at a constant step (about 1 km), necessary to perform the Fast Fourier Transform (FFT);
- FFT and band-pass filtering between 5 and 100 km;

The filtered data are projected along tracks to produce magnetic anomaly maps. For the identification of magnetic anomalies, synthetic magnetic profiles (Fig. 1.4) are computed using the Geomagnetic Time Scale of Harland et al. (1990). Huchon et al. (1994) used an average depth to the top of the magnetic layer (layer 2) of 2.7 km, a thickness of the magnetic layer of 0.5 km, and a magnetization value of 0.01 emu/cm.

An example of magnetic anomaly identification is given in Figure 1.4, where Anomalies 1 to 2A are clearly displayed. The identification of magnetic anomalies is facilitated by the good control we have on the location of the active spreading axis using swath bathymetry as well as observations *in situ* . Magnetic anomaly maps of the three zones studied are presented in Part III.

1.2.3. GRAVIMETRY

Measurements of the gravitational attraction of the Earth provide information about the structure of the lithosphere and mantle. Gravity anomalies are much smaller than the mean surface gravity value of 9.81 m/s^2 and they are quoted in milligal (mGal), which is 10^{-5} m/s^2 (10^3 Gal). Gravimeters are usually located in the most stable parts of the ships and have a resolution of 10^{-2} mGal. Two types of gravity anomaly are considered in marine geophysical studies:

Free-air anomalies

The free-air gravity anomalies are dominated by the attraction of seafloor topography and they mimic the bathymetric structure. Thus, anomaly lows are associated with the greater depths and positive anomalies appear over topographic highs and graben flanks. Free-air grids are obtained using the cubic B-spline approach (Inoue, 1986), and then free-air anomaly maps are obtained, like those presented in Part III.

The free-air gravity anomaly across mid-ocean ridges is not zero, indicating that the ridges are not in total isostatic equilibrium. In the ridges presenting an axial valley, the free-air anomaly is negative and of large amplitude (Cochran, 1979; Collette et al., 1980; McKenzie and Bowin, 1976). In contrast, in the ridges showing an axial high, the free-air anomaly is positive and of low amplitude (Davis and Lister, 1974; Lewis, 1981; Madsen et al., 1984).

Mantle Bouguer anomalies

Mantle Bouguer anomalies are obtained using the classical approach developed by Prince and Forsyth (1988) and Kuo and Forsyth (1988). Mantle Bouguer anomalies are generated by subtracting the attraction of seafloor topography and the effect of the crust-mantle interface from the free-air anomaly. The gravity effect of the water/crust and crust/mantle interfaces are usually computed assuming a crustal thickness of 6 km. Here, crust and mantle densities were assumed to be uniform, 2.7 and 3.3 Mg/m^3 respectively, while sea water density was taken as 1.03 Mg/m^3 (Fig. 1.5). The gravity effects of the two interfaces are processed at each node of the grid with the FFT algorithm of Parker (1972). Mantle Bouguer anomaly maps are presented in Part III (Chapters 7 and 8).

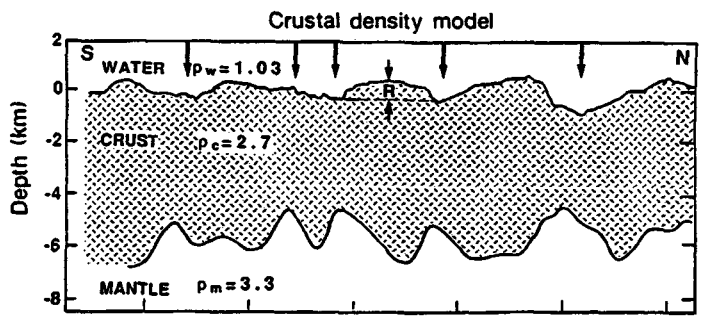

Fig. 1.5. A cross-sectional view of the crustal structure of the Mid-Atlantic Ridge. R is the axial topographic relief. Water, crust and mantle densities are given. The arrows correspond to bathymetric discontinuities. The crust in this model is predicted to be thickest near the segment midpoints and thinnest at the segment ends (Lin et al., 1990).

1.3. Submersible data

The best way to explore the nature of the ocean floor in detail is by using a submersible. The main problem is that the cost of building and maintaining a scientific submersible capable of diving with passengers down to depths of thousands of meters is too high for most countries to afford. However, at least seven deep scientific submersibles are still in use (Table 1.II).

Submersibles	Shinkai 2000	Cyana	Alvin	Mir I-II	Nautile	Shinkai 6500
Country	Japan	France	USA	Russia	France	Japan
Year	1981	1970	1964	1987	1985	1989
Depth (m)	2000	3000	4000	6000	6000	6500
Length (m)	9.3	5.7	7.6	7.8	7.6	9.5
Weight in air (T)	24	8.3	16	18.7	18.5	26
Max. Speed (kn)	3	3	1.5	5	2.5	1.8
Work aut. (h)	?	10	10	10	13	6
Safety aut. (h)	?	72	72	?	130	120

Table 1.II. *Main characteristics of the scientific deep submersibles in use. Aut: Autonomy.*

Submersibles permit marine geologists to do what land geologists do in the field. Submersible activities comprise *in situ* rock, sediment and water sampling, imaging (high quality video and photos), and measuring of water temperature, salinity and depth. The navigation system is based on several acoustic beacons communicating the submersible with the mothership which allow the submersible to use satellite GPS navigation at depth. This information allow scientists to make a detailed "geological mapping" of the seafloor.

In situ studies are fundamental for understanding the ocean ridge system. Thus, one of the best sections through the oceanic crust was recorded by the submersible Nautile along the sides of the Vema Fracture Zone (Auzende et al., 1989). In addition, several hydrothermal sites have been explored by submersibles in mid-ocean ridge environments. Such as the Mid-Atlantic

Ridge at 23°22'N (Gente et al., 1991), or in backarc setting, as the Lau Basin active sites (Fouquet et al., 1991).

Data and results obtained from dives of the Nautile and Shinkai 6500 in the Central Spreading Ridge of the North Fiji Basin are presented in section 7.3.

Chapter 2

NEW INSIGHTS INTO OCEAN RIDGE STUDIES

Ocean ridges mark accretive plate margins where the new oceanic lithosphere originates. They represent the longest, linear uplifted features of the Earth's surface, and can be traced by a belt of shallow-focus earthquakes which follow the ridges and their transform faults. The total length of the ridge system is about 70,000 km, and their crests are commonly 2-3 km higher than neighbouring ocean basins.

New swath mapping sonar systems and complementary geophysical methods (described in Chapter 1) have revealed the structure of the mid-ocean ridge and surrounding deep ocean floor with unprecedented clarity. These images show that the global ridge system is partitioned into discrete accretionary segments, each of which is separated from its neighbour by ridge axis discontinuities of various tectonic character. They have been studied and classified into a hierarchical system, comprising four principal orders (Macdonald et al., 1991). These range from the most fundamental first-order discontinuities, such as fracture zones, which are large, stable features linking ridge segments along strike-slip fault zones, to less stable second-, third- and fourth-order ridge axis discontinuities, which are considered to be more direct manifestations of the volcanic and tectonic controls governing the geometry of spreading centres. The changes in spreading rate, symmetry and direction, together with variations in temperature and magma supply, all affect crustal accretion processes. Much of contemporary oceanographic research is now focused on these features.

2.1. Superficial structure

The shallow structure of oceanic ridges can be approached in two different ways: temporal (structural variability across the axis), and spatial (structural variability along the axis).

2.1.1. ACROSS-AXIS MORPHOLOGY

The study of the across-axis morphology may give detailed information about the evolution of the ridge over time. We distinguish between axial and off-axial morphology.

Axial zone

The study of numerous bathymetric profiles orthogonal to the ridge axis suggested two different types of axial morphology: with axial high and with axial graben (Menard, 1967). The presence of each type of axial morphology depends on the spreading rate (e.g. Menard, 1967; Macdonald, 1982 and 1986). Thus, an axial depression is characteristic of slow spreading rates, whereas an almost flat profile and a topographic high are systematically observed at intermediate and fast spreading rates (Macdonald, 1982 and 1986). Macdonald (1982) considered three different types of axial morphology as a function of the full spreading rate (Fig. 2.1).

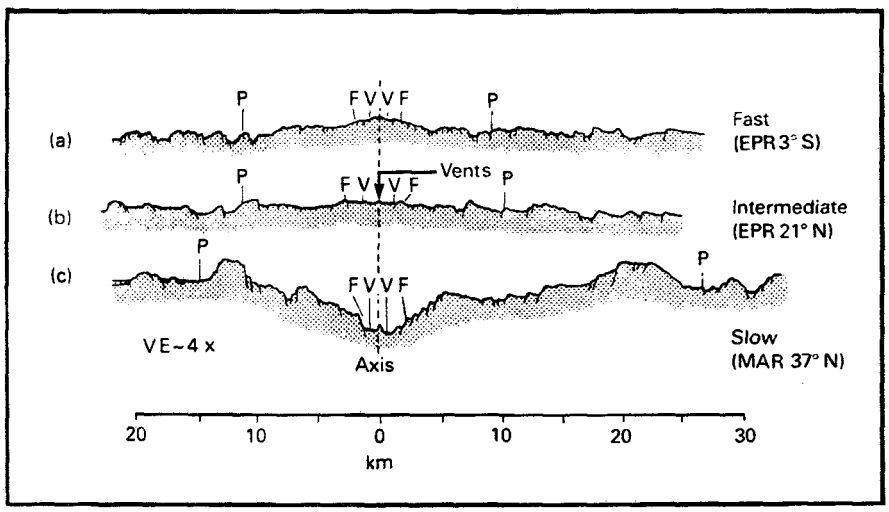

Fig. 2.1. High resolution bathymetric profiles of ocean ridges at fast, intermediate and slow spreading rates. EPR: East Pacific Rise, MAR: Mid-Atlantic Ridge, V: Neovolcanic zone, F: Zone of fissuring, and P: Extent of active faulting (Macdonald, 1982).

- **Fast.** At fast spreading rates (> 80-90 mm/yr) the most common feature is a wide, smooth axial high (Fig. 2.1), as the East Pacific Rise south of 15°N (Macdonald et al., 1992a). Some exceptions are observed, where a fast spreading ridge contacts an old, cold lithosphere, and then a deep axial valley develops (Malinverno, 1993) (e.g. Pito Rift, Martinez et al., 1991).

• **Intermediate.** They have a spreading rate between 50 and 90 mm/yr, and a morphology showing an axial high locally split by a 50 to 200 m deep graben (Fig. 2.1). Examples of intermediate ridges are the East Pacific Rise near 21°N and the Galapagos Ridge (Klitgord and Mudie, 1974). Exceptions are parts of the Juan de Fuca Ridge, the Australian-Antarctic Ridge, and Pacific-Antarctic Ridge, where a rift valley can be present along the ridge (Kappel and Ryan, 1986; Palmer et al., 1993; Marks and Stock, 1994).

• **Slow.** At slow spreading rates (< 40-50 mm/yr) the most common feature is an axial rift valley (Fig. 2.1). The axial valley width ranges between 10 to 50 km, and the height, difference in depth between the top of the flanks and the valley floor, is usually about 1000 m, sometimes reaching 2000 m (Le Douaran and Francheteau, 1981). Exceptions to this general trend are noticed in parts of the Mid-Atlantic Ridge near hot-spots where axial highs are found at slow spreading rates, such as the Reykjanes Ridge (20 mm/yr), or south of the Azores, at 37°40'N (23 mm/yr) (Laughton et al., 1979; Vogt, 1979).

Off-axis

The difference in topographic roughness between fast and slow spreading ridges is also found off-axis (Cannat, 1990). The maximal amplitude of the abyssal hills associated with fast spreading ridges is about 200-300 m. In contrast, the amplitude of the topographic features at the flanks of slow spreading ridges may reach 1000 m (Gente, 1987). The distribution of abyssal hills is not regular, and does not follow a simple periodicity law (Malinverno and Pockalny, 1990). This irregularity of the off-axis morphology suggests a temporal variability of the present-day axial morphology (Lewis, 1979).

In addition, a marked variation in fault-facing direction with the spreading rate has been observed on the flanks of mid-ocean ridges. Based on interpretation of SeaMARC II side-scan sonar data, Carbotte and Macdonald (1990 and 1994) demonstrated that on slow and intermediate rate spreading centres inward-facing faults predominate, whereas on fast spreading ridges, large numbers of both inward- and outward-facing faults are observed (Fig. 2.2). These authors suggested that this variation in fault-facing direction may reflect differences in the mean stress on potential fault

planes through the oceanic lithosphere, which might favour inward- versus outward-facing faults at different spreading rates (Fig. 2.2).

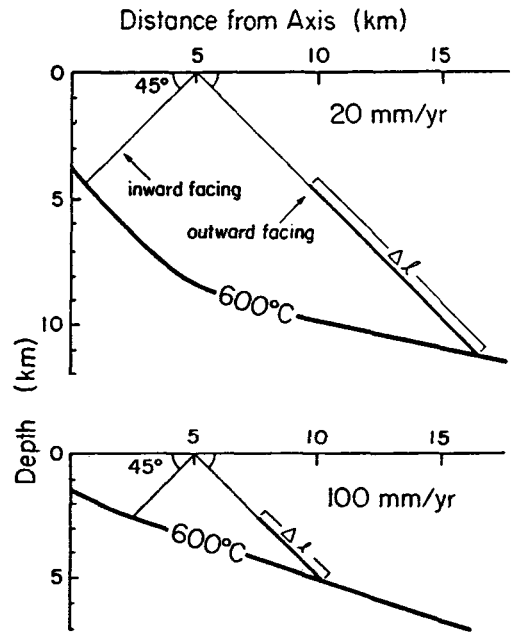

Fig. 2.2. Location of the theoretical 600°C isotherm within the oceanic lithosphere from the thermal model of Lin and Parmentier (1989) for spreading rates of 20 and 100 mm/yr. Figure illustrates relative difference in length (Δl) of outward- and inward-facing faults inclined at 45°, at slow and fast spreading rates. On the basis of this model, outward-facing fault dipping at 45° will be 2.6 times longer than inward-facing fault at a total opening rate of 20 mm/yr, but only 1.8 times longer at 100 mm/yr. Given these differences in fault length, greater mean stress on the longer fault plane will require greater shear stress to initiate failure, hence the predominance of inward-facing faults. At faster rates, however, as differences in length between inward- and outward-facing faults diminishes, so will relative differences in mean stress associated with failure; hence, both inward- and outward-facing faults are observed on fast spreading ridges, although there is still a predominance of inward-facing faults (Carbotte and Macdonald, 1990).

2.1.2. ALONG-AXIS MORPHOLOGY

When viewed in along-axis perspective, the axial depth and continuity of mid-ocean ridges is segmented at various scales (see section 2.2) by different types of discontinuities (Fig. 2.3). Two wavelength scales are distinguished (Macdonald et al., 1991):

- Long wavelength. The along-strike profile of the ridge is characterized by a broad swell with length in excess of 1000 km. The crests of these swells are determined by hot-spots, associated with anomalously shallow levels, and permanent magmatic budgets. One example is the Mid-Atlantic Ridge near Iceland and the Azores (Anderson et al., 1973).

• Short wavelength. The along-strike profile of the ridge is characterized by a short wavelength, between 20 to 100 km, independent of the spreading rate. The ridge system is partitioned into discrete segments by axial discontinuities showing distinctive structural signatures (Whitehead et al., 1984).

Independent of segment length, most segments have arched along-axis topographic profiles: the shallowest part is located approximately midway along the ridge segment, and depths increase towards the segment ends (Fig. 2.3). The extent to which axial depths increase from central high to segment ends ranges from tens to thousands of metres, with the largest changes in relief associated with segments along slow spreading ridges. At fast spreading ridges, the axial high increases steadily in cross-sectional area with increasing proximity to the elevated mid-sections of individual segments (Macdonald and Fox, 1988; Macdonald et al., 1992b; Scheirer and Macdonald, 1993).

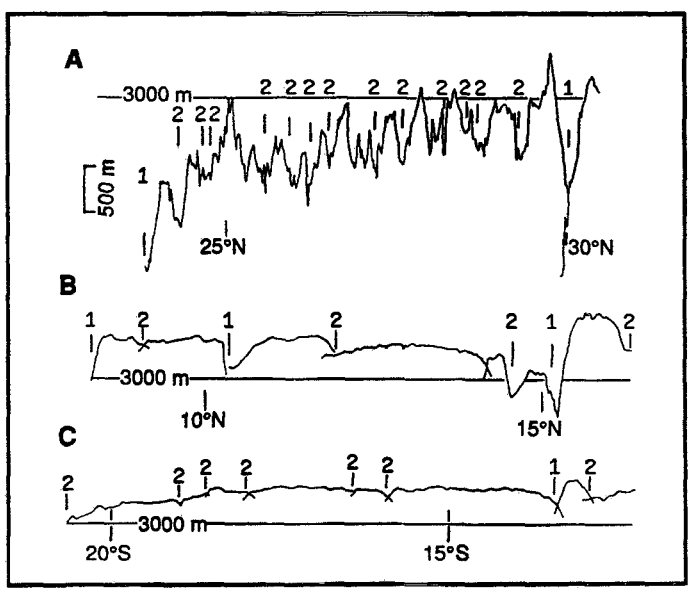

Fig. 2.3. Axial depth profiles for (A) slow spreading, (B) fast spreading, and (C) ultra-fast spreading ridges. Discontinuities of orders 1 and 2 occur at local depth maxima. The segments at fastest spreading rates are longer and have smoother axial depth profiles than those at slow spreading rates. Vertical exaggeration is 150 (Macdonald et al., 1991)

2.2. Segmentation and discontinuities

Since most of the observations support the concept of a hierarchy in the segmentation of mid-ocean ridges, a classification scheme from orders 1 to 4 has been proposed (Schouten et al., 1985; Langmuir et al., 1986; Macdonald and Fox, 1990; Macdonald et al., 1988 and 1991). Table 2.I represents these four-orders of segmentation as a function of some parameters like length and longevity of the ridge segments, and offset, age and off-axis trace of the discontinuities.

Segments	Order 1	Order 2	Order 3	Order 4
Length (km)	600 ± 300 (400 ± 200)	140 ± 90 (50 ± 30)	50 ± 30 $(15 \pm 10?)$	14 ± 18 $(7 \pm 5?)$
Longevity (yr)	$> 5 \times 10^6$	$< 5 \times 10^6$ $(0.5 - 10 \times 10^6)$	$\sim 10^4 - 10^2$ (?)	$\sim 10^2 - 10$ (?)
Discontinuities				
Offset (km)	> 30	2.0 - 30	0.5 -2.0	< 1
Age (yr)†	$> 0.5 \times 10^6$	$< 0.5 \times 10^6$	~ 0	~ 0
Off-axis trace	Fracture Zone	V-shaped discordant zone	None	None

Table 2.I. Characteristics of ridge segmentation (after Macdonald et al., 1991). Information is for fast spreading (> 60 mm/yr) ridges. If this differs from that for slow spreading ridges, it is marked in parentheses.
† The age of seafloor that is juxtaposed to the spreading axis at a discontinuity.

2.2.1. FIRST-ORDER

The first-order segmentation of the ridge is defined tectonically by major transform faults and large propagating rifts at both slow and fast spreading ridges (Fig. 2.4). We remind readers of the definition of these first-order discontinuities:

- Transform faults are large offsets of opposing ridge segments in terms of both distance (tens to hundreds of kilometres) and age (from one to tens of millions years) (Wilson, 1965). Transform faults represent a first-order discontinuity along which accretionary processes truncate and along which strike-slip strains are narrowly focused defining a

small circle about the pole of opening (Langmuir et al., 1986; Macdonald et al., 1988; Fox et al., 1991).

• Propagating rifts are non-transform ridge axis discontinuities that migrate up or down the axis with time. Propagating rift is the name given to a new spreading centre that grows at the expense of an old ridge when a change occurs in the spreading direction (Hey, 1977; Hey et al., 1980).

The segments limited by first-order discontinuities are very long (600 ± 300 km for fast spreading ridges, and 400 ± 200 for slow spreading ridges) and have longevity of more than 5 Ma (Table 2.I).

2.2.2. SECOND-ORDER

The second-order discontinuities represent an offset in the ridge characterized by morphotectonic patterns, both on- and off-axis, that are spatially complex and heterogeneous (Fox et al., 1991). Large overlapping spreading centres* on fast spreading ridges (Macdonald and Fox, 1983; Lonsdale, 1983), and oblique, *en echelon* offsets along slow spreading ridges (Rona and Gray, 1980; Sempere et al., 1990) are examples of second-order discontinuities (Fig. 2.4).

*We recall that:

• Overlapping spreading centres (OSC's) are non-rigid discontinuities where the spreading centre of a ridge is offset by a distance of 0.5 to 10 km, with the two ridge portions overlapping by about three times the offset (Macdonald and Fox, 1983).

Segments limited by second-order discontinuities are 140 ± 90 km long for fast spreading ridges and 50 ± 30 km for the slow ridges. The segment longevity is 0.5 Ma to 5 and 10 Ma, for fast and slow spreading ridges, respectively (Table 2.I). Second-order discontinuities leave an off-axis trace but this does not create alignments parallel to flow lines. They are considered a non-rigid offset and the on- and off-axis expressions of these features are called discordant zones (Fox et al., 1991). Second-order segmentation patterns may migrate along-strike, leaving a V-shaped wake of abandoned ridge tips and basins; or they may remain approximately in the same place, but oscillate back and forth along the ridge (Lonsdale, 1985; Macdonald et al., 1987; Wilson, 1990).

2.2.3. THIRD-ORDER

The third-order segmentation is characterised by small offset overlapping spreading centres on fast spreading ridges (Macdonald et al., 1984 and 1988) and inter-volcano gaps on slow spreading ridges (Fig. 2.4). Characteristic segment length for third-order segments ranges between 50 ± 30 km for the fast spreading ridges and 15 ± 10 km for the slow ridges. The longevity of the segment varies between 100 and 10,000 years (Table 2.I). The magnitude of a third-order offset is relatively small (< 2 km), and they leave no off-axis trace indicating that they are not long-lived features (Fox et al., 1991).

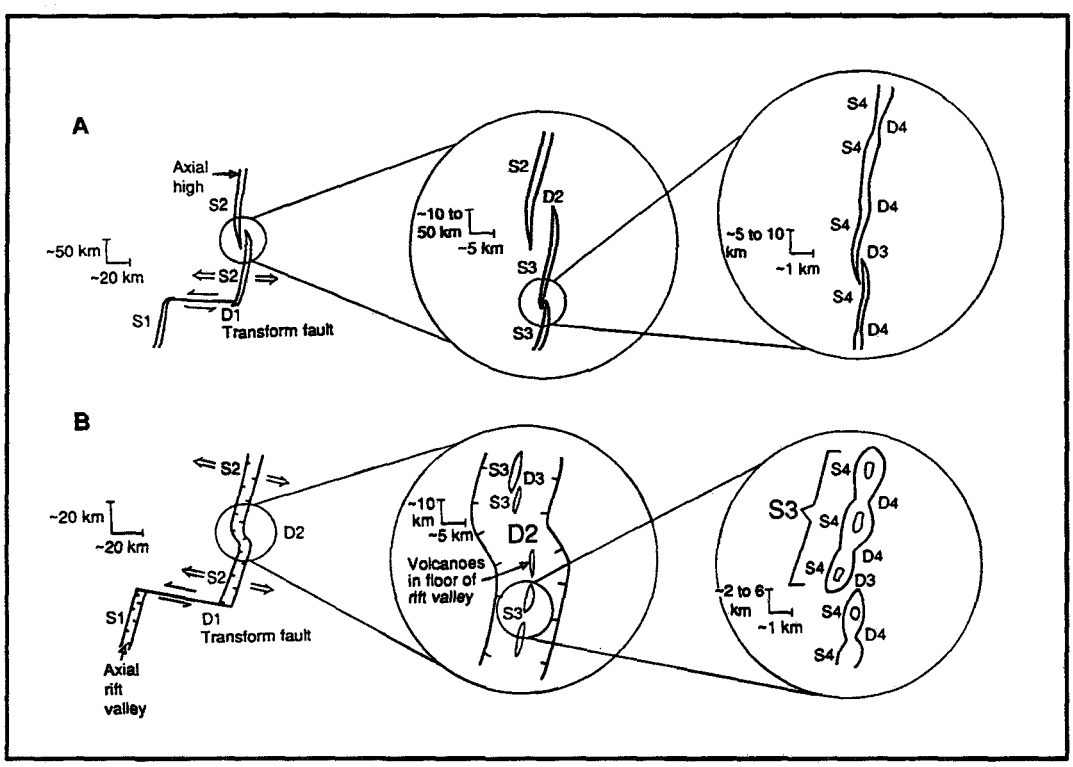

Fig. 2.4. A proposed hierarchy of ridge axis discontinuities of orders 1 through 4 for fast (A) and slow (B) spreading centres. S1, S2, S3, and S4 are ridge segments of order 1, 2, 3, 4, and D1, D2, D3, and D4 are ridge axis discontinuities of order 1, 2, 3, 4, respectively. Thus a segment is first-order if it is bounded at both ends by first-order discontinuities, and second-, third-, or fourth-order if it is bounded at one (or both) end(s) by second-, third-, or fourth-order discontinuities. Intermediate rate spreading centres (40-90 mm/yr) tend to have the characteristics of slow spreading segments and discontinuities when they are magmatically starved, and those of fast spreading centres when they are magmatically robust (Macdonald et al., 1991).

2.2.4. FOURTH-ORDER

Fourth-order discontinuities do not represent termination of ridge axis structures, rather they represent changes in the character of axial structures. They include features like DEViations from Axial Linearity (DEVAL's) resulting in slight bends or lateral offsets of the axis of less than 1 km on fast

spreading ridges (Langmuir et al., 1986), and intra-volcano gaps on slow spreading ridges (Macdonald et al., 1988) (Fig. 2.4). The fourth-order segments are very short, between 5 and 30 km long, and very short lived, between 1 to 100 years (Table 2.I). High resolution imaging and sampling of the ridge axis in some areas has defined morphological and geochemical changes along-strike that suggest that this finer, fourth-order scale of segmentation is superimposed on the long segmentation discussed above (Langmuir et al., 1986).

This hierarchy of segmentation may really be a continuum. It has been established, for example, that fourth-order segments and discontinuities can grow to become third-, second-, and even first-order discontinuities and vice-versa at both slow and fast spreading centres (Macdonald et al., 1991).

2.3. Deep structure

The tectonic and morphological segmentation of the ridges presented above is also accompanied by a deep segmentation evidenced by gravity data, and especially marked in slow spreading ridges (Lin and Phipps Morgan, 1992). In contrast, gravity studies along intermediate and fast spreading ridges, such as the Cocos-Nazca Ridge or East Pacific Rise, do not show significant variations of the along-axis deep gravity structure (Madsen et al., 1990; Lin and Phipps Morgan, 1992). Thus, along-axis mantle Bouguer anomaly gradients at the Mid-Atlantic Ridge vary from 0.3 to 1.2 mGal/km, whereas at the East Pacific Rise they vary only from 0.1 to 0.2 mGal/km. In addition the amplitude of the mantle Bouguer anomaly is also greater along the Mid-Atlantic Ridge (30-60 mGal) than in the East Pacific Rise (10-20 mGal) (Lin and Phipps Morgan, 1992).

Gravity observations collected along the Mid-Atlantic Ridge provide constraints on the characteristics of segmentation, and suggest that magmatic accretion is focused near segment centres (Kuo and Forsyth, 1988; Lin et al., 1990; Morris and Detrick, 1991). The Mantle Bouguer anomalies (for definition see section 1.2.3), show circular gravity lows centred near the midpoints of morphologically defined slow spreading segments. These concentric negative anomalies are usually named "bull's eye" anomalies. The interpretation of these gravity anomalies is that magmatic accretion is focused near the centre of a segment and that the vigour of magmatic activity at the midpoint of a segment increases with segment length (Lin et al., 1990).

Two specific hypotheses have been proposed to interpret the mantle Bouguer anomalies (Lin et al., 1990):

- Along-axis variations in crustal thickness. Since the mantle Bouguer correction is calculated for a fixed crustal thickness, any departure from this structure will appear as an anomaly. Consequently, the mantle Bouguer anomaly pattern could arise from a thick crust near the centre of a ridge segment and a thinner crust near the segment ends.

- Variations in upper-mantle density structure. In this hypothesis the anomalies are attributed to a buoyancy-driven mantle upwelling.

Recent 3-D numerical modelling (Phipps Morgan and Forsyth, 1988; Parmentier and Phipps Morgan, 1990) suggested that mantle contributions to the gravity can be significant only near large offset transforms. At the more commonly observed non-transform ridge offsets, gravity anomalies will mainly reflect variations in crustal thickness (Lin and Phipps Morgan, 1992).

2.4. Crustal accretion and mantle upwelling

Analysis of the along-axis gravity data indicates that the amplitude of the along-axis crustal thickness variation decreases when the spreading rate increases (Lin and Phipps Morgan, 1992). The authors suggested that the spreading rate crustal accretion style may originate in the mantle. Two contrasting types of crustal accretion pattern can be distinguished depending on the spreading rate (Lin and Phipps Morgan, 1992) (Fig. 2.5).

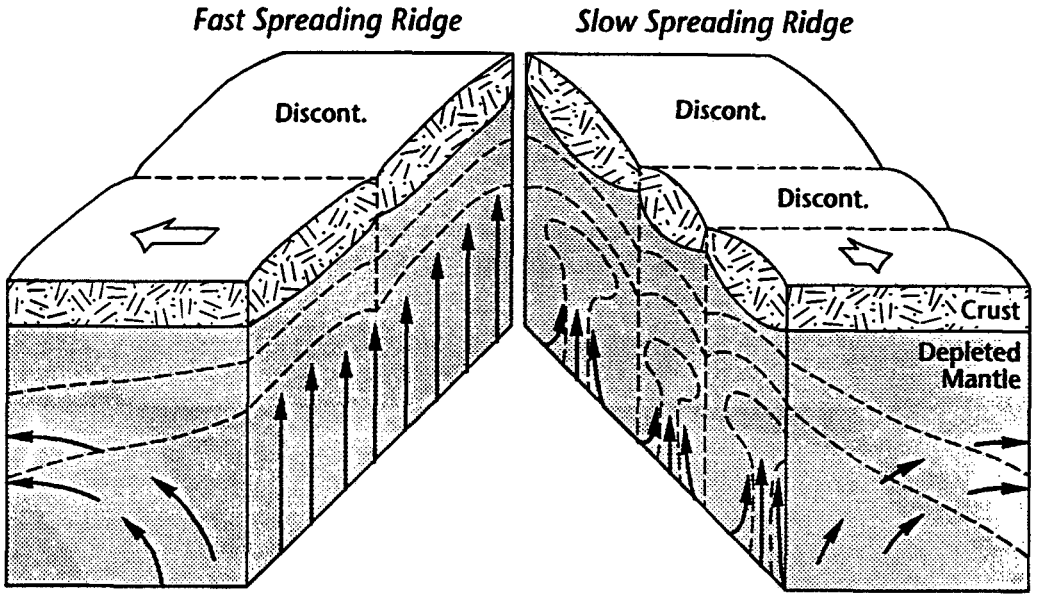

Fig. 2.5. A spreading-rate dependent model of crustal accretion and mantle upwelling that is consistent with the gravity and bathymetry observed on ocean ridges. Solid arrows show mantle flow directions. Open arrows show plate motion vectors. Dashed lines in the mantle show isotherms. Such contrasting crustal accretion patterns may result from a dominantly plume-like upwelling and melting beneath a slow spreading ridge and sheet-like mantle upwelling and melting beneath a fast spreading ridge (Lin and Phipps Morgan, 1992).

- **Sheet-like accretion.** Gravity analyses indicate that the crustal density structure is relative uniform beneath a fast spreading ridge, and a constant crustal thickness is expected. In consequence, crustal accretion is more sheet-like (2-D) (Fig. 2.5, left). However, smaller amplitude 3-D upwellings may still occur at a fast spreading ridges, but their effects on crustal thickness variations will be reduced by along-axis melt flows along a persistent magma chamber.

• **Plume-like accretion.** Gravity analyses over slow spreading ridges show a variable crustal density structure, suggesting strong variations in along-axis crustal thickness, even if the segment is bounded by non-transform offsets. Finite-amplitude mantle upwelling is intrinsically plume-like (3-D) beneath a slow spreading ridge (Fig. 2.5, right).

Chapter 3

GENERAL ASPECTS OF BACKARC BASINS

The last ten years have seen fundamental changes in the understanding of tectonics, volcanism, hydrothermalism and sedimentation in backarc basins (Taylor, 1995). This results from exploration and detailed studies using some of the tools described in Chapter 1, as well as other methods, such as multi-channel seismics, remotely operated vehicles, and deep ocean drilling.

As explained in the Foreword, this Thesis is based on the study of three extensional zones (see Part III) located within the North Fiji and the Bransfield basins, both backarc basins. Thus, this chapter is devoted to a synthesis of the main characteristics of backarc basins, from their definition and origin to the most recent models of backarc opening and evolution. Other dynamic processes occurring in this particular setting, such as backarc hydrothermalism, are also presented at the end of the chapter.

3.1. Definition and characteristics

3.1.1. MARGINAL AND BACKARC BASINS

The terms "marginal basin" and "backarc basin" are often mixed up or not used appropriately. Karig (1971) defined marginal basins as semi-isolated basins lying behind the volcanic chains of island arc systems, taking the Western Pacific basins as typical. This definition is based primarily on the tectonic position "back-of-the-arc". Subsequent studies (e.g. Weissel and Watts, 1979) have shown that not all the marginal basins are located in a backarc position, and Karig's (1971) definition was too restrictive. Taylor and Karner (1983) used the term "marginal basin" following Menard's (1967) definition as a small ocean basin, but they added the condition that the basin must have an oceanic crust. The same authors (Taylor and Karner, 1983) defined the backarc basins as marginal basins located behind active or inactive trench systems and having an origin related to subduction

processes. In this study we use the term "backarc" as defined by Taylor and Karner (1983).

Backarc basins are situated above or beyond the Wadati-Benioff seismic zones that trace the descending oceanic lithosphere from submarine trenches into the mantle (Taylor, 1995). Not all subduction zones have associated active arc and/or backarc volcanism, sometimes because the above wedge of mantle is missing and/or because there is compressional coupling between the subducting and the overriding plates (Taylor, 1995).

The formation of backarc basins involves the splitting of volcanic arcs, initially forming rifts (elongated depressions bounded by faults) and subsequently backarc spreading centres. They may form within continental or intraoceanic arcs (Taylor, 1995). Thus, the two basins studied in this work, North Fiji (intraoceanic) and Bransfield (intracontinental), may both be considered as backarc basins. Active backarc basins occur in the Western Pacific, Caribbean and Scotia Sea regions.

3.1.2. GEOPHYSICAL CHARACTERISTICS

In this section we summarize some geophysical aspects characterizing the backarc basins, such as crustal structure, seismic wave attenuation, heat flow and magnetic anomalies.

Crustal structure

Early seismic refraction studies suggested that backarc basins may have a thin oceanic crust (Karig, 1971; Sclater et al., 1976). Subsequent studies, however, showed a range of velocity-thickness crustal sections indistinguishable from the range of major oceanic sections. Thus, LaTraille and Hussong (1980) with data from the Mariana Trough, reported crustal thicknesses of 4-5 km, whereas results of Bibee et al. (1980) in the same area indicated a crustal thickness of 6.6 km.

Seismic wave attenuation

Seismic wave attenuation may be a useful measurement of the temperature regime and the degree of partial melting under backarc basins. Differences in seismic amplitude are quantitatively described in terms of the Q-factor, the inverse of the specific attenuation factor. A zone of very high attenuation (extremely low Q of about 50) has been defined in the uppermost mantle above the downgoing slab in a region about 300 km wide

stretching between the active island arc (Tonga Islands) and backarc ridge (Lau Ridge) (Barazangi and Isacks, 1971; Oliver et al., 1973; Barazangi et al., 1975) (Fig. 3.1). It implies that the mantle beneath the backarc basin (Lau Basin) is much weaker than elsewhere or that the lithosphere is considerably thinner (Barazangi and Isacks, 1971).

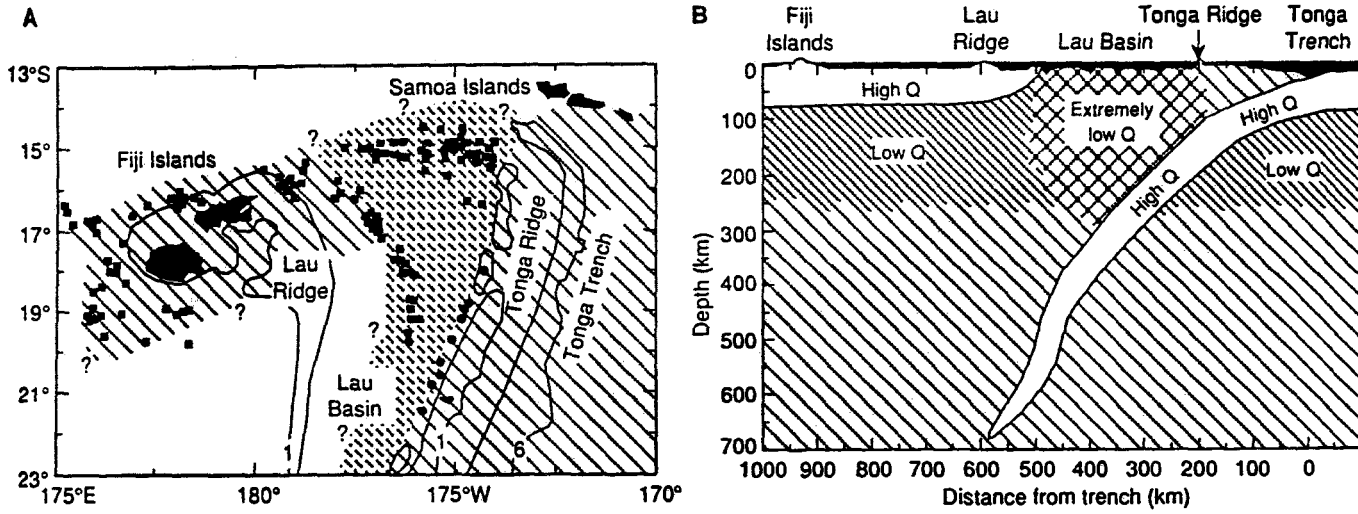

Fig. 3.1. Map (A) and cross-section (B) of the North Fiji Basin-Lau Basin-Tonga Trench region showing inferred and extrapolated extent of the region of high and low attenuation in the uppermost mantle. (A) Historically active volcanoes of the Tonga Arc are shown as solid circles. Loci of shallow earthquakes are shown as solid squares. Depth contours are at 1 and 6 km. (B) Note that the Lau Basin is underlain by mantle with extremely low Q (very high seismic attenuation) (Barazangi and Isacks, 1971).

Heat flow

Karig (1971) classified the marginal basins according to their heat flow. He distinguishes three different types: active basins with high heat flow, inactive basins with high heat flow, and inactive basins with normal heat flow. Later in 1977, Toksöz and Bird reclassified the backarc basins by their heat flow value as well as their stage of evolution, and considered four different types of backarcs.

- Undeveloped basins, those that have not reached the spreading stage. They show low heat flow values.

- Active basins, those showing active spreading parallel to island arcs, and characterized by high heat flow.

- Mature basins, those that have undergone several spreading phases. They are characterized by very high heat flow.

- Inactive basins, those old basins that have long passed the spreading stage. They show normal oceanic heat flow.

The high heat flow measured in active and mature backarc basins (Watanabe et al., 1977) correlates with the region of very low Q-factor in the upper mantle (Fig. 3.1) and supports the interpretation of this area as a zone of partial melting (Kearey and Vine, 1990).

Magnetic anomalies

Many authors (Sclater, 1972; Karig, 1974; Hawkins, 1976; Uyeda, 1977) suggested that the mode of spreading in backarc basins may be substantially different from that in major ocean basins. This assumption was mainly based on the less developed (low intensity and difficult identification) magnetic lineations in backarc basins. As an explanation for that, Lawver and Hawkins (1978) proposed a model of diffuse backarc spreading, in which accretion occurs simultaneously at a number of spreading ridges.

However, symmetric magnetic lineations correlatable with the magnetic reversal time scale are found in several active and inactive backarc spreading centres, such as Manus, Lau, North Fiji, and East Scotia (Taylor and Karner, 1983). Only the basins formed near the magnetic equator by N-S spreading do not show recognizable magnetic pattern. Thus, Bibee et al. (1980) and Weissel (1981) proposed that backarc basin crustal accretion takes place in a narrow zone by processes similar to those of mid-ocean ridges. In agreement with the last authors, Taylor and Karner (1983) suggested that the irregular but correlatable magnetic pattern of some backarc basins is largely a function of the scale rather than a function of fundamental differences in spreading processes.

3.2. Origin

The mechanism of backarc origin has been the matter of much debate, and since the 1970's, several models have been proposed. Taylor and Karner (1983) and Tatsumi et al. (1990) reviewed the main hypotheses to explain backarc basins.

3.2.1. DIAPIRISM IN THE MANTLE WEDGE

This model proposes that extension in backarc basins is caused by injection of hot low-density mantle diapirs that rise buoyantly from sub-lithospheric depth (Karig, 1971) (Fig. 3.2a). The source of this diapir may be the magmas mobilized from the top of the descending slab by shear strain heating. A variation of the initial model was presented by Karig (1974), in which dewatering of the slab would cause partial melting and diapiric rise of the overlying mantle.

The fundamental problem with this model is that they cannot explain the temporal and spatial distribution of backarc basins and their spreading centres (Taylor and Karner, 1983). In addition, the geophysical evidence presented to support this hypothesis, such as high heat flow, seismic attenuation, and low density mantle (Karig, 1971; 1974), is indicative of spreading, but not necessarily of mantle diapirism (Taylor and Karner, 1983).

3.2.2. INDUCED ASTHENOSPHERIC CONVECTION

Another mechanism is the convective motion induced in the asthenosphere by the subducting lithosphere (Andrews and Sleep, 1974; Toksöz and Bird, 1977; Toksöz and Hsui, 1978). The convective current induced in the asthenospheric wedge above the slab delivers hot mantle material to the base of the plate behind island arcs (Fig. 3.2b). The combination of material upwelling, heating of the lithosphere and flow-induced tension initiates spreading and the formation of a backarc basin (Toksöz and Hsui, 1978).

This model also presents major disagreements, such as the lack of explanation for backarc spatial distribution or why backarc basins are absent in some arc-trench systems, and its unrealistic prediction about the emplacement of backarc spreading centres (Taylor and Karner, 1983).

3.2.3. INTERACTION OF MAJOR PLATES

Problems with the above "local" models of backarc formation have prompted alternative models in which backarc extension is considered a consequence of the global interaction of major plates (Taylor and Karner, 1983) (Fig. 3.2c). All these models (Molnar and Atwater, 1978; Uyeda and Kanamori, 1979; Dewey, 1980) emphasize the role of relative plate motion between the over- and underriding plates in the formation of extension within the overriding plate (Tatsumi et al., 1990).

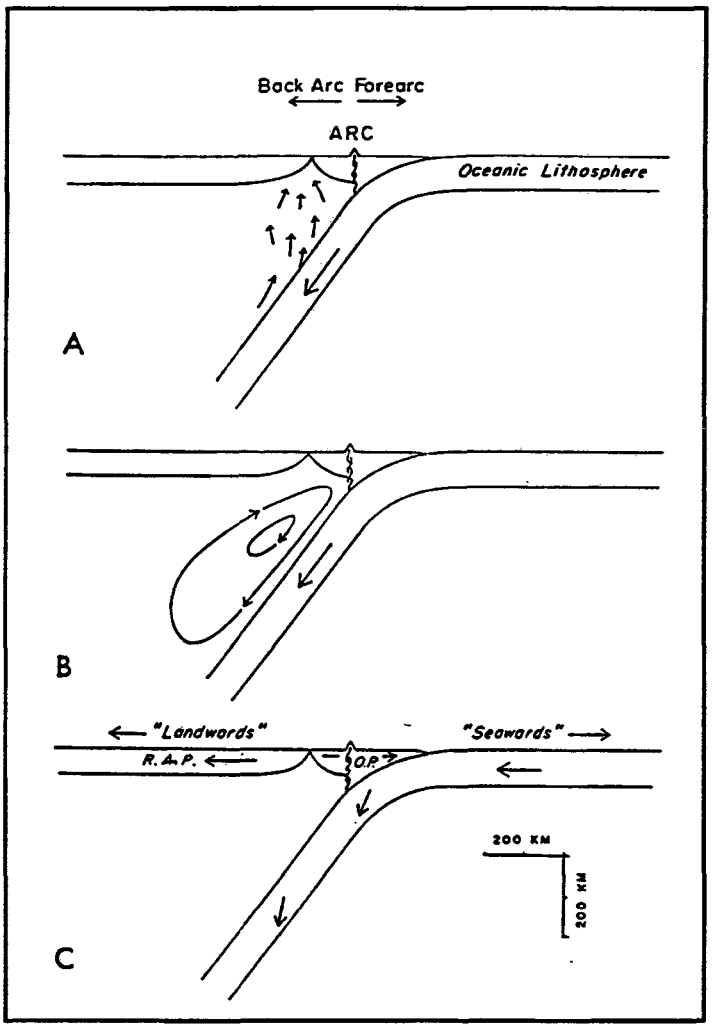

Fig. 3.2. Hypothetical models of backarc basin formation. a)Active diapirism resulting from heat and/or water generated along the Benioff zone (Karig, 1971; Karig, 1974). b) Convective flow induced in the mantle by the subducting lithosphere (Andrews and Sleep, 1974; Toksöz and Bird, 1977; Toksöz and Hsui, 1978). c) By-product of major plate interactions on a global scale (Molnar and Atwater, 1978; Dewey, 1980). OP: Overriding plate, RAP: Remnant plate (Taylor et al., 1983).

Two models can be distinguished in terms of the role of the subducted slab (Tatsumi et al., 1990).

Anchored slab model

This model, based on Uyeda and Kanamori (1979), simply assumes that the subducted slab is fixed (or anchored) relative to the deeper mantle, and suggests that the landward motion of the overriding plate produces the backarc extension. This model cannot be applied to some of the backarc systems in which the overriding plate migrates trenchwards, as in the North Fiji Basin (Taylor and Karner, 1983).

Sinking slab model

Molnar and Atwater (1978) suggested that the old, cold lithosphere sinks into the asthenosphere under its own weight causing the trench to migrate seaward. They proposed that the density of oceanic lithosphere increases with age and inferred that trenches subducting Mesozoic lithosphere should move seaward faster than trenches subducting relatively younger lithosphere. Thus, they proposed that backarc spreading may result if the velocity of seaward trench migration exceeds the convergence rate. One problem of this model is that there is no clear correlation between seaward motion speed and the age of the subducting lithosphere (Carlson and Melia, 1984).

In 1980, Dewey proposed that backarc origin is mainly controlled by the "absolute" motion of the overriding plate and by the migration of the hinge of the downgoing plate. Thus, hinge migration, named rollback, is fundamental to the understanding of the geodynamics of backarc regions (Dewey, 1980). Carlson and Melia (1984) estimated the rate of hinge migration from the rate of backarc extension and the motion of the overriding plate. Rates of rollback range from values of 100 mm/yr at the Tonga Arc, 50-70 mm/yr at the South Sandwich Arc, and zero at the New Hebrides Arc, and negative values (advancing trench) at the Izu-Bonin Trench.

Based on numerical analysis of subducting slab stability, Dvorkin et al. (1993) suggested a new model for the origin of backarc basins. They show that a horizontally wide slab is always stable in its inclined position. This stability is due to the lifting force produced by the negative pressure (suction) into the corner between the slab and the overriding plate. Dvorkin et al. (1993) suggested that there is a common feature associated to all backarc basins: the narrow width of their associated subducting slabs. In the case of a narrow slab, sideways asthenospheric flow into the slab/overriding plate

corner eliminates the suction force, which results in the rapid sinking of the slab. This sinking causes a fast migration of the slab hinge and the associated arc (rollback) leading to a rapid opening of a backarc basin (Fig. 3.3). They show that the hinge of an unstable narrow slab can migrate quite rapidly at rates of 100-200 km per million years.

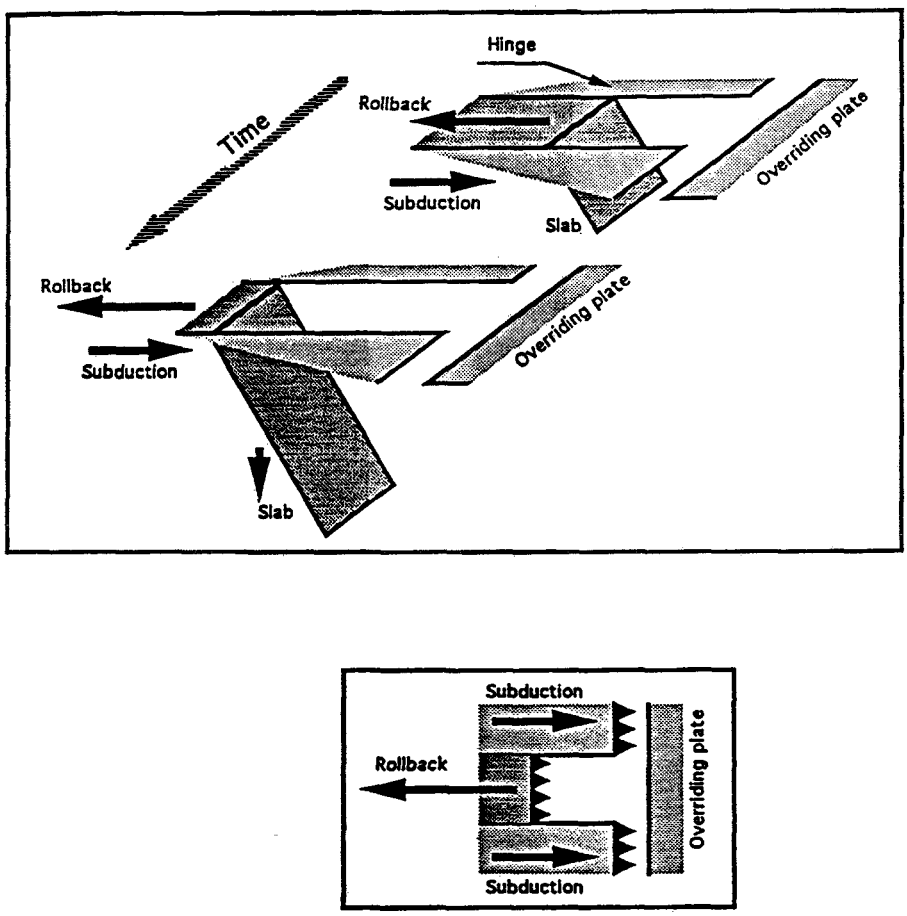

Fig. 3.3. A scenario of backarc rollback resulting from the instability of a narrow slab. Up: The slab sinks vertically, which results in the hinge rollback away from the overriding plate. Down: Map view of the backarc opening (Dvorkin et al., 1993).

3.3. Modes of backarc evolution

Two modes of backarc opening have been suggested by Tamaki (1985) from a comparative study of the Bonin Arc and the Japan Sea. These two modes are: single-rift type and multi-rift type.

Single-rift type

The single-rift type (Fig. 3.4) is based on the study of the rifting of the Bonin Arc. The volcanism is concentrated on the volcanic front where an active volcanic ridge is formed because of the high dip angle of the subducting slab (60°) (Isacks and Barazangi, 1977). The rifts are maturing and may eventually join together to make a single-rift system parallel to the trench.

The rifting features of the Bonin Arc demonstrate that when the arc is extensional the break-up of the arc occurs near the volcanic zone. This is basically the model of Dewey (1980), which is illustrated in Figure 3.4. Dewey (1980) consider three plates for modelling the tectonics of island arcs: backarc plate, fore-arc sliver, and subducting oceanic plate (Fig. 3.4, stage 1). The divergent movement between the backarc and the fore-arc sliver generates rifts along their boundary, which is the arc volcanic zone (Fig. 3.4, stage 2). In the case of the Bonin Arc, a single rift system is generated along its active volcanic chain and arranged in a single line. Further divergent tectonics may cause a new backarc basin and a linear remnant arc (Fig. 3.4, stage 3). The spreading system developed from the single-rift system usually causes a single lineated remnant arc, such as the Kyushu-Palau Ridge and West Mariana Ridge in the Philippine Sea (Tamaki, 1985).

Multi-rift type

This second type of backarc opening is based on the example of the now inactive Japan Sea. This basin is characterized by the presence of many submarine volcanoes and fragments of rifted continental crust along the margins of the basin.

In the multi-rift case, many parallel rifts appear to have been formed in a broad volcanic zone. This reflects a low dip angle of the subducting slab (Fig. 3.5, stage 1). Extension across the broad zone caused many rifts rather than a single rift system (Fig. 3.5, stage 2). Some of the rifts failed and became

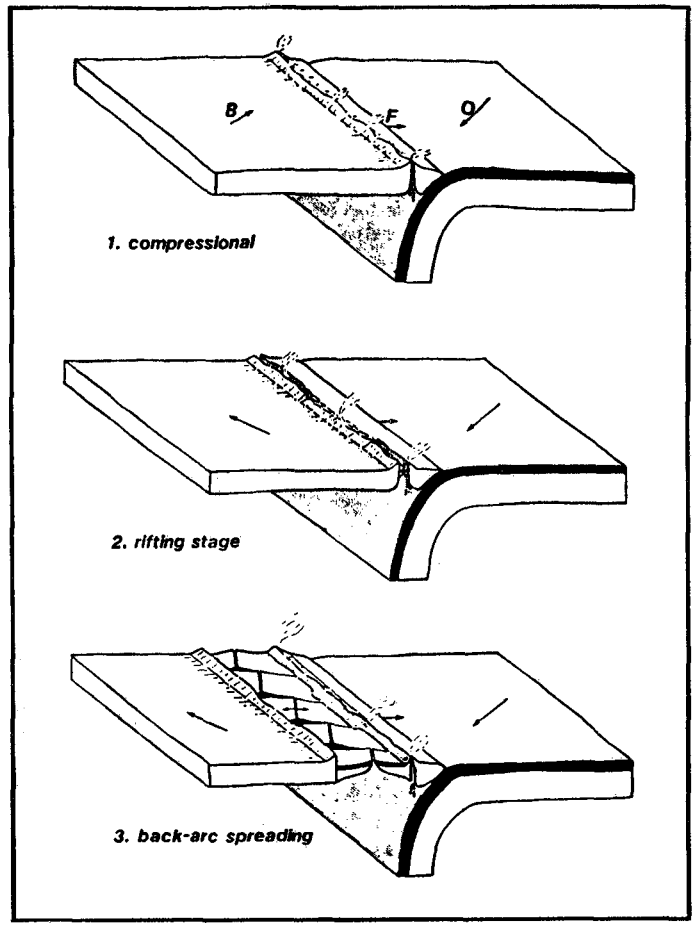

Fig. 3.4. Model of stages of single-rift backarc spreading. Arrows show motion vector of each plate. O: oceanic plate, F: forearc sliver, B: backarc plate. Motion of forearc sliver is coupled with that of trench hinge line. Rifting stage shows present-day evolution of the Bonin Arc (Tamaki, 1985).

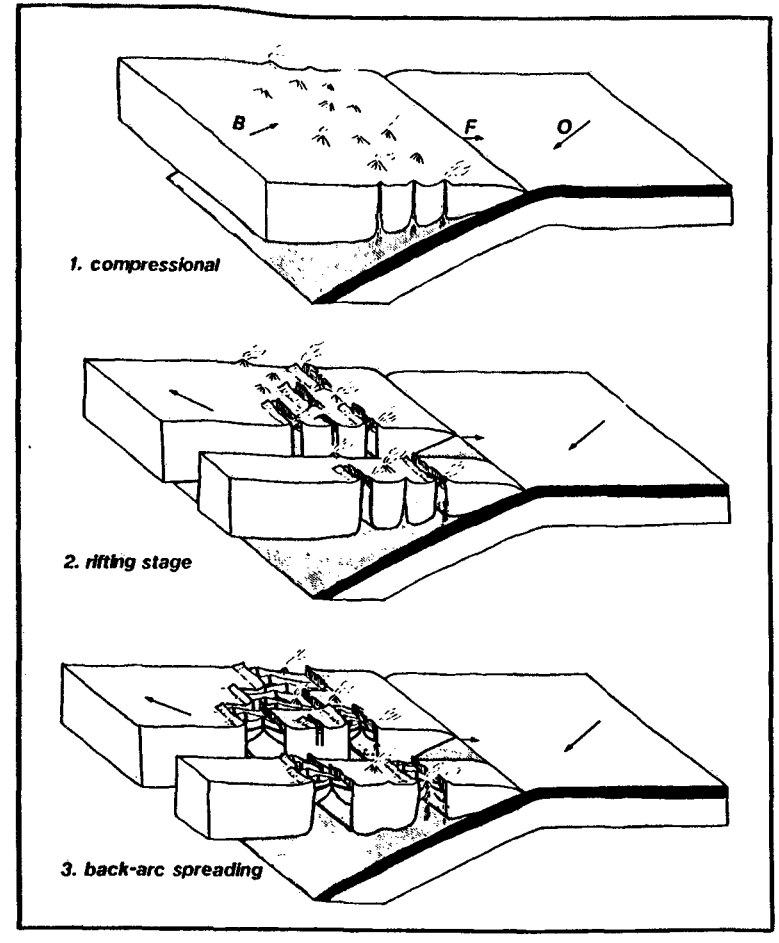

Fig. 3.5. Model of stages of multi-rift backarc spreading. O: oceanic plate, F: forearc sliver, B: backarc plate. Present-day evolution of Japan Sea corresponds to cessation of backarc spreading shown in stage 3 (Tamaki, 1985).

remnant rifts, and others joined together and developed into spreading centres of the backarc basin (Fig. 3.5, stage 3).

In summary, there are fundamental geological variations between the two types. In the single-rift type, the remnant arc is single and continuous, seamounts are rare, the crust is purely oceanic, and aborted rifts are rare. In contrast, in the multi-rift type the remnant arc is segmented, seamounts are abundant, the crust is overprinted by island-arc volcanism, and aborted rifts are common features. The two types are end-members, and there are probably many gradual variations between them (Tamaki, 1985).

Recent studies, mainly based on results obtained from the Ocean Drilling Program (ODP) in backarc basins (e.g. Lau Basin, Hawkins, 1994), are revealing greater importance than previously recognized of the role of rift stage in the evolution of backarc extension. Thus, based on data from the northern Mariana Trough, Martinez et al. (1995) proposed the following four stages model of evolution of backarc rifting (Fig. 3.6):

- A) Initial rifting starts near the arc volcanic line (Fig. 3.6a), the locus of arc volcanism characteristic of subduction zones. The arc volcanic line has been proposed as the most favourable location for rifting to initiate, based on rheological and physical considerations (Steckler and ten Brink, 1986).

- B) Extension in the overriding plate, caused by the rollback of the subduction zone hinge, can generate an asymmetric rifting mechanism since the arc volcanic line will remain on the subducting slab side of the rift. The volcano-tectonic zone migrates seaward following the weak zone above the locus of arc magma generation and rift into the frontal arc crust. At this stage, a large proportion of the magmas which erupt within the volcano-tectonic zone have an arc composition. However, because the arc lithosphere is thinning, there may also be a component of extensionally induced advection of the underlying mantle, which may generate some MORB-like melts (Fig. 3.6b).

- C) The volcano-tectonic zone separates from the arc line, in a process named "localization". This process begins to establish a well defined plate boundary within the backarc, allowing the forearc platelet to migrate passively with the seaward rollback of the subducting plate and

allowing arc magmatism to rebuild the arc volcanoes. Separation of arc magma source from the zone of concentrated extension may lead to a less magmatic phase forming deep tectonic grabens (Fig. 3.6c).

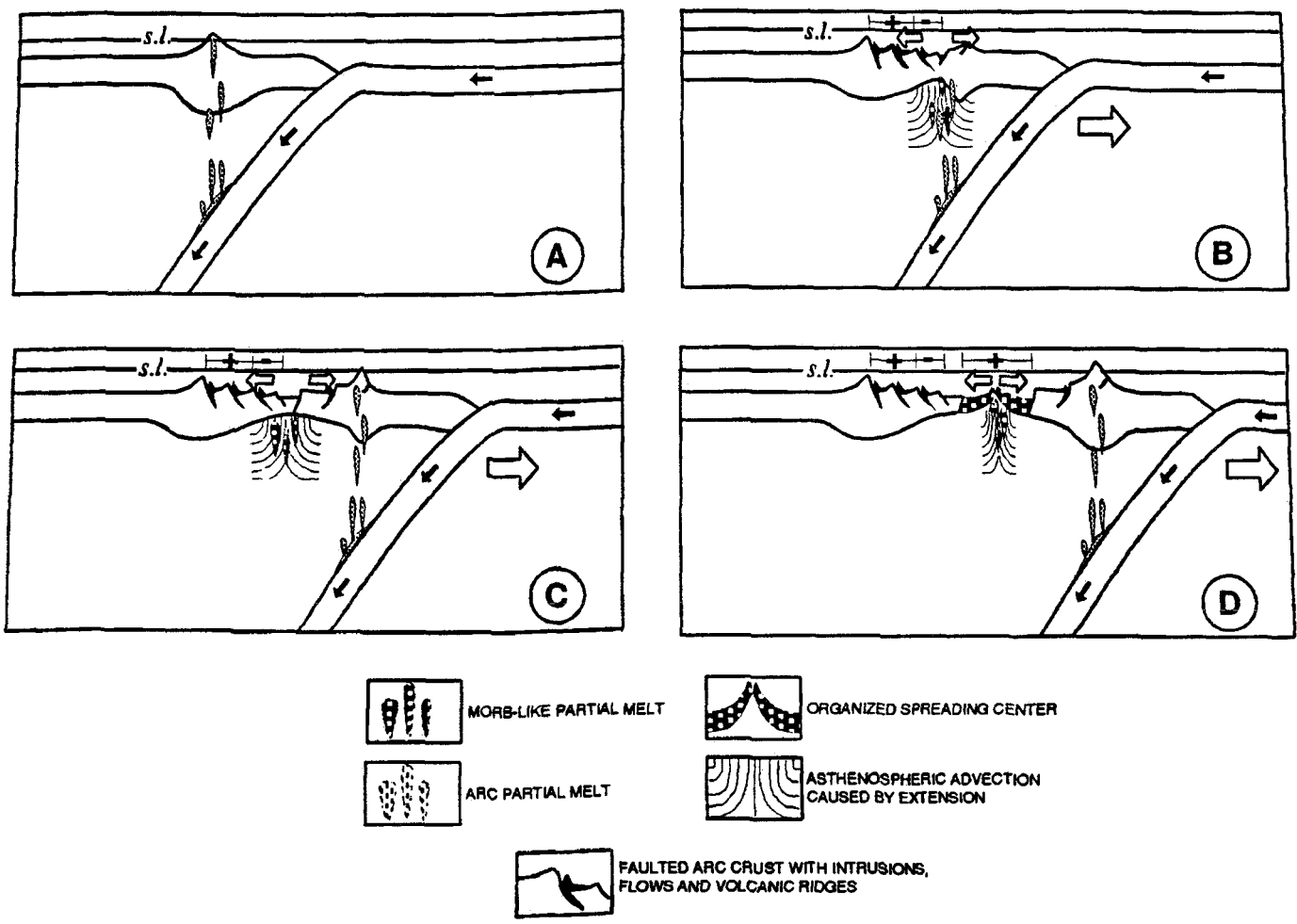

Fig. 3.6. Sketch illustrating the tectonic evolution of a backarc basin with increasing amounts of extension. a) Initial configuration of the arc-slab system prior to extension. Partial melt of arc composition released from the subducting slab is shown as rising diapirs coloured in light grey. Solid arrows: motion of the descending slab; s.l.: sea level. b) Extension of the overriding plate is caused by the rollback of the subduction zone hinge (large outlined arrow). Region of concentrated extension is indicated by the diverging outlined arrows. Both arc and MORB-like melts may intrude and erupt within the rifting backarc basin. c) The zone of focused extension becomes weaker than the volcanic arc and "localizes", producing the separation of the arc magma source from the zone of concentrated extension. d) Organized seafloor spreading begins and accommodates extension by accreting new material from MORB-like melts (Martinez et al., 1995).

• D) Continued rifting results in an increasingly focused zone of extension creating greater upward advection and volumes of partial melt of underlying mantle. Organized seafloor spreading begins and accommodates all of the subsequent extension by accreting new

material from MORB-like melts within a narrow boundary zone (Fig. 3.6d).

Tamaki (1995) after the ODP drilling results in the Japan Sea (e.g. Jolivet and Tamaki, 1992) suggested that part of this basin was probably formed by rifted and extended continental crust instead of true oceanic crust formed by seafloor spreading (Tamaki, 1985).

3.4. Hydrothermal activity

Five or six years after the discovery of hydrothermal mineralization at the East Pacific Rise (Francheteau et al., 1979) reports of similar seafloor hydrothermal activity were noted in the Western Pacific (Both et al., 1986; Hawkins and Helu, 1986; Craig et al., 1987a,b). Continued exploration showed that the Western Pacific region has as much seafloor hydrothermal mineralization associated with it as with mid-ocean ridges. However, mineralization in the Western Pacific appears to have wider variations in tectonic setting, mode of occurrence, and chemistry of fluids and deposits than those of mid-ocean ridges (Ishibashi and Urabe, 1995).

About 75% of backarc basins worldwide occur in the Western Pacific region, and six of them have active spreading centres: Mariana Trough, Andaman Sea, Manus Basin, Woodlark Basin, North Fiji Basin, and Lau-Havre Basin (Tamaki and Honza, 1992). It is reasonable to expect vigorous hydrothermal activity at most of the active volcanic centres in this systems. Thus, one sixth of the known sites of seafloor hydrothermal activity has been discovered in backarc basins in the Western Pacific (Taylor, 1995). In recent years, several cruises with deep diving scientific submersibles (Shinkai 2000 and 6500, Nautile, Alvin, and Mir) have contributed to successive discoveries of hydrothermal occurrences (Ishibashi and Urabe, 1995).

Ishibashi and Urabe (1995) reviewed some major sites of hydrothermal mineralization associated with three major tectonic settings: backarc spreading centre, backarc rift, and volcanic front. Examples of these hydrothermal occurrences found in backarc spreading centres and rifts as well as their location, water depth, geologic structure, water temperature of vents, and type of hydrothermal deposit are represented in Table 3.I.

Site name	Location	Depth (m)	Geologic structure	Water Temp. (°C)	Type of deposit
Backarc spreading centre					
Station 4	North Fiji (Central Ridge)	1980	Split axial high near a triple junction	290	Anhydrite chimneys on a sulfide mound
Station 14	North Fiji (Central Ridge)	2720	Collapsed lava lake on a flat rectangular dome	5.2	10 m high extinct sulfide chimneys
Vienna Woods	Central Manus	2500	Axial rift graben covered by pillow lavas	?	20 m high active sulfide chimneys
Pacmanus Field	Eastern Manus	1650	Top of a ridge composed of dacite flows	?	4 m high active sulfide chimney
Vai Lili	Lau (Valu Fa Ridge)	1707 - 1764	Normal fault along a ridge crest	400	17 m high black-white smokers and sulfide ores
Hine Hina	Lau (Valu Fa Ridge)	1832 - 1887	Dome of highly vesiculated and brecciated andesite	40	Fossil sulfide covered by Mn crust
White Church	Lau (Valu Fa Ridge)	1946 - 1966	Top and flanks of a ridge formed by pillow lavas	-	10-15 m high inactive barite-sulfide chimney
Franklin Seamount	Western Woodlark	2143 - 2366	Propagating rift west tip composed of basaltic andesite	20 - 30	Inactive barite silica chimneys, oxide mounds
Alice Spring Field	Central Mariana	3600 - 3700	Flank of an axial split volcano of basaltic andesite	287	1 m high active barite sulfate chimneys
Backarc rift					
Minami-Ensei knoll	Northern Okinawa	690 - 705	Volcanic depression with pumice, and diorite fragments	267 - 278	Anhydrite chimneys on a sulfide mound
Iheya Ridge	Middle Okinawa	1400	Axial ridge with vesicular pillow basalts	100 - 220	Carbonate precipitates with sulfides
Izu-Ogasawara	Sumisu rift (Bonin Arc)	1550	Flank of a rhyolite dome	-	Fossil barite-silica chimneys

Table 3.I. Synthesis of the main backarc hydrothermal sites (modified from Ishibashi and Urabe, 1995).

PART II:
GEOLOGICAL SETTING

In this part, composed of two chapters, we overview the geological setting of the Bransfield Basin (Chapter 4) and the North Fiji Basin (Chapter 5). The first section of each chapter deals with the regional geodynamic setting and history of the areas where the two basins are located, the Scotia Arc and the southwest Pacific, respectively. A short review of other active backarc basins, and a brief description of the regional geodynamic evolution are presented.

Subsequently, we introduce the characteristics and structural elements of the Bransfield and North Fiji basins, such as location, limits and main geological-geophysical traits, based on previously published studies (bathymetry, seismicity, magnetics, seismic reflection and refraction, gravity, heat flow, hydrothermalism, and petrology). Finally, we focus on the reconstructions and geodynamic evolution of the Bransfield and North Fiji basins since their formation.

Chapter 4

THE BRANSFIELD BASIN

The Bransfield Basin is the narrow, elongated basin located at the northern tip of the Antarctic Peninsula, forming the southwestern edge of the Scotia Arc. The Bransfield Basin/northern Antarctic Peninsula area is one of the most accessible parts of Antarctica. Thus, since the first studies carried out in the 1970's (e.g. Ashcroft, 1972), the solid earth's structure of this area has been extensively studied by teams of scientists from Europe, Asia, North and South America.

4.1. Geodynamic setting: The Scotia Arc

4.1.1. GENERALITIES

The Scotia Arc is the name of the eastward-closing curved loop of mountains, submarine ridges, and islands which connects the Andean Cordillera of South America to the Antarctic Peninsula and encloses the Scotia Sea (Barker et al., 1991) (Fig. 4.1). The Scotia Arc region is dominated by the E-W strike-slip displacement between the two major surrounding plates, South-America and Antarctica (Dalziel, 1989). Two main plates are located within the Scotia Arc, the small Sandwich Plate in the extreme east, and the much larger Scotia Plate filling the remaining area and limited in the western part by the Shackleton Fracture Zone (Forsyth, 1975) (Figs. 4.1 and 4.2).

A 10 mGal contour satellite-derived free-air gravity map of the Scotia Arc region shows the principal structures in high resolution (Fig. 4.1). The present-day plate tectonic setting and the main morphostructures of the Scotia Arc are shown in the interpretative sketch of the satellite-derived map (Fig. 4.2).

- Active subduction occurs along the South Chile Trench (pre-Mesozoic to Present, Barker et al., 1991) and South Sandwich Trench

(Mid Eocene/Early Oligocene to Present, Barker and Hill, 1981) (Figs. 4.1 and 4.2).

- The South Chile Trench is where subduction of the Antarctic Plate under the South American continent occurs. The trench is marked by negative free-air anomalies reaching up to -160 mGal.

- The South Sandwich Trench is the eastern limit of the Scotia Plate, and where the western edge of the South American Plate is being subducted at present. The South Sandwich Trench is strongly marked by curved free-air anomalies reaching more than -250 mGal, whereas the volcanic arc, parallel to the trench, shows positive values of 180 to 200 mGal (Figs. 4.1 and 4.2).

• Passive subduction occurs along the South Shetland Trench. This trench, west of the intersection with the South Scotia Ridge and the Shackleton Fracture Zone, represents the last surviving segment of a subduction zone that originally extended along the western margin of the Antarctic Peninsula (e.g. Hawkes, 1981). The South Shetland Trench shows negative free-air anomaly values, up to -120 mGal.

• Present-day left-lateral strike slip motion occurs along the Scotia Ridge, and marks the northern and southern boundaries (North and South Scotia ridges, respectively) of the Scotia Plate (Pelayo and Wiens, 1989).

- The North Scotia Ridge (Fig. 4.2) is composed of a series of elevated blocks from Tierra del Fuego to South Georgia Island, showing strong positive anomalies (> 80 mGal) (Fig. 4.1). South Georgia Island represents a fragment of the South-American continent displaced 1600 km to the east (e.g. Dalziel et al., 1975). The northern margin of this ridge, with negative free-air anomalies up to -180 mGal (Fig. 4.1), has been interpreted as the collision zone between South America and Scotia plates (Ludwig and Rabinowitz, 1982).

- The South Scotia Ridge (Fig. 4.2) is also composed of a series of fragmented blocks showing high values on the free-air anomaly map (Fig. 4.1). From the South Orkney Islands to the Bransfield Basin, the ridge is composed by two continuous, parallel crests limited by deep inner depressions. The South Scotia Ridge

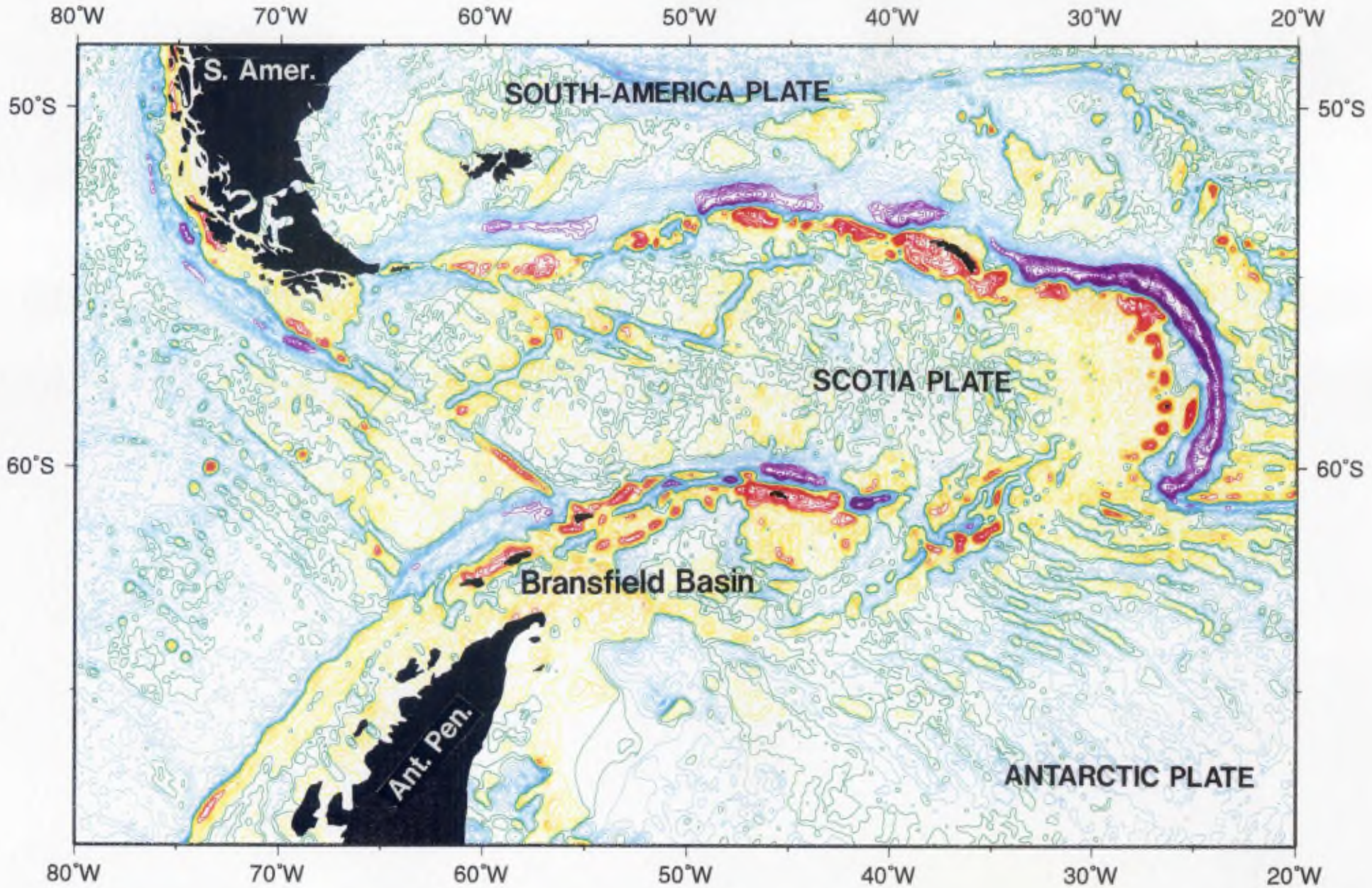

Fig. 4.1. Contour satellite-derived free-air gravity map of the Scotia Arc and northern Antarctic Peninsula area. Contour every 10 mGal. Colour ranges are red: 300/80 mGal; orange: 80/40 mGal; yellow: 40/30 mGal; light green: 30/20 mGal; dark green: 20/0 mGal; blue: 0/-100 mGal and purple: -100/-300 mGal.

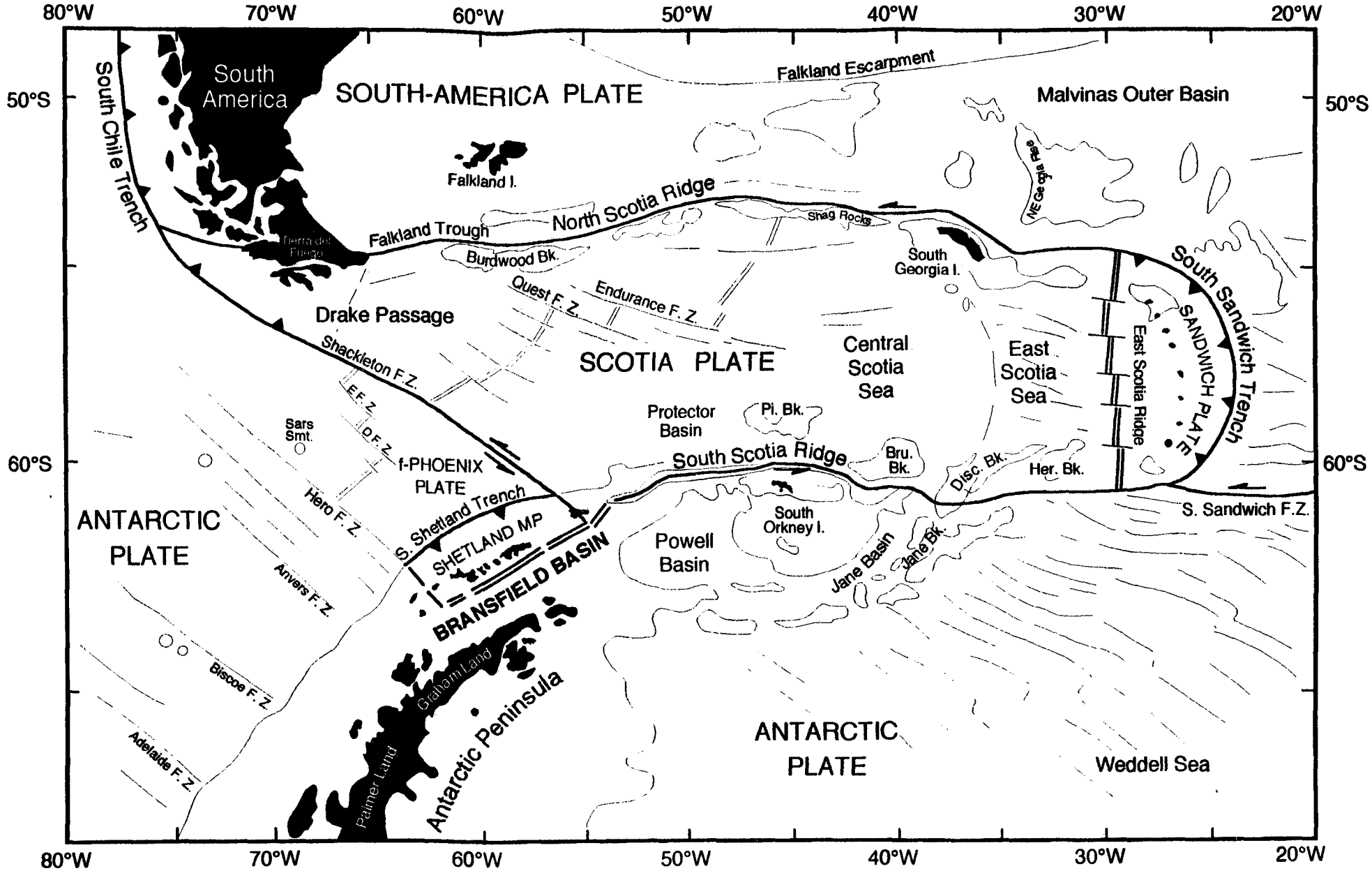

Fig. 4.2. Present-day plate tectonic setting and main structural features of the Scotia Arc and Antarctic Peninsula area from interpretation of Figure 4.1. Double lines indicate spreading centres, aligned triangles denote a subduction zone with triangles pointing to the overriding plate. Thick lines indicate present-day plate boundaries. Location of features are from Barker (1982), British Antarctic Survey (1985), and Lawver et al. (1995).

emerges from the sea on the South Orkney Islands, interpreted as a micro-continental fragment originally contiguous with the Antarctic Peninsula (Dalziel, 1984).

• Dead spreading centres can be observed within the Scotia Plate (Fig. 4.1). Three inactive spreading regimes have been recognized within the Scotia Sea overlapping in time: the Drake Passage, the Central Scotia Sea and Protector Basin (Barker and Burrell, 1977; Hill and Barker, 1980; Barker et al., 1991) (Fig. 4.2). However, only one of them (Drake Passage) is clearly seen in the free-air anomaly map. This fossil spreading centre is characterized by a WNW-ESE trending double ridge and pronounced fracture zones showing negative anomalies (-50 mGal) (Fig. 4.1). This system stopped spreading at magnetic Anomaly 5 (11 Ma), Late Miocene (Barker and Hill, 1981).

• Small marginal basins occurring within the Scotia Arc region, such as the Powell and Jane basins flanking the South Orkney micro-continent, and those separating Pirie, Bruce, and Discovery banks (Fig. 4.2), show weak negative anomalies (Fig. 4.1). Some of them have an oceanic crustal structure (Barker, 1972), but their ages can not be determined precisely (Barker et al., 1991).

• Active extensional backarc basins, such as the East Scotia Sea and the Bransfield Basin, are also clearly identified on the free-air anomaly map (Figs. 4.1 and 4.2).

- The East Scotia Sea is characterized by higher regional anomalies (10-50 mGal) than those of surrounding areas, such as the old Central Scotia Sea (-10 to 10 mGal). The East Scotia Ridge is the active backarc spreading centre (Barker and Hill, 1981), and appears as a small (10-40 mGal) linear gravity low flanked with gravity highs (Livermore et al., 1994) (Figs. 4.1 and 4.2). More detailed information about this structure is presented in section 4.1.3.

-The Bransfield Basin shows weak negative free-air anomalies associated with bathymetric lows (Figs. 4.1 and 4.2). The Bransfield Basin may represent the present-day episode of backarc extension with respect to a possible active subduction along the South

Shetland Trench (Pelayo and Wiens, 1989). For more details see section 4.2.

The seismicity of the region is concentrated along the bathymetric features which surround the Scotia Sea, providing evidence for a kinematically distinct Scotia Plate (Forsyth, 1975) (Fig. 4.3). Apart from the seismicity related to the active subduction along the South Sandwich island arc, the most active seismic zone follows the bathymetric trend of the South Scotia Ridge (Pelayo and Wiens, 1989). The North Scotia Ridge shows a seismicity level lower than the South Scotia Ridge, and the most important activity is found near Burwood Bank (Figs. 4.2 and 4.3).

The earthquakes along the North Scotia Ridge have E-W nodal planes with a left-lateral sense of shear, and a compressional component also indicated by focal mechanisms (Fig. 4.4). Moreover, earthquakes along the South Scotia Ridge also have E-W trending nodal planes with a left-lateral shear sense, but display elements of extension (Fig. 4.4). The results suggest about 6 mm/yr of left-lateral motion with a component of compression along the North Scotia Ridge, and about 10 mm/yr of left-lateral motion with a component of extension along the South Scotia Ridge (Pelayo and Wiens, 1989).

4.1.2. ACTIVE BACKARC BASIN: THE EAST SCOTIA SEA

The East Scotia Sea is the basin located backarc from the curved South Sandwich volcanic arc and trench (Fig. 4.2). The East Scotia Sea provided the first reported example of active backarc extension generating well developed oceanic magnetic lineations (Barker, 1970 and 1972). The dominant feature of the basin is the spreading centre located approximately along 30°W, and defined very precisely by lineated magnetic anomalies (Barker and Hill, 1981). In the northern and central sections of the East Scotia Ridge well formed magnetic anomalies are identified to at least Anomaly 5 (11 Ma) on the western flank. Farther south, anomalies can be identified only out to Anomalies 2 (2 Ma) or 2A (3.5 Ma). Spreading is essentially E-W, but a slight discordance between the older anomalies on each flank suggests the possibility of earlier complexity. For the last 1.7 Ma, spreading was up to 15% asymmetric, favouring accretion to the arc flank, within an overall rate of 65 mm/yr (Barker, 1995).

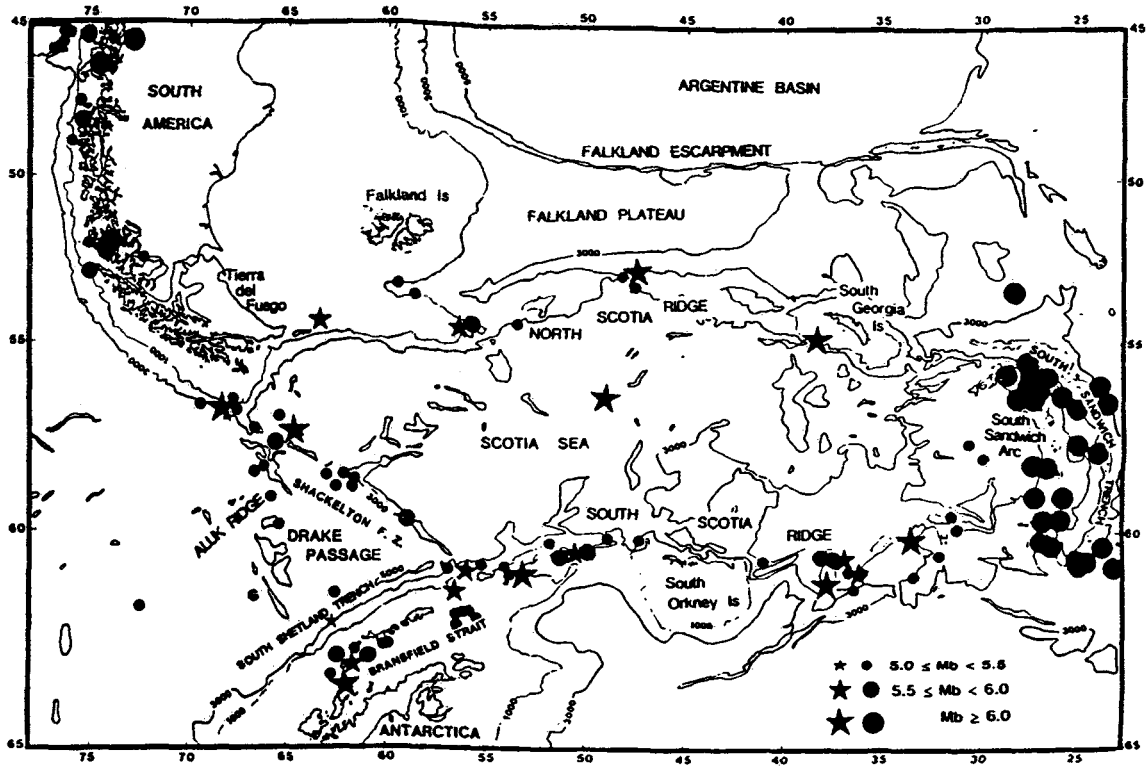

Fig. 4.3. The 1963-1985 seismicity of the Scotia region (m_b > 5.0). Stars represent events for which source parameter inversion results were obtained (see Fig. 4.4). Only earthquakes with m_b > 6.0 are plotted east of 30°W. They represent events along the South Sandwich island arc and the South Sandwich Fracture Zone (Pelayo and Wiens, 1989).

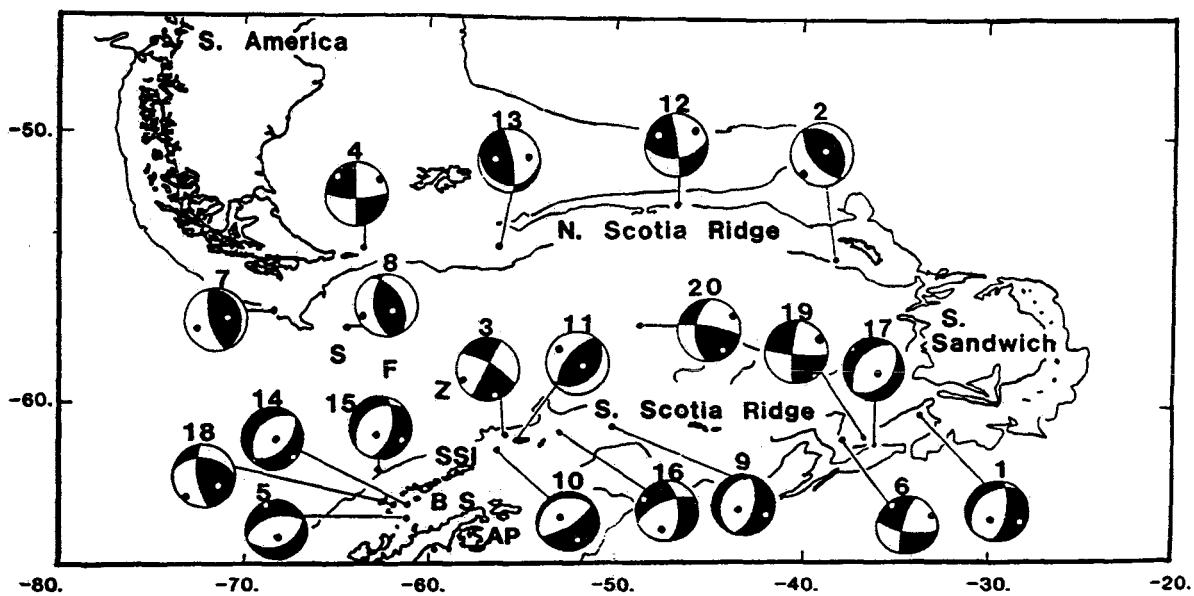

Fig. 4.4. Focal mechanisms solutions determined from body waveform inversion. Each mechanism solution is shown as lower hemisphere equal-area projection of the focal sphere with solid quadrants representing compressional P-wave first motions. The P- (maximum compression) and T- (minimum compression) axes are shown as filled and unfilled small circles, respectively. Events numbered from 1 to 20. SFZ: Shackleton Fracture Zone, SSI: South Shetland Islands, BS: Bransfield Strait, and AP: Antarctic Peninsula (Pelayo and Wiens, 1989).

The East Scotia Ridge comprises seven or more N-S oriented ridge segments, separated by short (less than 30 km), mainly sinistral, offsets. The axial morphology of the East Scotia Ridge varies along strike, although a median valley may be recognized along most of the central part. The valley can reach 1200 m in depth and 20 km in width, although it most commonly appears as a central trough 500-800 m deep and 6 to 10 km wide (Barker, 1995). The amplitude of the axial free-air anomaly lows is larger (around 40 mGal) in the central part of the ridge, between 57°S and 58°S (Figs. 4.1 and 4.2). Towards the northern and southern ends, presumably a ridge-transform-transform (RFF) triple junction, the amplitude of the free-air anomalies is reduced to 10/20 mGal, making it difficult to locate the axis precisely (Livermore et al., 1994).

4.1.3. THE SCOTIA SEA EVOLUTION

Based on the identification of marine magnetic anomalies, Barker et al. (1984 and 1991) and Barker (1995) presented a series of reconstructions of the Scotia Sea, from the present-day back to 30 Ma ago, in three steps 10 Ma each (Fig. 4.5). Some uncertainties affect the reconstructions, such as the age and nature of many parts of the Scotia Ridge, the southern Scotia Sea, and the small marginal basins.

Present-day

The identified magnetic anomalies of the Scotia Sea and northern Weddell Sea are depicted in Figure 4.5a. Note that within the Scotia Arc region, active spreading and extension occur only along the East Scotia Ridge and the Bransfield Basin, respectively.

Late Miocene (10 Ma ago)

During this period, the Bransfield Basin and the dividing trough of the western South Scotia Ridge are both closed. The whole East Scotia Sea is eliminated, and small sections of the young ocean floor are removed from the Drake Passage and Central Scotia Sea. The southern part of the South Sandwich Trench becomes parallel to the Discovery Bank. South Georgia Island is located at the same place as it is today (Fig. 4.5b).

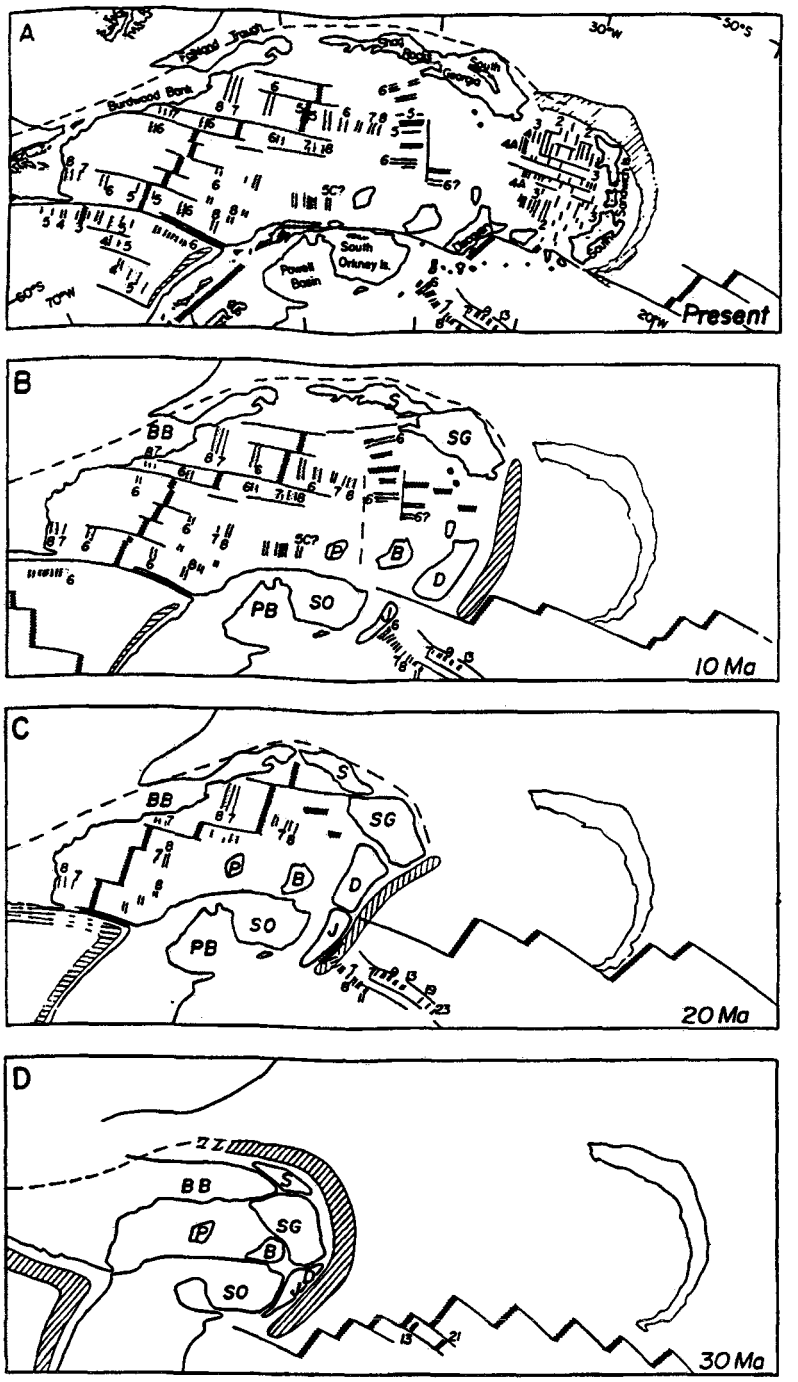

Fig. 4.5. Tectonic evolution of the Scotia Sea region over the past 30 Ma (Barker et al., 1984 and 1991). Small blocks are BB: Burdwood Bank, S: Shag Rocks, SG: South Georgia, H: Herdman Bank, D: Discovery Bank, J: Jane Bank, SO: South Orkney, B: Bruce Bank, P: Pirie Bank, and PB: Powell Basin. These are micro-continental fragments, dissected intra-oceanic island arcs, and accretionary prisms. (A) Present-day geodynamic setting with the identified magnetic anomalies in the Scotia Sea and northern Weddell Sea. South Sandwich trench is shaded. (B, C and D) Reconstructions to 10, 20 and 30 Ma, respectively. The "ghost" of the present South Sandwich Trench is given for scale (Barker, 1995). See section 4.1.3. for further explanations.

Early Miocene (20 Ma ago)

For the 20 Ma reconstruction, all the Central Scotia Sea and Protector Basin are removed. Collision with a ridge crest section of the South America-Antarctic boundary has stopped subduction at the southern section of the trench, and Jane and Discovery banks are aligned. This implies that the small basins lying between these banks are older than 20 Ma. The North Scotia Ridge is shorter and the South Georgia block lies further west, protected from accretion to the north by the Shag Rocks block (Fig. 4.5c).

Early Oligocene (30 Ma ago)

This reconstruction is more speculative than the previous ones. Oceanic floor in Drake Passage is removed to Anomaly 8 (28 Ma). The basins lying between Jane Bank and South Orkney Islands, and Discovery and Bruce banks are removed, but not the basin between Pirie and Bruce banks. This is based on the similar width and position of the first two basins, and the age estimation of 25 Ma for the Jane Basin from heat flow data (Lawver et al., 1985). The bathymetric reconstruction suggests that the Powell Basin may be younger than 30 Ma (King and Barker, 1988). The result of this reconstruction is a compact continental connection between South America and the Antarctic Peninsula (Fig. 4.5d). Thus, the paleo-Pacific margin of South America appears to have continued to the eastern end of the South Georgia block, in the same way as the Antarctic Peninsula continued to the eastern end of the South Orkney block.

4.2. Main characteristics

An overview of the main geological and geophysical characteristics of the Bransfield Basin is presented in this section.

4.2.1. LOCATION AND LIMITS

Geographically, the Bransfield Strait is the body of water extending between the South Shetland Islands and the northern tip of the Antarctic Peninsula (Lawver et al., 1995) (Fig. 4.6). At the northern part of the Strait, in a backarc position with respect the South Shetland Island lies the Bransfield Basin *sensu stricto*. The Bransfield Basin is a young, active rift basin (Saunders and Tarney, 1984; Fisk, 1990; Grad et al., 1992; Lawver et al., 1995) that separates the Shetland Microplate from the Antarctic Plate, at the southwestern edge of the Scotia Plate (Fig. 4.2). The Bransfield Basin is located between longitudes 62°W and 54°W, and latitudes 61°S and 64°S. The basin extends more than 400 km from Low Island to Clarence Island, and up to 80 km in width (González-Ferrán, 1985). The limits of the Bransfield Basin are (Fig. 4.2):

- to the north, the South Shetland Islands. The central South Shetland Islands are mainly composed of volcanic and plutonic rocks, constituting part of a magmatic arc of Cretaceous to Mid-Tertiary age, with few sedimentary rocks intercalated (Trouw and Gamboa, 1992). The youngest rocks in the South Shetland Islands are ensialic alkaline volcanics probably related to the extension (Smellie, 1987). Behind the islands lies the curved South Shetland Trench. In cross-section it shows a classic trench asymmetric profile: very steep slope landward and gentle slope seaward (Henriet et al., 1992).

- to the south, the Antarctic Peninsula margin. The Antarctic Peninsula forms part of the same Mesozoic-Tertiary magmatic arc as the South Shetland Islands. Consequently, the rock units are essentially the same. The Antarctic Peninsula is apparently a higher uplifted, and therefore deeper eroded, part of the magmatic arc, resulting in the predominance of basement outcrops, such as the Permian-Triassic turbiditic sequences of the Trinity Peninsula Group, intruded by Middle Jurassic to Cretaceous batholiths. Few remainders of Late Tertiary and

Quaternary volcanics cover the older sequences locally (Trow and Gamboa, 1992).

• to the west, the extension of the Hero Fracture Zone. This feature has been surveyed by seismic reflection lines, and it appears as a mighty ridge, towering more than 1500 m above the surrounding seafloor. Only the southern flank of the fracture is covered by a 200 m thick sedimentary layer (Henriet et al., 1992).

• to the east, the extension of the Shackleton Fracture Zone. This is an elevated ridge feature having a transpressive character, manifested by deep diapirs, normal faults, and shallow folds with reverse faults deforming the sediments. The intersection between the Bransfield Basin, the South Scotia Ridge, and the southeastern tip of the Shackleton Fracture Zone is a complex triple junction (Maldonado et al., 1994).

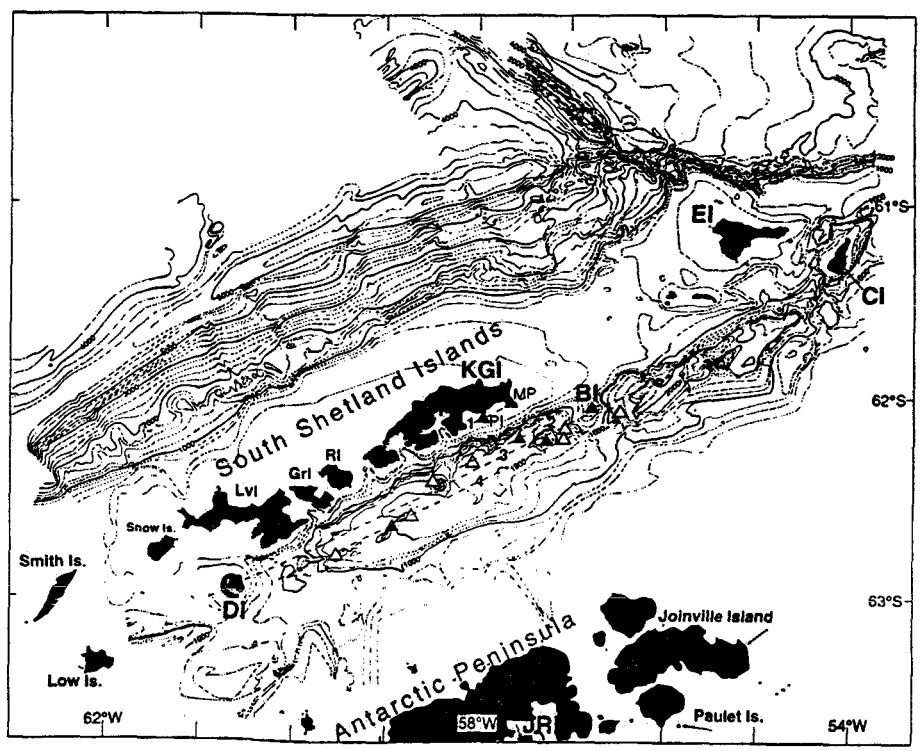

Fig. 4.6. Bathymetric map of the Bransfield Basin region (contour interval is 200 m). Solid triangles are locations of submarine and subaerial Quaternary volcanism that were sampled and analyzed by Keller et al. (1992). Hollow triangles denote submarine locations where fresh basalts were recovered by Keller et al. (1994) but not yet analyzed. Dashed numbered lines (1 to 4) are volcanic lineations explained in the text. BI: Bridgeman Island, CI: Clarence Island, DI: Deception Island, EI: Elephant Island, Grl: Greenwich Island, JRI: James Ross Island, Lvl: Livingston Island, MP: Melville Peak, PI: Penguin Island, and RI: Robert Island (Lawver et al., 1995). Compare to the new sets of bathymetric maps presented in Chapter 6.

4.2.2. GEOLOGY AND GEOPHYSICS

Bathymetry

Important aspects of the bathymetry of the Bransfield Basin have been discussed by previous authors, as Ashcroft (1972). The Bransfield Basin is an asymmetric trough, trending NE-SW and with an average depth of 1900 m, bounded by a steep slope from the South Shetland Islands and wider from the Trinity Peninsula margin (Jeffers et al., 1991). Several deep troughs, roughly aligned with the bays of the South Shetland Islands, cut the platform of Trinity Peninsula (British Antarctic Survey, 1985). Irregular topography is exposed on the seafloor, mainly as an alignment of seaknolls between Deception and Bridgeman Islands (Jeffers et al., 1991). A compilation of all the bathymetric data acquired in the area was published by Klepeis and Lawver (1994), and is presented in Figure 4.6. Note the higher resolution along the bands where multibeam bathymetric data were acquired. Dashed lines between bands correspond to interpolated values.

Seismicity

Seismicity associated with the South Shetland Trench is weak, showing no evidence of shallow earthquakes along the thrust zone except near the intersection of the trench, the Shackleton Fracture Zone and the South Scotia Ridge (Figs. 4.3 and 4.4). Similarly, deep events which would indicate a downgoing slab are rare (Pelayo and Wiens, 1989). Most of the earthquakes in the Bransfield Basin are shallow events related to extension and volcanic activity, and located near Deception and Bridgeman islands.

Magnetism

Marine magnetic and aeromagnetic surveys of the Bransfield Basin region found a central positive anomaly along the axis of the basin. This central high has been modelled as a large, positive magnetized igneous body associated with the inferred axis of rifting (Roach et al., 1978; Parra et al., 1984; Garrett, 1990; González-Ferrán, 1991). Roach et al. (1978) hypothesize that spreading has occurred only during the past 1.3 Ma. Parra et al. (1984 and 1988), modelling aeromagnetic data, suggest an age of 1.8 Ma for the start of the basin spreading, at an average full rate of 9 mm/yr. González-Ferrán (1991) suggests from aeromagnetic data interpretation an average full spreading rate of 2.5-7.5 mm/yr for the past 2 Ma. What seems clear is that magnetic anomalies are difficult to identify in the Bransfield Basin. The young age of the basin makes the magnetic patterns still diffuse, and the thick sediment cover containing interbedded basalt flows hides the

basement topography (Lawver et al., 1995). This difficulty in analyzing marine magnetic anomalies is a common characteristic of the young backarc basins of the southwest Pacific, as suggested by Lawver and Hawkins (1978).

Seismic refraction and gravity

Early seismic refraction work found an anomalously thin layer beneath the Bransfield Basin with a seismic velocity lower than of normal mantle material but higher than typical continental crust (Ashcroft, 1972). Later studies carried out by a Polish research group (Guterch et al., 1985, 1991; Grad et al., 1992 and 1993) found a crustal thickness of 30-33 km in the South Shetland Islands to 38-45 km near the coast of the Antarctic Peninsula. Guterch et al., (1991) observed a seismic discontinuity with velocities of 7-7.2 km/s at a depth of about 10 km beneath the Bransfield Basin. The subducted slab can be detected beneath the South Shetland Islands (Grad et al., 1993) dipping at an angle of 25° to the southeast (Fig. 4.7). A 10 km wide body with velocity $v_p \approx 6.8$ km/s has been assimilated by Grad et al. (1993) to the active Bransfield rift (Fig. 4.7).

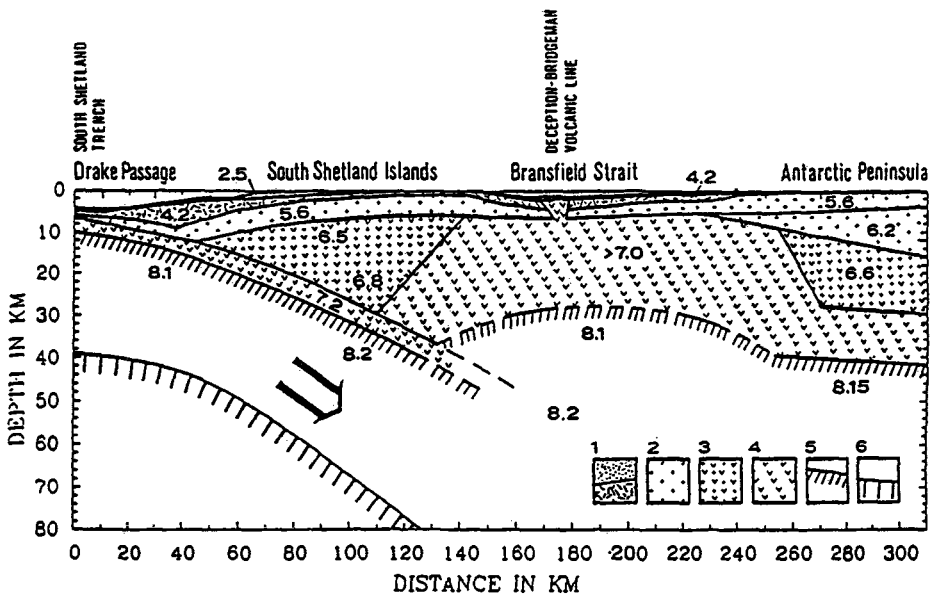

Fig. 4.7. Seismic model of the lithosphere from the Drake Passage through Bransfield Strait and onto the Antarctic Peninsula. 1: sediments, v_p= 2.5-4.2 km/s; 2: upper crust, v_p= 5.4-6.3 km/s; 3: middle crust, v_p= 6.4-6.8 km/s; 4: lower crust and high velocity body in Bransfield Strait, v_p> 7.0 km/s; 5: Moho boundary, v_p> 8.0 km/s; 6: Reflection boundary in the lower lithosphere (Grad et al., 1993)

Large negative free-air gravity anomalies were observed by Garrett (1990). Bouguer gravity anomalies (Renner et al., 1985; Garrett, 1990) of up to 100

mGal correlate with the anomalous crustal structure found by Grad et al. (1993) under the South Shetland Islands and Bransfield Basin.

Seismic reflection and sedimentary record

Numerous multi-channel and single-channel seismic lines from the Bransfield Basin were collected and published by researchers from Brazil (e.g. Gamboa and Maldonado, 1990), Belgium (e.g. Henriet et al., 1992), Poland (e.g. Guterch et al., 1985), Spain (e.g. Acosta et al., 1992), United Kingdom (e.g. Larter and Barker, 1989), and United States (e.g. Jeffers and Anderson, 1990). Neovolcanic intrusions within the Bransfield Basin were first detected by Guterch et al. (1985) in single-channel seismic profiles. Jeffers and Anderson (1990) determined that sedimentation is mainly dominated by glacial-marine processes with associated lithofacies. The same authors stated that the volcanic ridge may act as a sedimentary barrier. The thickness of the ponded turbiditic sediment within the Bransfield Basin is less than 1 second (Gamboa and Maldonado, 1990). Line-drawings presented by Acosta et al. (1992) show the southwestern flank of the South Shetland Islands faulted in horst and graben structures and intruded by dykes and plugs. Barker and Austin (1994) imaged, from multichannel data, complex fan-shaped faulting patterns along the Antarctic Peninsula margin. They interpreted these patterns as resulting from crustal diapirism, suggesting diffuse zones of extension within the Bransfield Basin.

Heat flow and hydrothermalism

Heat flow measurements were made in the King George Basin, located south of King George Island (Lawver et al., 1995). The heat flow values range from 49 mW/m^2 to 626 mW/m^2, with about 25% of the values greater than 220 mW/m^2. The highest values were recorded in the central part of the basin and along the southeast and northeast edges of the basin (Lawver et al., 1995). Most of these values are typical of regions with active hydrothermal circulation (Nagihara and Lawver, 1989; Lawver et al., 1995). Evidence of hydrothermal activity were found in the water column and in the sediments where the highest heat flow measurements were recorded (Lawver et al., 1995). ^3He increment with depth has been interpreted as resulting from injection of ^3He into the water by backarc rifting (Schlosser et al., 1988). Mn concentration and temperature also increase with depth (Suess et al., 1988). Thermogenic hydrocarbons found in surface sediments (Whiticar et al., 1985) may be also associated with hydrothermal activity in the Bransfield Basin.

Volcanism

Quaternary volcanism in the Bransfield Basin is recorded at Deception, Penguin and Bridgeman islands (Weaver et al., 1979) as well as at few other places on the South Shetland Islands (Smellie, 1990), and on the seamounts and ridges between Deception and Bridgeman islands (Fisk, 1990; Keller and Fisk, 1992). Lawver et al. (1995) suggested at least four parallel lines of active and incipient volcanism in the Central Bransfield Basin (Fig. 4.6). The first line would be located within the shelf of the South Shetland Islands and includes Penguin Island and Melville Peak (Birkenmajer, 1992). The second would be defined southeast of King George Island (along the King George Basin margin), and comprises small circular volcanoes. The third line would be the main rift axis and includes Deception and Bridgeman islands and at least two major submarine volcanoes. The fourth lineation would be defined by a ridge, the maximum heat flow values, and a recent extrusion at the northeastern part of the basin.

Samples recovered from the Bransfield Basin seamounts are fresh glassy basalts less than 300,000 years old (Fisk, 1990; Birkenmajer and Keller, 1990; Keller et al., 1992), classified as backarc basin basalts, a hybrid of arc and mid-ocean ridge basalt composition (Fisk, 1990). The Bransfield Basin is one of the few modern examples of a marginal basin within an ensialic arc (Keller and Fisk, 1992).

4.3. Origin and evolution of the basin

The Bransfield Basin is an example of basin formed by rifting within a continental volcanic arc, but the history of extension and evolution of the Bransfield Basin is still not well constrained.

Cenozoic plate convergence occurred at the Pacific margin of the Antarctic Peninsula (Barker and Dalziel, 1983). The seafloor created at the Antarctic-Phoenix ridge was subducted beneath the Antarctic Plate, and a succession of ridge-trench collisions started about 50 Ma at the south of the Pacific margin of the Antarctic Peninsula (Barker, 1982; Larter and Barker, 1991) (Fig. 4.8). The trailing flank of the ridge crest and the overriding lithosphere at the trench were both part of the Antarctic Plate, and in consequence, the rate of convergence at the trench was equal to the full spreading rate at the ridge crest (Barker, 1982). After each collision, seafloor spreading and subduction both stopped. Trench basement topography was eliminated and the margin became passive (Larter and Barker, 1991). Through time, additional segments of the ridge were subducted to the northeast until about 4 Ma ago, when the spreading centre immediately southwest of Hero Fracture Zone reached the trench (Barker, 1982). The last segment of the Antarctic-Phoenix ridge (between Hero and Shackleton fracture zones) was then abandoned offshore of the trench and the remnant of the Phoenix Plate became part of the Antarctic Plate (Lawver et al., 1995) (Fig. 4.8).

Barker (1982), Barker and Dalziel (1983), Barker et al., (1991), and Lawver et al. (1995) have suggested that the Bransfield Basin is opening because the subducting plate (former Phoenix Plate, see Fig. 4.2) is continuing to sink by oceanward migration of the hinge of subduction. According to these authors, a mechanism of trench rollback may result in the opening of the Bransfield Basin, and the amount of trench rollback would be comparable to the amount of extension in the basin. Barker and Dalziel (1983) suggest an age between 4 and 1.3 Ma for the start of the extension.

Jeffers et al. (1991) presented the evolution of the basin from the marine sedimentary record. Those authors agree with Barker and Dalziel (1983) that the basin is relatively young (less than 4 Ma), and considered that extension in the Bransfield Basin began with the cooling and sinking of the subducted slab. Jeffers et al. (1991) suggested that the segmentation of the basin could be

related to the segmentation of the subducting slab into three pieces and their differences in the age. Then, the older and denser slab sinking faster below the northeastern part of the Bransfield Basin would drive extension more rapidly there than further southwest.

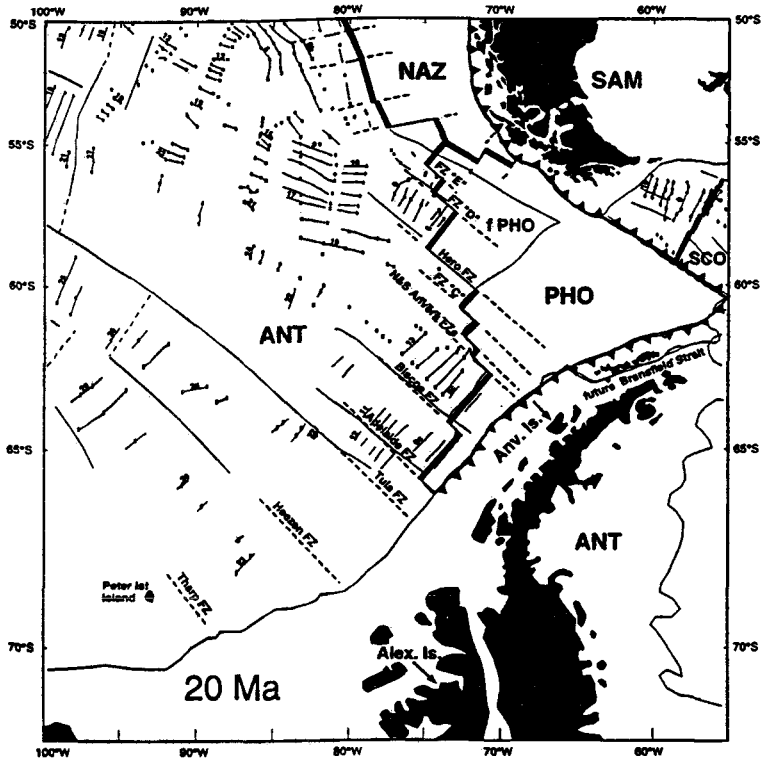

Fig. 4.8. Reconstruction of southeast Pacific and Antarctic Peninsula regions for 20 Ma. Dashed fracture zones and spreading centres are taken from Larter and Barker (1991). Magnetic anomaly picks are shown as small squares. Rifting in the Bransfield Basin has been closed up. The shaded region corresponds to the seafloor that was subducted since 20 Ma. NAZ: Nazca Plate, PHO: Phoenix Plate, SAM: South-America Plate, SCO: Scotia Plate, ANT: Antarctic Plate, FZ: Fracture zones, Alex.: Alexander Island, Anv.: Anvers Island (Lawver et al., 1995).

A completely different model of evolution of the Bransfield Basin has been presented by Birkenmajer (1992 and 1994). That author considered that the oldest evidence for rifting in the area derives from Oligocene deposits and volcanics. This "old" age for the Bransfield Basin contrasts with the "young" Pliocene age (4 Ma) proposed by Barker (1982) and many other authors. Birkenmajer (1992 and 1994) suggested that incipient rifting started at the end of Oligocene, 26 to 22 Ma, and continued at a slow rate through Early Miocene. This is evidenced by a system of faults cutting through Upper Oligocene and older rocks at the outer margin of the rift. Between Early (22-20 Ma) to Mid (14 Ma) Miocene, several successions of basaltic to andesitic dykes and plug intrusions occurred. From Late Miocene to Pliocene stages, there is a gap in geological evidence of the rift evolution. Finally, the

Pleistocene to Recent stages are characterized by alkaline to calc-alkaline volcanic activity along the rift axis. Birkenmajer (1992) concluded that the Bransfield Basin continues to be at an early stage of rifting evolution underlined by continental-type crust, despite its Oligocene age.

Tokarski (1991) considered that the Bransfield Basin is not a backarc basin and its origin is not directly related to the subduction of the Drake Plate, as suggested by many authors (e.g. Weaver et al., 1979; Barker and Dalziel, 1983). Instead, he proposed that the volcanic features and extension along the Bransfield Basin are simply signs of the internal deformation of the Antarctic Plate due to the stress regime set up by the surroundings spreading centres. Thus, after ceasing the subduction, a NE-SW compressional component, probably related to the accretion near to the Scotia Sea, would have determined a NW-SE extension leading to the basin opening.

Chapter 5

THE NORTH FIJI BASIN

The North Fiji Basin is a large, triangular basin located in the south-west Pacific region. Little was known about the geology of the basin and its structures 10 years ago. Only large-scale heat flow and seismicity studies were conducted in the North Fiji Basin, although they already supported the hypothesis of its formation by seafloor spreading (Sclater and Menard, 1967; Chase, 1971). Numerous studies carried out during recent years within international scientific programs, have provided a more accurate picture of the structures and history of this basin (Crook et al., 1991).

5.1. Geodynamic setting: The southwest Pacific

5.1.1. GENERALITIES

The southwest Pacific region is a complex transitional area located between Australia and the Central Pacific Basin (Fig. 5.1). It is composed by continental fragments, oceanic trenches, island arcs, marginal basins, fracture zones, and seamounts, created by the interactions between the Pacific and Indo-Australian plates during the Cenozoic (Kroenke, 1984). The southwest Pacific region (Fig. 5.1), extending from New Guinea to Tonga, is then dominated by the E-W plate convergence and lateral displacement between the two major plates (Chase, 1978; Minster and Jordan, 1978).

The southwest Pacific region is still referred to as the Melanesian Borderland (Coleman and Packham, 1976), as it constitutes the "border" between the Pacific and Indo-Australian plates. The convergence along the Melanesian Borderland is expressed by both shallow and deep seismicity and Quaternary volcanism associated (Hamburger and Isacks, 1987).

A 10 mGal contour satellite-derived free-air gravity map shows the main structures of the region (Fig. 5.1). The diverse morphologies across this area, such as long linear submarine ridges and troughs, broad plateaus, extensive

basins, and curved island arcs and trenches (Fig. 5.1), depict the complex history of the region (Kroenke, 1984):

- Present-day (from Late Miocene to Present) convergence occurs along New Britain - San Cristobal - New Hebrides - Tonga - Kermadec trenches (Yan and Kroenke, 1993) (Fig. 5.2). These features are marked by strong negative anomalies reaching up to -200 mGal (Fig. 5.1).

- A succession of inactive subduction zones (from Early Eocene to Late Oligocene) (Yan and Kroenke, 1993) trending NW-SE, as Manus - North Solomon - Cape Johnson - Vityaz trenches (Fig. 5.2), are also recognizable by negative anomalies (-100 mGal) of lower amplitude than the active trenches.

- Seamount chains, as the Tasmanid, Lord Howe, Louisville and Samoan seamounts (Fig. 5.2), are clearly visible by alignments of circular and strong positive anomalies (Fig. 5.1). All these seamounts are formed by development over the hotspots of the same names, respectively (Yan and Kroenke, 1993).

- Old marginal basins, such as New Caledonia, Coral Sea, Loyalty, West Torres, Solomon, and South Fiji basins (Fig. 5.2), are also identified on the gravity map (Fig. 5.1). They correspond to basins formed during extensional episodes from Late Cretaceous to Oligocene (Yan and Kroenke, 1993).

- Active backarc basins are expressed as elevated areas in the free-air anomaly map (Fig. 5.1). Four main basins can be easily identified: Manus, Woodlark, North Fiji and Lau, from west to east respectively (Fig. 5.2).

5.1.2. ACTIVE BACKARC BASINS

In this section, we highlight the main traits of the Manus, Woodlark and Lau basins in terms of active seafloor spreading.

Manus Basin

The Manus Basin (Fig. 5.2), included within the Bismarck Sea, is a backarc extensional structure situated north of the New Britain subduction zone and volcanic arc. A seismic lineation formed by strike-slip events marks the

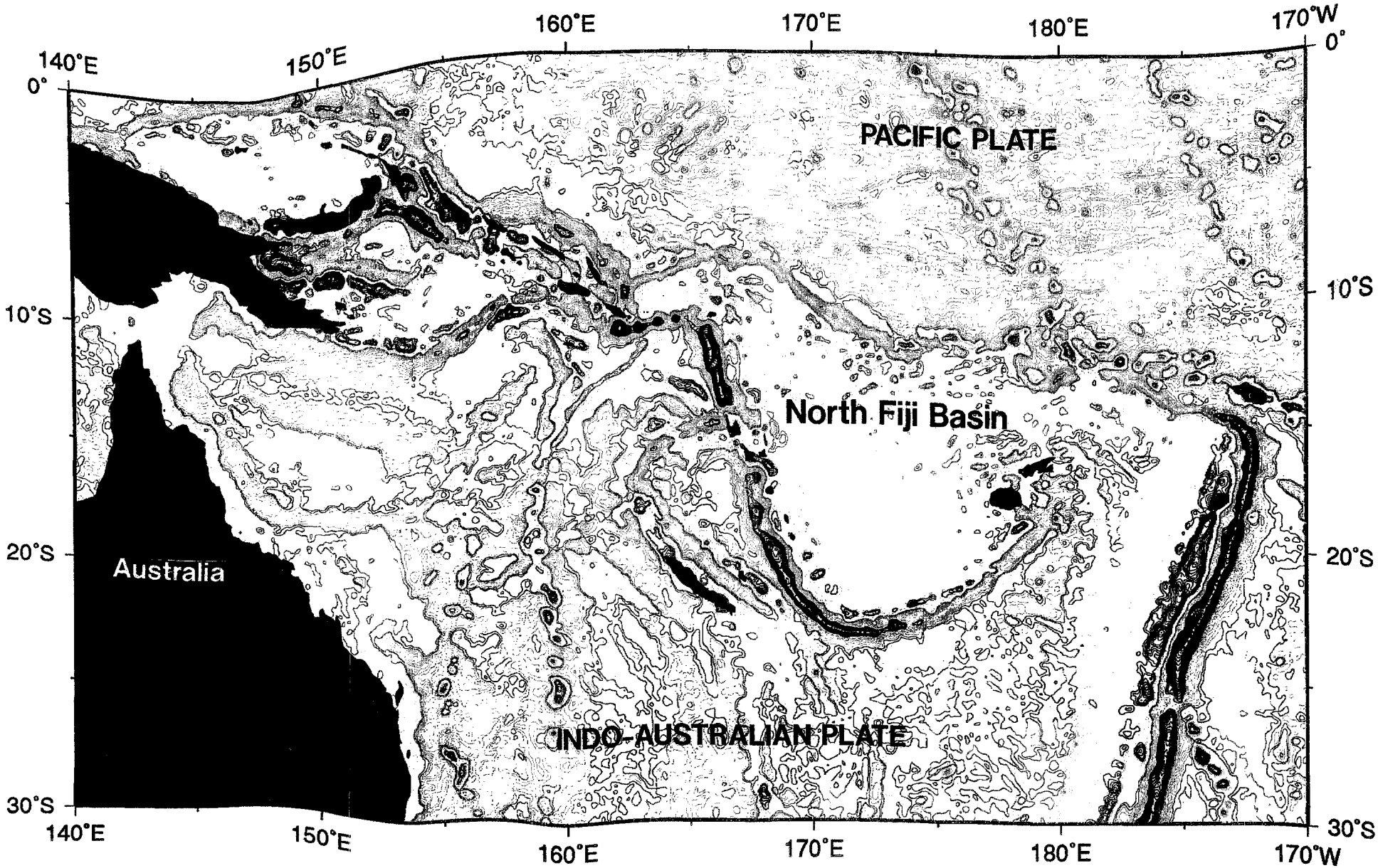

Fig. 5.1. Contour satellite-derived free-air gravity map of the southwest Pacific region. Contour every 10 mGal. Colour ranges are the same as for Figure 4.1.

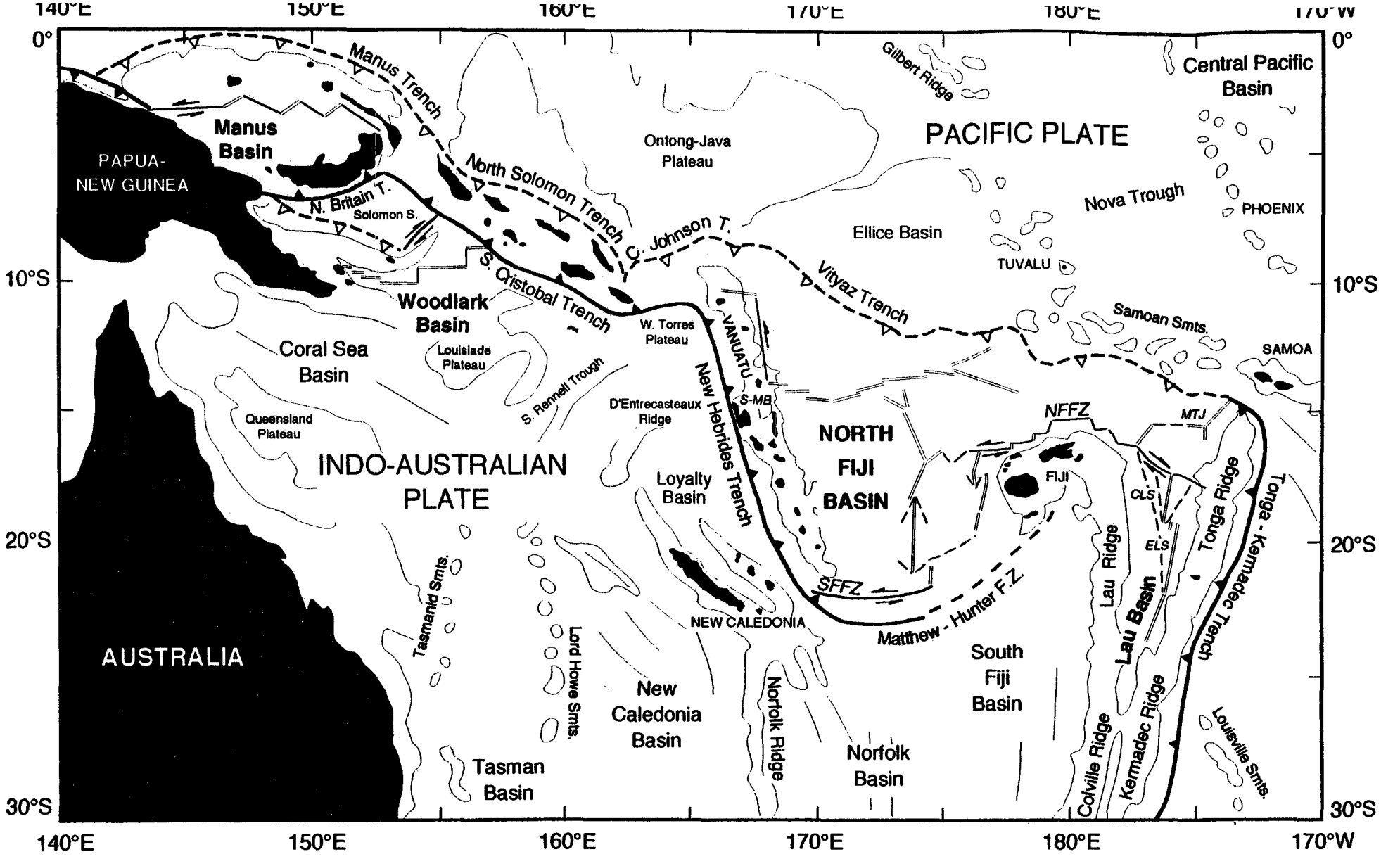

Fig. 5.2. Present-day plate tectonic setting and main features of the southwest Pacific from the interpretation of Figure 5.1. SMB: Santo-Malekula block, MTJ: Mangatolu Triple Junction, NFFZ: North-Fiji Fracture Zone, CLS: Central Lau Spreading Centre, ELS: Eastern Lau Spreading Centre. Black aligned triangles denote active subduction zones with triangles pointing to the overriding plate. White aligned triangles denote fossil subduction zones. Double lines indicate active spreading centres, located from Benes et al. (1994) for the Manus Basin; Taylor et al. (1995), for the Woodlark Basin; Auzende et al. (1995c) and Gràcia et al. (1996b), for the North Fiji Basin; and Parson and Hawkins (1994), for the Lau Basin.

present-day boundary between the Pacific and Bismarck plates (Taylor, 1979). The Manus Basin spreading centre is formed by three discrete segments limited by highly oblique left-stepping and left-lateral transform faults (Fig. 5.2). An extensional transform zone was identified at the intersection between the Willaumez Fracture Zone and the Central Manus Spreading Centre (Taylor et al., 1994).

The identification of magnetic anomalies indicates that asymmetric seafloor spreading in a direction averaging N60 has formed the Manus Basin in the past 3.5 Ma. A total spreading rate of 132 mm/yr was calculated, which represents 74 and 58 mm/yr half spreading rates for the western and eastern flanks of the ridge, respectively (Taylor, 1979). Two zones of basalt-dominated seafloor spreading in the central and western portions of the basin are each associated with hydrothermal activity (Binns and Scott, 1993; Scott and Binns, 1995).

Woodlark Basin

The Woodlark Basin is located between the Solomon Islands and the southeast tip of Papua New Guinea, at the southern part of the Solomon Sea (Figs. 5.1 and 5.2). The basin it is largely floored by mafic oceanic crust generated along a spreading axis which separates formerly contiguous continental rocks (Taylor et al., 1995). Seafloor spreading started 5 Ma ago in the extreme east of the basin, where the Woodlark axis is being subducted beneath the Solomon Arc, and has propagated episodically westward at an average rate of 120 mm/yr (Taylor, 1987). Magnetic profiles indicate decreasing spreading rates westward, from 60 mm/yr at 156°E to 2.7 mm/yr at 152°E (Hill et al., 1984). The V-shaped Woodlark Basin shallows towards its western end, where evidence of initial seafloor spreading and rift propagation into the continental crust has been recognized (Benes et al., 1994; Taylor et al., 1995). Earthquake source parameters indicate that low-angle (10°-25°) normal faulting is active in the region of incipient continental separation (Abers, 1991). At the western part of the basin, hydrothermal activity associated with seamount volcanism in a continental margin setting has been observed (Binns et al., 1993; Scott and Binns, 1995).

Lau Basin

The Lau Basin (Figs. 5.1 and 5.2) is a trapezoidal-shape backarc basin that separates the inactive Lau Ridge remnant volcanic arc from the Tonga Ridge (Karig, 1970) behind the westward dipping Tonga-Kermadec

subduction zone (Figs. 5.1 and 5.2) (Hawkins, 1995). The Lau Basin was considered as the "typical" example of world's backarc basins formed by arc splitting (Karig, 1971). Two major spreading centres located in the central part of the basin, Central Lau Spreading Centre (CLSC) and Eastern Lau Spreading Centre (ELSC) (Fig. 5.2), are propagating southward as suggested by the triangular shape of the basin (Parson et al., 1990; Parson and Hawkins, 1994). At the northeastern part of the Lau Basin, a ridge-ridge-ridge (RRR) type triple junction (Mangatolu Triple Junction) presenting modern volcanism has been identified (Nilsson et al., 1989).

Seafloor spreading may started about 5.5 to 5 Ma ago (Parson and Hawkins, 1994) by the southwards propagation of the present ELSC. A further development of a second propagator (1.5 Ma ago) cut the previously created seafloor (ELSC) and formed the present CLSC (Parson et al., 1990, Parson and Hawkins, 1994). The two spreading centres overlap and are separated by complex seafloor with traces of pseudofaults, abandoned ridges, and relay zones (Hawkins, 1995). At present, the northern Lau Basin opens in an E-W direction at a rate of 120 to 145 mm/yr decreasing southwards. Along the southern ELSC (named Valu Fa Ridge) seismic reflection data evidence a magma chamber underneath the present-day axis (Collier and Sinha, 1990 and 1992). At this part of the ELSC, three major active hydrothermal fields have been discovered (Fouquet et al., 1991).

5.2. Main characteristics

An overview of the main characteristics of the North Fiji Basin and its structures is presented in this section.

5.2.1. LOCATION AND LIMITS

The North Fiji Basin is an extensional basin (Packham and Falvey, 1971; Karig, 1971) located along the Vityaz Trench and between two active subduction zones of opposite polarity: the New Hebrides and the Tonga-Kermadec trenches (Fig. 5.1). The North Fiji Basin is located between longitudes 168°E and 180°E, and latitudes 10°S and 25°S. The basin extends along 1200 km from north to south, and 700 km from west to east (Lafoy, 1987; Bendel, 1993). The limits of the North Fiji Basin are (Fig. 5.1 and 5.2):

- to the north, the Vityaz Trench. This structure trending WNW-ESE extends from the northern part of the New Hebrides Arc to 175°E. Farther east, it is marked by a series of discontinuous, irregular bathymetric troughs at depths of 4-5 km considered as remnants of the formerly continuous trench (Brocher, 1985). The Vityaz Trench appears as a well-defined bathymetric low, locally over 6000 m deep (Kroenke et al., 1983). Its morphology is similar to that of active trenches (Halunen, 1979), but shallow seismicity and Quaternary arc-related volcanism are absent (Hamburger and Isacks, 1987). However, recent studies show present-day compressive structures across the Vityaz Trench (Pelletier and Auzende, 1994).

- to the west, the New Hebrides-Vanuatu Arc. This structure is a bathymetric high extending 1200 km. The geology of the New Hebrides records a history of arc volcanism that began in the Late Eocene (Carney and Macfarlane, 1982). The New Hebrides Arc trends NNW-SSE and is parallel to the New Hebrides Trench. The New Hebrides Trench extends from 11°S to 23°S, reaching 8000 m deep in the north (Kroenke et al., 1983). The trench is interrupted in the central segment where the Santo-Malekula block overrides it (Hamburger and Isacks, 1987) (Fig. 5.1). However, plate convergence is observed along the entire length (Isacks et al., 1981), with abundant shallow earthquakes associated (Hamburger and Isacks, 1988).

• to the south, the Matthew-Hunter Fracture Zone. This curvilinear belt of ridge/trough topography extends from the Fiji Islands to the southern New Hebrides Arc. At its western end it intersects the southern termination of the New Hebrides Trench. The average depth decrease progressively eastwards. Malahoff et al. (1982a) and Gill et al. (1984) proposed that this zone accommodated subduction of the South Fiji Basin until Early Quaternary. However, the absence of an inclined seismic zone and shallow thrust focal mechanisms suggests that the Matthew-Hunter Fracture Zone is not accommodating plate convergence at present (Hamburger and Isacks, 1987).

• to the east, the Fiji Islands Platform. It is defined physiographically as a broad, apostrophe-shaped, shallow platform, less than 2000 m deep (Kroenke et al., 1983). The Fiji Islands represent the exposed portion of a remnant island arc (Hamburger et al., 1988 and 1990). Their exposed rocks reveal a complex history of arc volcanism and deformation beginning in the Late Eocene and extending into the Quaternary (Gill et al., 1984; Rodda and Kroenke, 1984).

5.2.2. GEOLOGY AND GEOPHYSICS

An exhaustive review of the marine data acquired in the North Fiji Basin before the STARMER project is presented by Lafoy (1987). In this section we will highlight only the main points characterizing the basin geology and geophysics.

Bathymetry

The North Fiji Basin has an average depth of 3000 m (Karig, 1970; Chase, 1971), and seems bathymetrically homogeneous, if we look at the scale of the whole southwest Pacific (Fig. 5.1). The basin is elevated of 2000 m with respect to the adjacent seafloor of the Central Pacific Basin. This is why it was named North Fiji "Plateau" (Sclater and Menard, 1967). Falvey (1975) was the first to name the area as North Fiji "Basin", taking into account its origin by oceanic accretion. A compilation of all the available bathymetric data made by J.P. Mazé is presented in Fig. 5.3. This compilation at 1:1,000,000 scale, combines classical bathymetric surveys with the swath-bathymetry data from the Seapso 3 cruise (1985) and from the whole STARMER project (1987-1992).

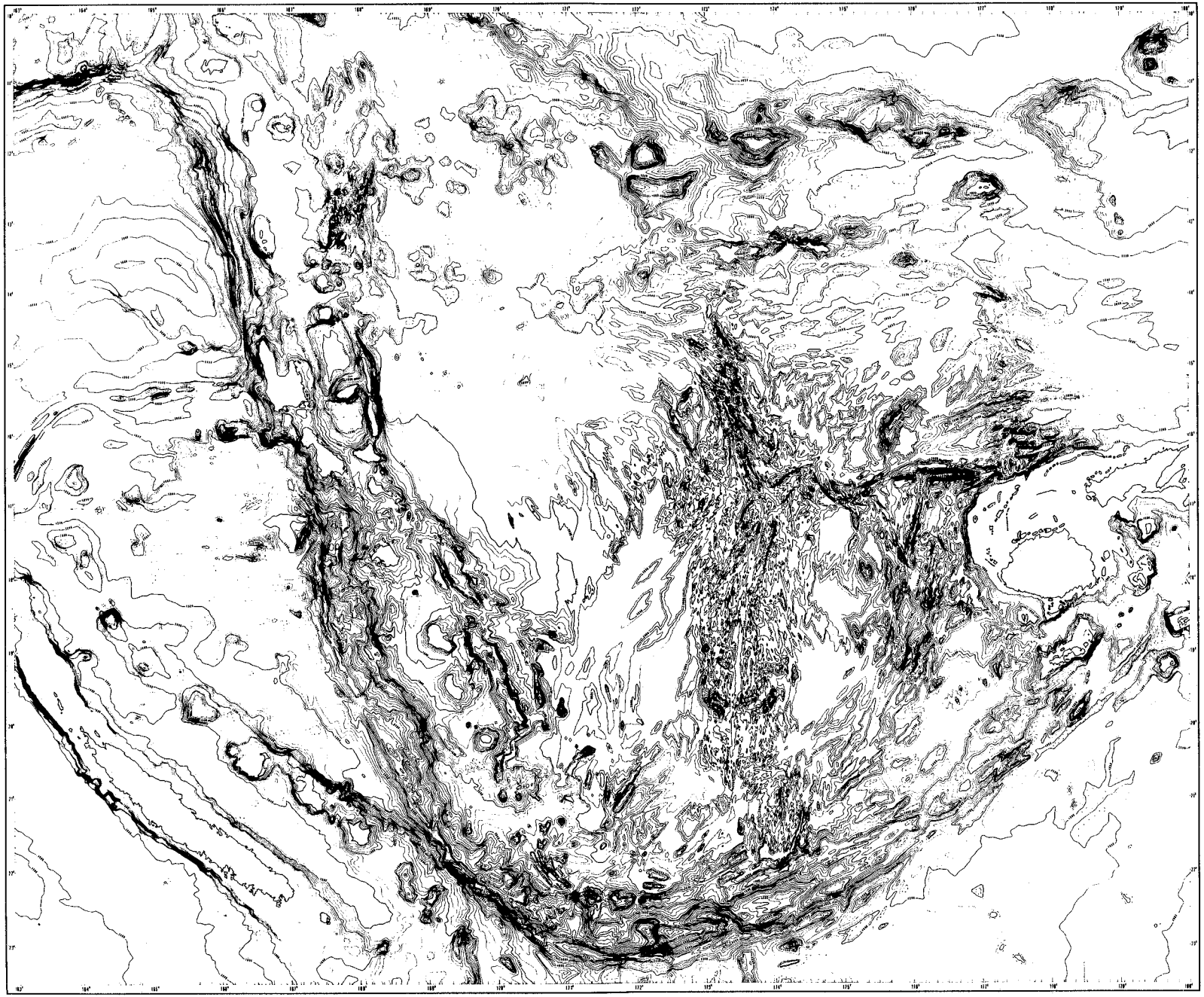

Fig. 5.3. Bathymetric map of the North Fiji Basin. This map results from a compilation made by J.P. Mazé of the whole bathymetric data set until 1993. The contour interval is 200 m (Auzende et al., 1995b).

Seismicity

A swarm of shallow earthquakes (depth < 70 km) are associated along the New Hebrides and the Tonga trenches (Hamburger et al., 1988) and contrast with the diffuse earthquakes located within the inter-arc region, the area between the dashed lines on Figure 5.4a. Shallow earthquake epicentres are aligned along the North Fiji Fracture Zone, and the Matthew-Hunter Fracture Zone.

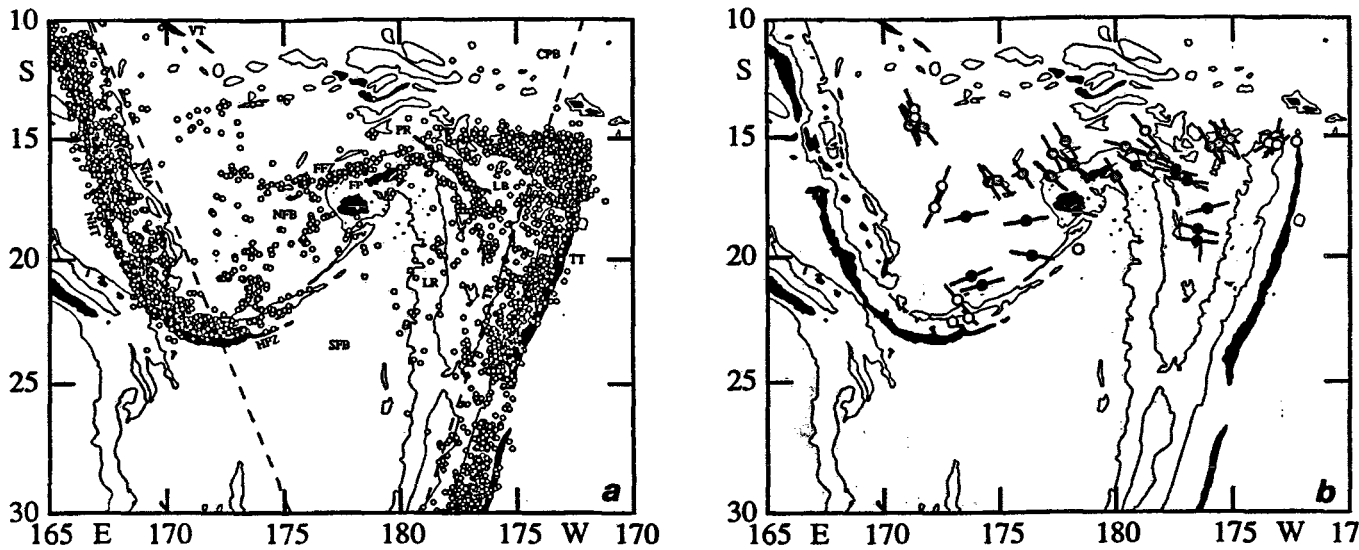

Fig. 5.4. Earthquake distribution and focal mechanism solutions in the inter-arc region of the southwestern Pacific. a) Compilation of well-located shallow events (depth < 70 km) is shown for the inter-arc region (within dashed lines); events along the Tonga and New Hebrides plate boundaries are shown for comparison. Light shading areas > 2 km depth, heavy shading shows areas > 5 km. Bathymetric features: CPB: Central Pacific Basin, FFZ: Fiji Fracture Zone, FP: Fiji Platform, HFZ: Hunter Fracture Zone, LB: Lau Basin, NFB: North Fiji Basin, NHA: New Hebrides Arc, NHT: New Hebrides Trench, PR: Peggy Ridge, SFB: South Fiji Basin, TR: Tonga Ridge, TT: Tonga Trench, VT: Vityaz Trench. b) Summary of focal mechanism types. Earthquake types are defined by consistent orientations of principal stress axes. Heavy bars indicate horizontal projections of mechanism tension (T) axes. Shaded circles: Type-1 events; Filled circles: type-2 events. Other mechanisms are shown by open circles (Hamburger and Isacks, 1988).

The central part of the North Fiji Basin is characterized by a concentration of earthquakes in discrete areas. This is interpreted as related to the present-day accretionary systems (Malahoff et al., 1982a; Louat and Pelletier, 1989). The focal mechanisms in the inter-arc region fall into two groups (Hamburger and Isacks, 1988): type-1 earthquakes, close to and north of the Fiji Platform are defined by NE-trending compression (P) axes, NW-trending tension (T) axes and nearly E-W fault planes, and type-2, south of Fiji, defined by E-W T axes, N-S P axes, and NW- and NE-striking fault planes (Hamburger and Isacks, 1988). Both fault planes are interpreted in

terms of relative left-lateral strike-slip motion between the Pacific and Indo-Australian plates. Thus, Hamburger and Isacks (1988) based only on this seismic data erroneously claimed that there are no steady-state spreading centres in the North Fiji Basin, but only diffuse extensional zones located within a wide strike-slip boundary between the Pacific and Indo-Australian Plates.

Deep earthquakes are associated with the present-day location of subduction zones. Thus, the New Hebrides Trench, site of eastward subduction of the Indo-Australian Plate, marks the surface trace of a Wadati-Benioff zone dipping steeply (about 70°) towards the northeast (Louat et al., 1982) to a maximum depth of 350 km (Cooper and Kroenke, 1993). The Tonga-Kermadec Trench is the site of the westward subduction of the Pacific Plate. The Tonga-Kermadec subduction zone has one of the deepest (> 650 km) and most active Wadati-Benioff zones of the world. Deep earthquakes (550-650 km) within the North Fiji Basin probably occur in pieces of lithosphere spatially detached from the New Hebrides slab (Cooper and Kroenke, 1993).

Magnetism

The study of magnetic anomalies suggests an age of Late Miocene (10-8 Ma) for the basin with a calculated opening rate of 70 mm/yr (Malahoff et al., 1982a). Paleomagnetic results from Vanuatu and Fiji (Viti Levu Island) indicate a clockwise rotation of the New Hebrides Arc and counterclockwise of the Fiji Platform (Malahoff et al., 1982b). An aeromagnetic survey carried out by the National Oceanographic and Atmospheric Administration (NOAA) in 1979 defined magnetic lineations revealing the structural complexity of the basin (Cherkis, 1980). Magnetic data are fundamental for reconstructions of the basin opening (see section 5.4).

Gravity and seismic refraction

Strong positive free-air anomalies (30 to 50 mGal) have been measured on the basin (Kogan, 1976) corresponding to a geoid anomaly. This anomaly has been interpreted by Larue et al. (1982) as an astenospheric swelling. Seismic refraction data indicate a crustal thickness of 5 to 7 km, and seismic wave propagation indicates a low velocity zone in the upper mantle (7.1 to 7.7 km/s). Both results suggest the formation of the basin by accretionary processes (Larue et al., 1982).

Seismic reflection and sedimentary record

A progressive thickening of the sedimentary cover from the middle of the basin (less than 100 m) to the margins (up to 1200 m), where the sedimentary input is substantial, is observed from seismic reflection data. The sedimentation rate varies from 1 to 5 cm/ky, based on measurements of sediment cores (Chase, 1971). Sediments accumulated across the basin are dominated by the remains of pelagic carbonate, organisms from surface waters and fine volcanic debris from surrounding volcanic centres (Eade and Gregory, 1993).

Heat flow and hydrothermalism

Heat flow values are high in the central North Fiji Basin, reaching 116 mW/m^2 (Sclater et al., 1972; Macdonald et al., 1973; Halunen, 1979). This value is similar to those recorded on mid-ocean ridges (e.g. Sclater and Francheteau, 1970). In the northern part of the basin, north of the Hazel-Holme Ridge (see section 5.3.3), the heat flow values are very low if the volcanism related to the New Hebrides Arc is subtracted (Halunen, 1979). These low values can be related to the age of the crust in this part of the basin or to hydrothermal circulation (Auzende et al., 1995b). Two active hydrothermal sites and several fossil sites have been recognized in the Central Spreading Ridge using deep submersibles (Auzende et al., 1990b, 1991). For more details about these results, see section 7.3.

Petrology

The first petrologic samples of the area were tholeiitic basalts obtained by Hawkins and Batiza (1975) in the central part of the North Fiji Basin (15°30'S-173°30'E). Sinton et al. (1985) recognized the co-existence of at least two different types of lava in the basin: Low potassium MORB (Mid-Ocean Ridge Basalt), similar to the ones found in mid-ocean ridges, and old basaltic lavas enriched with incompatible elements, interpreted as associated with an old spreading centre. More details about the petrologic characteristics of each of the structures within the basin will be developed in next section.

5.3. Structural elements

Several extensional structures and spreading centres have been identified within the North Fiji Basin (Figs. 5.3 and 5.5). However, the most widely explored and known is the Central Spreading Ridge, located in the central part of the basin. The name "central" was firstly given by Brocher and Holmes (1985) to differentiate it from the other structures also present within the basin that have been interpreted as spreading centres or fracture zones, but are smaller or less explored. These features are: the South Pandora and Tripartite Ridges, the Hazel-Holme Ridge, the West-Fiji Ridge and the North-Fiji Fracture Zone (Fig. 5.5). In this section we summarize their main characteristics.

5.3.1. THE CENTRAL SPREADING RIDGE

The Central Spreading Ridge (Figs. 5.3 and 5.5) was locally recognized using sparse magnetic and bathymetric profiles (Chase, 1971; Malahoff et al., 1982a; Maillet et al., 1986), but it was mapped with swath-bathymetry systems for the first time during the Seapso 3 cruise in December 1985 (Auzende et al., 1986a, 1988b). During the French-Japanese STARMER project, the Central Spreading Ridge was completely mapped between 14°30'S and 21°40'S on more than 1 degree width by multibeam bathymetric full coverage (Auzende et al., 1990a; Urabe et al., 1992).

The basalts accreted along the Central Spreading Ridge are predominantly MORB-type, suggesting that is one of the most evolved spreading zones in the North Fiji Basin (Auzende et al., 1988a, b, 1990 and 1991). However, a geochemical backarc signature has been identified on the northern and southern parts of the spreading centre (Eissen et al., 1991 and 1994; Lagabrielle et al., 1994b). Magnetic anomalies indicate that seafloor spreading began at the central part of the ridge about 3 Ma ago. More recently, about 1.5 Ma ago, changes in the geodynamic setting and a successive plate-motion reorganization resulted in the present-day ridge segmentation (Auzende et al., 1988a; Huchon et al., 1994). Multi-channel seismic data show a relatively thin crust, with no evidence for an axial magma chamber reflector (Kisimoto et al., 1994). There is extensive low-temperature hydrothermal activity, in addition to some sites of vigorous high-temperature venting along the Central Spreading Ridge (Auzende et al., 1990b and 1991; Bendel et al., 1993).

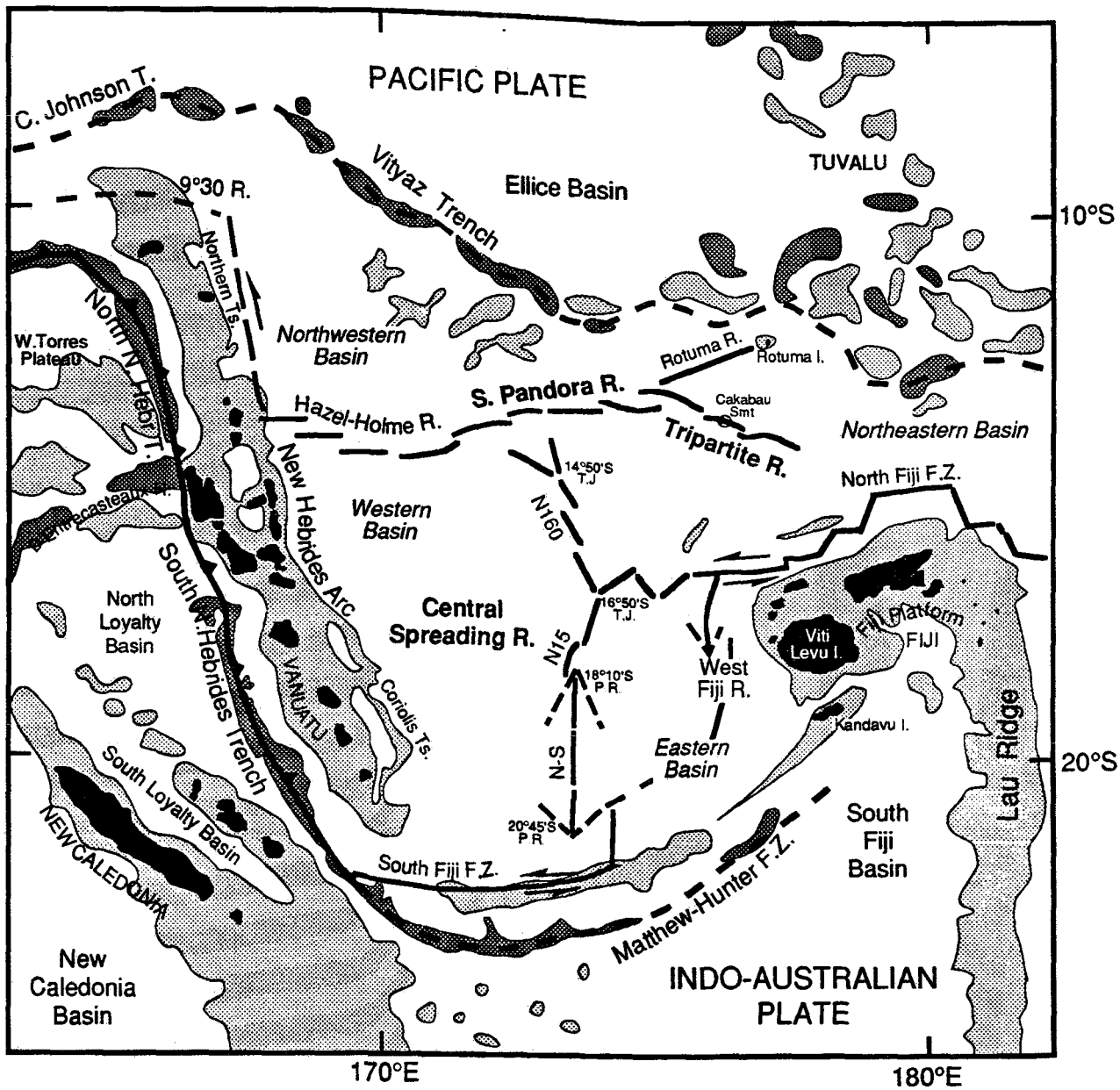

Fig. 5.5. Main structures of the North Fiji Basin. The two study areas: Central Spreading Ridge and South Pandora/Tripartite Ridges are marked by bold letters. Thick lines mark the position of the present-day spreading axis and fracture zones. Islands are in black, shallow areas in light grey, and deep areas and trenches in dark grey. Ck. Smt.: Cakabau Seamount, F.Z.: Fracture Zone, P.R.: Propagating Rift, R.: Ridge, T.: Trench, T.J.: Triple Junction, Ts.: Troughs.

The axis extends along 800 km, is 8-10 km wide, and trends roughly N-S changing in direction to the N160 and N15, north and south of the 16°50'S latitude, respectively. The axial depth ranges between 4300 m and less than 2000 m. Three main segments, N160, N15 and N-S are observed along the Central Spreading Ridge (Auzende et al., 1988a and 1990b; Gràcia, 1992; Gràcia et al., 1992 and 1994; Huchon et al., 1994; Tanahashi et al., 1994) bounded by four main discontinuities (Fig. 5.5).

The 14°50'S triple junction is located at the northern tip of the N160 segment, where three grabens seem to converge (Gràcia, 1992; Gràcia et al., 1992; Auzende et al., 1994a). This triple junction is of RRR type (ridge-ridge-ridge) following the McKenzie and Morgan (1969) classification, and its morphological expression is a deep depression of more than 4000 m (Gràcia, 1992; Gràcia et al., 1992; Auzende et al., 1994a). The 16°50'S triple junction is located at the intersection between the N160 and N15 segments and the North Fiji Fracture Zone (Lafoy et al., 1990; Jarvis and Kroenke, 1993). This triple junction is of RRF type (ridge-ridge-fracture zone) following the McKenzie and Morgan (1969) classification, and its characterized by a broad and large dome reaching the shallowest point of the Central Spreading Ridge (1800 m). The 18°10'S propagating rift occurs at the northern tip of the N-S segment where a clear V-shape structure is observed. The N15 failing rift retreats progressively whereas the N-S segment propagates northwards (De Alteriis et al., 1993; Ruellan et al., 1994). De Alteriis et al. (1993) and Tanahashi et al. (1994) also suggested that the N-S segment could be propagating southwards at 20°40'S. The gravity data we present in Chapter 7 confirm this.

5.3.2. THE SOUTH PANDORA AND TRIPATITE RIDGES

The South Pandora Ridge (Fig. 5.5) is located at the northern part of the basin, one of the less explored areas of the North Fiji Basin. It is part of the named "Hazel-Holme Fracture Zone" (Chase, 1971) and corresponds to a broad, complex arch, trending globally E-W, and showing a strong linear fabric. On a previous bathymetric map (Kroenke et al., 1983) it appears as a pair of discontinuous ridges flanking an axial trough and separated by numerous offsets. The strong E-W linear fabric of the South Pandora Ridge was clearly revealed by Sea-MARC (Price and Kroenke, 1991) and GLORIA (Jarvis and Kroenke, 1993; Tiffin, 1993a; Jarvis et al., 1994) side-scan sonar imagery, ran over widely-spaced small surveys.

An active spreading centre in this part of the northern North Fiji Basin was first proposed from the analysis of magnetic anomalies (Lapouille, 1986). Hamburger and Isacks (1990) pointed out that this interpretation was difficult to reconcile with the focal mechanism solutions from earthquakes indicating a dominant strike-slip character along the ridge. The ridge has finally been interpreted as an active spreading ridge (Kroenke et al., 1993b) based on bathymetry and gravity profiles, and freshness of the pillow basalts

dredged (Price and Kroenke, 1991). Towards the east, the South Pandora Ridge bifurcates in two branches, named Tripartite and Rotuma Ridges (Figs. 5.3 and 5.5).

The Tripartite Ridge is an elongated feature, trending N110, which connects to the South Pandora Ridge (Figs. 5.3 and 5.5). It has been interpreted by Kroenke et al. (1993b) as a very young spreading axis. The Tripartite Ridge was sampled and explored in detail only near the region of Cakabau Seamount during the SeaMARC II survey aboard the R/V Moana Wave in 1987 (Price et al., 1990; Price and Kroenke, 1991).

The Rotuma Ridge is a volcanic ridge trending N75, which is shallower than 1000 m. The ridge is bounded by two parallel troughs, 3000 m deep each. Rotuma Ridge consists of an alignment of seamounts but it has not been interpreted as a spreading axis. The Rotuma Island is located at the eastern tip of the Rotuma Ridge. It exposes very fresh alkali-olivine basalts and hawaiite of Late Pleistocene and Recent age (Woodhall, 1987).

5.3.3. THE HAZEL-HOLME RIDGE

The Hazel-Holme Ridge is located on the northwestern part of the basin, at the western end of the South Pandora Ridge (Fig. 5.5). Focal mechanisms show dextral, sinistral, or even compressional motions along this feature (Luyendyck et al., 1974; Halunen, 1979; Hamburger and Isacks, 1988). The segment of the Hazel-Holme Ridge located west of 171°E corresponds to the western part of the "Hazel-Holme Fracture Zone" of Chase (1971), and has recently been surveyed and interpreted as an active extensional zone (Pelletier et al., 1988 and 1993).

Pelletier et al. (1993) describe the ridge as composed of several parallel narrow ridges and troughs trending N80-N90 and extending over a maximum width of 120 km. The troughs are 3500-4000 m deep on average and are bounded by 500 to 1000 m high scarps. West of 168°30'E, the width of the ridge decreases, the lateral troughs disappear, and a unique 2500-3000 m deep trough appears. This trough ends at 168°10'E, where it connects with the northern New Hebrides backarc troughs.

The Hazel-Holme Ridge is seismically active (Louat and Pelletier, 1989). A WNW-ESE seismic belt correlates all along the area between the New Hebrides backarc and the northern tip of the N160 segment of the Central

Spreading Ridge. Concerning the magnetic anomalies, an E-W trending magnetic fabric is associated with the Hazel-Holme Ridge, and interpreted as the present-day opening and extension (Pelletier et al., 1993).

5.3.4. THE WEST FIJI RIDGE

This area is located between the Fiji Islands and the Central Spreading Ridge (Figs. 5.3 and 5.5). Despite the lack of detailed data, in 1967 Sclater and Menard mapped a pair of troughs seismically very active at the western part of the Viti Levu Island (Fiji). They were the first to interpret the area as the result of active seafloor spreading. Later, this spreading centre was also proposed taking into account different parameters, such as magnetism (Chase, 1971; Malahoff et al., 1993), plate reconstructions (Brocher and Holmes, 1985; Kroenke et al., 1993a), and seismicity (Louat and Pelletier, 1989). Auzende et al. (1986b) carried out a swath-bathymetry and geophysical survey in a one-square-degree zone located immediately west of the Fiji Islands. Taking into account structural arguments, Auzende et al. (1986b and 1988a) interpreted the area as a right lateral strike-slip deformation zone, refusing an active spreading axis. Finally, the area has been re-interpreted in terms of propagating rift (Auzende et al. 1993, 1994b and 1995b, c; Huchon et al., 1994). The area of the West Fiji Ridge comprised between 17°10'S and the intersection with the North Fiji Fracture Zone (16°30'S-176°10'E Triple Junction) has been recently surveyed during the German HYFIFLUX cruise (Auzende et al., 1995a), confirming active spreading.

This area is characterized by two overlapping curved grabens separated by a central plateau with sinuous trends. Auzende et al. (1995 a and b) distinguished three domains in the West Fiji Ridge. The Western Domain, is composed by a N-S trending ridge that propagates southward at an overall propagation velocity of about 100 mm/yr, and is bordered by two deep grabens converging to the south (Auzende et al., 1995b). The Eastern Domain is characterized by an axial graben trending N10 abutting on a N150 scarp. The Central Domain shows a fan-shaped succession of highs and lows. The close structural similarities between this area and the 95.5°W Galapagos Propagator (Hey et al., 1986) confirms the interpretation of an active spreading axis (Auzende et al., 1995 b and c).

A NNE-SSW trending line located near 176°E, between 17°S and 20°S underlines the West Fiji Ridge (Auzende et al., 1995c). Events with strike-slip or normal fault type focal mechanism solutions have been detected

(Pelletier and Louat, 1989). Magnetic anomalies also favour active spreading. In the western graben, corresponding to the propagating system, a well defined magnetic Anomaly 1 has been observed. Anomalies 1 and J have been identified on both grabens, and the spreading rates calculated are of 40 to 50 mm/yr (Auzende et al., 1993 and 1995c; Huchon et al., 1994). Free-air gravity anomalies follow the seafloor topography, and West Fiji Ridge anomaly lows are associated with the greater depths and positive anomalies over topographic highs and graben flanks. A V-shaped positive Mantle Bouguer Anomaly associated with the Western Domain, is consistent with the idea of a propagating rift structure (Auzende et al., 1995c).

5.3.5. THE NORTH FIJI FRACTURE ZONE

The North Fiji Fracture Zone (Figs. 5.3 and 5.5) has a major role in the plate tectonic framework of the northern Melanesian Borderland (Auzende et al., 1988b). This structure, located immediately north of the Fiji Platform, marks the site of the present-day southern boundary of the Pacific Plate (Fig. 5.5). Sinistral motion along the North Fiji Fracture Zone was first suggested by Isacks et al. (1969), based upon seismic activity, and was placed into a plate tectonic framework by Chase (1971).

Before the SOPAC-GLORIA side-scan imagery survey, the North Fiji Fracture Zone (Hughes Clarke et al., 1993; Tiffin, 1993b) appeared in most models as an E-W trending simple zone of sinistral shear taking up plate boundary motion from the 16°50'S triple junction of the central North Fiji Basin (Lafoy et al., 1990) to the northern tip of the Tonga Trench (Pelletier and Louat, 1989). Hughes Clarke et al. (1993) detailed the location and orientation of the present-day areas of extension and translation along the North Fiji Fracture Zone. In particular, they determined that northwest of Fiji, the North Fiji Fracture Zone has a sinistral motion whereas in the northern Lau Basin, it is marked by dextral motion (Fig. 5.2). The precise location of the accommodation fault between the two areas is still uncertain. Some pull-apart basins have been observed along the North Fiji Fracture Zone between 177°E and 179°E (Pelletier and Louat, 1989; Jarvis et al., 1994).

5.4. Evolution of the basin

Several models have been proposed to explain the formation and geodynamic evolution of the North Fiji Basin (Chase, 1971; Gill and Gorton, 1973; Dubois et al., 1973 and 1977; Falvey, 1978; Colley and Hindle, 1984; Hamburger and Isacks, 1987; Auzende et al., 1988b). Although each model differs from the others, all the authors seem to coincide in that the North Fiji Basin opened at least 10 Ma ago, in part resulting from the clockwise rotation of the New Hebrides arc and the anti-clockwise rotation of the Fiji Islands after the dismemberment of a unique arc. About 3 Ma ago, a N-S spreading system start functioning in the south of the basin.

Auzende et al. (1995c), based on the recent data acquired on the northern and northwestern parts of the North Fiji Basin, completed the geodynamic evolution model previously proposed by Auzende et al. (1988b). The evolution of the North Fiji Basin is composed of six main phases, illustrated on Fig. 5.6.

Mid Miocene (12 Ma ago)

The Vityaz, New Hebrides, Fiji, Lau and Tonga arc alignment split, and the North Fiji Basin rifting started with the change of subduction polarity from the Vityaz to the New Hebrides system. The main part of the initial arc remained on the southern side of the spreading axis.

Late Miocene (10 Ma ago)

Spreading along a NW-SE axis was synchronous with the clockwise rotation of the New Hebrides arc and the anticlockwise rotation of Fiji Platform. The initial axis located north of Fiji Platform jumped southward between New Hebrides and Fiji. The crust created during this stage is mainly located in the western part of the basin.

Late Miocene (7 Ma ago)

The NW-SE spreading axis stopped and was replaced by an E-W trending spreading centre from the northwestern tip of the basin to the north of the Fiji Platform. This centre correspond to the 9°30'S, and proto-South Pandora Ridge. This opening induced a new subduction zone along the southern limit of the North Fiji Basin.

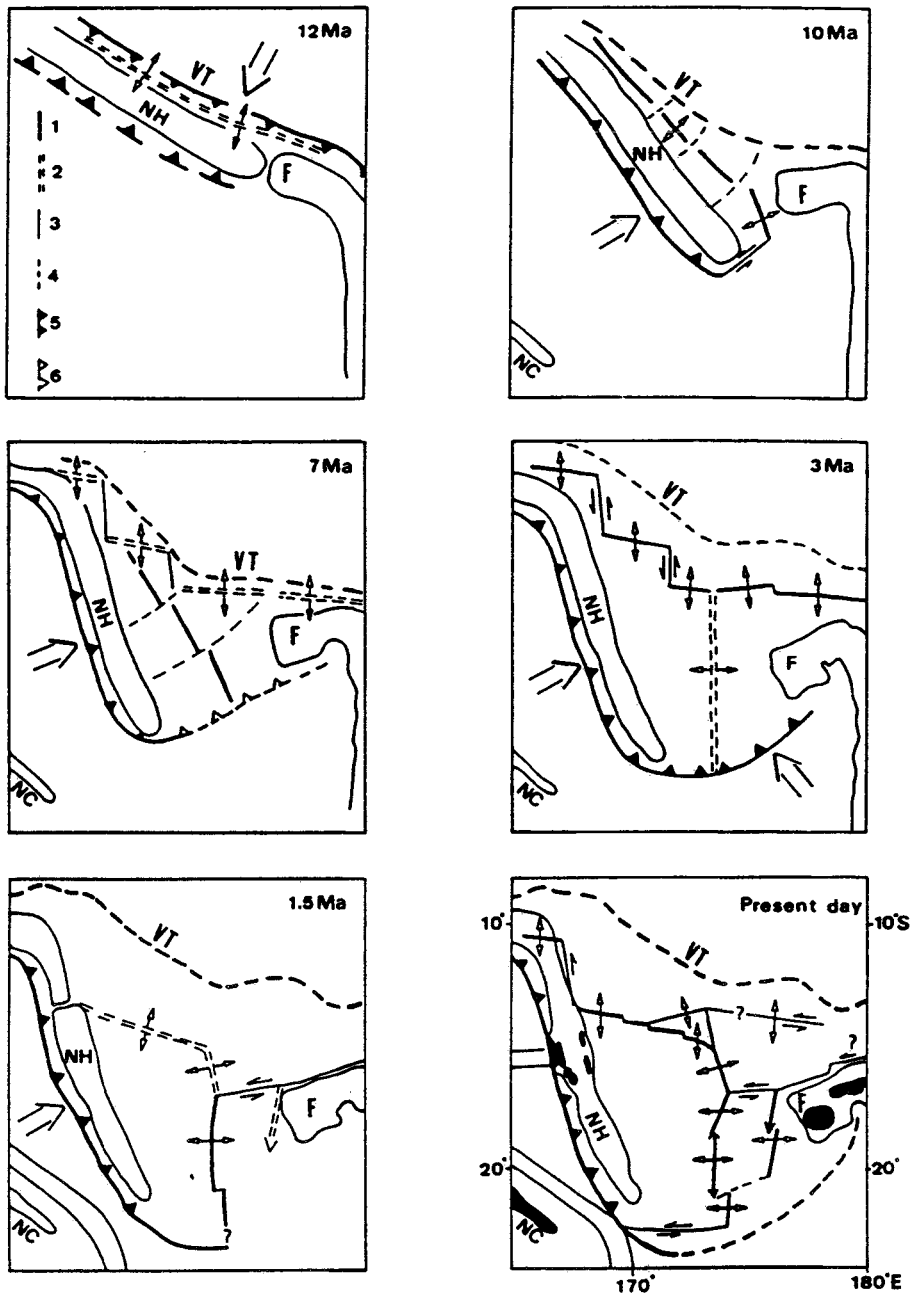

Fig. 5.6. Geodynamic evolution of the North Fiji Basin. 1: active ridge axis, 2: incipient ridge axis, 3: transform fault, 4: flow lines, 5: active subduction zone, 6: incipient subduction zone. VT: Vityaz Trench, NH: New Hebrides Arc, F: Fiji platform, NC: Nouvelle Calédonie (Auzende et al., 1995c)

Late Pliocene (3 Ma ago)

A triple junction was active around 3 Ma ago (Anomaly 2A) between the former E-W axis and the newly created N-S trending spreading centre. At this stage there was a major change in the stress direction from N-S to E-W. This period was synchronous with the beginning of spreading in the Lau Basin.

Pleistocene (1.5 Ma ago)

The opening along the E-W axis was reorganized by the development of the North Fiji Fracture Zone along the Fiji Platform up to the N-S axis, creating the 16°50'S triple junction. The left-lateral strike-slip motion along the North Fiji Fracture Zone induced the change of the direction of the N-S axis at the 16°50'S triple junction. The West Fiji and Hazel Holme Ridges developed to accommodate strike-slip motion along the North Fiji Fracture Zone.

Present-day

The spreading south of the North Fiji Transform Zone is distributed along the parallel Central Spreading Ridge and West Fiji Ridge, isolating an intermediate microplate. To the south, the southernmost spreading axis is connected to the New Hebrides trench by a large left-lateral strike-slip fault. North of the 16°50'S triple junction, opening occurs along the N160 segment and the Hazel-Holme Ridge. Crustal motion probably occurs in the north and the northeastern part of the North Fiji Basin along the South Pandora Ridge and its eastern prolongation. This system is connected with the N160 segment and Hazel-Holme Ridge by the 14°50'S triple junction.

PART III:
DATA AND RESULTS

In this part, we present the data and main results obtained in the three study areas: The Central and Eastern Bransfield Basins in Chapter 6, the Central Spreading Ridge in Chapter 7, and the South Pandora and Tripartite Ridges in Chapter 8.

The chapters are largely similar in organization. In the first section, we present the characteristics of bathymetric, magnetic and gravimetric methods of data acquisition. In the second section we describe the morphostructure of the ridges, focusing principally on three aspects: segmentation, axial morphology and seafloor fabric. The magnetic anomalies, which provide information about the spreading rate and age of the ridge, are then identified. In the final section we describe the free-air gravity anomalies and, where possible, include mantle Bouguer anomaly maps.

In addition to the above, specific results of single-channel seismic reflection data acquired in the Branfield Basin are presented in Chapter 6, while the main results obtained in those areas explored using submersibles in the Central Spreading Ridge are included in Chapter 7.

Chapter 6

THE CENTRAL AND EASTERN BRANSFIELD BASINS

6.1. Data base and methods

The field data described in this chapter were obtained during the GEBRA 93 cruise (Geological Evolution of the BRAnsfield), which took place between 2nd and 24th December, 1993 aboard the Spanish research vessel (R/V) Hesperides. The data consist of full bathymetric mapping of two of the three Bransfield Basins, Central and Eastern, located between longitudes 60°30'W and 54°30'W, and latitudes 61°24'S and 63°10'S (Fig. 6.1). Although, during the last decade, the Bransfield Basin has been the object of several geological and geophysical surveys (see Chapter 2), surprisingly, it had not previously been mapped using modern swath-bathymetry systems. Only a digital compilation of pre-existing data has been published by Klepeis and Lawver (1994) (see Fig. 4.6). In this chapter we present the first, full coverage swath-bathymetric maps of the Central and Eastern Bransfield Basins. Magnetic and single-channel seismic reflection profiles were also acquired (Canals et al., 1994), and are presented here in sections 6.3 and 6.4. No gravity data were acquired during the GEBRA 93 cruise, but in order to complete our data set, we present a free-air anomaly map of the study area obtained from the world satellite-derived gravity data (Sandwell et al., 1994).

6.1.1. BATHYMETRY

Bathymetric data were acquired using the multibeam echosounders Simrad EM-12, 81 beams covering twice the water depth in deep areas, and the EM-1000, 48 to 60 beams covering up to 7 times the water depth in shallow areas. A full coverage of the Central (10,366 km) and Eastern Bransfield basins (3,816 km), totalling a surface of about 14,200 km was produced (Fig. 6.1). The bathymetric survey covered the floors of both basins with 25 and 10 shiptracks, respectively, running NE-SW with a spacing of 2.7 to 3.7 km. Several DTM (see section 1.2.1 for more details) at different grid spacings (200, 400 and 1000 m) were obtained, but only the latter (1000 m grid spacing) is presented in this chapter (see section 6.2).

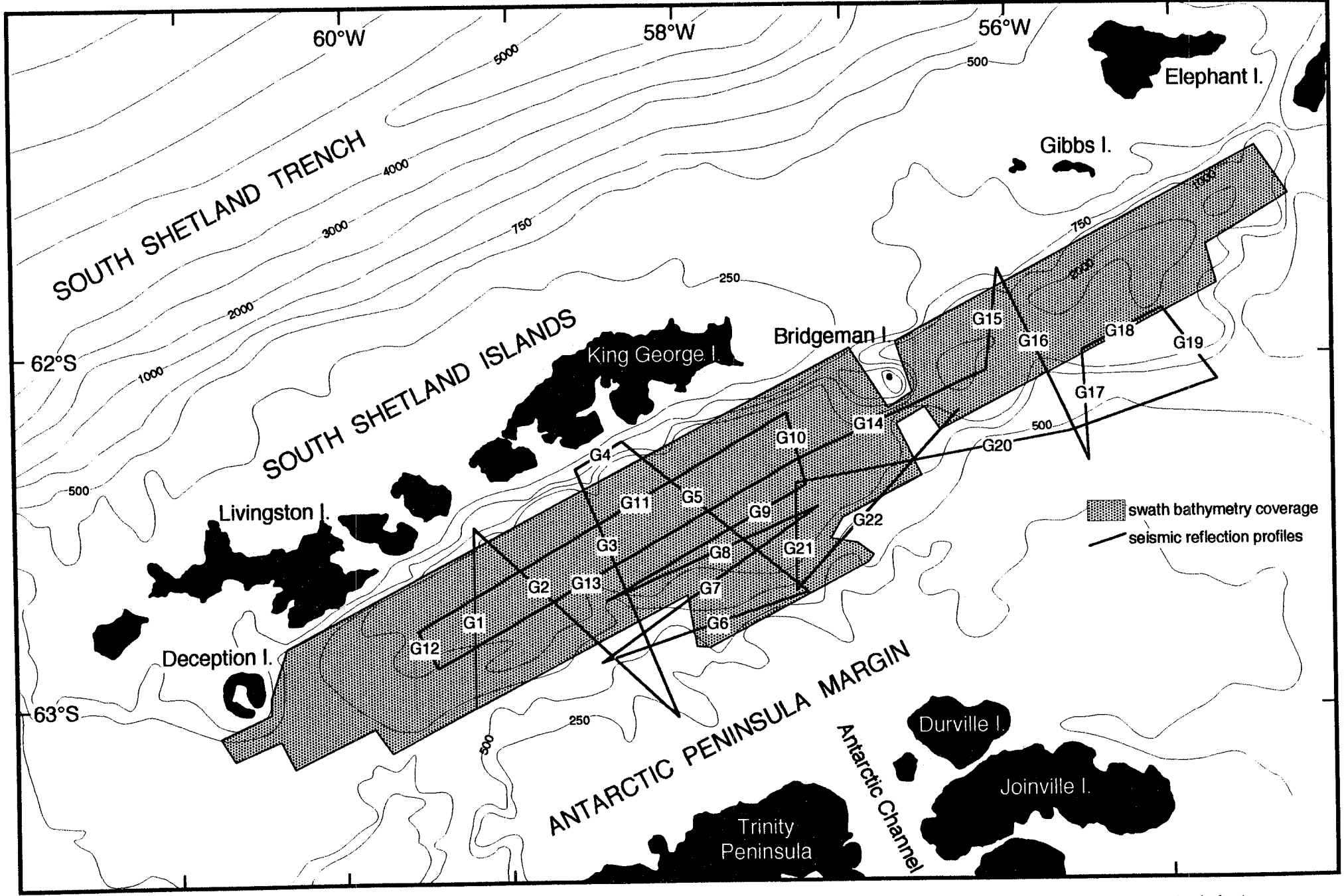

Fig. 6.1. Location map of the swath-bathymetry coverage (shaded box) and seismic reflection and magnetic profiles (numbers 1 to 22) acquired during the GEBRA 93 cruise.

6.1.2. SEISMIC REFLECTION

More than 1500 km (corresponding to 22 lines) of single-channel seismic reflection were recorded during the GEBRA 93 cruise. Longitudinal and transversal basin profiles were taken providing a full coverage of the central basin floor, the outer shelf of the South Shetland Islands and the Antarctic Peninsula margins (Fig. 6.1). Seismic profiles were shot every five seconds with a BOLT 1500 C airgun of 175 cubic inches (2.9 l) at a pressure of 2000 psi. The reflected signals were detected with a SIG 120 three channel streamer with an active section of 150 m. Digital acquisition was carried out with the ELICS Delph 2 system. Simultaneously, the analogic signal was recorded with an EPC 4800 S graphic recorder. Post-acquisition data processing, including bandpass, deco-filtering and scaling was carried out at the Renard Centre of Marine Geology in Ghent (Belgium) using the Delph2 and Phoenix vector processing systems. Most profiles yield a penetration of more than 1 s Two Way Travel Time (TWTT), which was sufficient to reach the basement in the basin and penetrate the Antarctic Peninsula Margin at considerable depths.

6.1.3. MAGNETICS

Together with the seismic reflection data, 22 magnetic profiles were acquired during the GEBRA 93 cruise. Total magnetic field intensity was measured using an EGG-Geometrics proton precession magnetometer towed 200 m behind the vessel.

6.1.4. GRAVITY

Satellite-derived gravity data from the northwest Antarctic Peninsula region have been extracted from the world-wide data grid (see section 1.1) and are presented as the free-air anomaly map of the region. This map enables us to understand better the general geodynamic location of the Bransfield Basin.

6.2. Morphostructure

The analysis and interpretation of the bathymetric maps allows detailed examination to be made of three features: basin segmentation, basin morphology, and the characteristics of the seamount population.

6.2.1. BASIN SEGMENTATION

Morphologically, the Bransfield Basin is composed of three small basins, Western, Central and Eastern, separated respectively by the highs of Deception and Bridgeman islands (Jeffers and Anderson, 1990) as can be observed in Figure 6.2.

A longitudinal bathymetric section along the axial part of the Central and Eastern Bransfield Basins shows a progressive deepening towards the northeast, while Bridgeman Island marks the boundary between the two basins (Fig. 6.3). The Central Bransfield Basin is characterized by a smooth, step-like topography, whereas the Eastern Basin shows both greater topographic roughness and depths (Figs. 6.2 and 6.3).

A detailed analysis of fault scarps and structural lineations from the bathymetric maps of both basins (at 1:250,000 scale) shows two main structural trends: N55-N60 for the Central Bransfield Basin, and N40-N45 for the Eastern Bransfield Basin (Fig. 6.4). A total of 866 directions have been measured, 424 for the Central and 442 for the Eastern Bransfield Basin. These are represented in rose diagrams with a 5° interval and a radius of 20% of the values (Fig. 6.4). Both basins differ greatly in size, morphology, and structure and are described separately below.

Central Bransfield Basin

The Central Bransfield Basin is located between longitudes 60°30'W and 56°50'W, and its along-basin extent is defined by the highs of Deception Island and Bridgeman Island (Fig. 6.2). The Central Bransfield Basin is 60 km wide, 230 km long, and 1950 m deep. A new bathymetric map (50 m isobath contour and 200 m colour change) of the Central Bransfield Basin is presented in Figure 6.5.

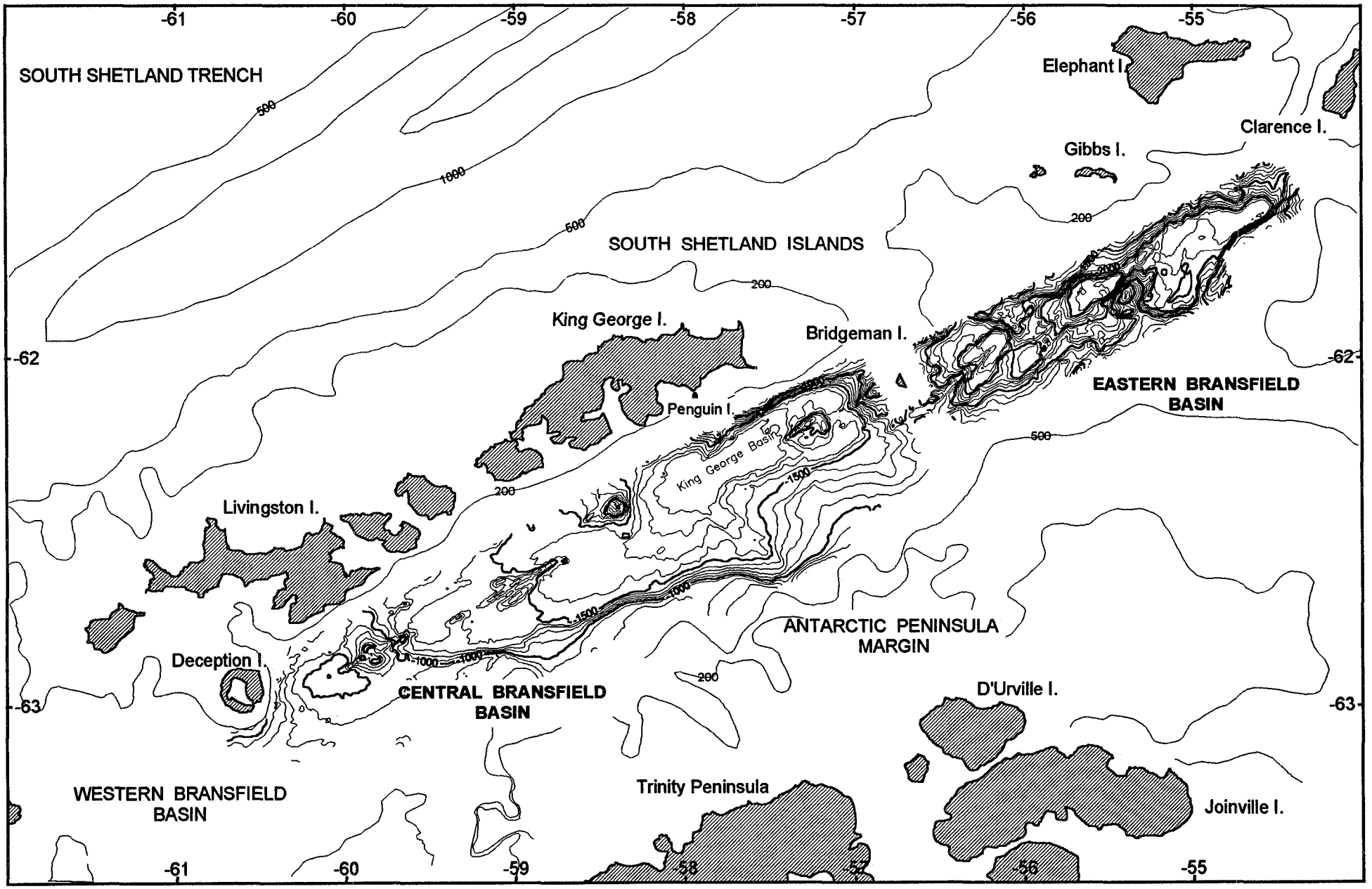

Fig. 6.2. Simplified bathymetric map of the Central and Eastern Bransfield Basins. Isobath contour is 100 m.

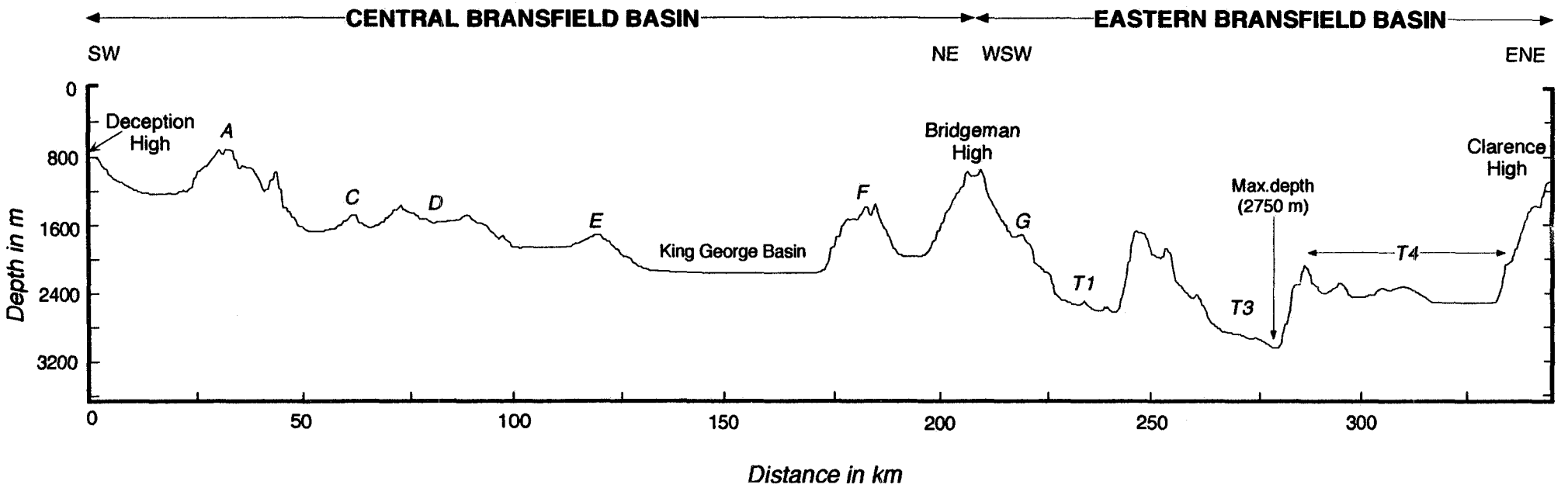

Fig. 6.3. Axial depth profile along the Central and Eastern Bransfield Basins. Edifices A, D, E, F and G, and troughs T1, T3 and T4 are depicted. Note the rough axial topography of the Eastern Basin in comparison with Central Bransfield Basin. Vertical Exaggeration: 20.

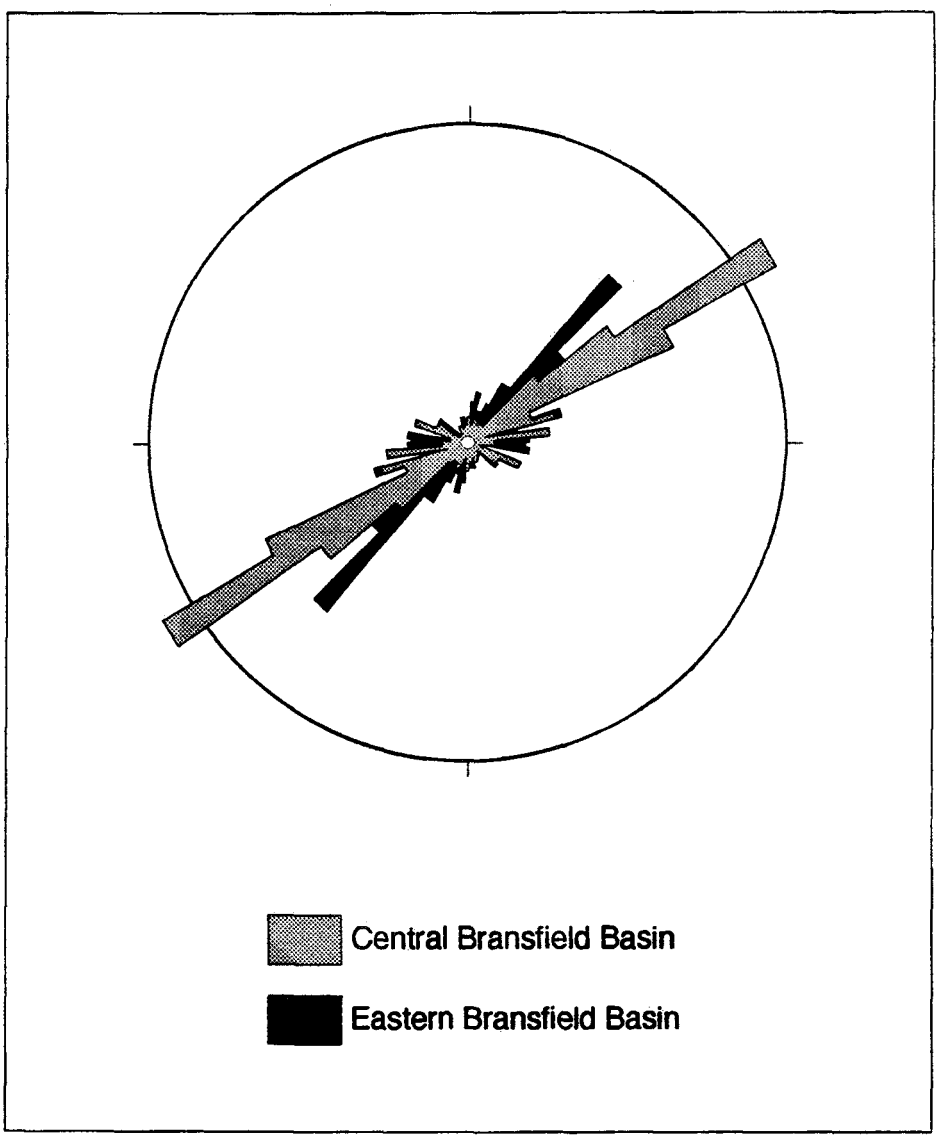

Fig. 6.4. Rose diagrams of the structural trend of lineations and fault scarps measured along the Central (grey) and Eastern (black) Bransfield Basins. Interval: 5°; Radius: 20%.

The margins of the Central Bransfield Basin are asymmetric. The South Shetland margin is steep (between 25° to 30° of maximum slope gradient), rectilinear and narrow, as can be observed along the swath-band surveyed at the northeastern edge of the bathymetric map (Figs. 6.5 and 6.6). This margin is dominated mainly by extensional faulting, with steep normal faults having as much as 4 km of downthrow to the southeast (Ashcroft, 1972). In contrast, the Antarctic Peninsula margin is more irregular and wider, deepening gently (from 8.5° to 3.2° of slope gradient) into the basin through a series of widely-spaced normal faults (Ashcroft, 1972). A 7-8 km wide valley is observed cutting into the slope, from the slope break at 800 m down

to the basin floor. This valley, named GEBRA Valley (Canals et al., 1994) is 30 km long, and is limited by flanks which rise up to 200 m.

A progressive deepening and widening of the basin can be seen towards the northeast. Four different levels are distinguished on the bathymetric map (Fig. 6.5), labelled 1 to 4 on the morphostructural interpretation (Fig. 6.6). The levels are demarcated by morphologic steps trending N145 which are interpreted as faults throwing to the northeast. These faults together with the longitudinally N55-N60 trending faults (Fig. 6.4) define the overall basin structure, and seem to correlate with features observed on land, e.g. on Livingston Island (Smellie et al., 1995) and King George Island (Birkenmajer, 1992). The deepest bathymetric level, level 4, corresponds to the King George Basin, which shows a very flat, thick sedimented seafloor, covering an area 10-18 km wide and 45 km long (Fig. 6.6).

Eastern Bransfield Basin

The Eastern Bransfield Basin lies between longitudes 56°40'W and 54°20'W, and is longitudinally demarcated by the highs of Bridgeman Island and Clarence Island. This basin is 42 km wide, 150 km long, and deeper than 2700 m in its central part (55°30'W) (Figs. 6.2 and 6.3).

The Eastern Bransfield Basin is limited to the north by the margins of Gibbs and Elephant Islands, the northeasternmost extension of the South Shetland Islands, and to the south by the Antarctic margin. The margins are more symmetrical than the Central Bransfield Basin margins (Fig. 6.7). The South Shetland margin is also steep and narrow but less linear than its homologue in the Central Bransfield Basin. The Antarctic margin is steep and irregular with a step-like morphology in plan-view poorly smoothed by sedimentation (Fig. 6.8).

6.2.2. BASIN FLOOR MORPHOLOGY

Central Bransfield Basin

The most striking features in the Central Bransfield Basin floor are the several volcanic edifices that rise above the sedimented seafloor (Figs. 6.5 and 6.6). Six large seamounts (labelled A to F) are on the edge of the N145 trending morphologic steps and several small cones have been distinguished. For each large seamount we recorded the longitude, latitude, height, depth (at the seamount top), morphology or shape, length, width, basal area, and the volume was calculated (Table 6.I).

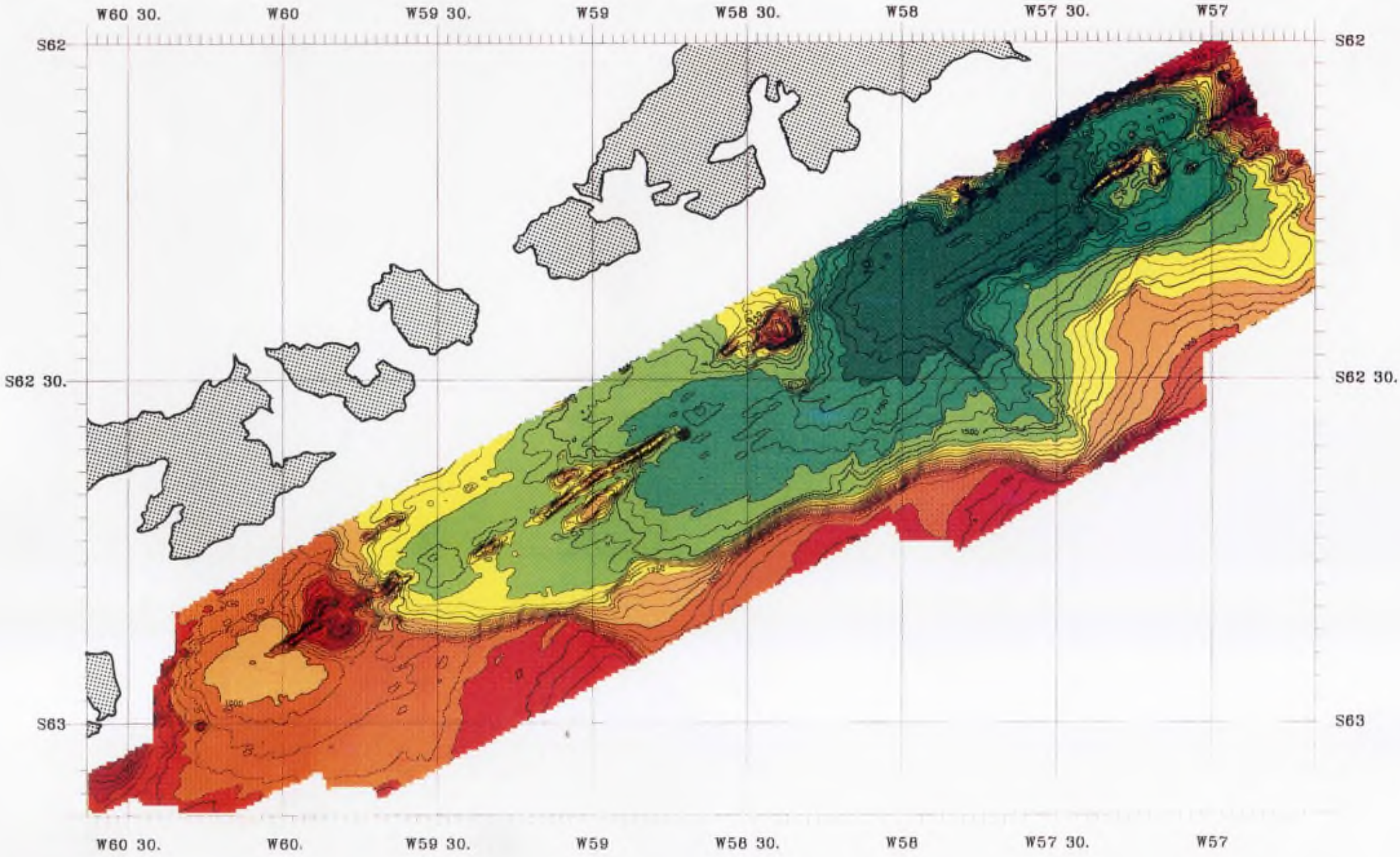

Fig. 6.5. Bathymetric map of the Central Bransfield Basin. Bathymetric contour: 50 m. Colour change: 200 m.

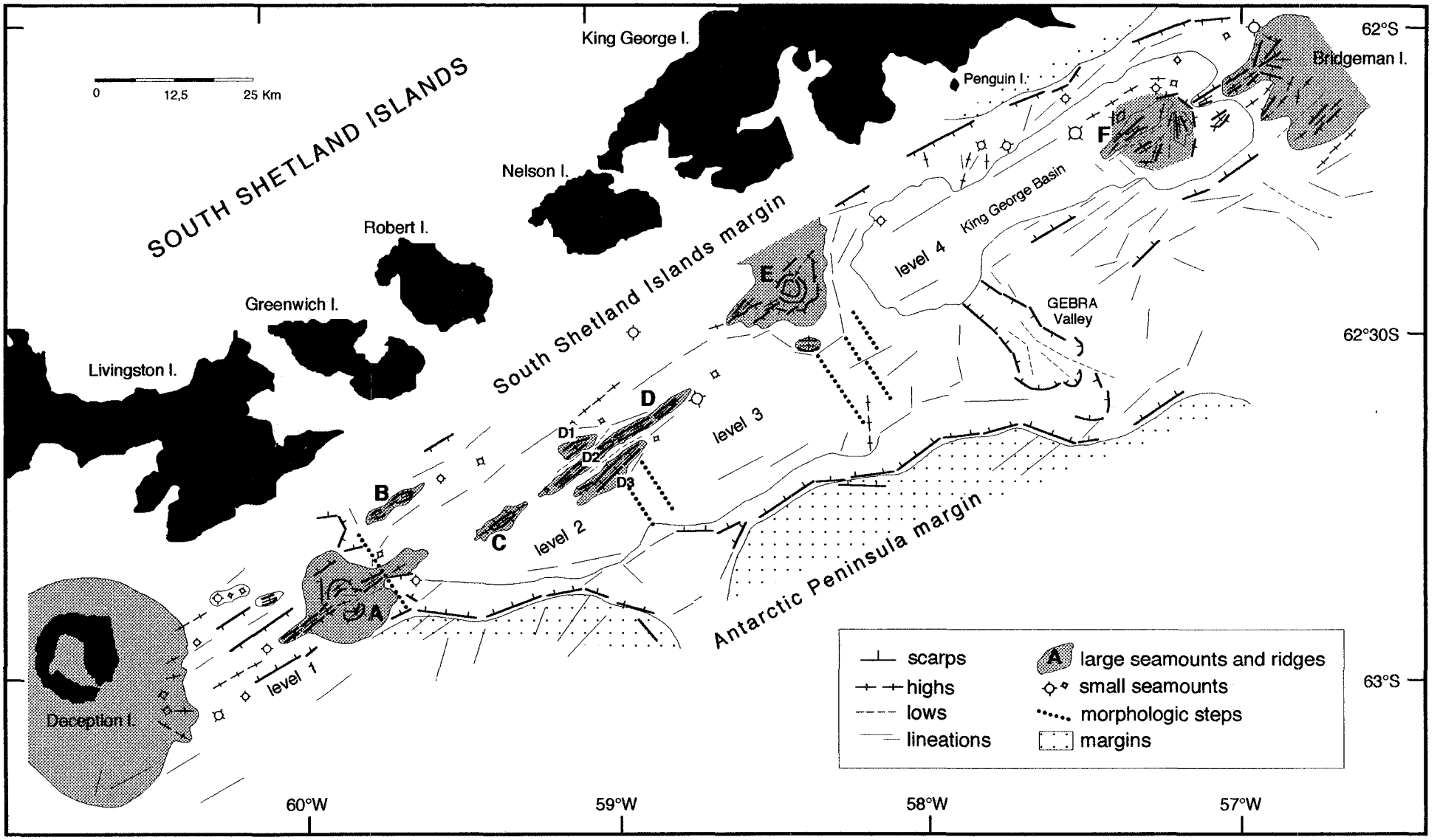

Fig. 6.6. Morphostructural interpretation of the Central Bransfield Basin. Note the six major volcanic edifices and lineaments (A to F), the small scattered volcanoes, and the four basin floor levels (modified from Gràcia et al., 1996a).

Edifice	Long. (W)	Lat. (S)	Height (m)	Depth (m)	Shape	Length (km)	Width (km)	Area (km^2)	Volume (km^3)
A	60°10	62°51.0	550	350	semi-circular	28	16.25	177.69	33282.16
B	59°42	62°42.7	325	1050	elongated	11.25	2.25	12.13	1166.08
C	59°20	62°44.6	250	1200	elongated	10.5	2.75	12.05	1004.16
D 1	59°04	62°38.5	300	1150	elongated	6.25	2.5	13	1300
D 2	59°00	62°38.6	350	1150	elongated	30	2.0	53.69	9395.75
D 3	59°00	62°41.2	300	1150	elongated	15	3.5	38.17	5725.5
E*	58°23	62°25.5	550	650	circular	11	10	114.82	19170.66
F	57°15	62°11.4	550	1150	circular	14.5	7	51.77	12725.75
G	56°35	62°04.1	475	900	elongated	33	5	94.72	22496

*Table 6.I. Main characteristics of the largest volcanic edifices in the Central (A to F) and Eastern (G) Bransfield Basins. *Edifice E corresponds to the ORCA volcano identified by González-Ferrán (1991).*

The seamounts are aligned parallel to the basin axis which is defined by a wide line between Deception and Bridgeman islands. All the volcanic features are concentrated between the South Shetland Islands margin and the basin axis (Figs. 6.5 and 6.6). Only two of the four parallel lines of volcanism suggested by Lawver et al. (1995) (see section 4.2 and Fig. 4.6) are identifiable on the new bathymetric map. Unlike Lawver et al. (1995), our observations suggest that one of the lineations comprises Deception Island, seamounts B, E, and small cones at the northern margin of King George Basin. The other lineation aligns edifices A, C, D and F with Bridgeman Island.

The seamounts present circular, semi-circular and elongated morphologies (Table 6.I and Fig. 6.6). Six cross-sections of the main edifices are shown in Figure 6.9. The largest circular and semi-circular seamounts have basal diameters of more than 16 km and heights of about 550 m, as edifice A, which in turn is similar in size to the emerged part of Deception Island. The flat top cone of edifice A is split by rectilinear faults which separate the two halves by a 3.3 km wide graben, as can be seen in cross-section in Figure 6.9. A discontinuous neovolcanic ridge (2.2 km wide) is found in its central part. Edifice E is another circular seamount with a 400 m deep caldera (Fig. 6.9) and shows few spurs following the main N55-N60 structural trend. Edifice F shows a circular basal area although it is composed of two perpendicular ridges, the main one elongated following the basin trend (Fig. 6.9).

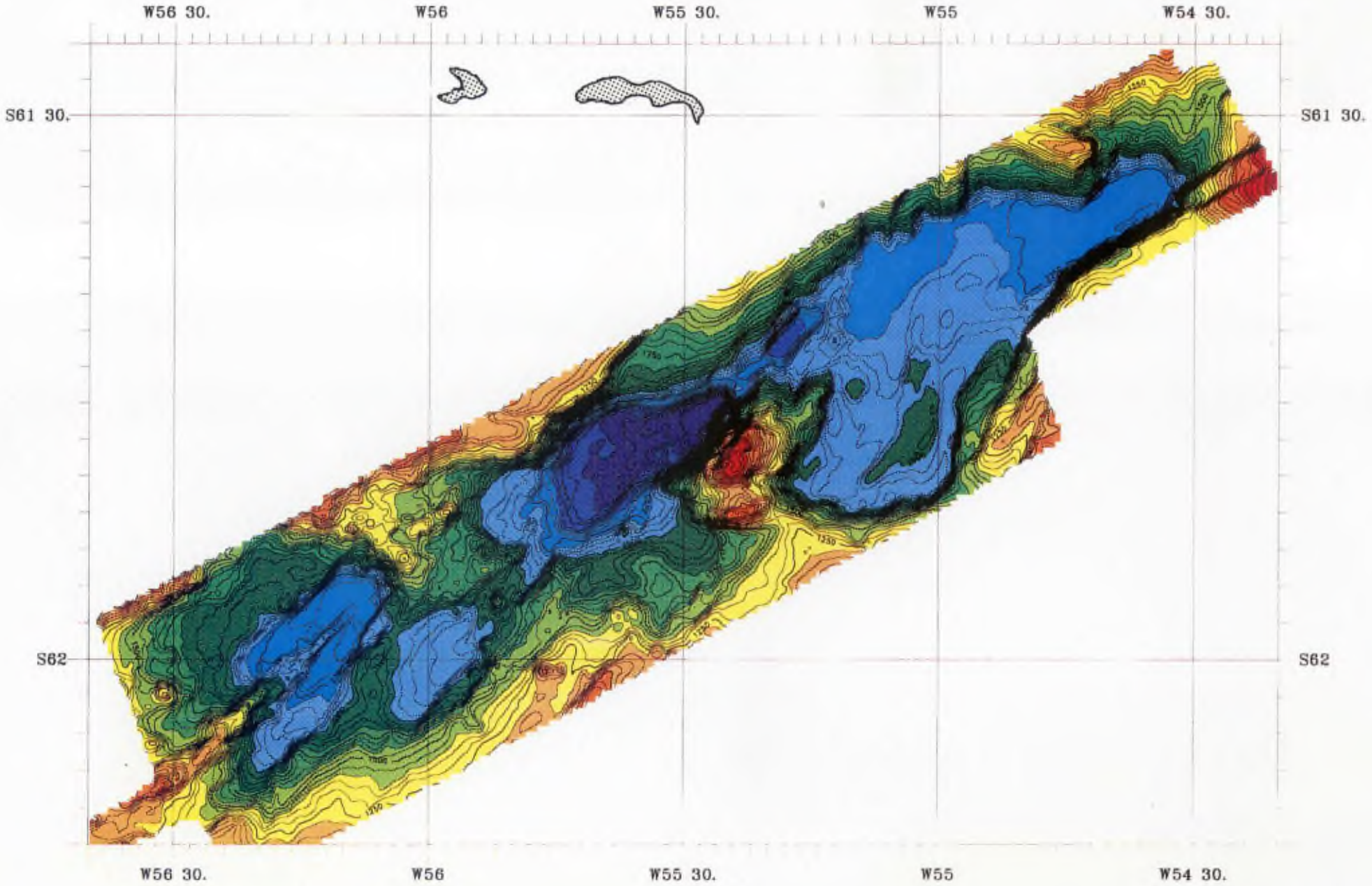

Fig. 6.7. Bathymetric map of the Eastern Bransfield Basin. Bathymetric contour: 50 m. Colour change: 200 m.

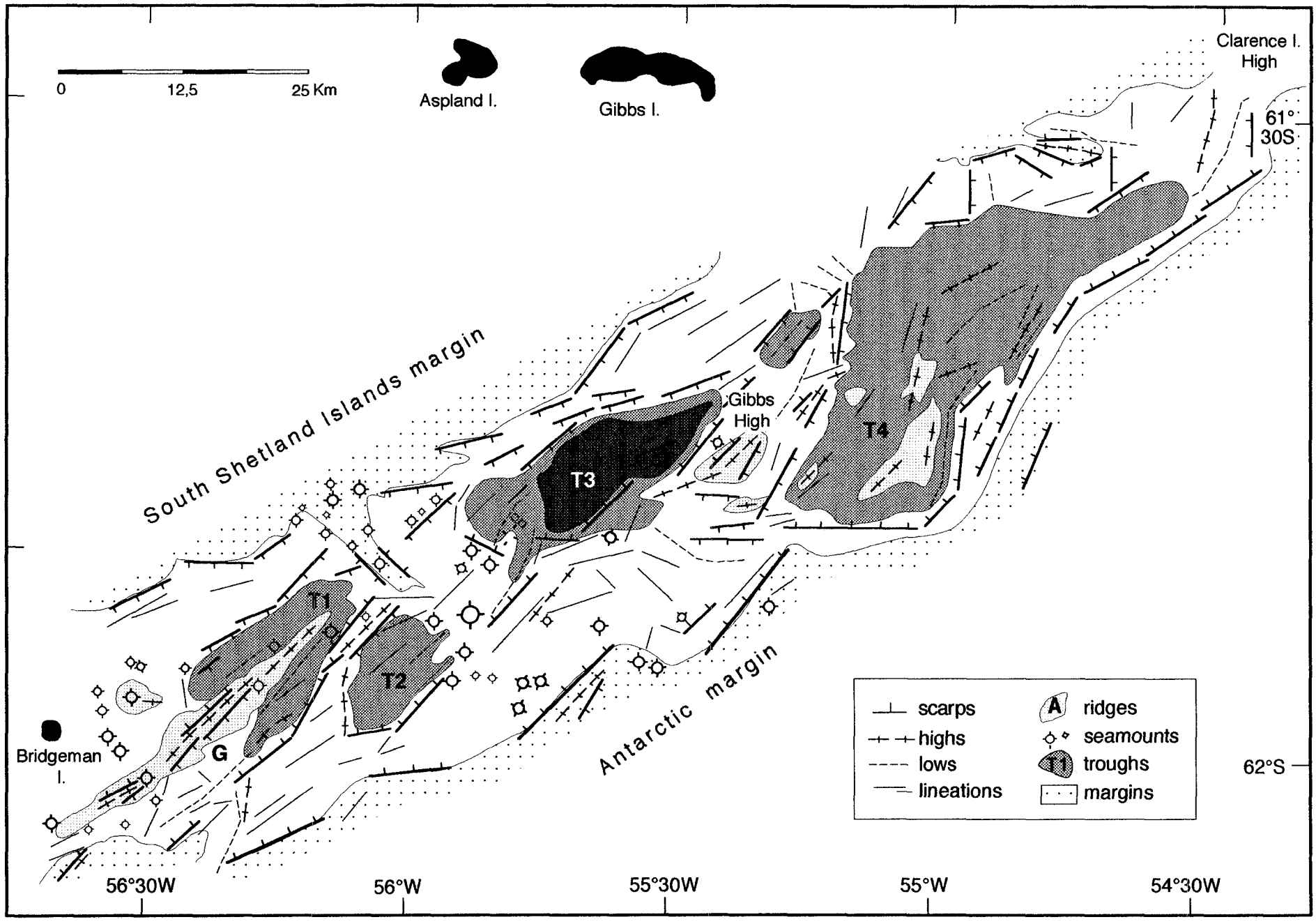

Fig. 6.8. Morphostructural interpretation of the Eastern Bransfield Basin. Note the four lozenge-shaped troughs (T1 to T4), the ridge G, and the scattered volcanoes (modified from Gràcia et al., 1996a).

The ridges (B, C and D) are 10 to 15 km long (reaching up to 30 km at edifice D), 2 to 3.5 km wide, 250 to 350 m high, and also trend N55-N60. Edifice D consists of three parallel features named D1, D2 and D3 (Figs. 6.6 and 6.9). Edifices D1 and D3 have inward facing flanks which are limited by rectilinear faults in contrast to their respective outward flanks which are smoother. This structure suggests that D1 and D3 result from the division of a previous single seamount. Edifice D2 is the neovolcanic ridge formed between the two halves (Fig. 6.9), and in plan-view it can be clearly seen that it is a coalescence of several mound-shaped small structures (Fig. 6.6).

Apart from the large structures, small isolated volcanic cones appear on the basin floor. They have a basal diameter about one sixth (2.5 km on average) of the volcanic edifices described above, but range up to 400 m in height, like the small volcano located at the northeast tip of ridge D2 (Figs. 6.5 and 6.9).

Eastern Bransfield Basin

The morphology of the Eastern Bransfield Basin is dominated by the presence of four deep troughs showing a lozenge shape on the bathymetric map (Fig. 6.7) and labelled T1 to T4, from south to north, on the morphostructural interpretation (Fig. 6.8). Figure 6.10 shows the along-axis variability of the Eastern Bransfield Basin morphology.

The trough T1 is 22 km long, 10 km wide, 2350 m deep, and limited by two steep scarps trending N45, strongly oblique to the basin margins. A neovolcanic ridge labelled G (see Table 6.I), 33 km long, 5 km wide and 475 m high, propagates within the central part of T1 (Figs. 6.8 and 6.10). This ridge shows a N60 trend on its southern part, changing progressively to N45 towards the north.

The trough T2 is located south of T1 and separated by a threshold culminating at 1850 m. The trough is 13,5 km long, 8 km wide, and 2150 m deep. Its southern margin is a very abrupt scarp composed of two rectilinear steps both of which are 200 m high (Figs. 6.7 and 6.8).

The central trough T3 is 25 km long, 11 km wide and more than 2750 m deep. The trough is located in the middle of the basin where the deepest part of the Bransfield Basin is found (Fig. 6.10). In contrast, the nearby structural

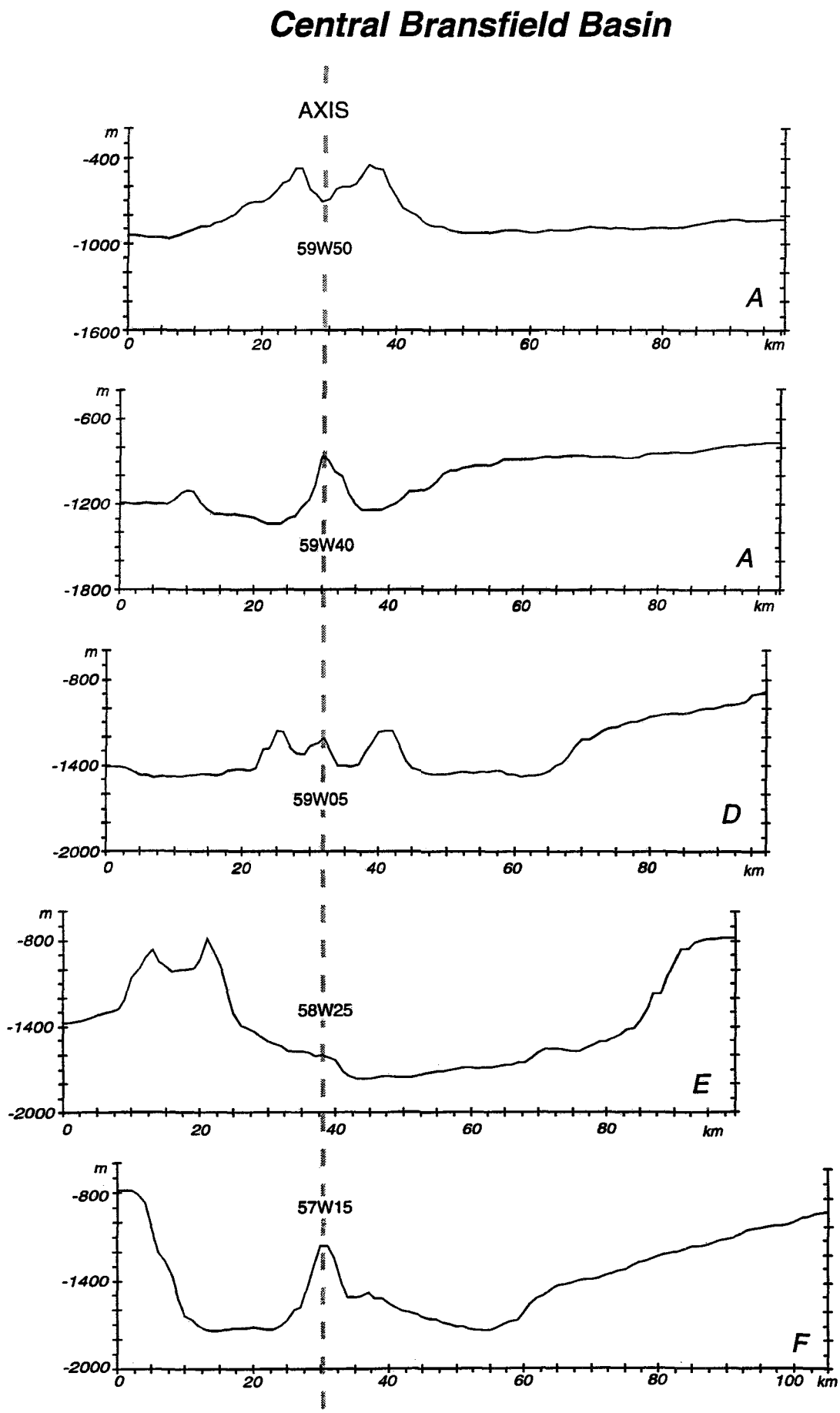

Fig. 6.9. Bathymetric sections across the Central Bransfield Basin. All the sections are taken following a N150 trend orthogonal to the axis. A, D, E and F are the volcanic edifices depicted. Vertical Exaggeration: 5.

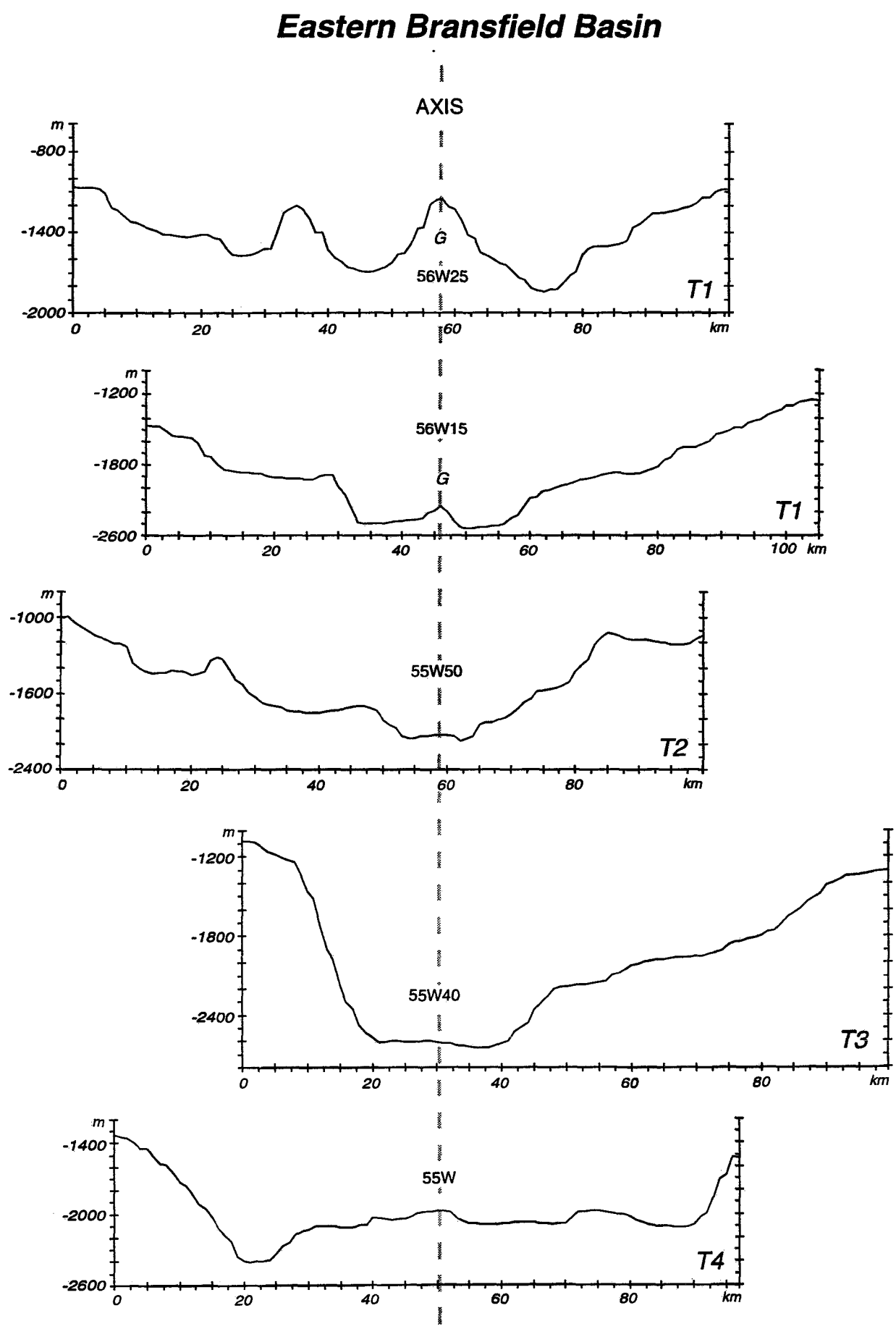

Fig. 6.10. Bathymetric sections across the Eastern Bransfield Basin. All the sections are taken following a N135-N140 trend orthogonal to the axis. T1, T2, T3 and T4 are the troughs depicted. Vertical Exaggeration: 5.

high located at 55°40'W that separates T3 from T4, named Gibbs High, shallows at 700 m.

The trough T4 located at the northern end of the Eastern Bransfield Basin, is 48,5 km long, 17,5 km wide and reaches 2250 m deep. The northern part of T4 shows a flat floor bordered by abrupt flanks (Fig. 6.10). The troughs have steep, linear flanks trending N40-45 and N80-90 (Fig. 6.4), which we assume to be fault scarps.

In addition to the neovolcanic ridge G located at the southwestern end of the basin (Fig. 6. 8), the rest of the volcanism on the Eastern Bransfield Basin is apparent in small scattered volcanic cones which are mainly concentrated on the south-central part of the basin between 56°30'W and 55°30'W. Some of the volcanoes seem to be aligned and trend N20, in a similar way to those between T2 and T3 (Fig. 6.8). The study of these seamounts together with those on the Central Bransfield is explained in more detail below.

6.2.3. SEAMOUNT POPULATION

We used bathymetric maps to study the fine scale volcanic morphology of the Bransfield Basin floor. Seamounts were identified from 25 m contour maps using criteria specified in prior studies (e.g. Batiza, 1982) in which they are defined as topographic highs having a relief greater than 50 m on all sides.

The plan shape of the seamounts was defined by drawing a closed curve, starting at the shallowest point where the base slope breaks and continuing until the feature was circumscribed, as in the work of Smith and Cann (1992) on the Mid-Atlantic Ridge valley floor. The height of the cones and basal areas were measured for each singular edifice to calculate the volumes. Basal area was used rather than basal diameter (as was used for the Pacific and Atlantic seamounts, Batiza, 1982; Smith and Cann, 1992) because the shapes of the edifices are irregular and partly defined by linear trends, instead of being perfectly circular.

We report 122 volcanoes (Table 6.II) of different sizes and morphologies; 119 submarine (39 volcanic edifices of the Central Bransfield Basin and 80 of the Eastern Bransfield Basin) and 3 subaerial (Deception, Penguin and Bridgeman islands).

Height (m)	Number
Submarine volcanoes:	
0-50	1
50-100	44
100-150	31
150-200	12
200-250	10
250-300	7
300-350	8
350-400	1
400-450	1
450-500	1
550-600	2
650-700	1
Total seamounts:	119
Subaerial volcanoes:	
350	Penguin I.
1000	Deception I.
1050	Bridgeman I.
Total volcanoes	**122**

Table 6.II. Observed number of seamounts along the Central and Eastern Bransfield Basins. The data for the subaerial volcanoes are from González-Ferrán (1991).

From the interpretation of the bathymetric maps, three parameters will be discussed in detail: height, basal area, and volume of the seamounts.

Height

There is an exponential decrease in the number of edifices with increasing height (Table 6.II). In the Bransfield Basin up to 37% of the edifices are over 150 m high. In the Central Bransfield Basin (Fig. 6.11) heights are generally evenly distributed except for a concentration around 75-100 m, and two larger peaks between 200-325 m. Three edifices are more than 550 m high; edifices E, F and A. In contrast, in the Eastern Bransfield Basin there is a clear predominance of low edifices (50-125 m) (Fig. 6.11), with only one feature greater than 250 m in relief: ridge G (475 m) (Fig. 6.9).

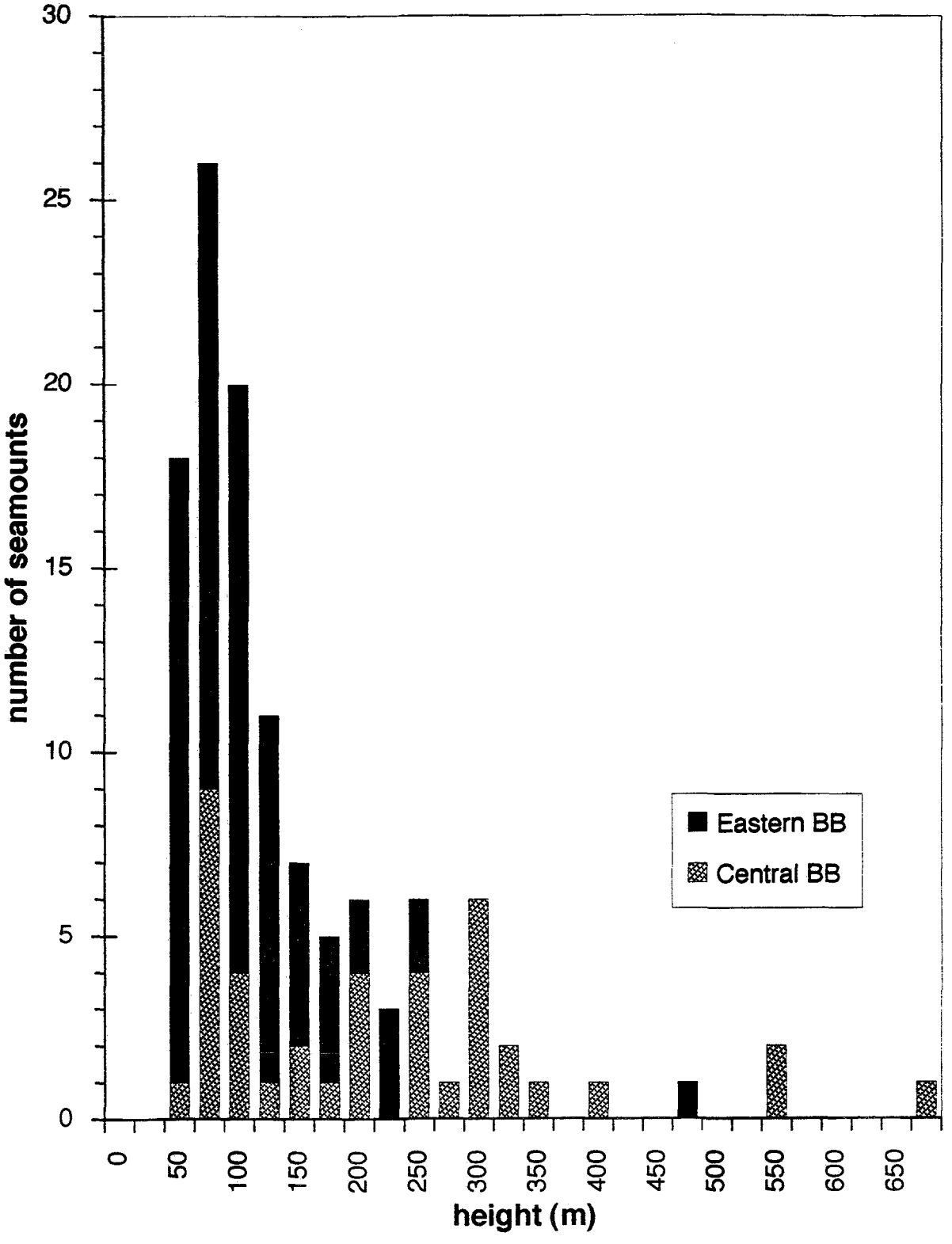

Fig. 6.11. Number of seamounts of the Eastern and Central Bransfield Basin plotted against summit height. Small edifices clearly predominate on the Eastern Bransfield Basin whereas on the Central Basin seamount population is more widely distributed.

Basal area

The basal area has been calculated automatically from the plan-shape of the edifices. The total basal area of the seamounts formed in the Central Bransfield Basin is about 522 km^2 whereas on the Eastern Bransfield Basin it is only around 150 km^2. The relationship between basal area and height is shown in Figure 6.12. Small edifices predominate on the Eastern Bransfield Basin, forming a highly homogeneous population. In the Central Bransfield Basin the seamounts exhibit a less homogeneous distribution with respect to size, the tallest being those with maximum basal area.

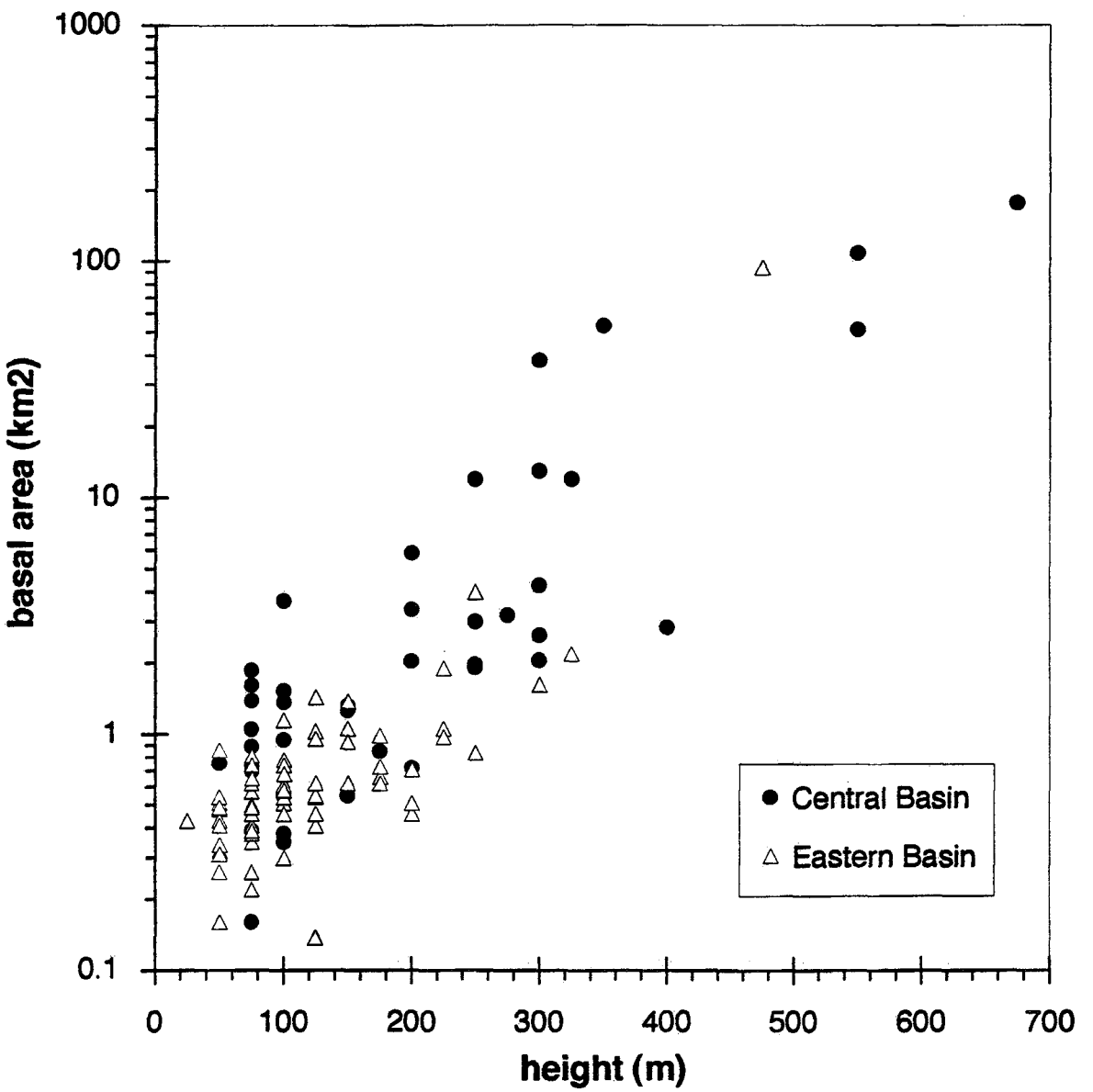

Fig. 6.12. Basal area plotted against height of the seamounts.

Volume

The volume has been calculated from the basal area and the height of the edifices. The total volume of seamounts in the Central Bransfield Basin is 87,000 km^3 while that of the Eastern Bransfield Basin is 25,000 km^3, less than a third of that of the Central Bransfield Basin.

6.3. Seismic reflection

In this section we discuss the main results obtained from the interpretation of seismic reflection profiles. These data are of particular interest in the Central Bransfield Basin due to the presence of a thick sedimentary cover that masks the underlying structure. In contrast, seismic reflection data allow us to identify a thin sedimentary cover on the Eastern Bransfield Basin, which determines its morphology, mainly dominated by structure.

On the seismic lines, we differentiate between acoustic basement, sedimentary cover, and volcanic edifices. They are described individually below.

6.3.1. BASEMENT STRUCTURE

The basement is characterized by a lack of internal reflectors, is highly faulted and arranged in horst and graben structures. The top of the acoustic basement shows a discontinuous, high amplitude and low frequency hyperbolic facies which is sometimes difficult to identify. The top of the acoustic basement is a pronounced erosional truncation (Prieto et al., 1995 and in press).

Central Bransfield Basin

As has been suggested by various authors, the basement of the Central Bransfield Basin seems to be formed by thinned continental crust (Ashcroft , 1972; Birkenmajer et al., 1992; Grad et al., 1992; Guterch et al., 1991) intruded by dykes. The top of the basement near the South Shetland Islands margin is relatively shallow (2 s Two-Way Travel Time) gradually deepening towards the Antarctic Peninsula margin, where it is found at 3-3.4 s (Fig. 6.13a). Along the basin, the basement is strongly faulted and shows a step-like deepening towards the northeast. This deepening is also evident in the bathymetric map as "morphologic steps" (see section 6.1). Across the basin, inward-facing normal faults parallel to the basin axis predominate (Fig. 6.13a). At 57°30'W, and towards edifice F and Bridgeman Island, the basement rises through a series of normal faults. This horst-feature is the threshold which limits the Central from the Eastern Bransfield Basin.

Eastern Bransfield Basin

Although no crustal studies of the Eastern Bransfield Basin have been undertaken, bathymetric data (Figs. 6.7 and 6.8) suggest that the basement may also be formed by thinned continental crust with isolated sills and dykes. The basement reaches a depth of 3 s in the deepest areas of the basin, but it is shallower (1 s) in the shelves. Seismic lines show that basement and volcanics crop out from the middle of the basin floor (Fig. 6.13b). Basement faults are very steep (sometimes almost vertical), and reach the seafloor.

6.3.2. SEDIMENTARY INFILL

The overlying sedimentary sequence is well stratified, of variable thickness, and organized in sedimentary units limited by discontinuities.

Central Bransfield Basin

The basement asymmetry of the Central Bransfield Basin is also reflected in the sedimentary cover, which is thicker near the Antarctic Peninsula margin (reaching 1 s) where sedimentary processes of shelf-progradation dominate, than on the South Shetland margin (less than 0.2 s). Several sedimentary terraces, some of which show ice scours, are found at different depths on the Antarctic margin (700-800 m and 1000-1100 m). Two major sedimentary sequences have been identified along the Antarctic Peninsula margin (Prieto et al., 1995 and in press) (Fig. 6.13):

- The lower sequence lies directly over the basement showing stratified, semitransparent seismic facies with reflections whose continuity and amplitude increase basinward. The top of the lower sequence is an erosional truncation surface.

- The upper sequence is a complex sedimentary sequence composed of several seismic units, classified in upper-slope prograding units and basinal units. The prograding units were formed during episodes of advanced ice-sheets, whereas the basinal units correspond to interglacial periods (Prieto et al., 1995 and in press).

The lower and upper sequences correspond to the tectonized syn-rift sequence (related to the basin opening), and an overlying post-rift sequence, respectively (Gamboa and Maldonado, 1990; Barker et al., 1991; Prieto et al., 1995). Both sequences are separated by the break-up discontinuity. For more

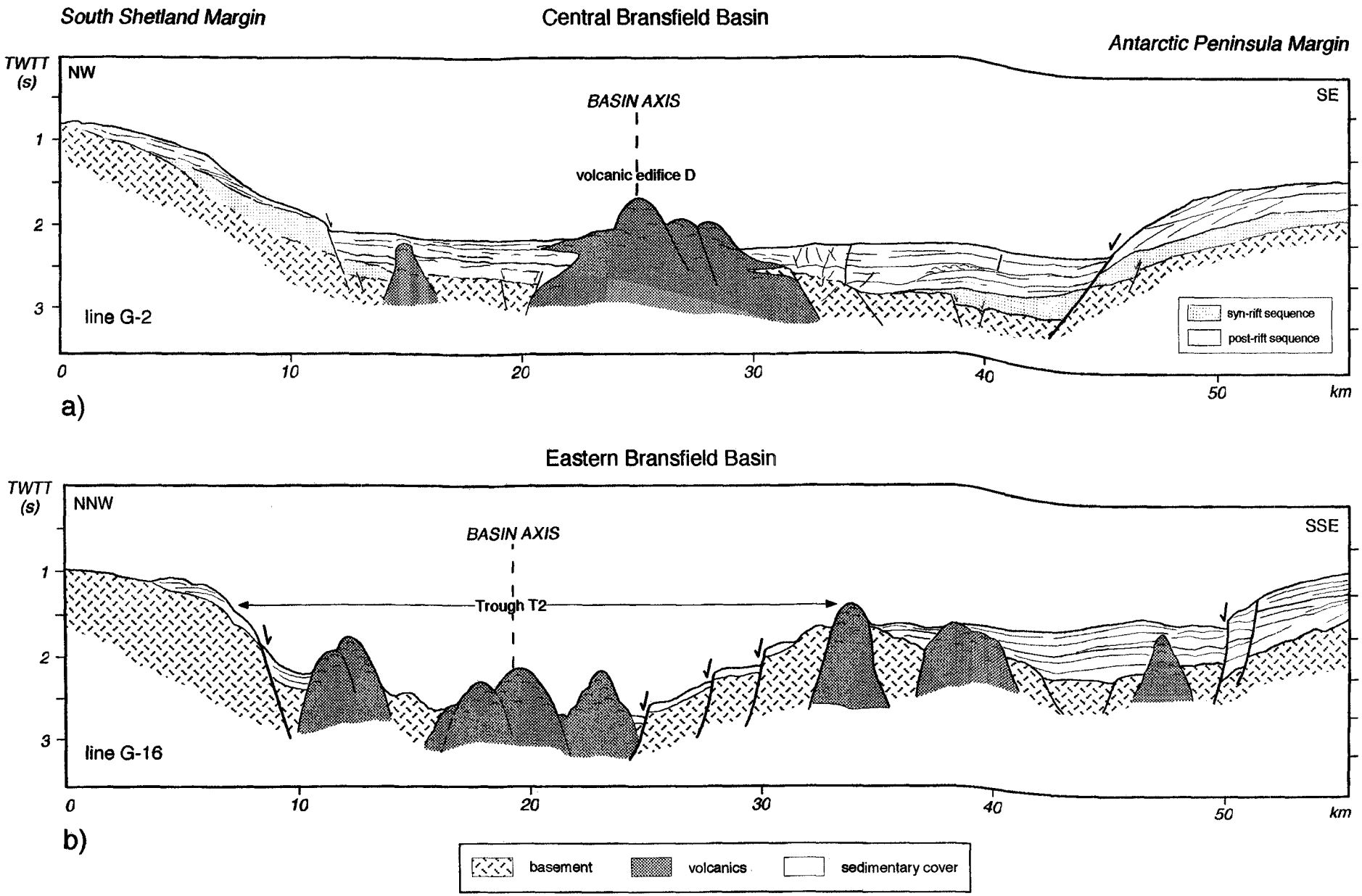

Fig. 6.13. a) Line-drawing corresponding to the interpretation of seismic profile G-2 across the Central Bransfield Basin. b) Line-drawing corresponding to the interpretation of seismic profile G-16 across the Eastern Bransfield Basin. See location lines on Figure 6.1.

details about seismic stratigraphy based on the interpretation of GEBRA 93 lines, see Prieto (1996).

Two elements determine the sediment distribution in the Central Bransfield Basin: differences in sediment supply and the presence of volcanic edifices. It seems that sedimentation in the Bransfield Basin is mainly dominated by glacial-marine processes (Jeffers and Anderson, 1990) and that sediment supply coming from the Antarctic Peninsula is greater than on the South Shetland Islands margin. Moreover, seamounts may be a local obstacle to the homogeneous distribution of sediment, but contrary to what Jeffers and Anderson (1990) suggested, they do not seem to constitute a real sedimentary barrier because the neovolcanic ridge is not a continuous feature.

Eastern Bransfield Basin

On this basin, the sedimentary cover is only observed along the continental shelves (Fig. 6.13). On the Antarctic Peninsula margin the sedimentary cover is relatively well developed (0.5 s), whereas on the South Shetland margin when it is present the cover is thin (0.2 s). Sediment supply on the Eastern Bransfield Basin is small due to the great distance separating it from the Antarctic Peninsula. This low sedimentary infill makes it almost impossible to recognize the two sequences (syn-rift and post-rift) found on the Central Bransfield Basin. Near the Antarctic Peninsula margin, sediments may be disturbed by intrusions which protrude through the sediment (Fig. 6.13b).

6.3.3. VOLCANIC EDIFICES

The volcanic edifices show chaotic seismic facies, with very low continuity and high frequency reflections in both basins. Bordering the edifices some faults can be identified. In the Central Bransfield Basin, interstratified lava flows, forming horizontal layers with flat or undulated morphologies, are observed (Fig. 6.13a) and attributed to batches of volcanic material (Prieto et al., in press). In the Eastern Bransfield Basin, in addition to the volcanic edifices cropping out from the middle of the troughs, there are some off-axis volcanic knolls partially buried by the sedimentary cover (Fig. 6.13b).

6.4. Magnetic anomalies

The magnetic anomaly map (Fig. 6.14) is a compilation of the data obtained during the GEBRA 93 cruise plus some lines obtained by Kim et al. (1992). The map shows a pronounced positive alignment referred to here as the Bransfield Rift Anomaly.

On the Central Bransfield Basin, this positive anomaly is characterized by its short wavelength and high amplitude (300-400 nT) and correlates well with the submarine volcanic edifices. In some places, it reaches values of more than 500 nT, e.g. near seamount A northeast of Deception Island (Fig. 6.14). Axial magnetic highs of profiles G1 and G2 (Figs. 6.1 and 6.14) are centred over the neovolcanic ridge of edifice D (D2). Edifice E, south of King George Island margin, and edifice F, at the northeastern end of the basin, also show highly positive associated magnetic peaks.

On two magnetic lines crossing the Eastern Bransfield Basin, a low amplitude positive anomaly correlates with the basin axis (Fig. 6.14). This anomaly may be associated to the ridge G cropping out from the southwestern edge of the basin. The only magnetic profile crossing the Western Bransfield Basin (Kim et al., 1992) (Fig. 6.14) also suggests the existence of isolated volcanic features south of Snow Island.

The Bransfield Rift Anomaly can be interpreted as forming part of the axial Central Anomaly or Anomaly 1 (0-0.71 Ma) following the magnetic reversal time scale of Harland et al. (1990). This normal polarity event is clearly related to an ongoing phase of extension and associated volcanism. In contrast, there is a long wavelength and high amplitude positive anomaly over the Antarctic Peninsula margin. This anomaly may be associated with either deep magnetic sources corresponding to the crystalline basement, as proposed by Kim et al. (1992), or with fault-controlled intrusions. Considering an oceanic origin for the Bransfield Rift Anomaly, and interpreted as the axial Central Anomaly, we may suggest a maximum age of 0.71 Ma for the beginning of spreading in the Central Bransfield Basin. The maximum full spreading rate, calculated from the magnetic anomalies, would be about 0.83 mm/yr at 59°W, suggesting an ultra-slow spreading rate, quite constant along the basin.

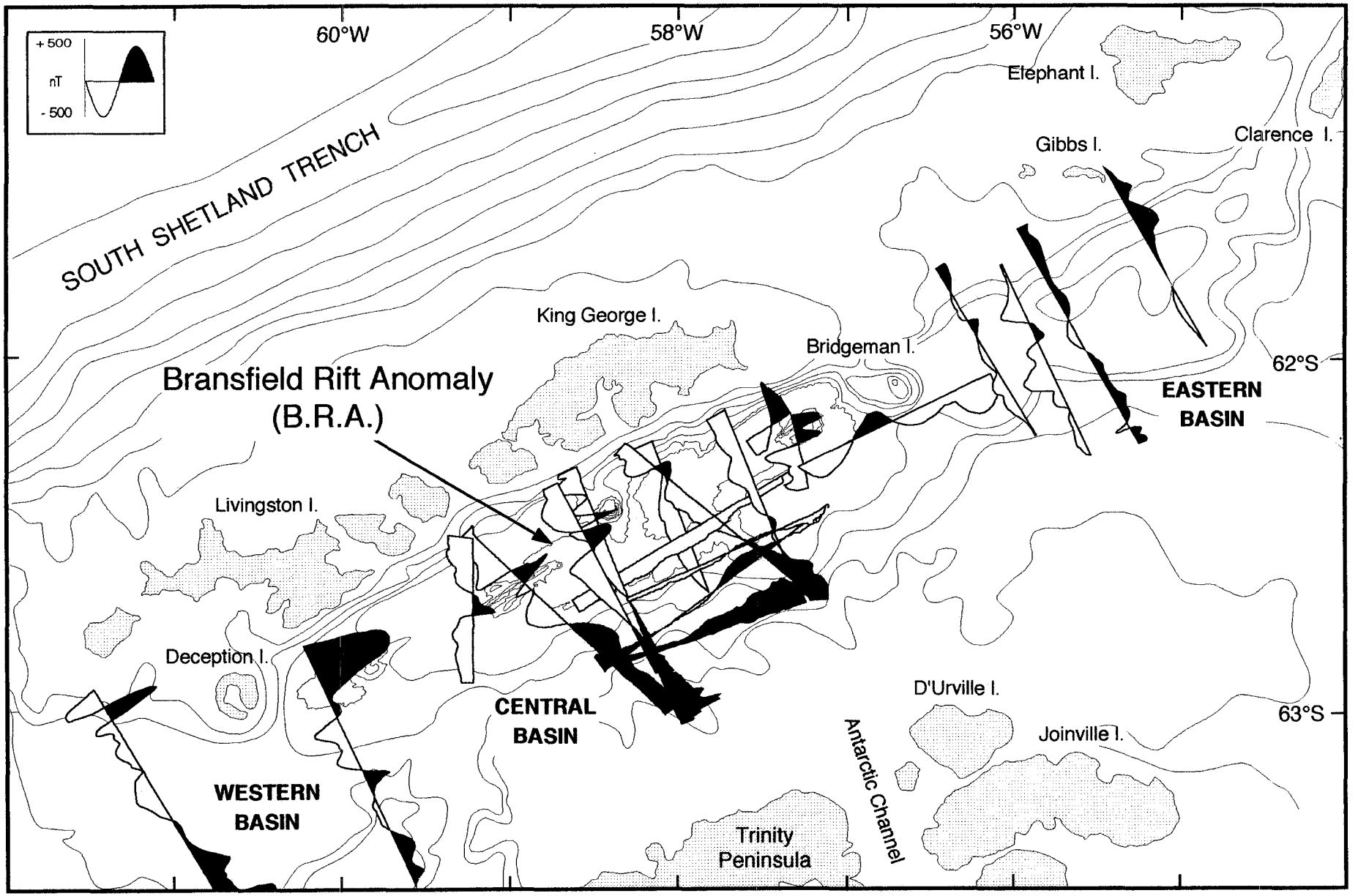

Fig. 6.14. Magnetic anomaly map of the Central and Eastern Bransfield Basins. Note the Bransfield Rift Anomaly interpreted as the Central Anomaly or Anomaly 1 (0-0.71 Ma). Compilation of magnetic data from the GEBRA 93 cruise and Kim et al. (1992).

6.5. Gravity anomalies

A 2 mGal contour satellite-derived free-air gravity map of the area between longitudes 67°W-43°W, and latitudes 58°S-64°S is presented in Figure 6.15. The free-air anomaly is dominated by the seafloor topography, and the map can thus be seen as a morphological map of the region. Red and orange colours correspond to gravity highs and blue and purple correspond to gravity lows.

The three basins forming the Bransfield Basin (Western, Central and Eastern) are clearly visible in Figure 6.15, as they show negative gravity lows (0 to -20 mGal), and are limited by the positive gravity anomalies produced by Deception and Bridgeman islands. The Western Bransfield Basin would seem to be connected to the South Shetland Trench via a narrow curved passage which separates Smith and Low Islands from the rest of the South Shetland Islands. The largest axial seamounts of the Central Bransfield Basin (A, D, E and F) are distinguishable in Figure 6.15. This provides additional evidence in support of the existence of these submarine features. Troughs T1, T3 and T4 of the Eastern Bransfield Basin are also shown in Figure 6.15, and are characterized by the largest negative anomalies of the three Bransfield basins (reaching up to -40 mGal), which also correlate with the maximum depths.

The South Shetland Trench shows an important negative anomaly of -130 mGal, whereas the South Shetland Islands show a positive anomaly of 100 mGal. The Shackleton and Hero Fracture Zones which delimit the Bransfield Basin to the north and south, respectively, are well marked by positive anomalies up to 80 mGal at the Shackleton Fracture Zone (Fig. 6.15). The present-day inactive Phoenix-Antarctic ridge, together with the fracture zones segmenting the spreading centre, are also well marked on the free-air anomaly map by positive anomalies up to 40 mGal.

East of Elephant Island, the South Scotia Ridge may be clearly identified by the presence of two ridges, the northern reaches 140 mGal and the southern reaches, 110 mGal. The ridges are separated by a deep narrow valley,

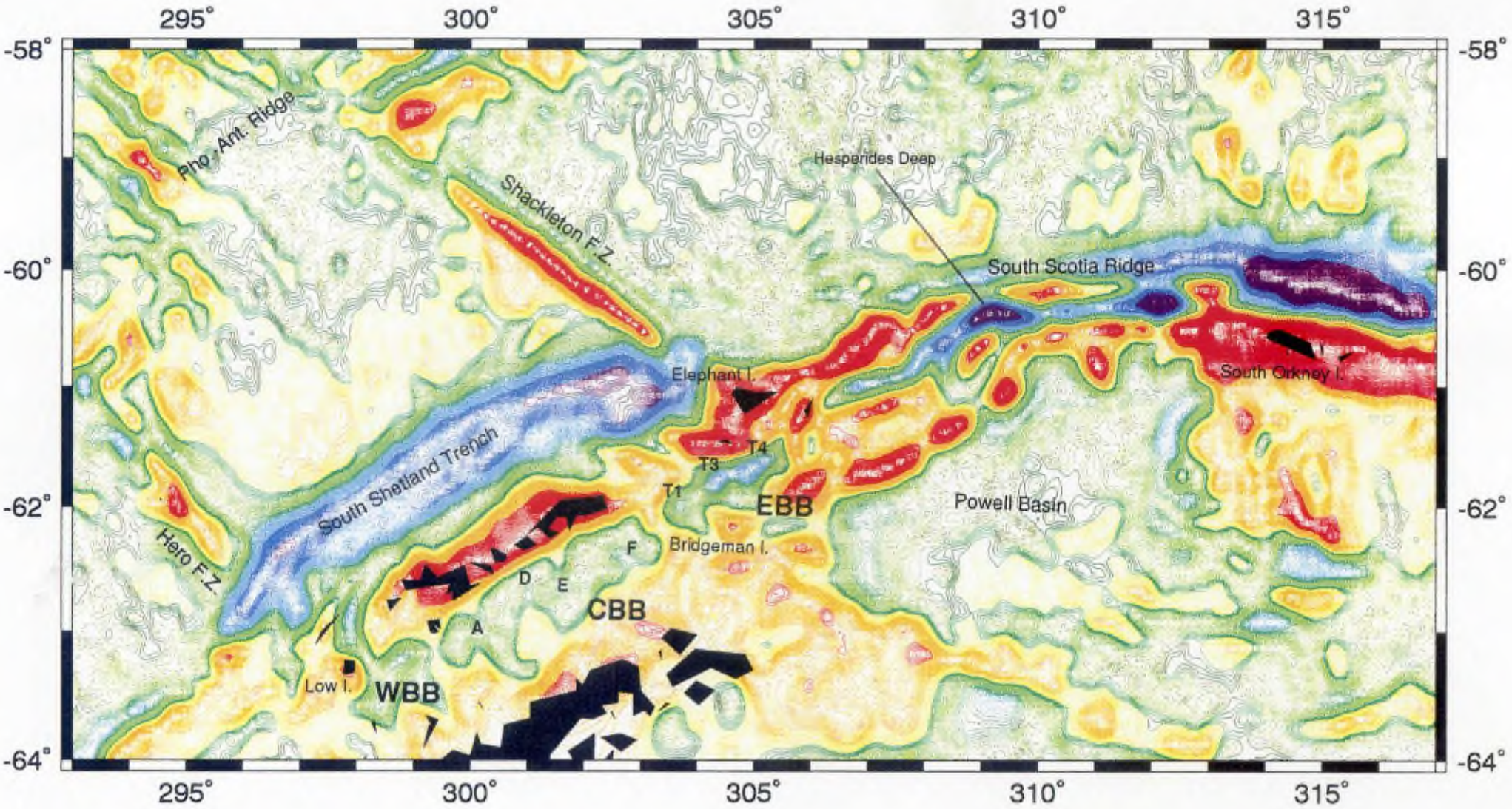

Fig. 6.15. Satellite-derived free-air anomaly map of the area between the western part of the South Scotia Ridge and the Bransfield Basin. Contour: 2 mGal. Edifices A, D, E, and F, and troughs T1, T3 and T4 may be observed at the resolution of this map. CBB: Central Bransfield Basin, EBB: Eastern Bransfield Basin, WBB: Western Bransfield Basin.

characterized by important gravity lows. At longitude 51°W, a maximum negative anomaly of -150 mGal is found, and the structures change from an E-W trend parallel to the South Scotia Ridge, to a NE-SW trend, parallel to the Bransfield Basin. The intersection area between these two sets of faults was completely mapped during the Scotia 92 cruise and named Hesperides Deep (Canals et al., 1992; Acosta et al., 1994) (Fig. 6.15). To the east and following the same E-W trend, another deep trough centred at 48°W and also showing a large negative anomaly is observed.

The Powell Basin is a quiet zone, with no major gravity anomalies. This basin has a curved enclosed shape, limited to the south by a narrow ridge showing positive anomalies of 20 mGal. In the northern margin, near the distinctive topography of the South Orkney Islands microcontinent, the anomalies are larger, reaching +190 mGal.

Chapter 7

THE CENTRAL SPREADING RIDGE

7.1. Data base and methods

The data used in this chapter were acquired during the French-Japanese STARMER project (1987-1992). The main objective of this project was an inter-disciplinary study of the Central Spreading Ridge of the North Fiji Basin, occupying the area located between latitudes 14°20'S and 21°40'S, and longitudes 172°30'E and 175°E (Fig. 7.1). During the project six cruises were undertaken in this area. Four of which (Kaiyo 87, Kaiyo 88, Kaiyo 89 and Yokosuka 90) were surface cruises, and included swath-bathymetric mapping, geophysics, water and geological sampling. The remaining two were submersible diving cruises: Starmer 89 and Yokosuka 91 (Auzende and Urabe, 1994) (Fig. 7.1).

We have available the whole data set acquired in the Central Spreading Ridge during STARMER project. Part of the data was previously processed and published during the project itself (see section 5.3.1). In addition, we have included further bathymetric and magnetic data from other data bases, and a compilation of pre-existing gravity data. All these data permit us to present a unique synthetic compilation of bathymetric and geophysical data of the Central Spreading Ridge, providing a detailed analysis of various features and aspects, such as ridge segmentation, near-axis seamount chains, axial morphology and spreading rate, and gravity anomalies, which have not previously been discussed.

7.1.1. BATHYMETRY

More than 800 km of bathymetric data, the length of the Central Spreading Ridge system, were acquired during STARMER. This extensive data set was collected using two different types of swath-mapping systems: firstly, the General Instruments Seabeam which was installed on board the R/V Kaiyo, and which has 2.7° x 19 narrow beams which make a 43.2° opening fan and cover up to 2/3 of the water depth in deep areas; and secondly, the Japanese Furuno HS10, installed on board the R/V Yokosuka,

and which has 2° x 45 narrow beams which make a 90° opening fan and cover up to twice the water depth in deep areas (Tanahashi et al., 1994).

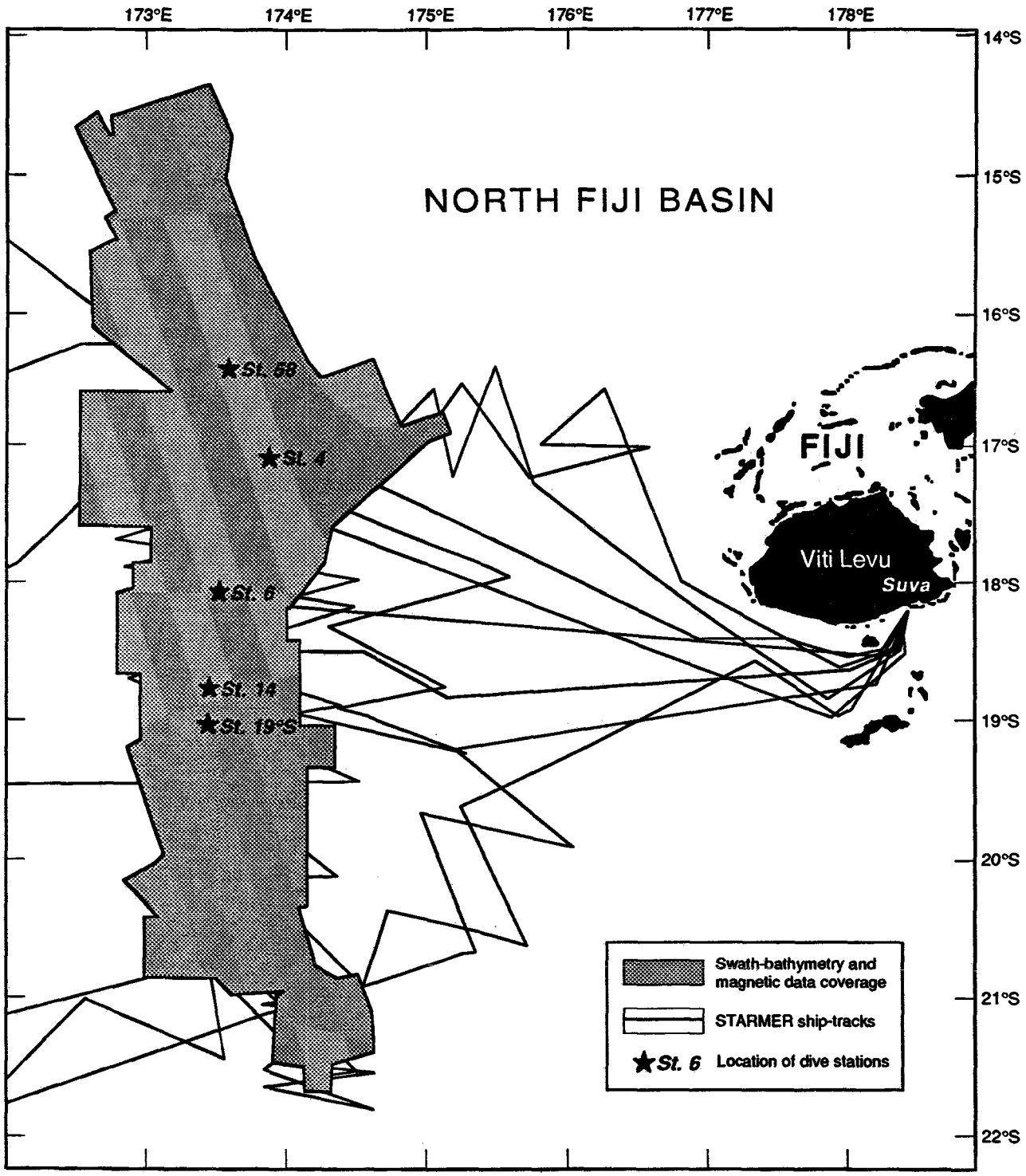

Fig. 7.1. Location of the swath-bathymetry data and geophysical surveys, and diving cruises carried out during the STARMER project in the Central Spreading Ridge.

The bathymetric maps presented in this chapter are a compilation of bathymetric data acquired during five STARMER cruises (Kaiyo 87, 88, 89 and Yokosuka 90 and 91) together with the Seabeam data obtained during the Seapso 3 cruise and data from the GEODAS database (NOAA/NGDC, 1992). Once the data was merged and homogenized, the post-processing to obtain bathymetric maps was the same as explained previously in section 1.2.1.

7.1.2. SUBMERSIBLE DATA

Two deep submersibles explored the Central Spreading Ridge during the STARMER project: the French submersible Nautile with the R/V Nadir (Starmer 89 cruise in June 1989), and the Japanese submersible Shinkai 6500 with its mothership R/V Yokosuka (Yokosuka 91 cruise in October, 1991). The Yokosuka 91 cruise was partly devoted to revisiting hydrothermal sites previously explored by the Nautile during the Starmer 89 cruise. In total 46 dives were carried out along the Central Spreading Ridge, focused on five dive-stations, from north to south (Fig. 7.1): station 58 on the N160 segment, stations 4 and 6 at the northern and southern tips of the N15 segment, respectively, and stations 14 and "19°S", both on the N-S segment.

The parameters recorded on the video image were time (hour/minutes/seconds), immersion, height to the bottom, submersible heading, and camera heading (when camera was mobile). All these parameters provide information about the nature of the seafloor, measure the orientation of structures, and establish detailed bathymetric and navigation maps. The main results obtained from submersible video data along the Central Spreading Ridge are presented in section 7.2.2.

7.1.3. MAGNETICS

Magnetic data were acquired during the STARMER cruises with a marine proton magnetometer EGG-Geometrics G866. The sensor was towed 230 m behind the ship, with an accuracy of 0.1 nT and a sampling rate of 10-second intervals. Thus, during the Kaiyo 87, Kaiyo 88, Kaiyo 89, Yokosuka 90 and Yokosuka 91 cruises, a total of 100,000 magnetic data points were recorded.

The STARMER data are compiled together with data obtained from other projects that also conducted cruises in the area. Magnetic data from the Hawaii Institute of Geophysics (Kroenke et al., 1993a; Jarvis and Kroenke,

1993), ORSTOM, Scripps Institute of Oceanography, and US Geological Survey were extracted from the GEODAS database (NOAA/NGDC, 1992). Taken together these cruises provide 180,000 magnetic data points (Huchon et al., 1994). The processing of the magnetic data of the Central Spreading Ridge was explained in detail by Huchon et al. (1994). A summarized version is presented in section 1.2.2.

7.1.4. GRAVITY

No gravity data were acquired during the STARMER project. Thus, we have compiled all the available shipborne gravity data from the GEODAS data base (NOAA/NGDC, 1992), comprising a total of 33,300 km, collected during numerous cruises and transits in this part of the North Fiji Basin. Due to the irregular quality of the data set, we performed a cross-over error analysis to check the consistency of the data between cruises. Profiles that had no cross-over were checked visually, and some were rejected. In one case (Seapso 3 cruise) the Eötvos correction was entirely recalculated, and good consistency with the remaining data was obtained. The whole data set were reduced to the same reference system (IGSN 71). Cross-over errors were computed and corrected for the data set using the algorithm of Hsu (1995). For details about processing the gravity data see section 1.2.3 in Chapter 1.

7.2. Morphostructure

This section is based on the analysis and interpretation of the bathymetric data, and three aspects are examined in detail: ridge segmentation, axial morphology and seafloor tectonic fabric.

7.2.1. RIDGE SEGMENTATION

Three parameters characterize segmentation along spreading ridges (Macdonald et al., 1991): the length of the segment, the longevity of the segment, and the offset separating the segments (see Chapter 2). Along the whole Central Spreading Ridge, neither the longevity nor the offset can be considered due to the youthfulness of the spreading centre and the lack of large offsets and transforms. Thus, the length of the segment is the only parameter we measured in order to characterize the Central Spreading Ridge segmentation. In Figure 7.2, a 200 m contour bathymetric map of the whole Central Spreading Ridge is presented, and the first-order segments N160, N15 and N-S are clearly differentiated. These three segments were previously identified and named after their main orientations by early STARMER workers (see section 5.3.1). Therefore, here we do not include rose diagrams of the structural trends for each segment, as is done for the Bransfield and South Pandora-Tripartite Ridges (see Chapters 6 and 8).

The axial depth profile (Fig. 7.3) shows a long-wavelength (150-250 km long) bathymetric pattern between the first-order segments separated by first-order discontinuities (14°50'S and 16°50'S triple junctions, and 18°10'S and 20°45'S propagating rifts). Superimposed on this long-wavelength segmentation is a shorter-wavelength (50-90 km) segmentation caused by second-order discontinuities. These smaller segments, second-order segments, have been labelled from north to south CSR1 to CSR8.

N160 first-order segment

The N160 segment extends 210 km, between the 14°50'S and the 16°50'S triple junctions. It is composed of three second-order segments (CSR1 to CSR3) which are a succession of long *en échelon* grabens, as can be observed on the bathymetric map and the morphostructural interpretation (Figs. 7.4 and 7.5). Segment CSR1 is 63 km long, between 7.5 km and 15 km wide and reaches a depth of more than 4200 m, the maximum depth measured along the whole Central Spreading Ridge. Segment CSR2 is offset 20 km to the

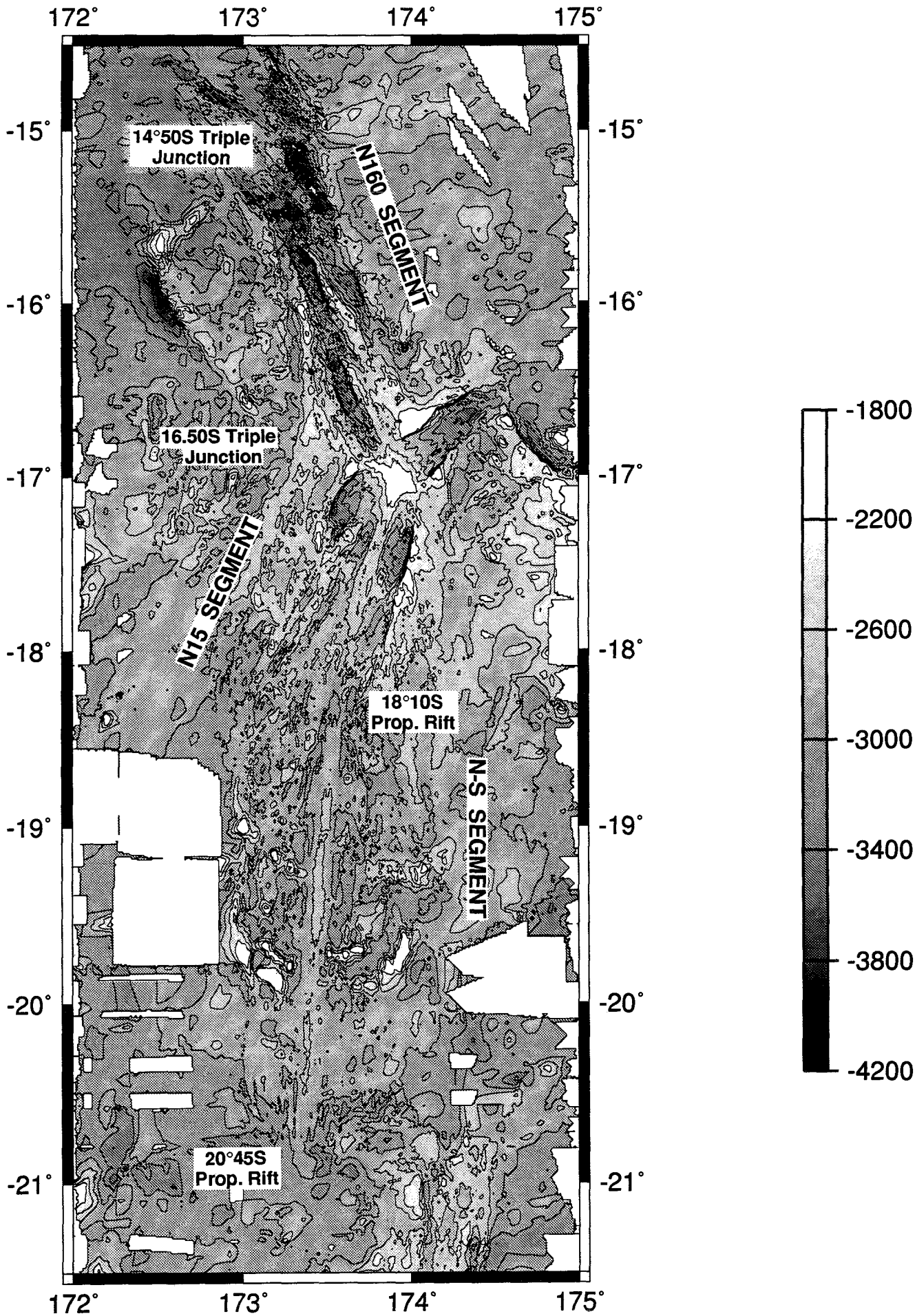

Fig. 7.2. Bathymetric map of the Central Spreading Ridge in 200 m contour interval. The three first-order segments (N160, N15, and N-S) and discontinuities are distinguished.

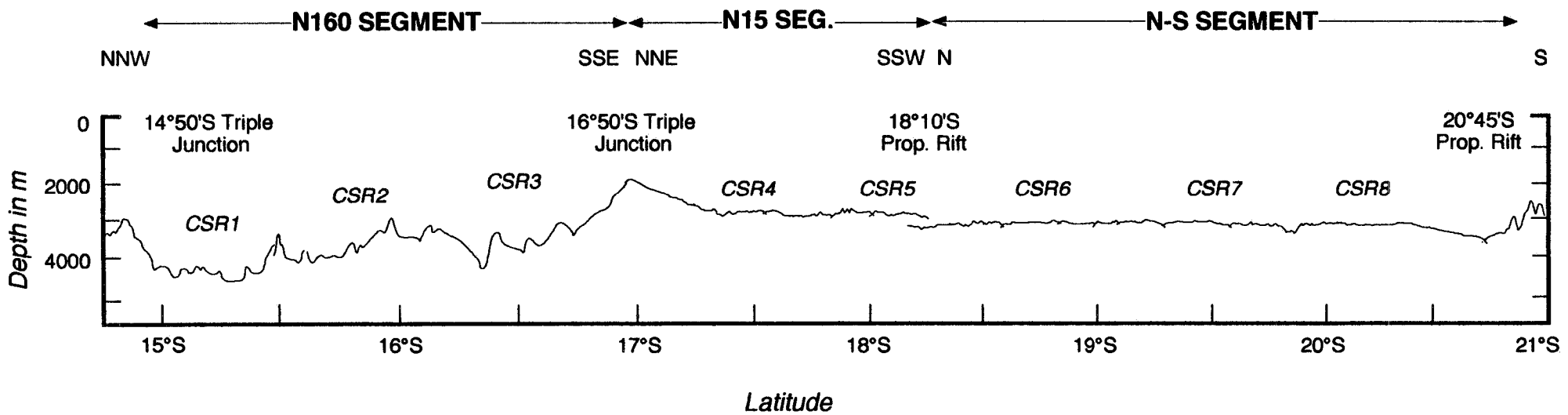

Fig. 7.3 Axial depth profile of the Central Spreading Ridge between 15°S and 21°S. Note the rough axial topography and the small order segmentation of the N160 segment (CSR1-CSR3) in comparison with the southern segments (CSR4 to CSR8). Vertical Exaggeration: 20.

east of segment CSR1 at 15°30'S. CSR2 is 82.5 km long, 12 km wide, and 3700 m deep. A 5 km right-lateral offset separates CSR2 and CSR3 at 16°15'S. Segment CSR3 is 78 km long, 10.5 km wide, and 3600 m deep (Figs. 7.4 and 7.5)

Segments CSR2 and CSR3 are bound by two volcanic constructions, 135 km long and 2100 m high that become progressively wider southwards, reaching a width of 40 km near the 16°50'S triple junction (Fig. 7.5). These ridges connect with the axial valley through a wall 1000 m high formed from several steps of inward facing scarps which would appear to be normal faults.

N15 first-order segment

The N15 segment extends from the 16°50'S triple junction to 18°10'S, and has a length of 165 km. It comprises the two second-order segments CSR4 and CSR5, separated from the 17°50'S offset. Segment CSR4 is 97 km long, and is characterized by a 500 m high and 10.5 km wide axial ridge with a small axial graben 1.5 to 3 km wide.

The axial zone is bound by two curved grabens, 60 km wide and 3500 m deep. Such grabens might be relict structures related to the functioning of the 16°50'S triple junction. CSR5 is 72 km long and characterized by a 3 km wide and 300 m high dome bordered by two elongated, curved depressions. The axis of segment CSR5 also shows a curved shape from 17°56'S to 18°34'S and overlaps with the northern portion of the N-S segment (Figs. 7.4 and 7.5).

N-S first-order segment

This segment extends from 18°10'S to 20°45'S and is 255 km long. Three second-order segments can be distinguished on the bathymetric map (Fig. 7.6). Segment CSR6 is characterized by a dome which is 67.5 km long, 9 km wide and 100 m high. A small offset at 19°05'S separates this segment from CSR7. A 71 km long dome, with the shallowest depth (2000 m) and the widest section (12 km), can be observed along the middle segment (CSR7). A small overlapping spreading centre at 19°50'S separates CSR7 and CSR8. This last segment is characterized by a 75 km long, 7.5 km wide and 100 m high axial dome. CSR6 propagates northwards whereas CSR8 seems to propagate southwards, as is suggested by the V-shaped pseudofaults (Figs. 7.6 and 7.7).

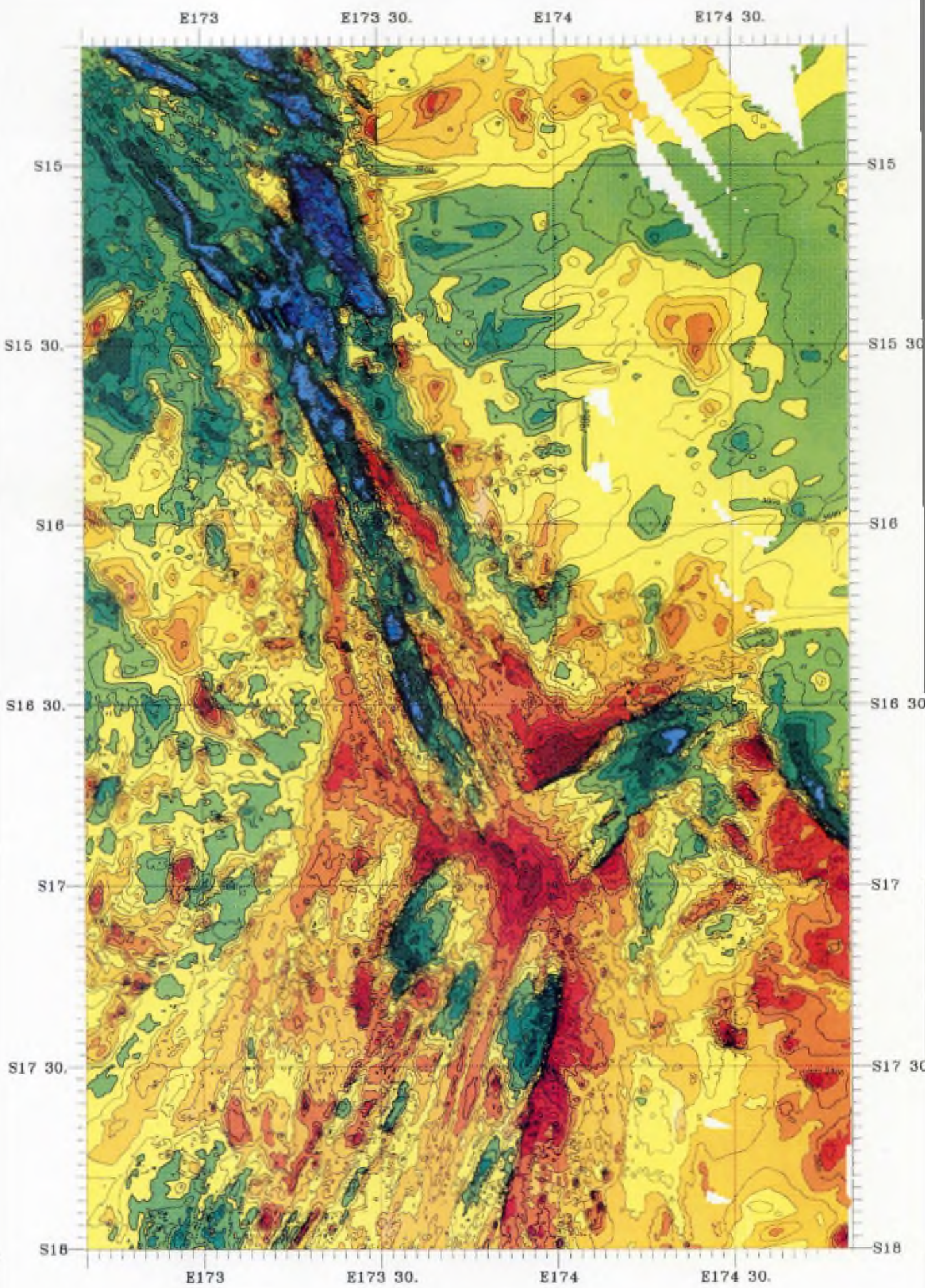

Fig. 7.4. Bathymetric map of the northern part of the Central Spreading Ridge between 14°40'S and 18°S, comprising the N160 and the northern part of the N15 segment. Bathymetric contour: 100 m. Colour change: 200 m.

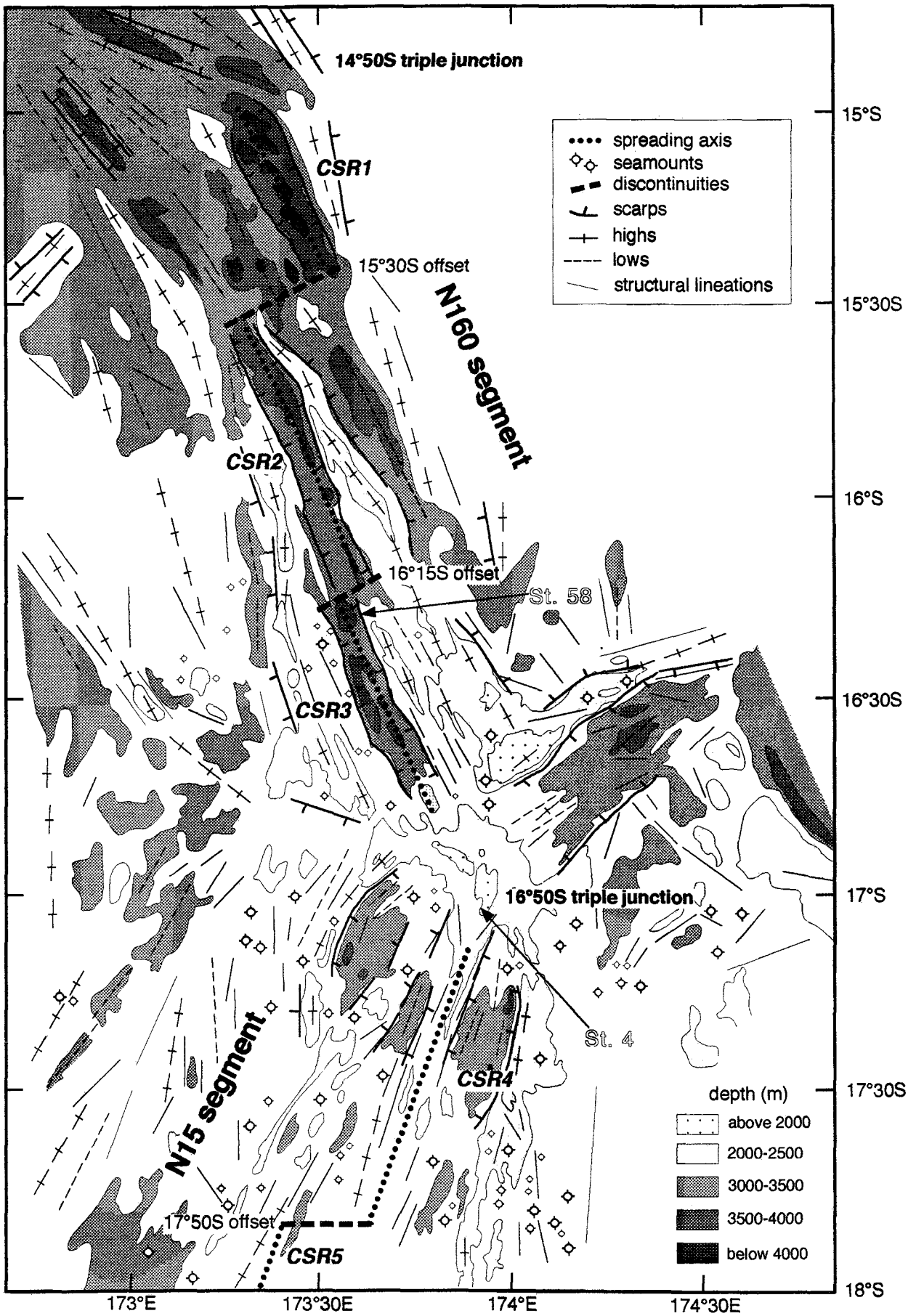

Fig. 7.5. Morphostructural interpretative map of the northern part of the Central Spreading Ridge. Second-order segments, axial discontinuities, and dive stations 58 and 4 are also indicated.

7.2.2. AXIAL MORPHOLOGY

Systematically spaced every 10 minutes, 40 transverse bathymetric profiles were made from 14°20'S to 21°S orthogonal to the axis. Some of these sections are presented in Figures 7.8, 7.9 and 7.10 for the N160, N15 and N-S segments, respectively.

A rift valley, on average 10 km wide and 1 km deep, runs along the crest of the N160 segment (Fig. 7.8). Present-day volcanism seems to be localized along the axial neovolcanic ridge. This discontinuous feature is about 500 m wide and 200 m high, and when present, is located in the middle part of the graben, as observed in the 16°30'S cross-section (Fig. 7.8). The inner flanks of the rift valley are very steep and formed by several scarps up to 35° of maximum slope gradient. The axial morphology of the N160 segment is similar to those reported for slow-spreading ridges, such as the Mid-Atlantic Ridge (Macdonald, 1986; Purdy et al., 1990; Grindlay et al., 1992).

The axial morphology of the N15 segment its characterized by a double ridge (2000 m deep) split by a 2 km wide and 200 m deep axial graben, as is observed along segment CSR4 (Fig. 7.9). The northern part of the CSR4 segment is particularly shallow (less than 1900 m) due to the proximity of the triple junction, as observed in the cross section at 17°10'S (Fig. 7.9). Towards the south, the axial morphology shows a flat dome topography more similar to the morphology of the N-S segment, as in segment CSR5 (Fig. 7.9).

The N-S segment morphology is characterized by a central flat rectangular axial rise locally cut by an axial summit caldera of 20 m depth. In the middle of segment CSR7 at 19°10'S-19°20'S a triangular dome-shape can also be observed (Fig. 7.10). Both axial morphologies, rectangular and triangular, are typical of fast-spreading ridges, such as the East Pacific Rise (Macdonald and Fox, 1988; Macdonald et al., 1992).

7.2.3. SEAFLOOR TECTONIC FABRIC

The shaded relief map corresponds to the topographic gradient derived from the swath-bathymetry data. Both black and white areas, which are the results of the direction of illumination, correspond to zones where the topographic gradient is very high, while grey areas are of intermediate value. The shaded relief maps (Figs. 7.11 and 7.12) reveal high angle-slopes

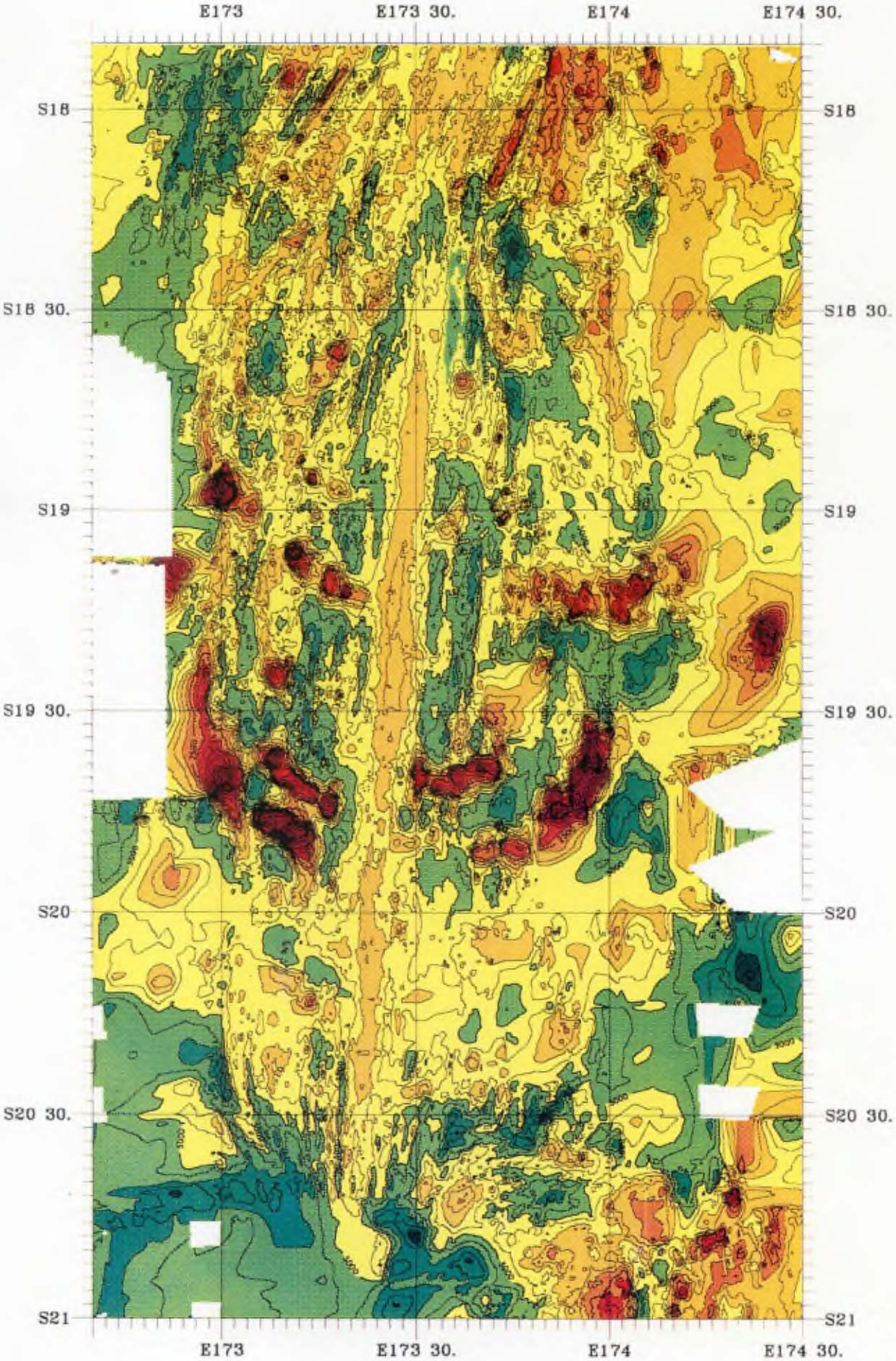

Fig. 7.6. Bathymetric map of the southern part of the Central Spreading Ridge between 17°50'S and 21°S, comprising the southern part of the N15 segment and the whole N-S segment. Bathymetric contour: 100 m. Colour change: 200 m.

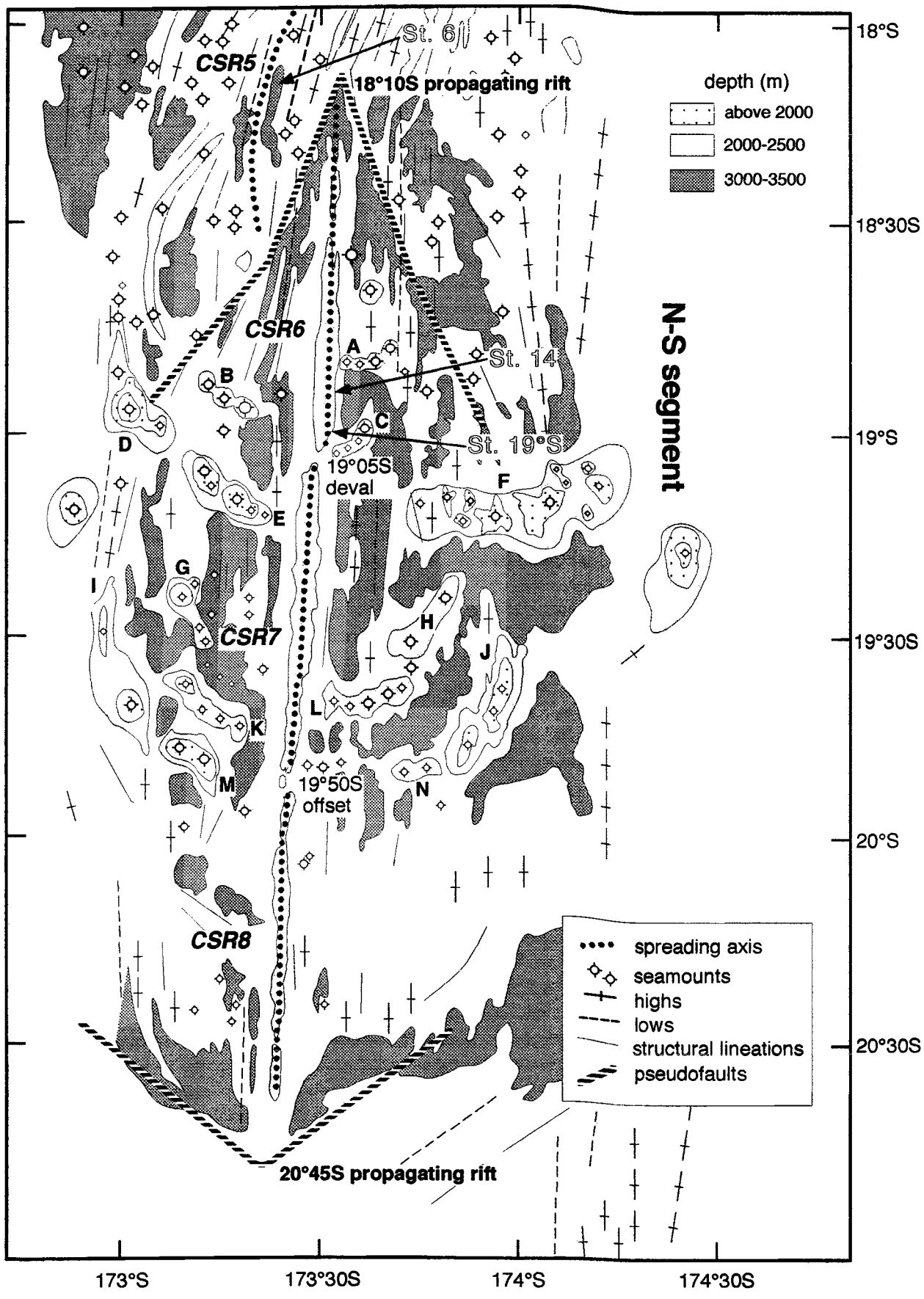

Fig. 7.7. Morphostructural interpretative map of the southern part of the Central Spreading Ridge. Note the near-axis seamount chains labelled A to N located at both sides of the N-S axis. Second-order segments, axial discontinuities, and dive stations 6, 14 and 19°S are also indicated.

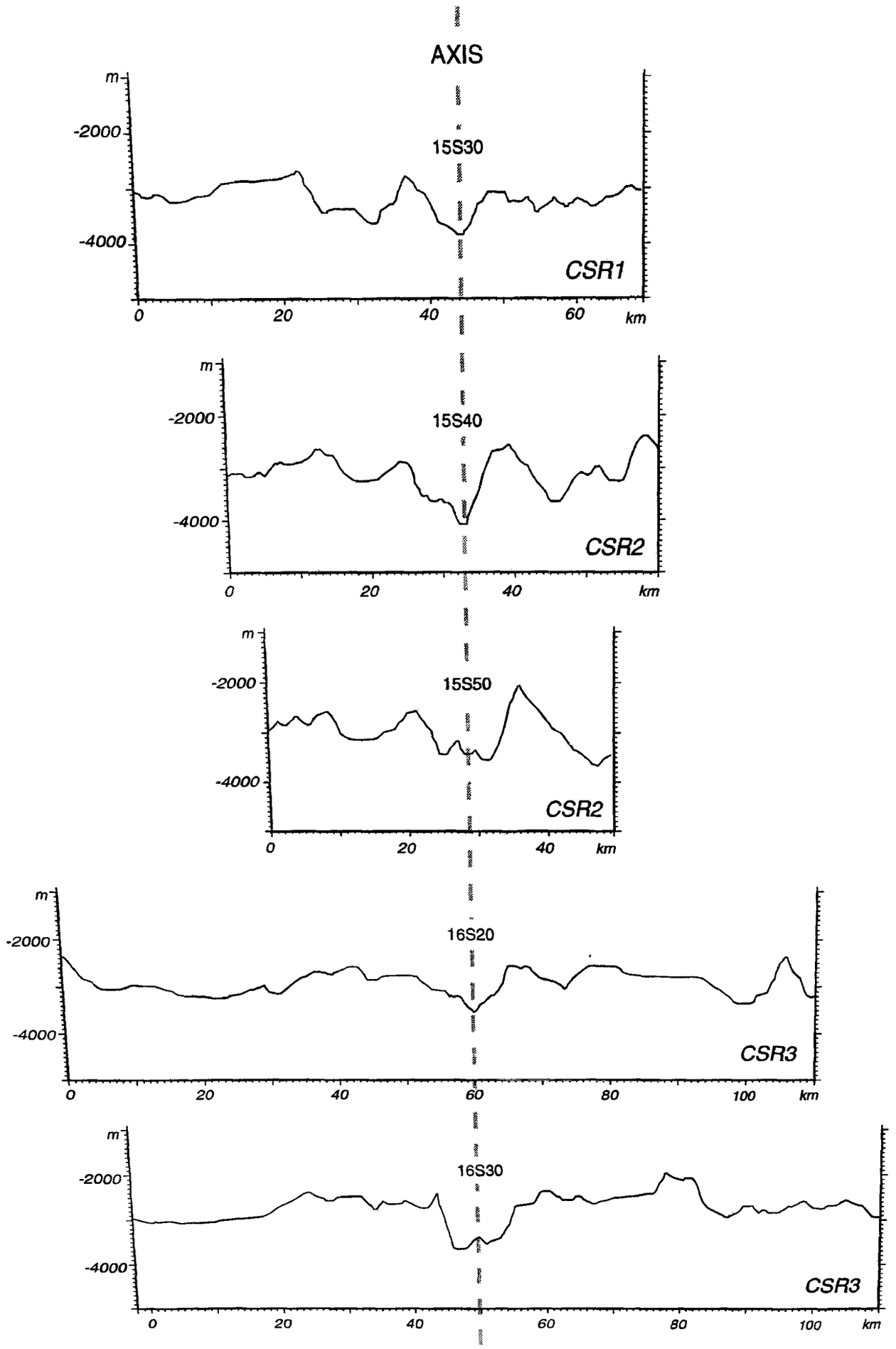

Fig. 7.8. Bathymetric sections across the N160 segment. All the sections are taken following a

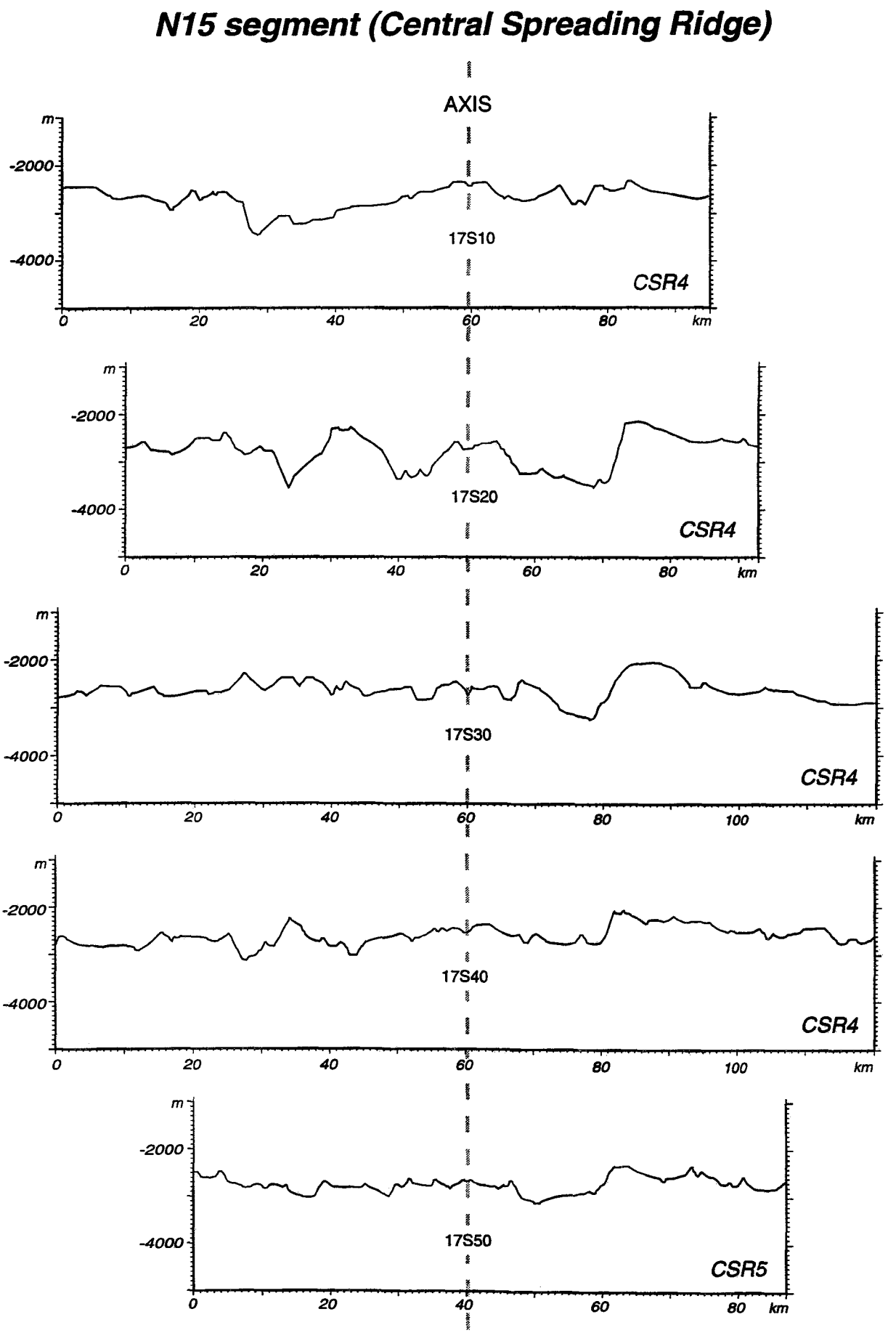

Fig. 7.9. Bathymetric sections across the N15 segment. All the sections are taken following a N105 trend orthogonal to the axis. CSR4 and CSR5 are second-order segments. Vertical Exaggeration: 7.

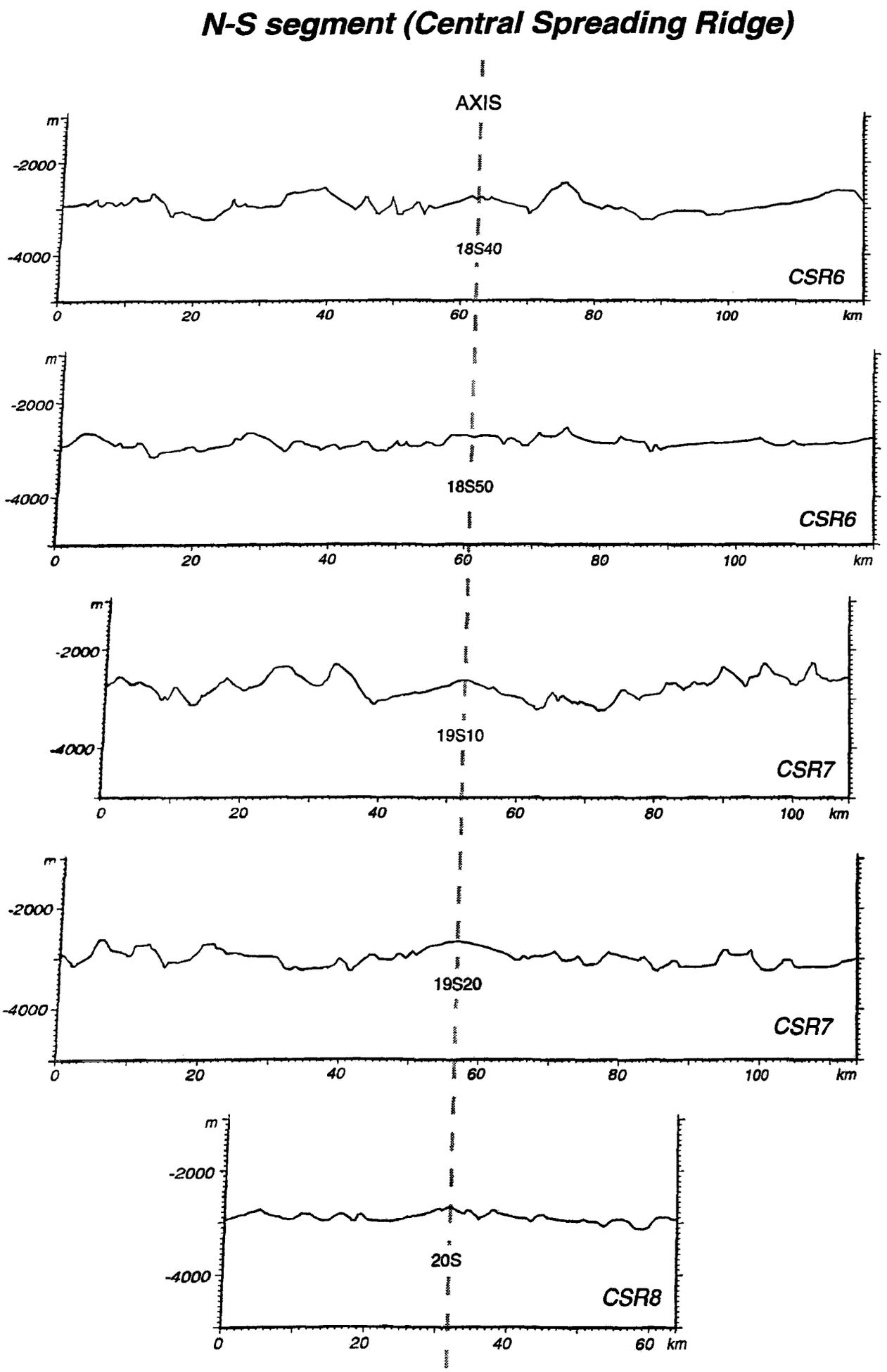

Fig. 7.10. Bathymetric sections across the N-S segment. All the sections are taken following a E-W trend orthogonal to the axis. CSR6, CSR7 and CSR8 are second-order segments. Vertical Exaggeration: 7.

that parallel the ridge axis, and are interpreted as being the expression of faults.

The topographic roughness seems to decrease towards the south from the N160 to the N-S segment, and the orientation of the fault pattern off-axis seems to mimic the present-day orientation of the ridge axis. It also clearly shows the dome-shaped topography along the N-S axis (Fig. 7.5).

The off-axis topography of the N160 and N15 first-order segments exhibits a series of topographic lows and highs also trending N160 and N15 respectively. They show a periodicity of 200,000 years, assuming a spreading rate of 50 mm/yr.

The off-axis topography of the N-S segment is rather flat, except along pseudofaults of the north and south propagating rifts where a series of topographic lows and highs occur every 120,000 years (Figs. 7.11 and 7.12). An important feature of the off-axis topography of the N-S segment is the existence of volcanic cones and seamount chains located between 18°30'S and 20°30'S, although its maximal concentration is off-axis of the CSR7 segment (Figs. 7.6 and 7.7). They are listed in Table 7.I, together with the latitude and longitude of their western and eastern limits (west and east ends, respectively), location with respect to the ridge flank, length, maximum height, orientation, and number of edifices forming the seamount chain.

We followed the same analytical approach as that undertaken by Scheirer and Macdonald (1995) for the near-axis seamounts of the East Pacific Rise. Each chain is composed of two or more seamounts over 200 m. Many smaller edifices and possibly lava flows and mass wasting deposits, which contribute to an irregular seafloor pattern, are located between the edifices of the chain. However, these are not included in Table 7.I.

We have identified a total of 14 seamount chains, labelled A to N. The chains range in length from 17 to 50 km, and some of them, such as chain I, extend beyond the multibeam coverage of the Central Spreading Ridge. These seamount chains exhibit conical volcanic edifices which have a basal diameter from 4-5 km up to 10-15 km and rise above the abyssal plain from between 300 to 1250 m. The seamount chains are generally linear, although a number of them contain distinct bends, and the two trends are given in

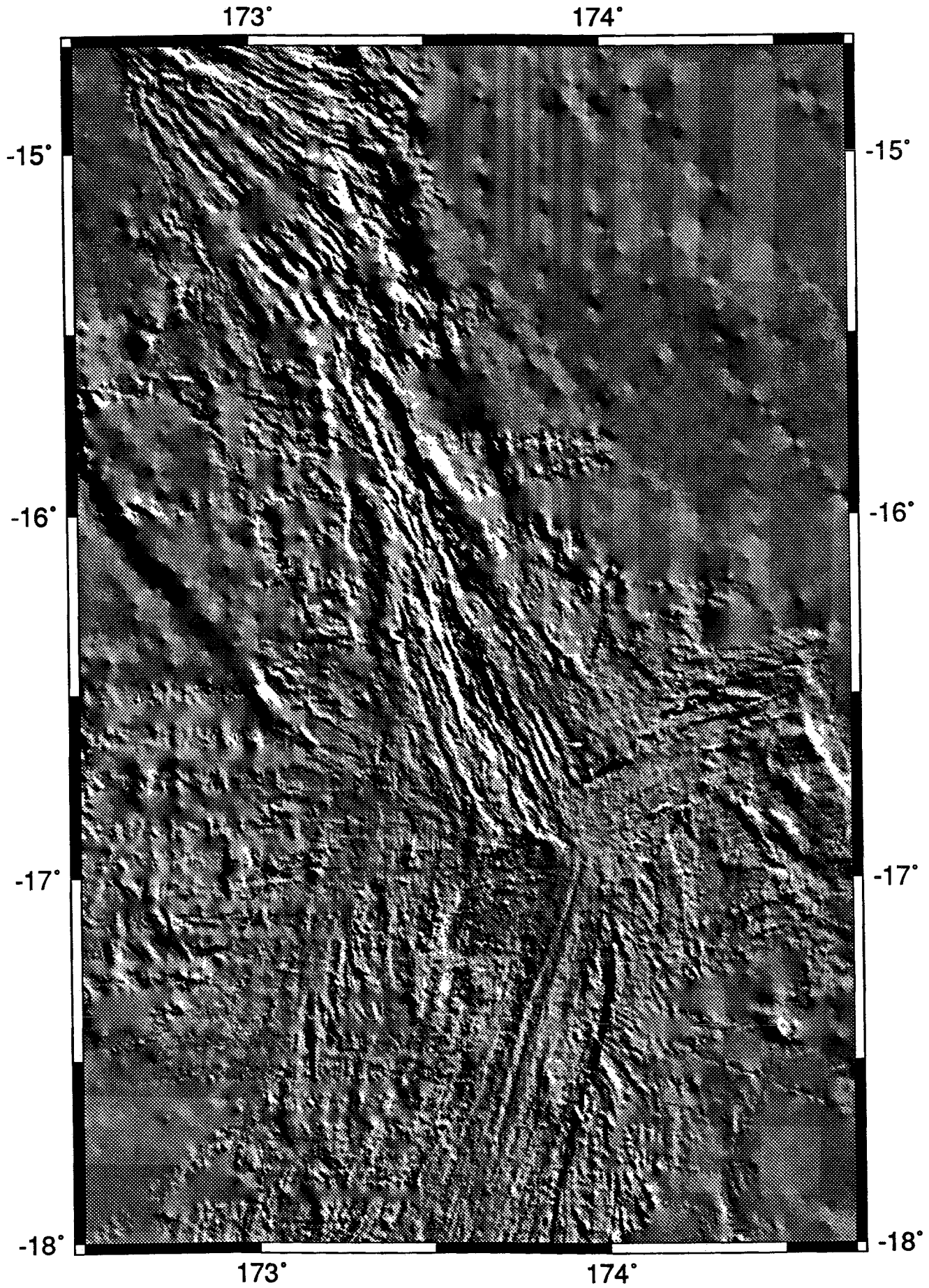

Fig. 7.11. Shaded relief map of the northern part of the Central Spreading Ridge. Illumination: N45, elevation: 30°. The areas with detailed survey are shown by rough, small-scale topography, whereas zones where the bathymetry is interpolated are much smoother.

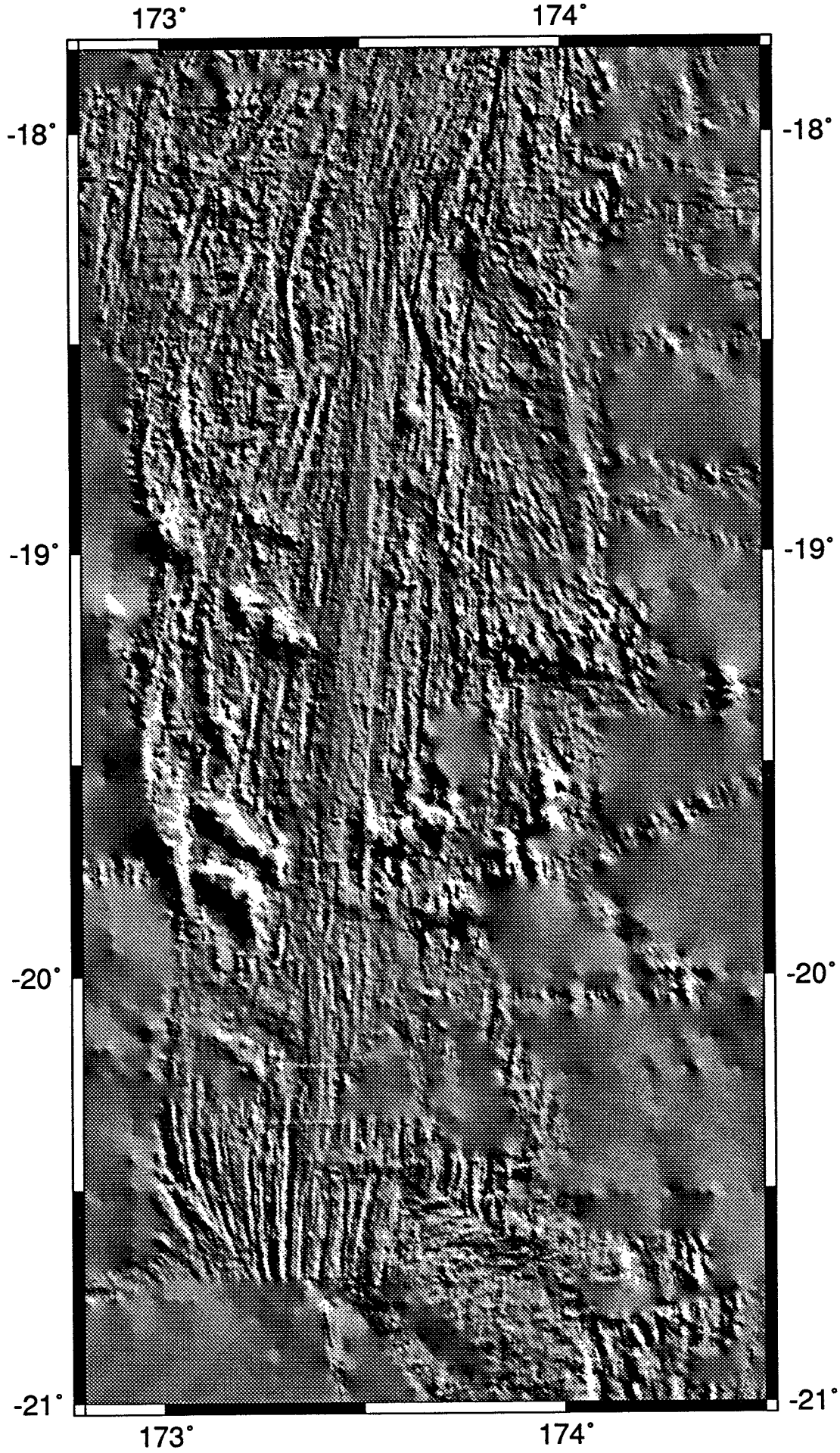

Fig. 7.12. Shaded relief map of the southern part of the Central Spreading Ridge. Illumination: N90, elevation: 30°.

Table 7.I. The trends of the chains range from perpendicular to almost parallel to the axis direction (Fig. 7.7).

Name	West end (lat °S/lon °E)	East end (lat °S/lon °E)	Flank	Length (km)	Height (m)	Trend (deg)	Edifices
A	18°52/173°31.5	18°47/173°40	E	17	350	90/49	4
B	18°52/173°11	18°59/173°20.1	W	29	500	129	3
C	19°06/173°30.5	18°56/173°38.5	E	24	300	26	4
D	18°52/172°57.3	19°03/173°05.6	W	23	950	140	3
E	19°04/173°09.5	19°10.5/173°23	W	28	1000	124	4
F	19°12/173°44	19°12/174°12.7	E	53	550	90	10
G	19°21.5/173°06	19°36/173°12	W	28	650	160	3
H	19°30/173°43	19°20/173°50.5	E	22	600	37	2
I	19°22/172°57.5	19°48/173°03	W	51	800	5/340	2
J	19°50.5/173°48	19°32.5/173°58	E	37	1250	27	3
K	19°35.5/173°05	19°45.2/173°17	W	27	750	127	4
L	19°43/173°28.5	19°34/173°42.5	E	28.5	850	71	5
M	19°46.7/173°03	19°54/173°13.5	W	21	1150	123	2
N	19°51/173°36.7	19°51/173°47.5	E	17.5	375	90	3

Table 7.I. Characteristics of the near-axis seamount chains observed along the N-S segment of the Central Spreading Ridge.

The small isolated volcanic cones appear scattered over the basin floor and have basal diameters which are 5 times smaller (1.5 km on average) than those described above in the seamount chains.

Inward facing faults seem to predominate on the N160 segment, whereas both inward and outward faulting appear along the N-S segment. This corresponds to observations made for slow and fast spreading ridges, respectively (Carbotte and Macdonald, 1990).

7.3. Dive results

In this section we describe the main results obtained at each of the five dive stations proceding from north to south, explored by submersible in the Central Spreading Ridge. Three principal aspects are presented in detail: structure, volcanism and hydrothermal activity, and are summarized from the works of Gràcia et al. (1994).

7.3.1. STATION 58

The site is located between latitudes 16°18'S-16°20'S and longitudes 173°32'E-173°34'E at the end of the CSR3 segment (N160 segment) (Figs. 7.1 and 7.5). The area is characterized by a 3800 m deep circular graben bordered by two 1000 m high vertical walls (Fig. 7.8). A N170 trending neovolcanic ridge culminating at less than 2800 m and slightly oblique to the graben axis is observed. Three dives were conducted to explore the median neovolcanic ridge, where significant methane and manganese anomalies were measured during surface cruises (e.g. Auzende et al., 1988a).

Structure

The most recent tectonic features on the graben floor are N130-140 trending funnel alignments indicating active fractures underneath the sediments, and narrow opened fissures (Gràcia et al., 1994). The scarps bordering the median ridge mainly trend N160-N170, and show steep slopes. The fault scarps are formed by a succession of small steps, 15-20 m high each, forming 100 m high main scarps. Mass wasting is very common along the wall, and debris and chaotic blocks are accumulated at the foot of the scarps.

Volcanism and Hydrothermalism

The most important outcrops of pillow lava and lava tubes are exposed on the fault scarps. Vertical sections of columnar jointed sheet-flows are observed on basaltic walls. At the edge of the neovolcanic ridge, white sedimentary patches associated with fissures cutting through the talus are observed. They are possible indications of fossil hydrothermal activity. In many places, dark-brown stained blocks are associated with temperature anomalies and major fissuration. This minor hydrothermal activity is characterized by sporadic discharges, as has been suggested by Nojiri et al. (1990) from the detection of hydrothermal plumes in the water column.

7.3.2. STATION 4

This station is located on the northern tip of the N15 segment (CSR4 segment), between longitudes 173°53'E-173°57'E and latitudes 16°57.5'S-17°02'S, very close to the 16°50'S triple junction (Figs. 7.1 and 7.5). Twenty-two dives were carried out in this area where an active white-smoker was discovered during deep-towed camera exploration (Jollivet et al., 1989). The main objectives of the dives were to explore and sample the most hydrothermally active part of the axial graben.

Structure

Three structural domains are distinguished from north to south along station 4 (Bendel, 1993; Gràcia et al., 1994). The northern domain (north of 16°58.5'S) is characterized by N15-N20 trending faults, although N160-N170 directions, reflecting the influence of the N160 segment, are also very common. The central domain (between 16°58.5'S and 17°S) was explored during most of the dives. The floor consists of 10-50 m high and 50-150 m wide horst and graben topography. The central horst, trending N-S/N05, is slightly oblique to the main N15 structures. Active tectonism on this domain is represented by fresh fissures, faults and aligned funnels (Fig. 7.13a). On the southern domain (between 17°00.5'S and 17°02'S) the axial graben is wider (2.5 km) than in the north, and scarps and fissures trend N15-N20.

Volcanism

Although the axial zone is almost completely covered by a thin sediment cover (Fig. 7.13a, b), there are still some basaltic outcrops. Basalts exhibit the most common lava morphologies observed in mid-ocean ridges (e.g. Ballard and Moore, 1977; Ballard et al., 1979), as pillow lavas and tubes, sheet flows, draped flows, lava lakes, and massive flows. Fluid lobate lavas form lava lakes, which exhibit collapse and pillar structures (Fig. 7.13b). Lava lakes cover the floor of the whole graben in the northern domain but are almost non-existent in the southern domain.

Hydrothermalism

Both fossil and active hydrothermal activities are found at station 4. Fossil deposits are represented by inactive sulfide mounds and chimneys. A 4 km^2 fossil field of sulfide chimneys (*Père Lachaise* field), some of them reaching heights of 20 metres, was discovered in the northern domain

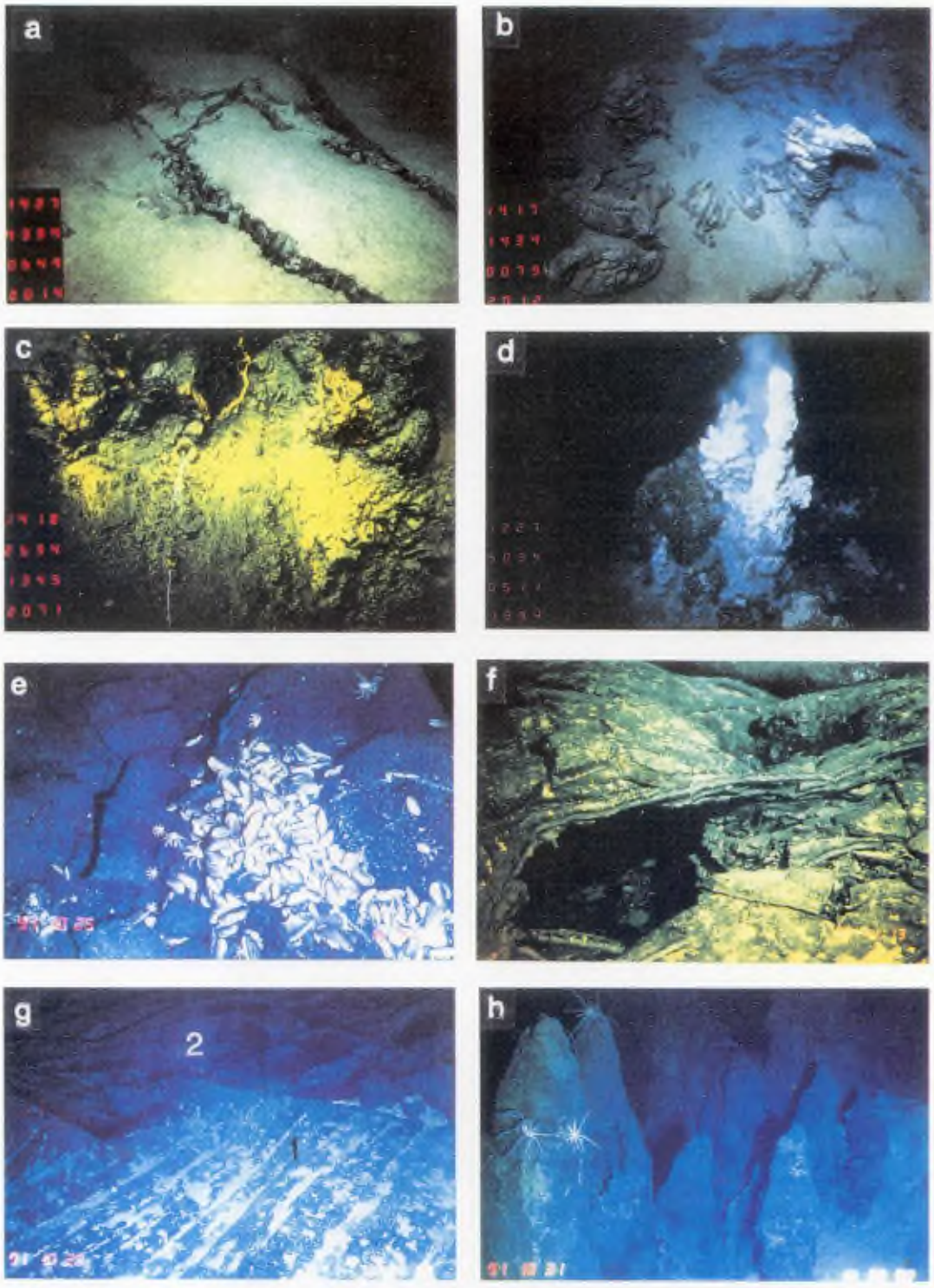

Fig. 7.13. Bottom photographs taken by the Nautile and Shinkai 6500 along different sites in the Central Spreading Ridge. Station 4: a) Open fissure at the bottom of the main graben, b) Basaltic pillars of foundered lava lakes, c) Yellow-ochre hydrothermal deposits located in a graben wall, d) the "White Lady" active smoker. Station 14: e) Animal colonies associated with low temperature diffusions, f) Top of a sediment free foundered lava lake, g) Contact between sheet flow lavas (1) and draped lavas (2). Station "19°S": h) Fossil chimneys forest with ophiuridae (Gràcia et al., 1994).

(Auzende et al., 1990b and 1991). Inactive hydrothermal deposits also occur in the surveyed area as yellow-brown patches along fault scarps (Fig. 7.13c). In the central domain, hydrothermal activity is observed in the area showing present-day fissuration. On the top of the central horst, a 3 m-high white anhydrite smoker venting at 285°C was discovered, and named the "White Lady" (Fig. 7.13d) (Auzende et al., 1991; Bendel et al., 1993). Other similar active white smokers are also found in this area, some of them venting at a temperature of 296°C ("Starmer II" site). Living animal communities including gastropods, shrimps, galatheans and crabs are associated with the active vents.

7.3.3. STATION 6

This station is located between 18°03'S-18°07'S and 173°24'E-173°34'E, at the end of the CSR5 second-order segment (Figs. 7.1 and 7.7). Four dives were carried out here following an E-W cross section. The objective was to locate with precision the N15 axis, in this area influenced by the 18°S propagating rift. All along the station, the seafloor is widely covered by sediments, although they tend to decrease towards the west, where the most tectonically active area is found and which was interpreted by Ruellan et al. (1994) as the N15 axial zone. Open fissures, N20 trending fault scarps, and fresh talus screes at the foot of the scarps can be observed. *In situ* pillow basalts crop out along the crest scarps and walls. No hydrothermal activity or indicators were found at station 6.

7.3.4. STATION 14

Station 14 is located along the CSR6 segment between 18°47.7'S-18°51'S and 173°29,5'E-173°30,5'E (Figs. 7.1 and 7.7). The station lies on the flat top axial dome, where a deep-tow camera survey revealed the existence of fossil hydrothermal activity (Jollivet et al., 1989). Sixteen dives were devoted to the exploration of this area.

Tectonics

Tectonic activity is not very important at this station which is dominated by volcanism. Only few *en échelon* N170-N10 trending fissures were observed along the axial summit caldera.

Volcanism

Extremely fresh basalts, mostly lava lakes, were observed on the floor of the axial graben. Lava lakes (Fig. 7.13f) exhibit drain-back features, 4 to 5 m

high vertical pillars aligned along a N-S direction, and lava debris. Sheet flows (Fig. 7.13g-1) and draped lavas (Fig. 7.13g-2) are also present. Sheet flows exhibit flow-lines, fresh volcanic glass, and a thin sedimentary cover, in contrast to the draped lavas lying over them. Sections of pillow lavas are exposed along the steepest slope scarps.

Hydrothermalism :

Diffuse vents of low temperature fluids (5°C) and brown-yellow stains associated with living animal colonies are frequent at the station. "Forests" of inactive chimneys, up to 10 m high, associated with dead animals are located within the axial summit caldera or along the first steps of the external walls (Bendel, 1993).

7.3.5. STATION "19°S"

Only one dive was carried out at the N-S axis at 19°S, 20 km south of station 14 (Figs. 7.1 and 7.7). At 19°S near the end of the CSR6 segment, the axial morphology consists of a 8 km wide dome, topped by two 40 m high ridges separated by a 300 m wide, 50 m deep, axial graben. The N-S trending walls are constituted by pillow-lava sections. Scree deposits at the foot of the scarps are indicators of recent tectonic activity. Pillow-lavas and lava-tubes are common volcanic features in the area. A sedimentary cover of a few centimetres is present all along the dive track. Forests of fossil sulfide chimneys are observed on the floor of the axial graben (Fig. 7.13h). Low temperature fluids vent in the axial graben, at the foot of the western wall, associated with yellow-brown inactive hydrothermal deposits.

7.4. Magnetic anomalies

On the magnetic anomaly map of the Central Spreading Ridge (Fig. 7.14) the axial anomaly or Anomaly 1, and the Anomaly J or Jaramillo Event can be clearly identified along the central N-S segment between 19°S and 20°30'S. Based on the profiles where the magnetic anomalies are easy to identify, and with the help of synthetic profiles (see section 1.2.2 and Figure 1.4), an identification of the magnetic anomalies along the whole Central Spreading Ridge was made (Fig. 7.14).

On the N160 segment only the Anomaly 1 (0.71 Ma to present) can be clearly identified. Along the N15 segment, up to Anomaly J (0.91 to 0.97 Ma) the anomalies follow the present-day structural trend, but older anomalies (Anomalies 2 and 2A) seem to follow an oblique N-S orientation, clearly visible on the eastern flank of the ridge (Fig. 7.14). This may be related to a ridge re-orientation, occurring at least 1 Ma ago. Along the N-S segment, the magnetic anomaly sequence up to Anomaly 2 (1.65 to 2.10 Ma) was previously identified between 20°S and 20°30'S by Maillet et al. (1986). Although not as clear as younger anomalies, magnetic Anomaly 2A (2.45 to 3.40 Ma) can also be identified on the central part of the N-S segment between 19°S and 20°10'S (Fig. 7.14).

The pattern of magnetic anomalies on the 18°10'S propagating rift (De Alteriis et al., 1993) shows that propagation began after Anomaly 2 and before Anomaly J (Fig. 7.14). This observation allows us to fix the age of the N15 segment between 1 and 1.6 Ma (see next section). Note that the N-S axial anomaly shows an increase in amplitude towards the tip of the propagating rift, which is the typical signature of the Fe-Ti enriched basalts formed in this setting (Miller and Hey, 1986).

Because of the occurrence of the 18°10'S propagating rift, the N15 segment was much longer about 1.5 Ma ago than it is today. Based on bathymetric and magnetic data, its tip was located around 19°S (De Alteriis et al., 1993; Ruellan et al., 1994) which suggests a propagation rate of about 75 mm/a (Huchon et al., 1994). This value is similar to the value found at the Galapagos Propagating Rift (Kleinrock and Hey, 1989).

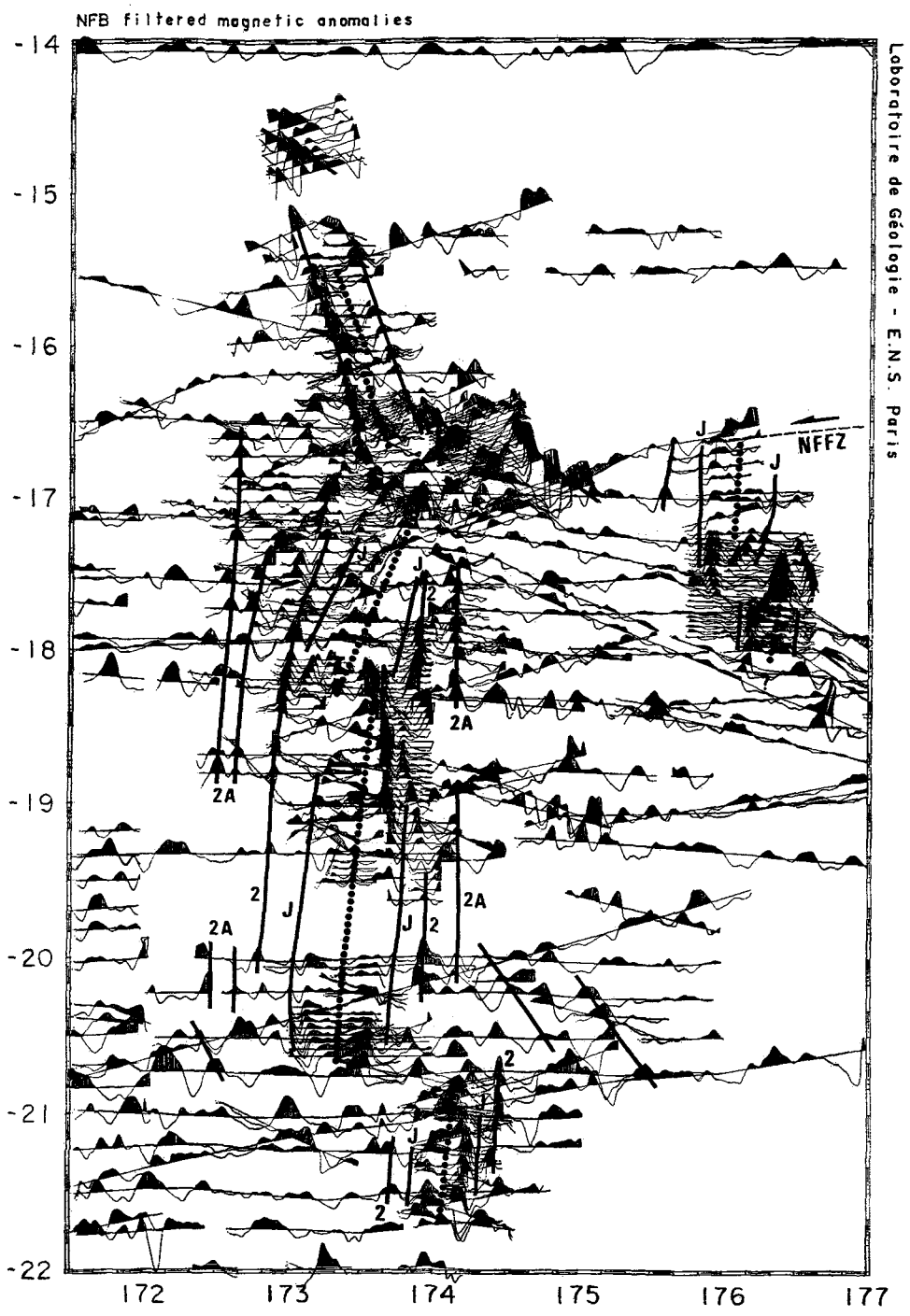

Fig. 7.14. Magnetic anomaly data projected along tracks of the Central Spreading Ridge between 14°S and 22°S and interpretation by Huchon et al. (1994). Dotted line: spreading axis, bold lines: identified magnetic anomalies, NFFZ: North Fiji Fracture Zone.

7.4.1. SPREADING RATE AND AGE

On the N160 segment, the spreading rate calculated from the magnetic anomalies has an intermediate value of 50 mm/yr (Huchon et al., 1994) and an age of less than 1 Ma (Auzende et al., 1991). Magnetic anomalies suggest

an age between 1 and 1.6 Ma for the N15 segment, whereas the calculated spreading rate decreases from 66 mm/yr at 18°S to 52 mm/yr at 16°50'S (Huchon et al., 1994). As has been suggested previously, magnetic anomalies up to 2A (3.5 Ma) have been identified along the N-S segment, and the calculated spreading rate decreases from 82 mm/yr at 20°S to 71 mm/yr at 19°S (Huchon et al., 1994).

Thus, the spreading rate is of an intermediate rate decreasing from 80 to 50 mm/yr along the Central Spreading Ridge. This northward decrease in spreading rate suggests that the pole of opening of the Central Spreading Ridge is located close to the north of the area. Assuming an E-W direction of opening, Huchon et al. (1994) estimated the latitude of the pole of rotation at around 9°S.

7.5. Gravity anomalies

To facilitate computation we separated the area in two sub-regions that overlap between latitudes 17°30'S and 18°30'S. These areas will be referred to hereafter as the northern and southern areas. The northern area has good gravity coverage from the Kana Keoki-1982 and Moana Wave-1987 cruises of the Hawaii Institute of Geophysics (Kroenke et al., 1993a; Jarvis and Kroenke, 1993).

For the southern area, CSR5 (N15 segment) and the whole N-S segment, the coverage is irregular, with sparse transit profiles, and only local full-coverage boxes, acquired during the Seapso 3 cruise (Auzende et al., 1988a). The central part of the southern area is particularly poorly covered, and anomalies with wavelengths shorter than 80 km cannot be resolved. In order to increase the spatial resolution in this central part we included free-air gravity anomalies derived from satellite altimetry (Sandwell and Smith, 1992). The spectral analysis of the free-air gravity computed from the satellite altimetry reveals that anomalies with wavelengths larger than 50 km can be correctly resolved. Thus, satellite-derived free-air gravity data were used to fill some data gaps.

In order to allow coherent comparisons to be made between the northern and southern areas, free-air grids were downgraded to remove wavelengths shorter than 50 km. The choice of the 50 km cut-off for the filter was determined by independent spectral analyses of both satellite and gridded marine data (for more detailed information see Gràcia et al., 1996b).

7.5.1. FREE-AIR GRAVITY ANOMALIES

The free-air anomaly map of the northern part of the Central Spreading Ridge between 14°S and 17°30'S, comprising the N160 segment and CSR4 (N15 segment) is shown in Figure 7.15a. The anomaly lows (-20 mGal) are associated with greater depths and rift valleys arranged *en échelon* along the N160 segment. Maximum positive anomalies (70 mGal) occur over topographic highs such as the 16°50'S triple junction, and the flanks of the CSR2, CSR3 and CSR4 segments (Fig. 7.15a).

On the downgraded free-air anomaly map of the northern part (Fig. 7.16a), the main features are still recognizable. The free-air anomaly map of

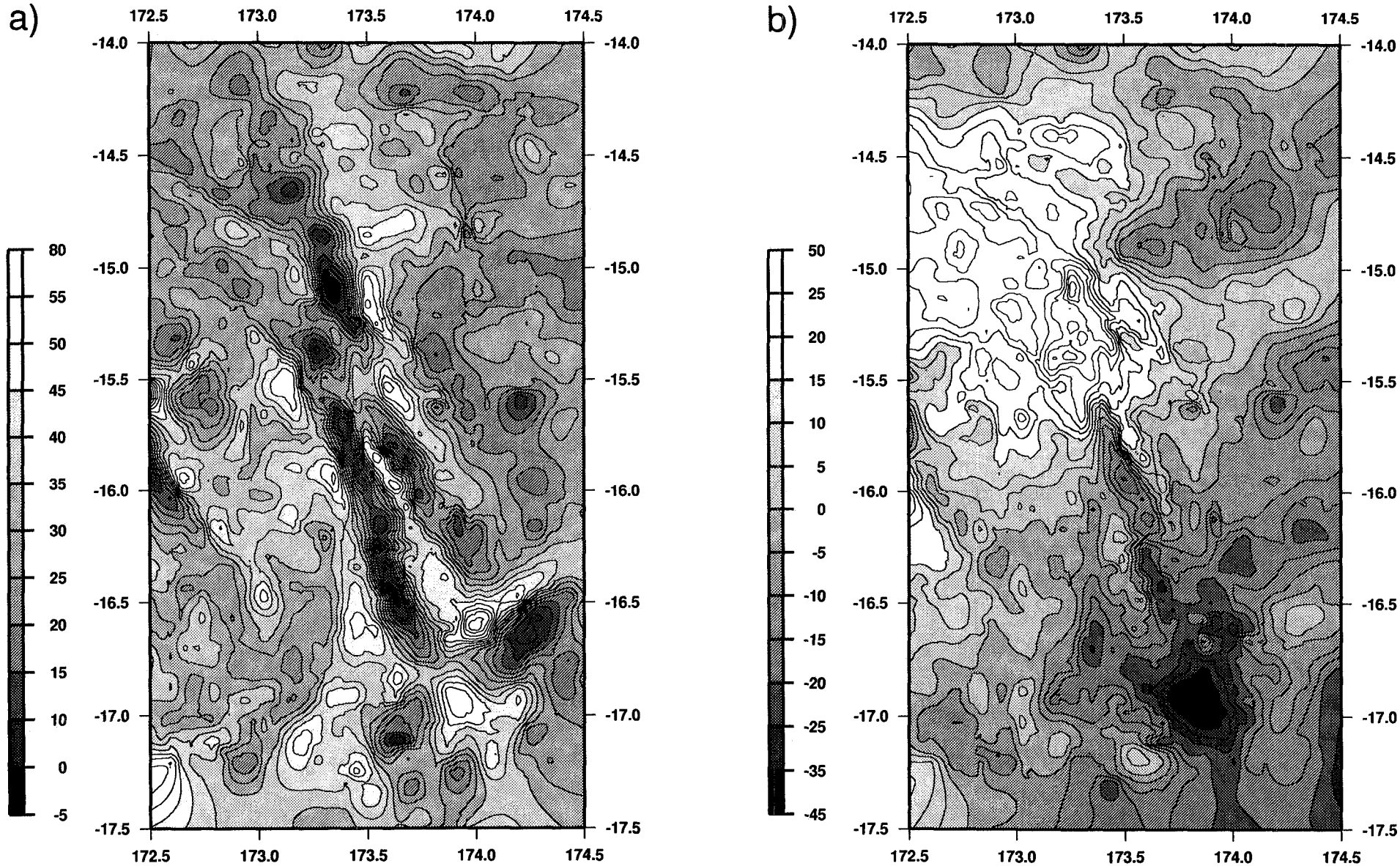

Fig. 7.15. a) Free-air gravity anomaly map of the northern part of the Central Spreading Ridge. b) Mantle Bouguer anomaly map of the northern part of the Central Spreading Ridge. These maps are created with the maximum resolution of the data. Contour interval is 5 mGal.

the southern part of the Central Spreading Ridge (17°30'S and 22°S), comprising the CSR5 (N15 segment) and the whole N-S segment is shown in Figure 7.16b. The N-S segment, is characterized by a small anomaly gradient (±10 mGal) consistent with its smooth axial topography. The off-axis seamounts are characterized by positive anomalies (more than 40 mGal).

7.5.2. MANTLE BOUGUER ANOMALIES

The mantle Bouguer anomaly is related to the sub-seafloor density structure (Figs. 7.15b and 7.16c,d) and reflects the gravity field arising from density anomalies in the crust or in the mantle. The interpretation of the mantle Bouguer anomaly can be made in terms of crustal thickness and density variations, mantle density variations thermally induced, or by a combination of these mechanisms (see section 2.3). In Figure 7.15b we present the resultant mantle Bouguer anomaly for the northern area. As for the free-air grid, the resultant mantle Bouguer anomaly for the northern and southern areas was also downgraded to remove wavelengths shorter than 50 km (Fig. 7.16c,d). A comparison between Figures 7.15 and 7.16 shows that downgrading preserves the main characteristics of the gravity field.

In the northern area (N160 segment) there is a strong negative signature (-50 mGal) passing from a "bull's-eye" (centred at the 16°50'S triple junction) to an elongated shape (Figs. 7.15b and 7.16c). Elongated "bull's-eye" anomalies (-25 mGal) appear also centred in the middle of segments CSR2 and CSR3, and may indicate the propagation of the CSR2 and CSR3 segments towards the north. The tip of the propagator is located at 15°50'S, at the point where the two triangular ridges bordering the rift valley end (Fig. 7.15a). From this point to the north, at about 14°20'S, the large positive anomaly (50 mGal) observed is possibly related to old and cold crust (Figs. 7.15b and 7.16c).

Fig. 7.16. Left: Downgraded free-air (a) and mantle Bouguer (c) anomaly maps of the northern part of the Central Spreading Ridge. Right: Free-air (b) and mantle Bouguer (d) anomaly maps of the southern part of the Central Spreading Ridge. The original data of (a) and (c) is presented in Figure 7.15 and has been downgraded to be compared with the southern part of the Central Spreading Ridge, where the gravity coverage is much more sparse. Superimposed, bold lines correspond to bathymetric contours to indicate the position of the rift-valleys, axial highs and seamounts. Contour interval is 5 mGal (Gràcia et al., 1996b).

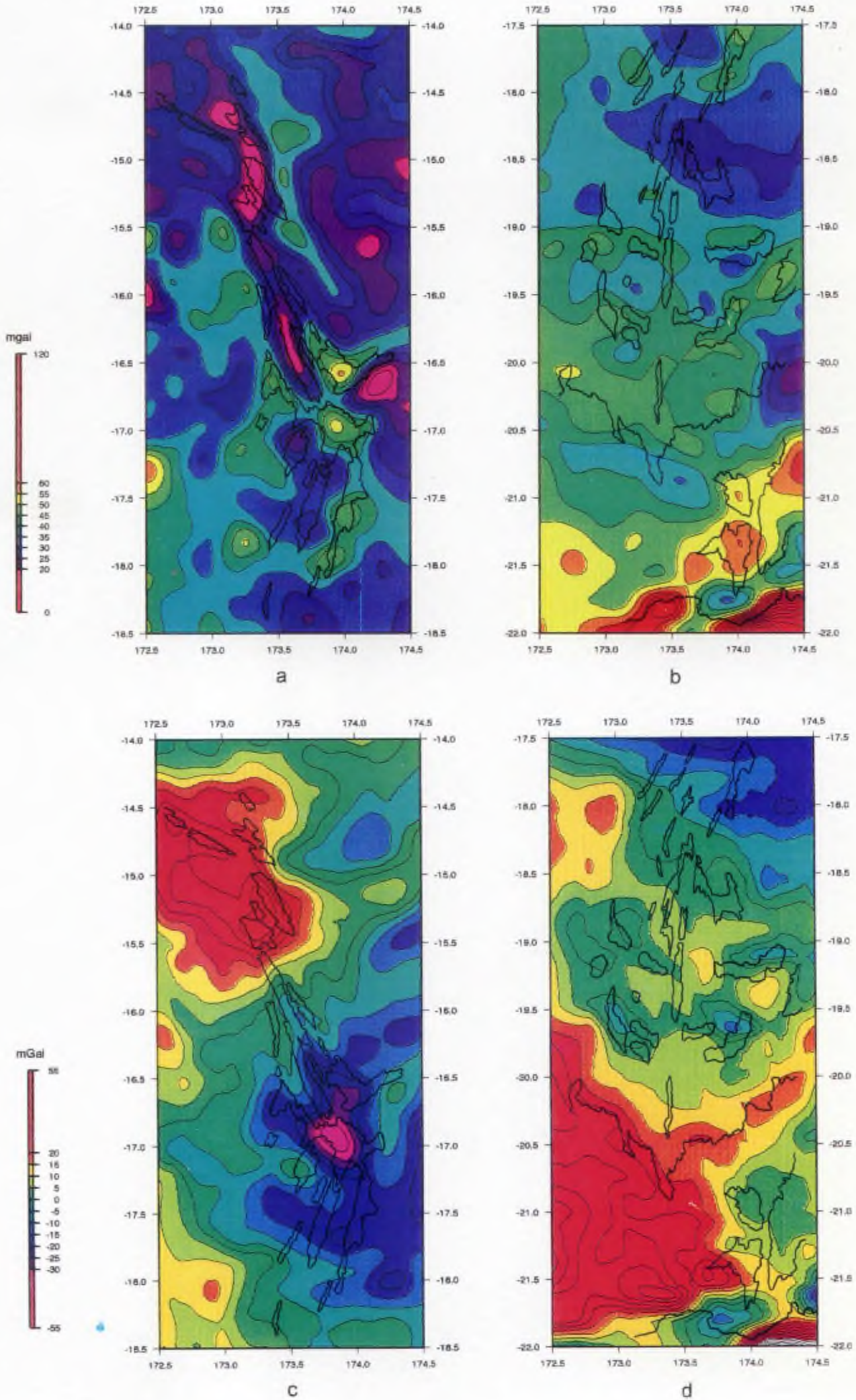
mgal
120
60
55
50
45
40
35
30
25
20
0
172.5
173.0
173.5
174.0
174.5
-14.0
-14.5
-15.0
-15.5
-16.0
-16.5
-17.0
-17.5
-18.0
-18.5
a
-17.5
-18.0
-18.5
-19.0
-19.5
-20.0
-20.5
-21.0
-21.5
-22.0
b
mGal
55
20
15
10
5
0
-5
-10
-15
-20
-25
-30
-55
c
d

The mantle Bouguer anomaly map of the southern part of the Central Spreading Ridge (Fig. 7.16d) shows a very uniform signature. The axis of the N-S segment shows anomaly variations from 5 to 10 mGal. The N-S segment propagates towards the north, as indicated in the bathymetric and structural maps (Figs. 7.6 and 7.7), towards the negative anomaly zone of the 16°50'S triple junction. Between 20°S and 21°S there is a V-shaped structure, visible both in the bathymetry and gravity, probably related to the southwards propagation of the N-S segment into a zone of old, cold crust with a very high positive gravity anomaly (55 mGal). The off-axis seamounts have a negative anomaly (-10 mGal) (Fig. 7.16d) which may be related to a locally thickened crust.

Chapter 8

THE SOUTH PANDORA AND TRIPARTITE RIDGES

8.1. Data base and methods

The data for this study come from the NOFI (NOrth of the North FIji Basin) cruise which took place between 25th August and 19th September, 1994 on board the French R/V L'Atalante. The area surveyed is located in the northern part of the North Fiji Basin, between 171°E and 178°E and 13°S and 14°40'S (Fig. 8.1). While maximum data coverage was obtained between longitudes 171°E and 175°30'E, between 175°30'E and 178°E, the data include only twelve widely spaced zig-zag tracks which were undertaken to explore the easternmost part of the ridge (Fig. 8.1)

The operations conducted during the NOFI cruise included swath-bathymetry and imagery, geophysics (seismic reflection, magnetic, and gravity profiles), and geological samples (dredges and piston core) (Lagabrielle et al., 1994a,b). In this chapter, we present only bathymetry, magnetic and gravity data.

8.1.1. BATHYMETRY

Bathymetric data were obtained with the Simrad EM-12 Dual multinarrow-beam echo-sounder for deep sea. This system provides precise swath mapping capability from 70 m to full ocean depth (11,000 m) with a normal accuracy of 0.25% of water depth. Integrated data processing enables detailed real time mapping. The maximum angular coverage of the EM-12 Dual is 150°. Two separate multibeam echosounders, one on port and one on starboard, generate 81 stabilized beams each, 11 of which are common (see Fig. 1.2). The swath width covered by the 162 beams is 7.4 times the water depth, so for 2800 m depth, the swath width is 20.7 km. In comparison with the EM-12 sounder on board the R/V Hesperides used during the GEBRA 93 cruise, it gives an increase in swath width of approximately 10 km in the 3000-6000 km range. Post-processing, in order to obtain the bathymetric maps, was performed as in section 1.2.1.

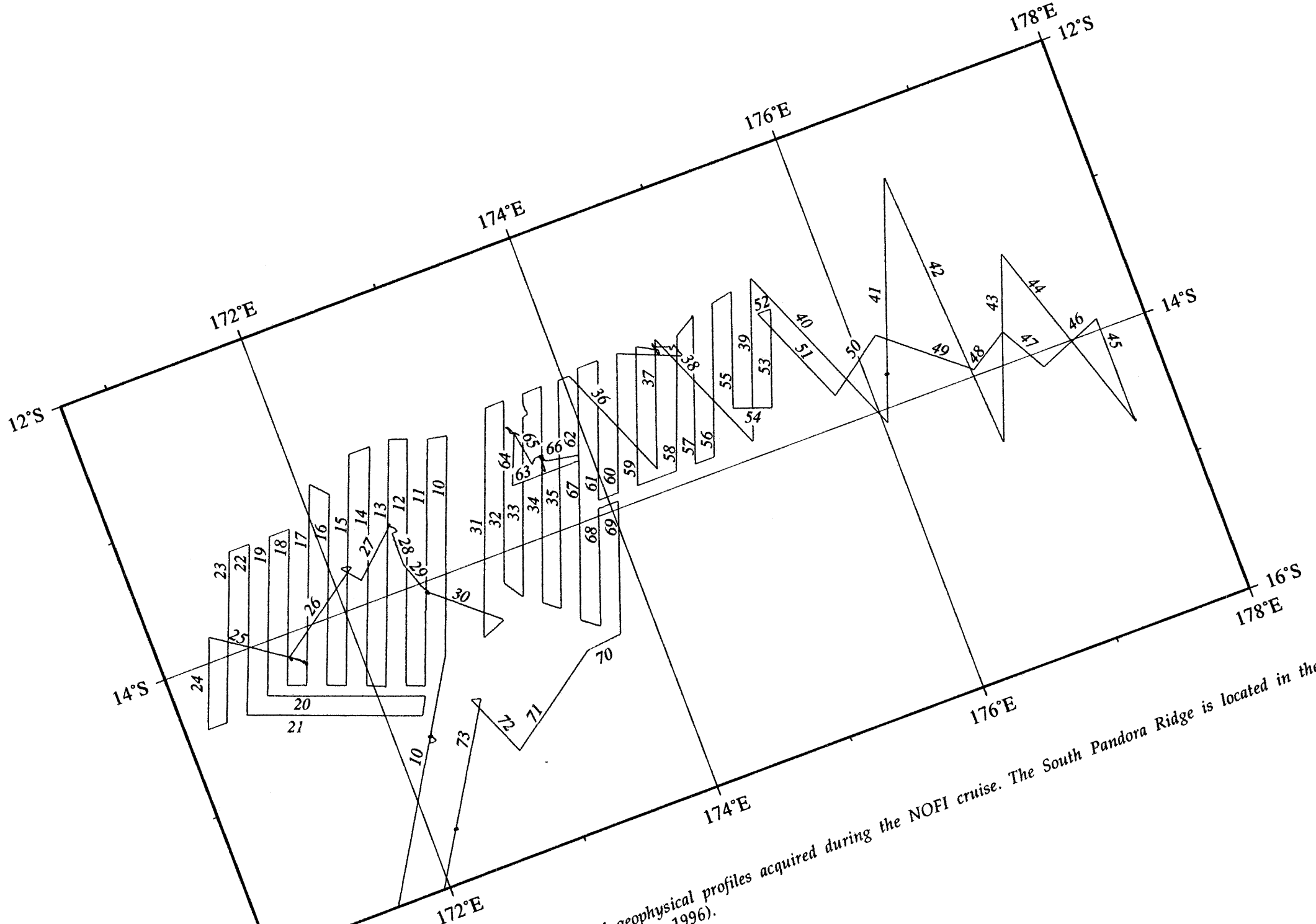

geophysical profiles acquired during the NOFI cruise. The South Pandora Ridge is located in the

1996).

8.1.2. MAGNETICS

The total amplitude of the magnetic field was recorded using a Barringer Research M-244 proton magnetometer. The sensor was towed from the ship's stern by a 280 m long cable, at a depth of about 15 m. The accuracy was 0.5 nT, and the sampling rate was 6 seconds. No correction was made for diurnal variations. In this chapter, we show the magnetic anomaly data and a preliminary identification of the anomalies, emphasizing the relationship of bathymetric and magnetic lineations. The parameters outlined in section 1.2.2 were used to calculate the synthetic magnetic profiles.

8.1.3. GRAVITY

Gravity data was measured using a Bodenseewerk KSS3 30 gravity meter, which was mounted on a KT 30 gyrostabilized platform, and installed at a point where ship motion was minimal. Short period noise was discernible in total gravity field data, and was clearly related to sea conditions. The noise amplitude was about 1 mGal in fair seas, but reached 3 mGal with 2-3 m swell and 30 knot wind-conditions which prevailed during most of the first half of the cruise. After smoothing the short period noise and cross-over errors between tracks, the data was considered suitable for interpretation. Gravity data were used to contour free-air anomaly and mantle Bouguer anomaly maps where there was sufficient data coverage. These maps were obtained following the procedure explained in section 1.2.3.

8.2. Morphostructure

As in Chapters 4 and 5, this section is based on the analysis of bathymetric maps, and consequently, we consider the same sections as in Chapter 5.

8.2.1. RIDGE SEGMENTATION

The South Pandora and Tripartite Ridges are located in the northern part of the North Fiji Basin and extend over more than 800 km. On the bathymetric map of the whole area (400 m contour), three main segments are distinguished according to their orientation: the N75 and E-W segments, which form part of the South Pandora Ridge (Green and Cullen, 1973), and the N110 segment also known as the Tripartite Ridge (Kroenke et al., 1993b) (Fig. 8.2).

The parameter used to determine segmentation order along the South Pandora-Tripartite Ridge was the segment length, also used for the Central Spreading Ridge. The axial depth profile (Fig. 8.3) shows a long wavelength (250-300 km) between the three first-order segments separated by the 172°10'E non-transform discontinuity and the 174°55'E offset. Superimposed on this long-wavelength there is also a shorter-wavelength (about 100 km) caused by smaller second-order discontinuities. The shorter segments are labelled from west to east, SPR4 to SPR0, and TR3 to TR1.

A detailed analysis of the fault scarps and structural lineations observed in the axial zone of each second-order segment was undertaken using 25 m contour bathymetric maps at 1:250,000 scale. A total of 777 directions were measured in the axial domain and grouped into first-order segments (163 for the N75 segment, 332 for the E-W segment and 282 for the N110 segment). They are represented in three rose diagrams with a 5° interval and a radius of 20% of the values (Fig. 8.4). Thus, in segments N110 and E-W the current axial structures follow the main segment trend. In contrast, part of the current axial structures in the N75 segment trend E-W, obliquely to the main segment trend (Fig. 8.4).

N75 first-order segment

This first-order segment extends 170 km, between 170°48'E and 172°12'E (Fig. 8.2). This segment corresponds to the westernmost part of the South

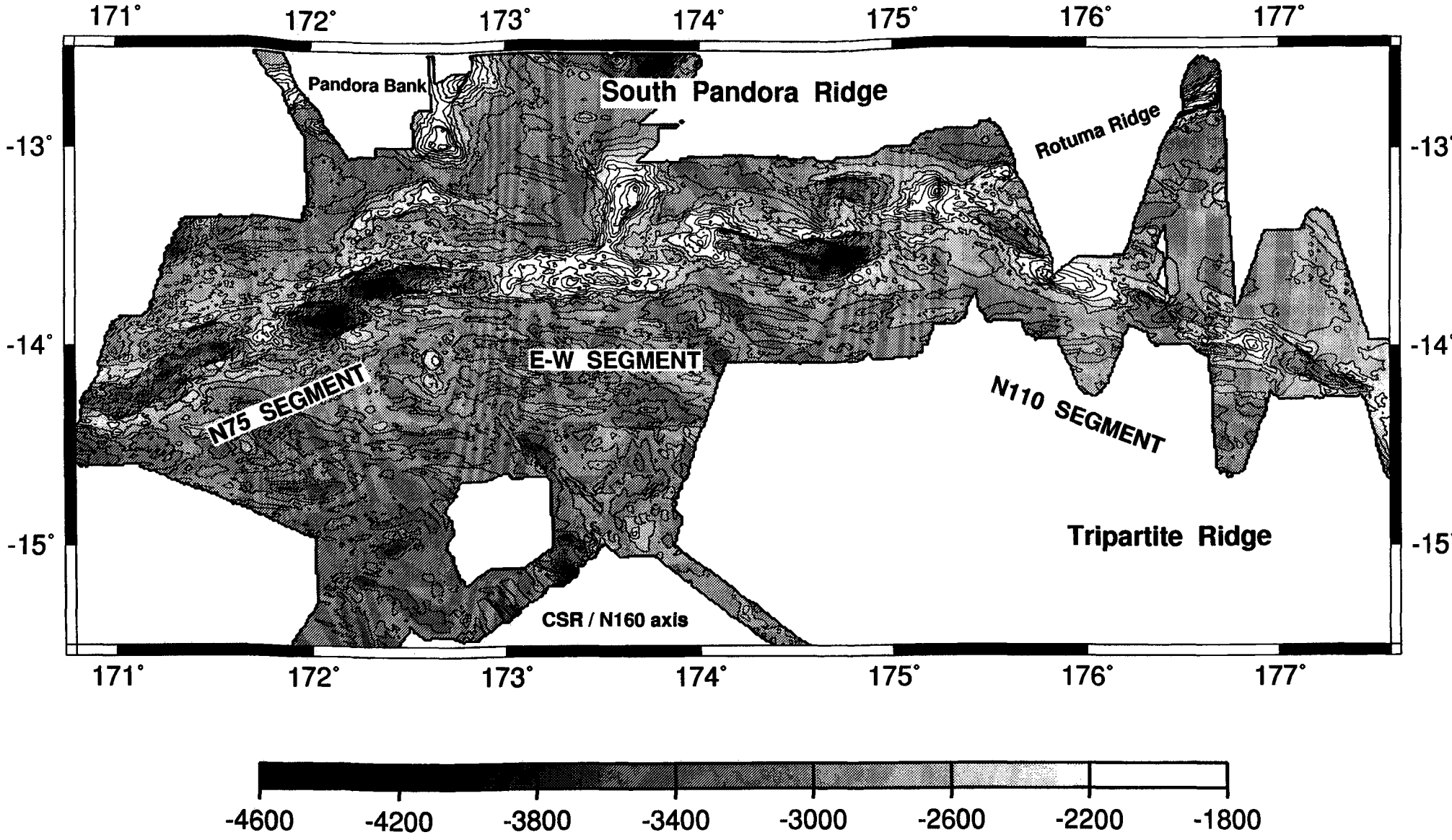

Fig. 8.2. Bathymetric map of the South Pandora and Tripartite Ridges in 200 m contour interval. The three first-order segments (N75, E-W, and N110), the Rotuma Ridge, and the N160 segment of the Central Spreading Ridge are identified.

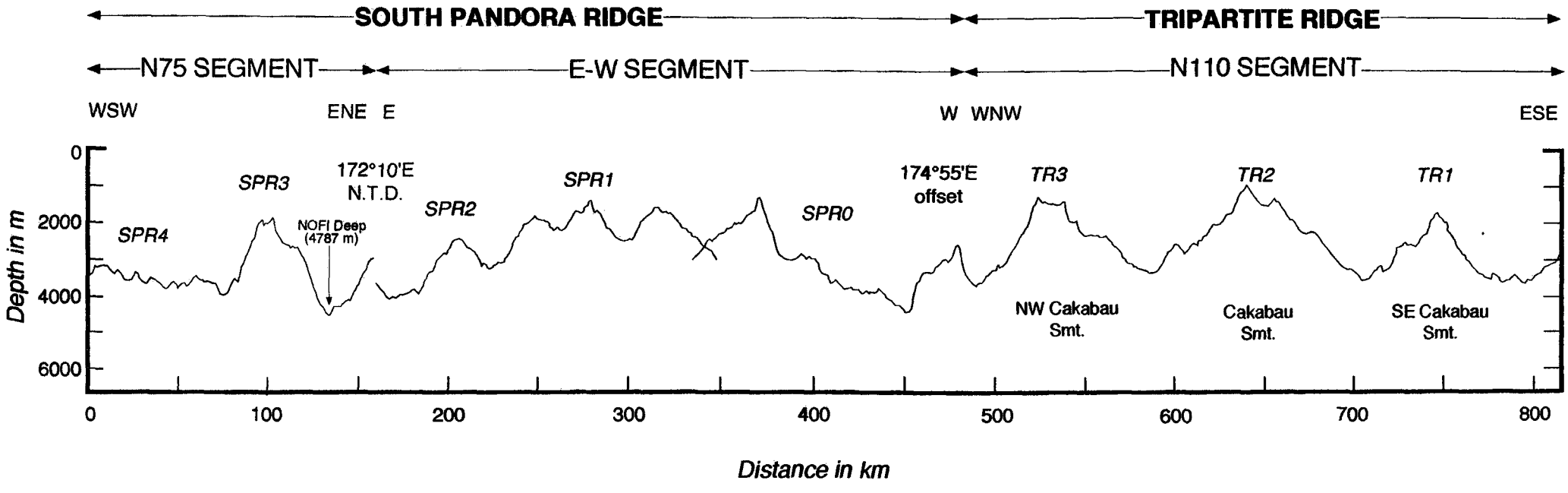

Fig. 8.3. Axial depth profile along the South Pandora and Tripartite Ridges. The three first-order and their respective second-order segments (SPR4 to SPR0 and TR3 to TR1), and the two first-order discontinuities are shown. Vertical Exaggeration: 20.

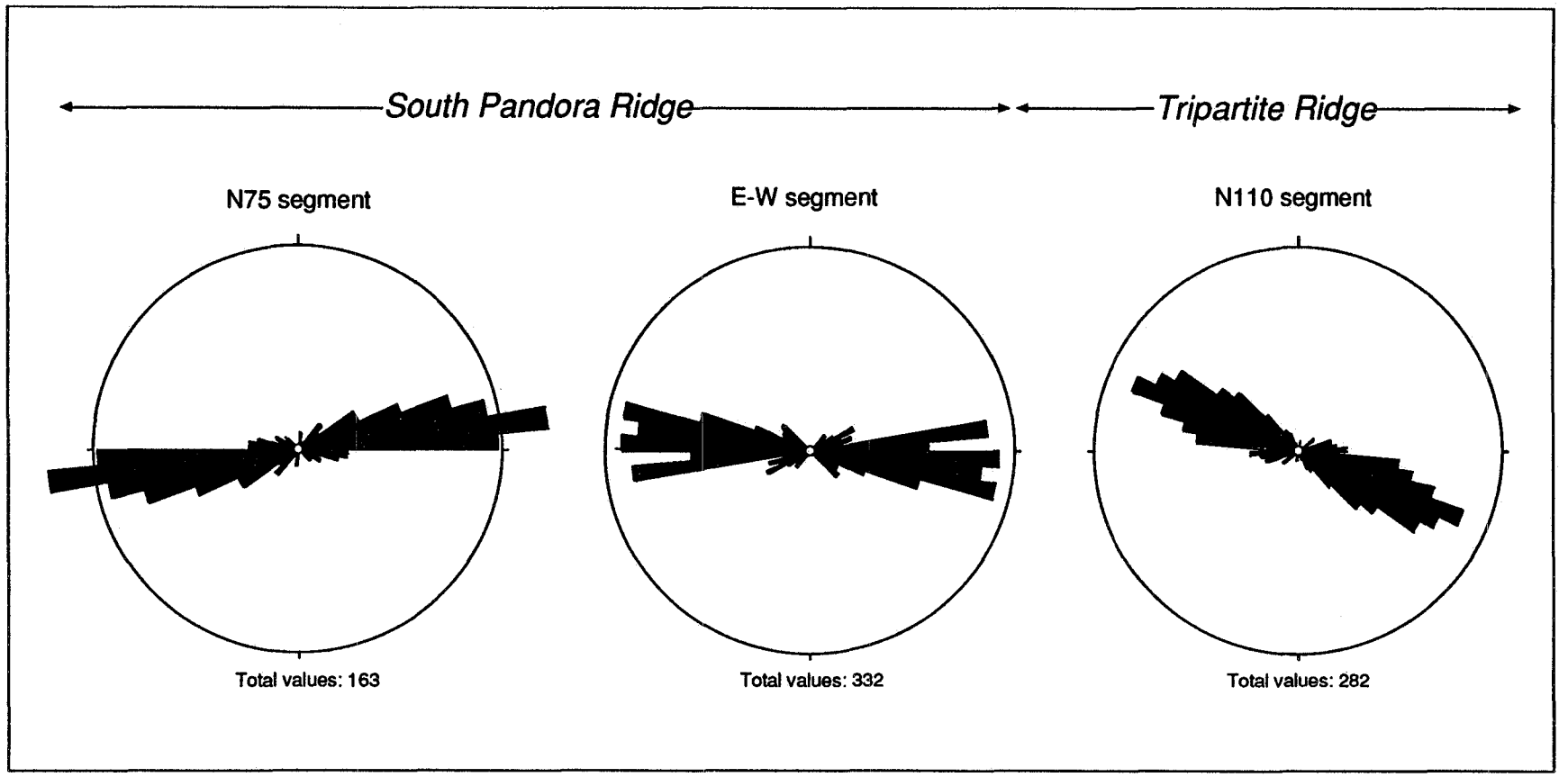

Fig. 8.4. Rose diagrams of the structural trend of lineations and fault scarps measured along the axial zones of the N75, E-W and N100 first-order segments. Interval: 5° and radius: 20%.

Pandora Ridge, and trends predominantly N70-N75 (Fig. 8.4). It is composed of two second-order segments (from west to east, SPR4 and SPR3), which can be seen on the bathymetric map (Fig. 8.5), while its morphostructural interpretation is included as Figure 8.6.

Segment SPR4 is located on the western edge of the survey area, and has not been completely mapped. It is at least 58 km long and seems to extend farther west with the same orientation. It shows an axial valley bounded by discontinuous lateral ridges trending E-W and which change to N75 towards the east (Figs. 8.4 and 8.6). A small offset located at 171°14'E separates segment SPR4 from SPR3.

Segment SPR3 is 125 km long, mainly trends N75 and is composed of a deep graben, with a large central volcanic high arranged *en échelon*. The axial zone of the segment is bordered by two narrow elongated ridges flanked by very steep scarps (Figs. 8.5 and 8.6). The northern ridge (5 km wide, 60 km long and N75 trend) is clearly shown on the bathymetric map (Fig. 8.5)., while the southern ridge is less continuous but also presents a marked N75 trend. Three third-order segments arranged *en échelon* , named SPR3a, SPR3b, and SPR3c, from east to west respectively, can be distinguished. The axis of these segments clearly trends E-W, and is oblique in respect to the N75 direction pattern of the SPR3 segment (Fig. 8.4).

- Segment SPR3a is 53 km long, 22 km wide with an average depth of 3800 m. It is characterized by an arcuate graben which might be the result of the two main structural trends, N75 and E-W, interacting (Figs. 8.5 and 8.6).

- Segment SPR3b is characterized by a 35 km-long and 24 km-wide topographic high protruding into the middle of the SPR3 segment, and bordered along-axis by two axial grabens. The central high appear to be rifted by faults trending E-W and N75 (Figs. 8.5 and 8.6).

- Segment SPR3c is a 43 km-long graben trending N85-E-W and flanked by abrupt walls clearly trending E-W. At the eastern part of this segment, a maximum depth of 4787 m, the greatest measured during the NOFI cruise whitin the North Fiji Basin, was recorded and named the NOFI Deep (Figs. 8.5 and 8.6).

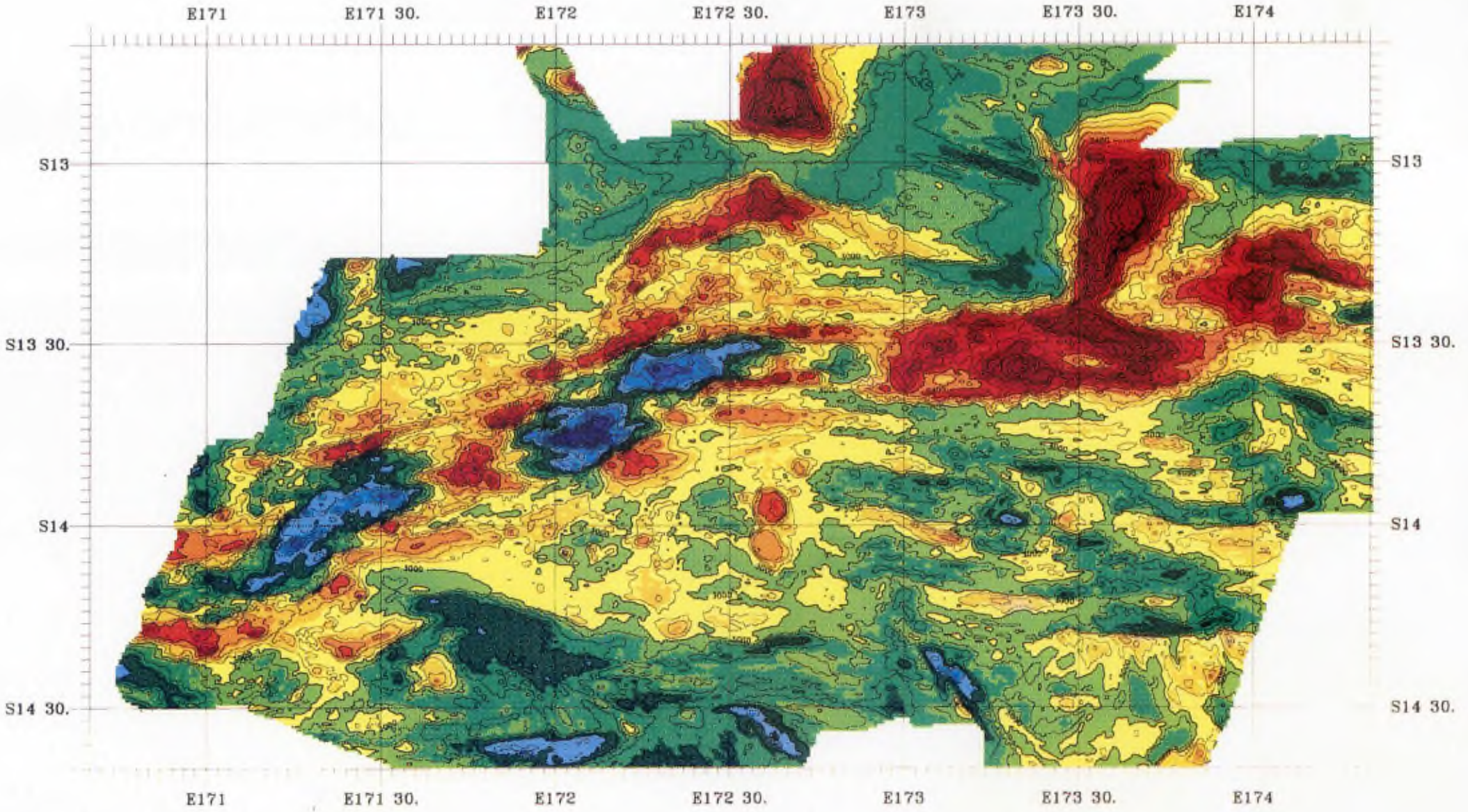

Fig. 8.5. Bathymetric map of the western part of the South Pandora Ridge between 170°40'E and 174°20'E, comprising the whole N75 segment and the western part of the E-W segment. Bathymetric contour: 150 m. Colour change: 200 m.

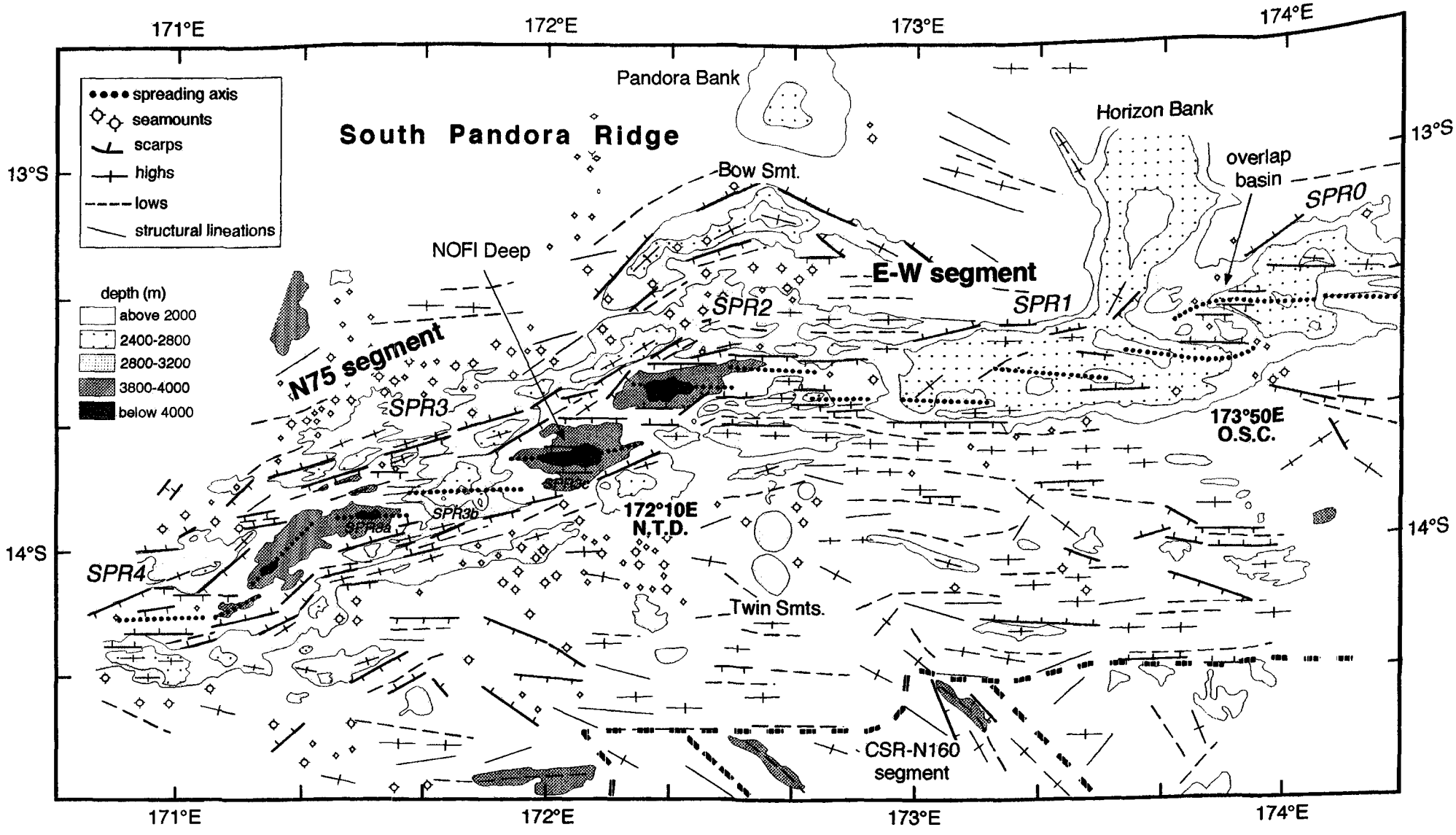

Fig. 8.6. Morphostructural interpretative map of the western part of the South Pandora Ridge. Second-order segments, axial discontinuities, and off-axis features are also indicated.

Around 172°12'E, a distinctive offset of 15-18 km, separates the axis of SPR3 from that of segment SPR2.

E-W first-order segment

This first-order segment is 300 km long and is located between 172°12'E and 174°54'E (Fig. 8.2). It corresponds to the eastern part of the South Pandora Ridge, trends predominantly E-W (Fig. 8.4), and is composed of three second-order segments, from west to east SPR2, SPR1, and SPR0, respectively (Figs. 8.5 and 8.6).

The 80 km-long segment SPR2 consists of a 12-14 km wide E-W trending graben flanked by two sharp narrow lateral ridges which are 5 km wide and culminate at a depth of 1800 m. The segment is composed of an axial graben that becomes progressively shallower and narrower towards the east. At 172°45'E the graben is only 5 km wide, and at this point the two bordering ridges reach their maximum elevation. Off-axis there is a high-and-low topography parallel to the main E-W trend. However, about 40 km off-axis there is a strong asymmetry between the northern and southern flanks. On the northern side, a 92 km-long ridge, showing a half-elliptical shape, is centred at 172°35'E, and named Bow Seamount (Fig. 8.6). North of this feature, a circular seamount which forms part of the Pandora Bank shallows at less than 1200 m. Around 40 km off-axis on the southern flank, two large circular-shaped seamounts, named Twin Seamounts, of 13 km diameter, disrupt the cyclic E-W seafloor pattern (Figs. 8.5 and 8.6).

Segment SPR1 is characterized by a very large volcanic high, which largely trends E-W and whose width varies between 18 to 30 km, with the widest part between 173°20'E and 173°30'E (Fig. 8.5). It is clearly rifted by two sets of faults trending E-W and N100-105. A median valley trending N100, whose depth reaches 2600 m, runs from the western tip of the segment to its eastern end and separates SPR1 into two main areas. In the western part of the segment, a small axial valley separates a volcanic high at the northern edge from an elongated and narrow ridge to the south. Towards the middle of the segment, at 173°30'E, a large near-axis seamount showing a triangular-shape is connected to the northern flank of the ridge segment. This feature corresponds to the Horizon Bank. The eastern tip of SPR1 segment is slightly curved towards the north whereas the western tip of SPR0 is curved towards the south, both overlapping at 173°50'E. The small depression formed

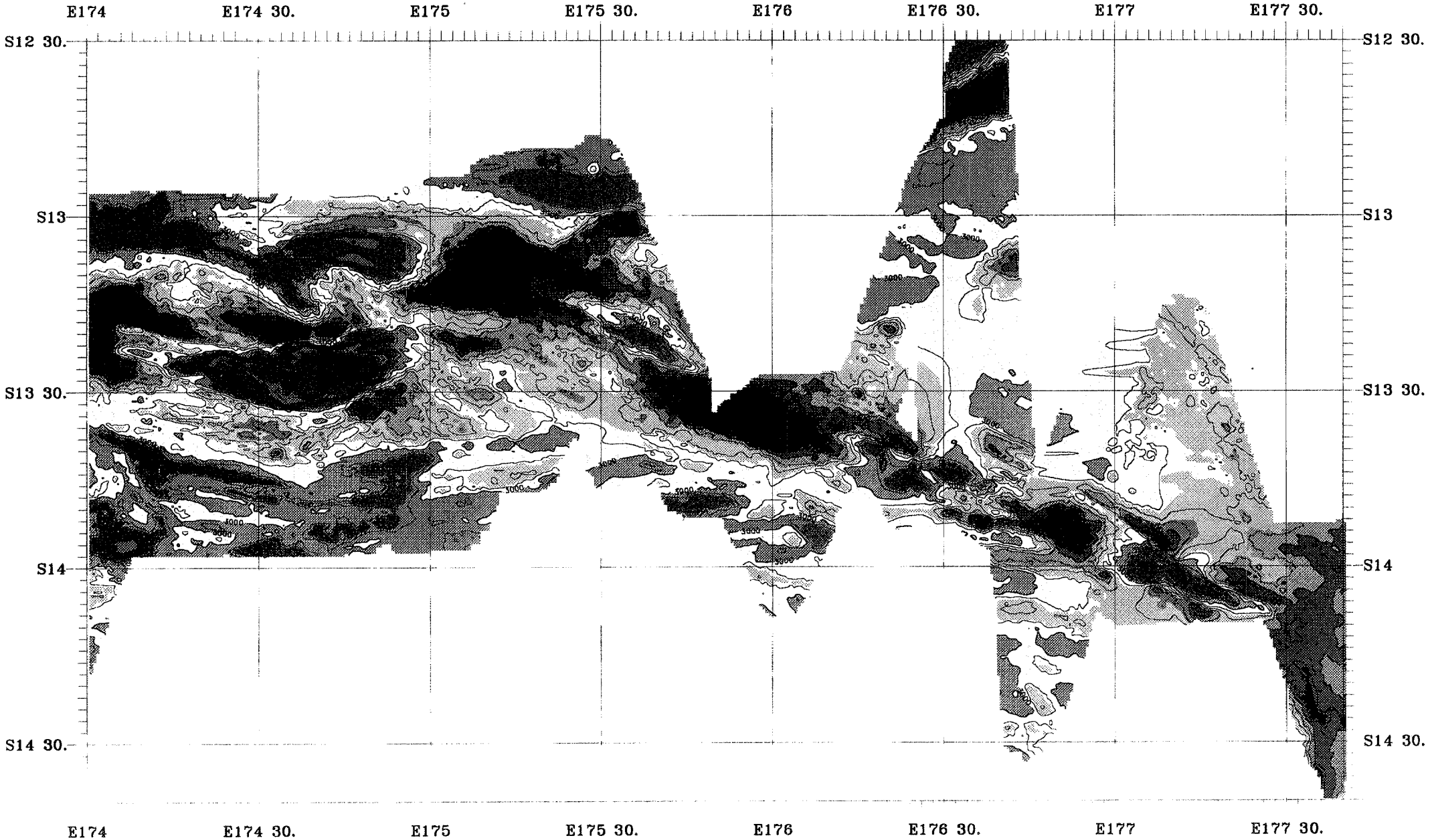

Fig. 8.7. Bathymetric map of the eastern part of the South Pandora Ridge between 174°E and 177°40'E, comprising the eastern part of the E-W segment and the whole N110 segment or Tripartite Ridge. Bathymetric contour: 150 m. Colour change: 200 m.

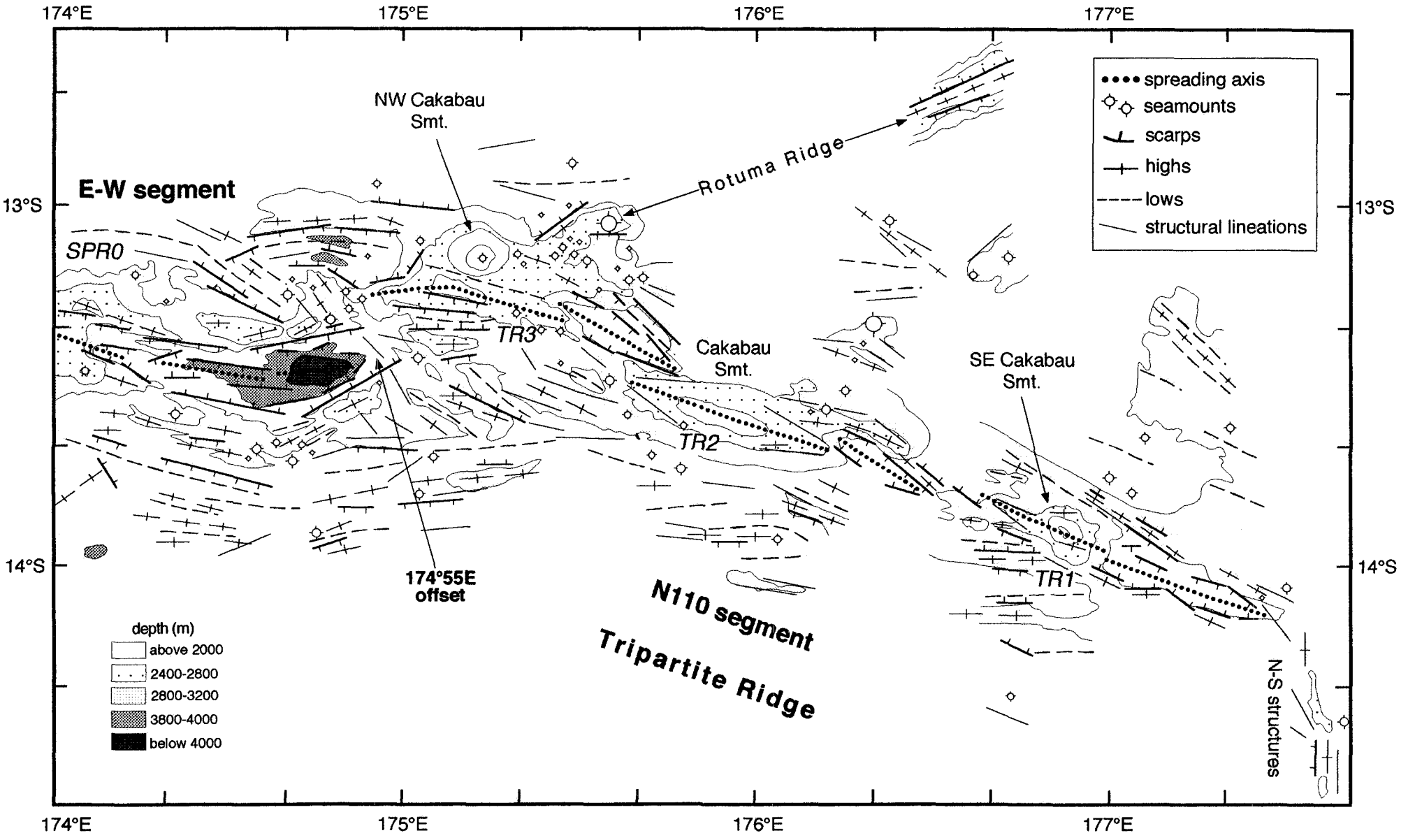

Fig. 8.8. Morphostructural interpretative map of the eastern part of the South Pandora Ridge and the whole Tripartite Ridge. Second-order segments, axial discontinuities, and off-axis features are also indicated.

between the two branches of the overlapping spreading centre corresponds to the overlap basin (Fig. 8.6).

Segment SPR0 is 135 km long, and is characterized by a split axial high which becomes an axial graben towards the east (Figs. 8.5 and 8.7). The northern half of the high is bow-shaped, with a steep rectilinear inner flank, and a smooth curved outer flank. The southern half of the high is dominated by a circular edifice centred at 174°E that elongates and curves to the west (Fig. 8.6). Around 174°10'E, an incipient axial graben may be observed, deepening and widening towards the east. Between 174°20'E and 175°E, the graben is bordered by two N105-110 trending elongated highs, both of which are 10 km wide and less than 2000 m deep. Off-axis and north of the axial domain at 174°45'E, a large curved graben can be observed (Figs. 8.7 and 8.8). Although this graben resembles a large overlapping spreading feature, geophysical data provides no evidence of present-day activity. An offset at 174°55'E is the discontinuity between SPR0 segment and the N110 segment.

Tripartite Ridge / N110 first-order segment

This first-order segment extends along 280 km, between 174°55'E and 177°30'E (Fig. 8.2). Also called the Tripartite Ridge, it trends predominantly N110 and is composed of three second-order segments from west to east, TR3, TR2, and TR1 (Figs. 8.7 and 8.8). Full bathymetric coverage of this first-order segment does not exist and only partial information is available along the axial zone.

Segment TR3 is located between 174°55'E and 175°45'E, is 106 km long and consists of a split axial high centred at 175°10'E which evolves towards the east into an axial graben. The central volcanic high, which we have named NW Cakabau Seamount (Fig. 8.8), corresponds to the intersection between the Tripartite, Rotuma, and South Pandora ridges. The graben bordering the NW Cakabau Seamount narrows progressively from 15 to 8 km, reaching a depth of 3600 m. The graben is limited by N120 trending and 750 m-high inner walls.

Segment TR2 is about 90 km long, and is composed of a large, slightly elongated axial volcano named Cakabau Seamount (Fig. 8.8), which was mapped with the SeaMARC II system by Kroenke et al. (1993a). A graben is located on its southeastern part. The Cakabau Seamount is centred at

175°55'E, and is 60 km long, 20 km wide and culminates at a depth of 400 m. The eastern graben is about 35 km long, 10 km wide and 3400 m deep.

Segment TR1 is 105 km long, and is located at the eastern limit of the Tripartite Ridge between 176°30'E and 177°30'E. This segment is composed of an axial seamount and a graben on its southeast end, as are the previous second-order segments of the Tripartite Ridge. The whole segment is bordered by two lateral ridges; the northern ridge trends N110-115 and shallows at about 2000 m, while the southern ridge trends almost E-W and is more discontinuous (Figs. 8.7 and 8.8). The axial volcano, named SE Cakabau Seamount (Fig. 8.8), is composed of a central round-shaped high 20 km wide and 25 km long centred at 176°53'E. At 176°46'E, the central volcano forks into two (200-2200 m high) elongated ridges. East of the seamount, a 50 km long elongated graben appears. This graben shows a triangular shape, narrowing progressively towards the end of the segment from 16 km to 3 km. The N110 structures stop abruptly at 177°30'E, where N-S trending structures appear.

8.2.2. AXIAL MORPHOLOGY

In common with the Central Spreading Ridge (Chapter 7), a succession of transverse bathymetric profiles orthogonal to the axis were undertaken. Some of these sections are presented in Figures 8.9, 8.10 and 8.11 for the N75, E-W and N110 segments, respectively. None of the three first-order segments shows a continuity in the along segment axial morphology.

The N75 segment is dominated by an axial graben morphology, disturbed only by the abrupt axial high of SPR3b. The rift valley of SPR4 segment extends from between a width of 10 to 15 km and a depth of 3800 m towards the segment end. The SPR3 segment shows a successive graben-dome-graben morphology, while SPR3a shows a rift valley 22 km wide, with a neovolcanic ridge in its middle (at 171°20'E) that disappears towards the east. Near 171°30'E, a maximum depth of 4200 m is observed (Fig. 8.5). In contrast, SPR3b is characterized by a triangular-shaped 22 km wide axial dome that culminates at a depth of 1875 m. Finally, SPR3c also shows a deep rift valley flanked by 1200 m high walls with an 18 km-wide inner rift (Fig. 8.9). The trough encloses the deepest part of the area, NOFI Deep, as explained in section 8.2.1.

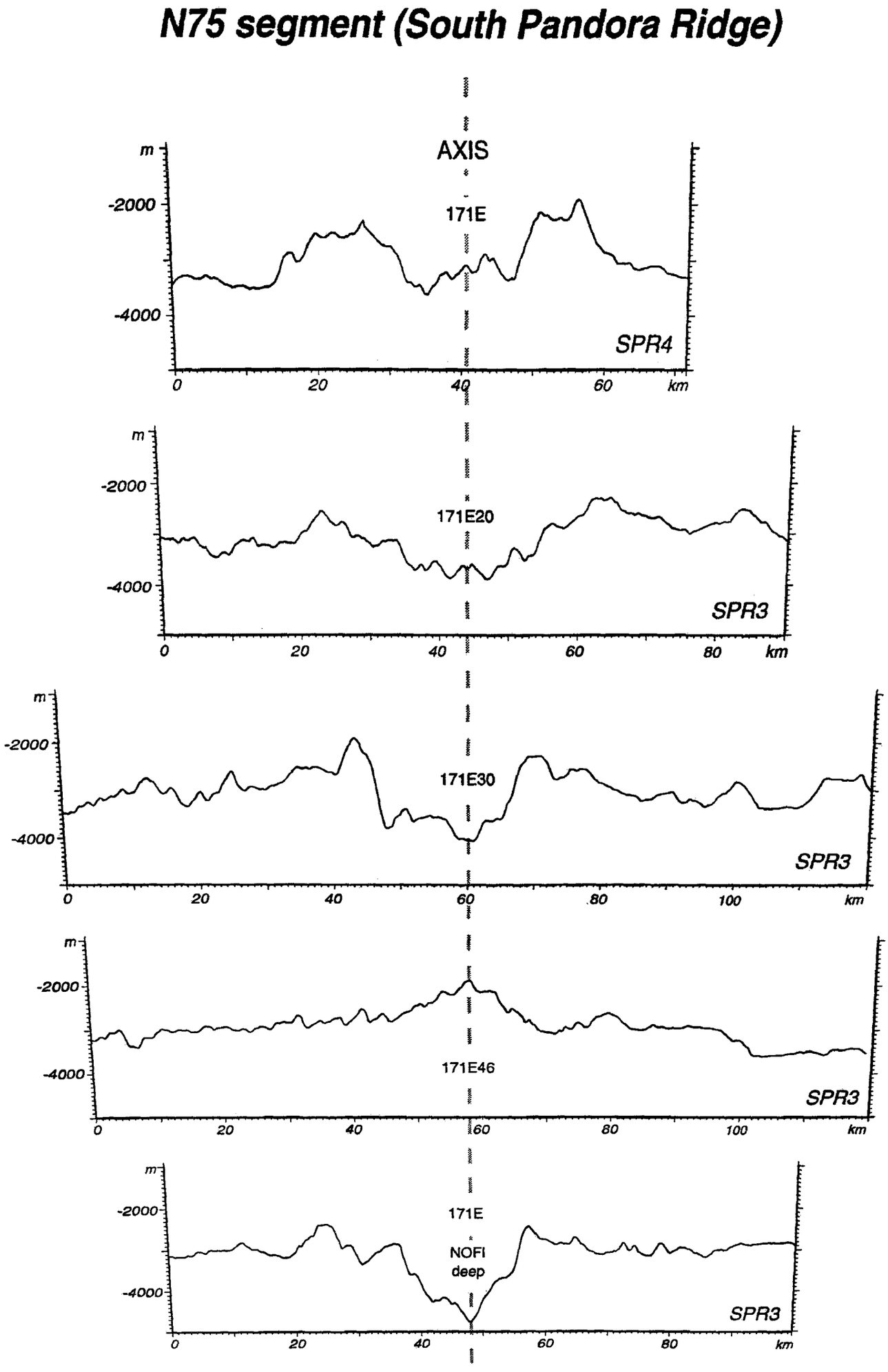

Fig. 8.9. Bathymetric sections across the N75 segment, western South Pandora Ridge. All the

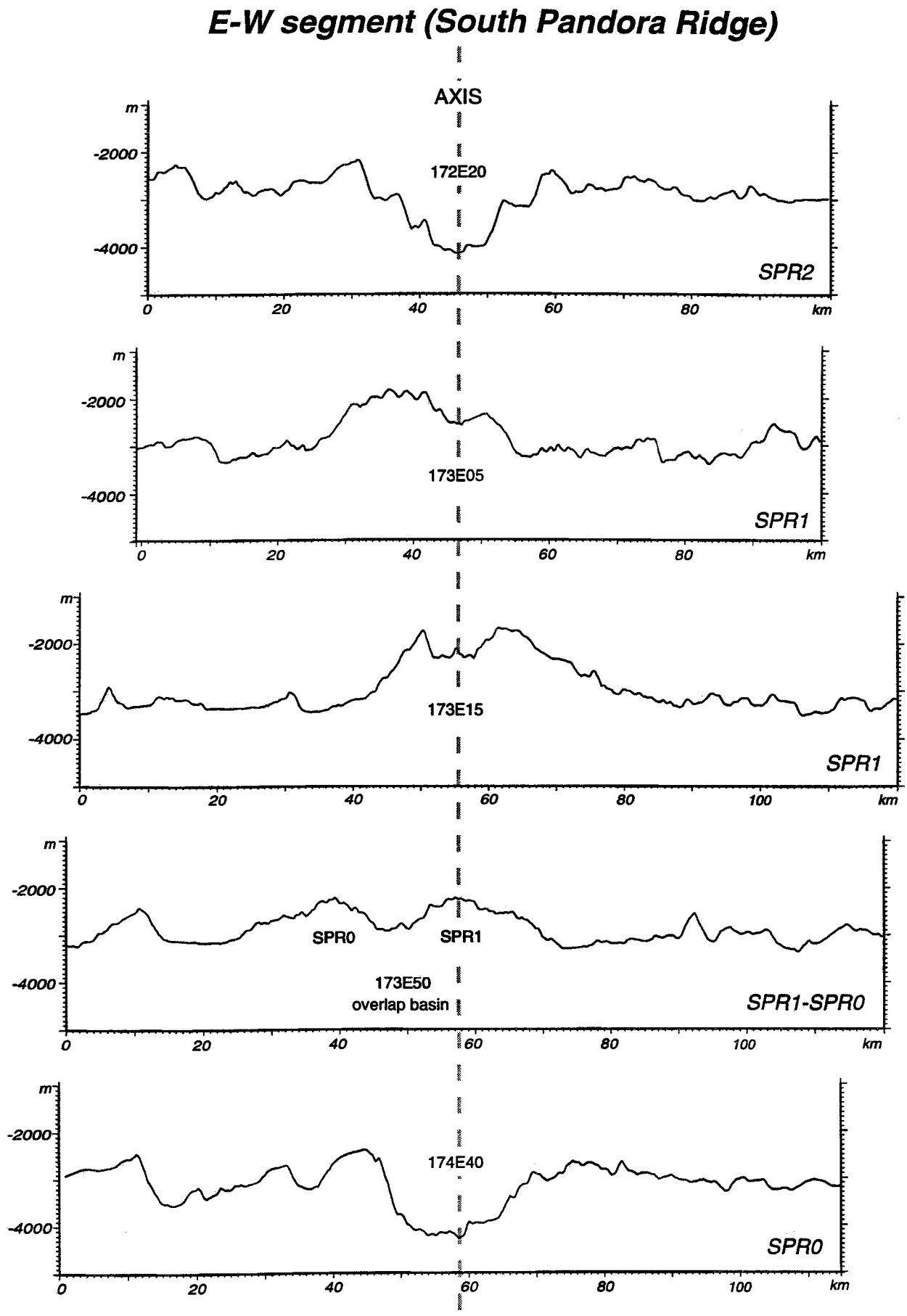

Fig. 8.10. Bathymetric sections across the E-W segment, eastern South Pandora Ridge. All the sections are taken following a N-S trend orthogonal to the axis. SPR2, SPR1 and SPR0 are second-order segments. Vertical Exaggeration: 7.

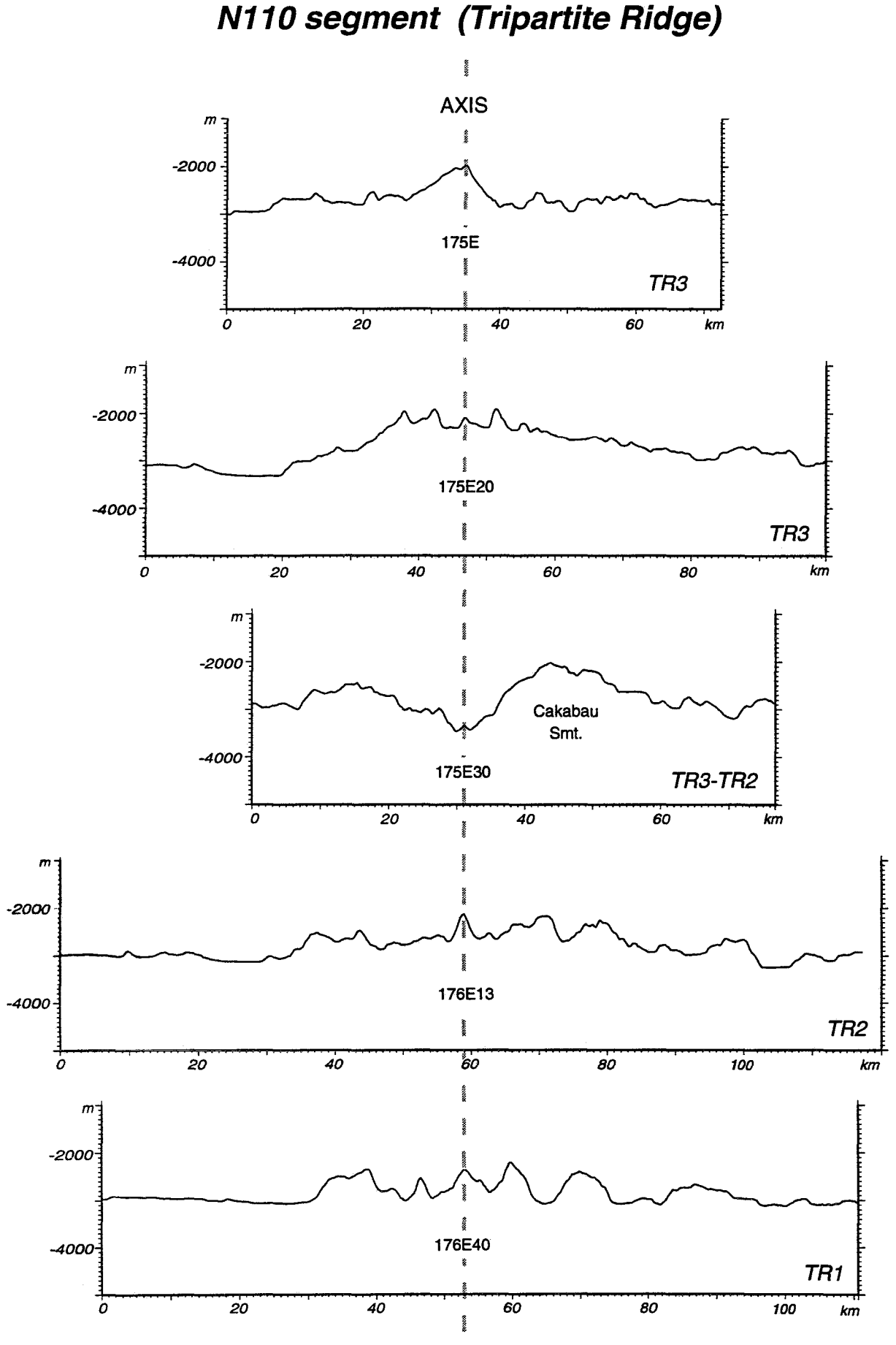

Fig. 8.11. Bathymetric sections across the N110 segment, Tripartite Ridge. All the sections are taken following a N20 trend orthogonal to the axis. TR3, TR2, and TR1 are second-order segments. Vertical Exaggeration: 7.

The E-W segment also shows a contrasting longitudinal morphology. The SPR2 segment is characterized by an axial valley topography. A typical slow spreading cross-section may be observed at 172°20'E (Fig. 8.10), where the rift valley is formed by several steps of inward faults of 750 m high each. The axial valley shallows from 4200 m at the western tip of the segment to 2800 m at the eastern one. The width of the axial graben also decreases eastwards from 12 to 5 km. The SPR1 segment shows an axial high culminating at 1200 m and split by a graben that reaches 10 km wide and 500 m deep at 173°13'E (Fig. 8.5). Finally, the SPR0 segment is characterized by a split volcanic high culminating at 1600 m around 174°E, that passes to a 25 km wide and 4200 m deep rift valley at 174°50'E (Fig. 8.10).

The N110 segment morphology is characterized by several volcanic highs or seamounts, located on the middle of the second-order segments, and deep troughs at the segment ends. This alternating morphology is clearly represented in Figure 8.11.

8.2.3. SEAFLOOR TECTONIC FABRIC

On the shaded relief map (for explanation see section 7.2.3) of the South Pandora Ridge (Figs. 8.12 and 8.13) the axial zone where active spreading occurs, is represented by high topographic roughness, continuous E-W trending lineations (that we assimilate to faults), and high reflectivity (dark pattern) on the imagery data (Lagabrielle et al., 1994b). We can distinguish northern and southern domains in the off-axis area. The northern domain (Fig. 8.12) shows a flat smooth topography with some isolated lineations trending N110 and clearly cut by large volcanic edifices such as the Horizon and Pandora Banks. The southern domain is more complex (Fig. 8.12) and is composed by the following zones: the E-W trending southern domain, the central plateau, the southwestern area and the Central Spreading Ridge tip.

- The E-W trending southern domain is located south of segments SPR2, SPR1 and SPR0. It shows a rough topography, and it is characterized by a cyclic succession of high and low lineations trending E-W.

- South of segment SPR3 (Fig. 8.5 and 8.6), there is a flat elevated area named the central plateau. Its average depth is 3000 m, and is characterized by the occurrence of numerous small volcanoes of 1,5 -2 km in diameter, although a several may reach 12 km.

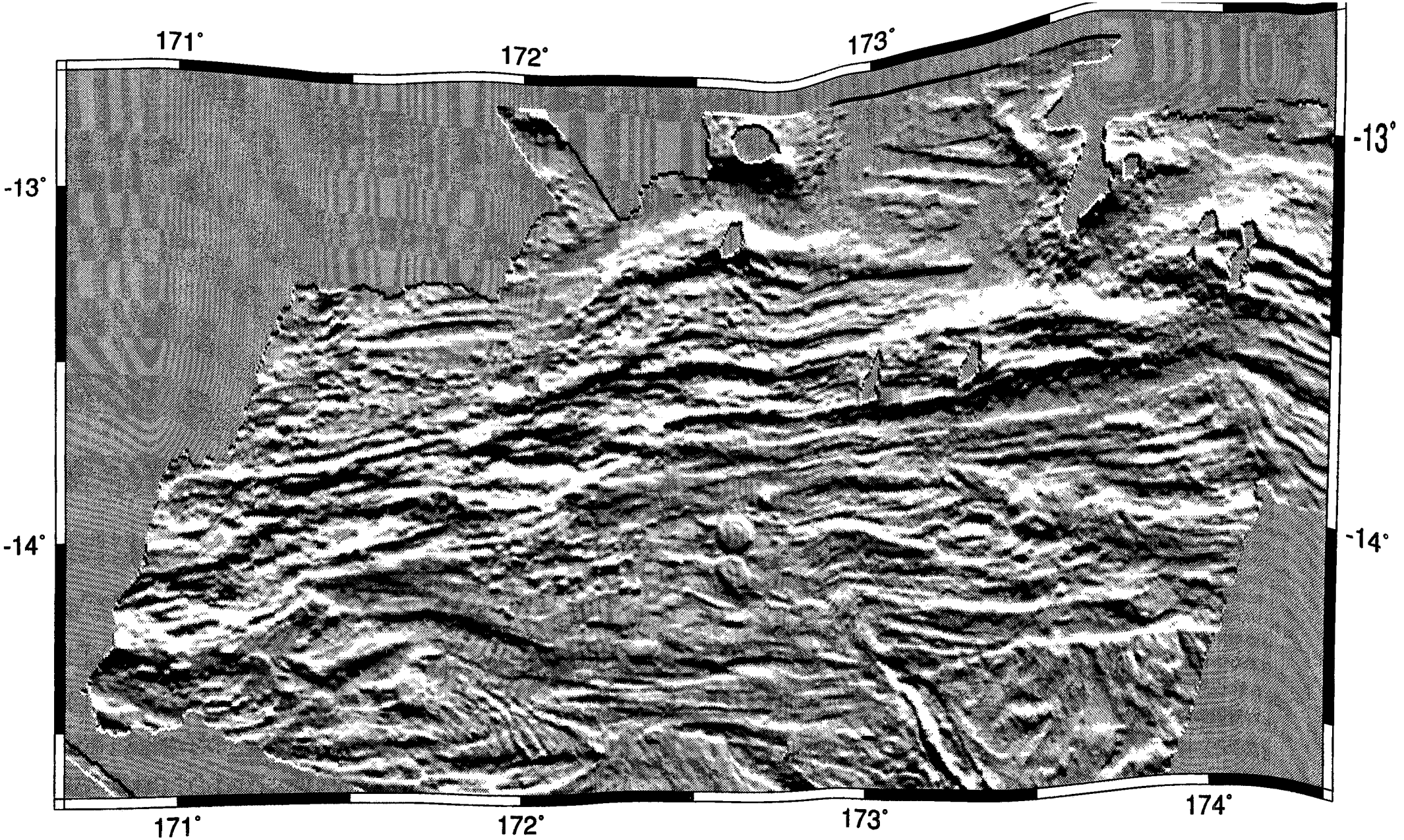

Fig. 8.12. Shaded relief map of the western part of the South Pandora Ridge. Illumination: N-S, elevation: 30°.

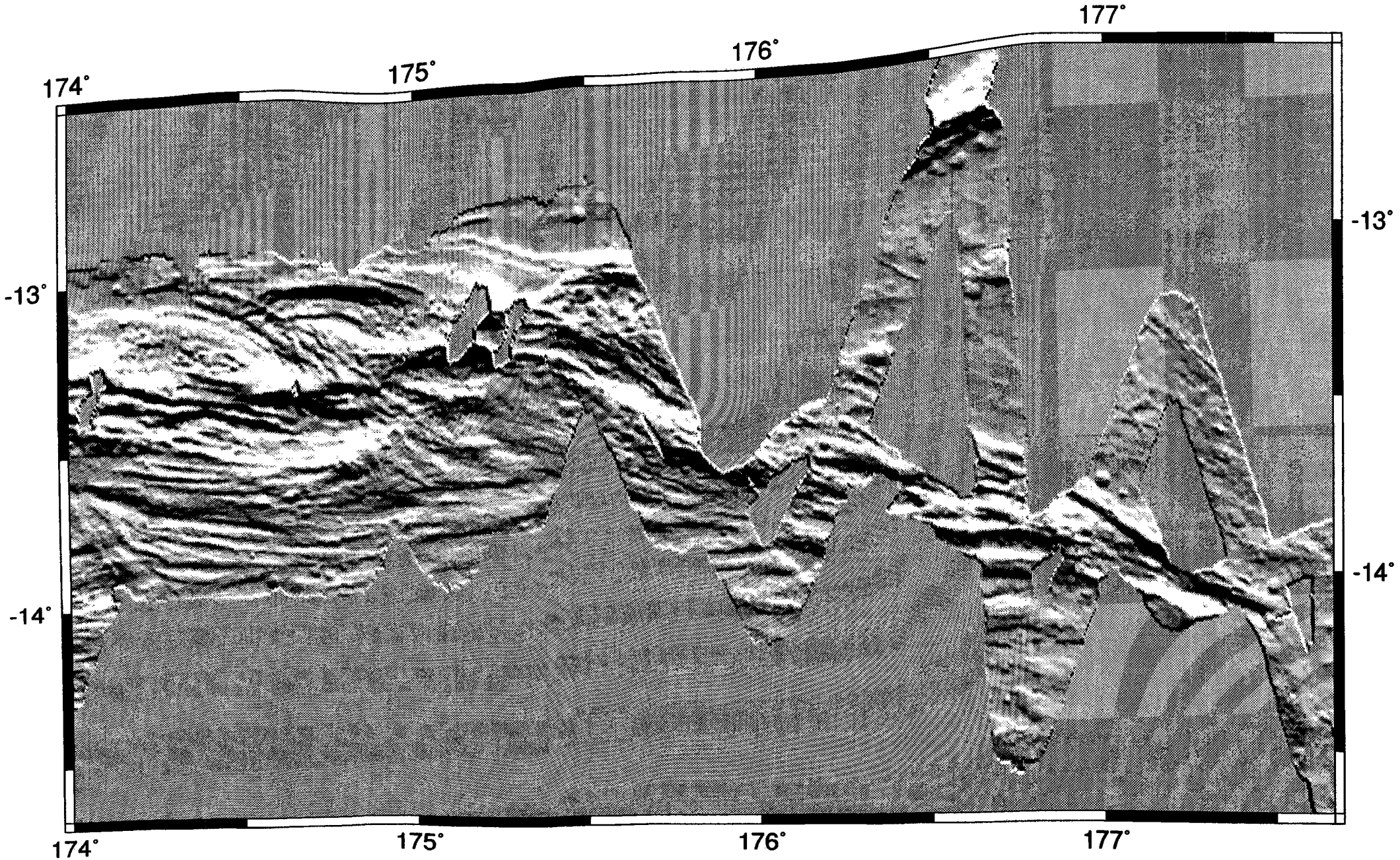

Fig. 8.13. Shaded relief map of the eastern part of the South Pandora Ridge and Tripartite Ridge. Illumination: N15, elevation: 30°.

- The southwestern area displays a widely curved tectonic fabric, with successive elongated grabens and horsts, separated by fault scarps, that locally are 90 km long.

- The Central Spreading Ridge tip corresponds to the northern part of the N160 segment, north of the 14°50'S triple junction (Gràcia, 1992; Gràcia et al., 1992; Auzende et al., 1994a) (see section 5.2). Two branches, one trending N150 and another one trending N120 are distinguished (Fig. 8.12). This system abuts abruptly against the E-W domain.

Along the N110 segment or Tripartite Ridge, there is a strong contrast between the axial and off-axis areas on the shaded relief map (Fig. 8.13). The axial part is associated to a high topographic roughness, whereas on the off-axis areas, the seafloor topography is almost flat only disturbed by some isolated features as the Rotuma Ridge at 176°30'E. The structural data suggest that the Tripartite Ridge may be a very young feature laying on a previously created and older oceanic domain.

8.3. Magnetic anomalies

Preliminary maps and the identification of magnetic anomalies are presented here based principally on the initial results of the NOFI cruise (Lagabrielle et al., 1996). Magnetic anomalies can be easily correlated among profiles navigated 15 km apart on the South Pandora Ridge, whereas anomalies are much harder to identify and correlate over the sparse zig-zag profiles along the Tripartite Ridge, as can be seen on the magnetic anomaly map (Fig. 8.14a).

Along the two first-order segments of the South Pandora Ridge, magnetic anomalies (mainly trending N75 and E-W) define lineations that mimic the bathymetric structures. Spacing of the recognized anomalies does not vary significantly along the South Pandora Ridge (Fig. 8.14a), suggesting a fairly constant spreading rate. Despite a poorer data coverage, the Tripartite Ridge is also associated with correlatable magnetic anomalies. The interpreted magnetic lineations become closer to the east on both flanks, suggesting a decreasing spreading rate in this direction (Fig. 8.14a). The Rotuma Ridge displays a narrow weak positive anomaly flanked by two negatives.

8.3.1. SPREADING RATE AND AGE

Identification of magnetic anomalies is not an easy task along the South Pandora-Tripartite ridges due to the complexity of structural patterns. Axial anomalies are the most easily recognized because they are associated with areas of highest reflectivity areas on imagery maps (Lagabrielle et al., 1996). Along the South Pandora Ridge, the axial anomalies are about 15 km wide displaying strong variations of amplitude, probably related to the axial variability (see section 6.2.2). Magnetic data along the Tripartite and Rotuma ridges are more difficult to identify. However, in both cases axial anomalies may be inferred, but no sequence of older conjugate anomalies has been recognized (Fig. 8.14 b).

Dyment et al. (1995) and Lagabrielle et al. (1996) recognize Anomalies 1 to 3A on both flanks along the South Pandora Ridge (Fig. 8.14 b) following comparisons between the observed magnetic profiles and a synthetic magnetic model. This may suggest that the ridge exists at least from 7 Ma, maximum age of Anomaly 3A. That may be followed along the whole E-W

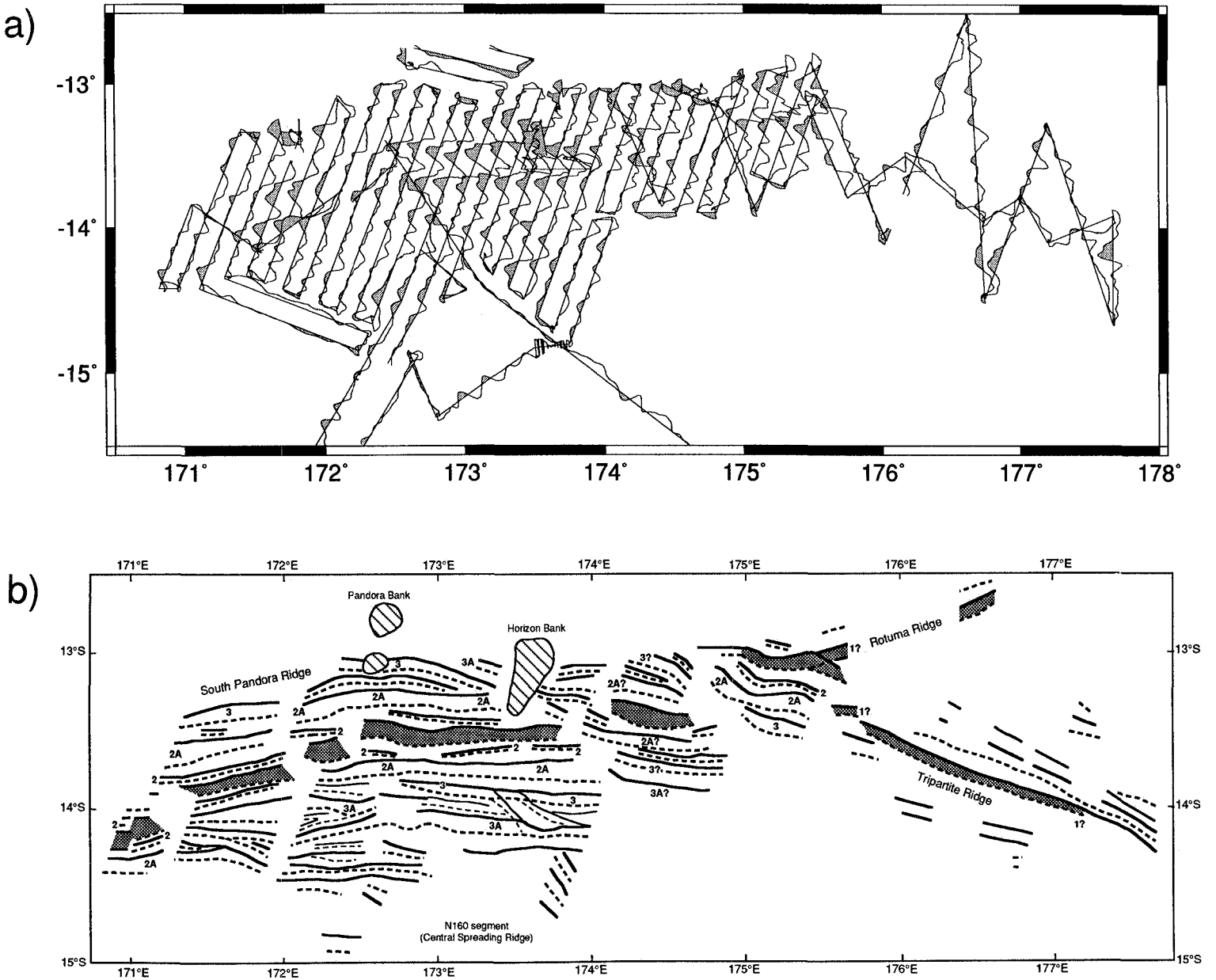

Fig. 8.14. a) Magnetic anomaly map projected along tracks of the South Pandora-Tripartite Ridges between 170°E and 178°E. Positive anomalies are shaded. b) Magnetic lineations identified by Lagabrielle et al. (1996). Solid lines: positive anomalies, dashed lines: negative anomalies.

first-order segment, although it is better represented along the SPR1 and SPR2 segments, indicating an average full spreading rate of 16 mm/yr.

Due to their lower amplitudes, anomalies are more difficult to interpret along segment N75 (Fig. 8.14 b). Anomalies 1 to 3 can be interpreted along segment SPR3, whereas only Anomalies 1 and 2 are identified on segment SPR4. Anomaly 1 and other unidentified anomalies are observed along the Tripartite Ridge (Fig. 8.14b). An approximate full spreading rate of 8.5 mm/yr over the last 0.71 Ma was calculated in the Tripartite Ridge at 176°15'E.

8.4. Gravity anomalies

Here we present the initial results of the gravity data from the NOFI cruise, partly based on the studies of Goslin et al. (1995) and Lagabrielle et al., (1996). The free-air anomaly and the mantle Bouguer anomaly maps were prepared between 170°40'E and 176°E as there was enough data to produce contour maps here. The whole of the South Pandora Ridge and the western edge of the Tripartite Ridge (comprising segments TR3 and the central part of TR2) are shown.

8.4.1. FREE-AIR ANOMALIES

The distribution of free-air anomalies (Fig. 8.15a) is strongly correlated with the main topographic features of the South Pandora Ridge, as revealed by the bathymetric maps. The two first-order segments (N75 and N110) are clearly differentiated, as well as their second-order segments.

The N75 first-order segment is characterized by negative anomalies, which follow the structure's trend and which are bordered by gentle gravity highs. From west to east, the SPR4 segment produces only a small negative anomaly, whereas the SPR3 segment is well marked by two gravity lows (Fig. 8.15a). The two negative anomalies, one of 20 mGal, and the other of -10 mGal, correspond to the grabens SPR3a and SPR3c respectively. The axial high between them (SPR3b) is poorly marked on the free-air anomaly map.

The segment SPR2, corresponding to the western tip of the E-W first-order segment, is characterized by two gravity lows that evolve towards a gravity high, as observed on the bathymetric map. The SPR1 segment produces two elongates and oblique positive anomalies, one of them reaching 100 mGal (Fig. 8.15a). The Horizon Bank, on the northern flank of SPR1 shows the highest positive anomaly recorded in the area (more than 120 mGal) and appears clearly connected to axial zone. Finally, the curved SPR0 segment is characterized by a maximum negative anomaly (less than -10 mGal) centred at 174°40'E.

The N110 segment, or Tripartite Ridge, is represented by a circular gravity high (100 mGal) corresponding to the NW Cakabau Seamount (TR3 segment) and by a small positive anomaly (70 mGal) over the Cakabau Seamount (TR2 segment) (Fig. 8.15a). A few off-axis features stand out on

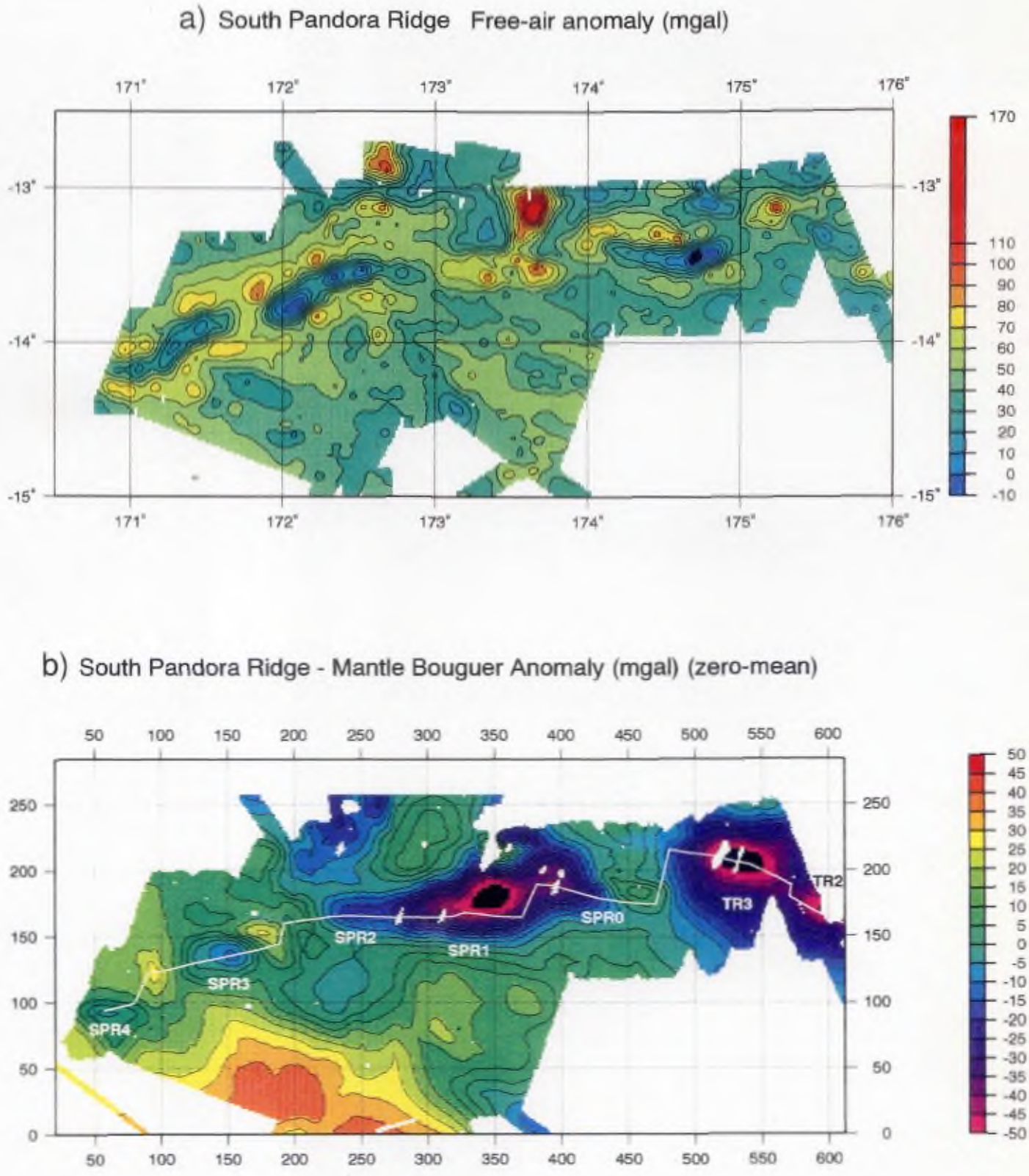

Fig. 8.15. a) Free-air gravity anomaly map over the South Pandora Ridge and western Tripartite Ridge. Contour interval is 10 mGal. b) Mantle Bouguer anomaly map over the South Pandora Ridge and western Tripartite Ridge taken from Goslin et al. (1995). White line: spreading axis and discontinuities. Second-order segments SPR4-SPR0 and TR3-T2 are depicted. Contour interval is 5 mGal.

the free-air anomaly map, including the Bow Seamount which is clearly visible due to the bending of the gravity contours, and the northern tip of the N160 segment of the Central Spreading Ridge, characterized by gravity lows.

8.4.2. MANTLE BOUGUER ANOMALIES

The mantle Bouguer anomalies of the area are depicted in Figure 8.15b. Along the western axial area, we can distinguish two circular negative anomalies (maximum -15 mGal) located in the centre of segments SPR4 and SPR3. The latter corresponds to the central volcanic high (SPR3b) and shows a small "bull's eye" signature (Fig. 8.15b). Towards the east, the three E-W segments (SPR2 to SPR0) are characterized by an extremely large elongated negative anomaly. A maximum "bull's eye" gravity low (more than -50 mGal) is centred in the middle of SPR1 (around 173°E), where the segment is more robust and flanked by the Horizon Bank (Fig. 8.15b).

The Tripartite Ridge, which bathymetrically shows central volcanoes flanked by troughs is also characterized by "bull's eye" anomalies. A very large circular gravity low (more than -50 mGal) is centred on the NW Cakabau Seamount (TR3). A similar anomaly is centred over the Cakabau Seamount (TR2).

In contrast to the axial domain anomalies, the off-axis area is characterized by weak, uniform, mainly positive anomalies. Only on the southwestern part of the area, an important positive anomaly reaching +40 mGal appears, which may be related to an old cold pre-existing crust.

PART IV:

DISCUSSION AND CONCLUSIONS

Five main points are discussed. First, each study area is classified in terms of backarc evolution, from pre-spreading rifting to mature spreading.

Secondly, a comparison between the backarc and mid-ocean ridge accretion is presented.

Next, we discuss the role of the seamount volcanism in the areas studied. We have seen in the previous chapters that large axial seamounts are common features in backarc areas. We attempt to elucidate their significance in the process of seafloor spreading.

The fourth point refers only to the Central Spreading Ridge of the North Fiji Basin. We apply a non-steady state thermal model in order to explain the morphological and gravitational differences observed between the northern (N160/N15 segments) and southern parts (N-S segment) of the ridge.

Finally, taking into account the whole data set over the three study zones, we present two end-member models of the accretionary processes in backarc basins.

In the last chapter (Chapter 10), we present a list of the main conclusions.

Chapter 9

DISCUSSION

9.1. Backarc evolution: From rifting to mature spreading

The three study areas presented in Part III, the Central-Eastern Bransfield Basin, the Central Spreading Ridge, and the South Pandora and Tripartite Ridges, can be classified in terms of backarc basin evolutive stages (see section 3.3). The three areas have been studied using almost the same conventional geological and geophysical methods (mainly swath-bathymetry, magnetics and gravity), and that constitutes the basis for comparison between them. Backarc rifting and incipient stages of seafloor spreading are both well illustrated in the Eastern and Central Bransfield basins, respectively (Fig. 9.1). In contrast, well developed seafloor spreading is characteristic of the North Fiji Basin spreading centres (Fig. 9.1). In this section, we discuss the evolution of the Bransfield and the North Fiji backarc basins, and compare them with other study cases.

9.1.1 THE BRANSFIELD BASIN: BACKARC RIFTING AND INCIPIENT SEAFLOOR SPREADING

As mentioned in Chapter 6, the Central and Eastern Bransfield basins are different in structure, dynamics, volcanism, and sedimentary cover. This suggests that slightly different processes may occur in both basins at present. In this section we propose that the Bransfield Basin is undergoing successive extensional stages from backarc rifting prior to spreading (Eastern Basin) to possibly incipient seafloor spreading (Central Basin).

The Eastern Bransfield Basin

Morphologically, the 150 km long Eastern Bransfield Basin is characterized by four deep rhombic troughs 13.5 to 48.5 km in length, 8 to 17.5 km wide, and with axial depths of 2150 to 2750 m. The troughs are arranged *en échelon*, showing a zig-zag pattern in plan view and trending slightly oblique to their margins. Considering the flanks of the troughs as normal faults, as suggested by bathymetric (Fig. 4.7) and seismic reflection data (Fig. 4.13), a possible left-lateral strike-slip motion in addition to a NW-SE extension would occur in the Eastern Bransfield Basin (Fig. 9.2). The

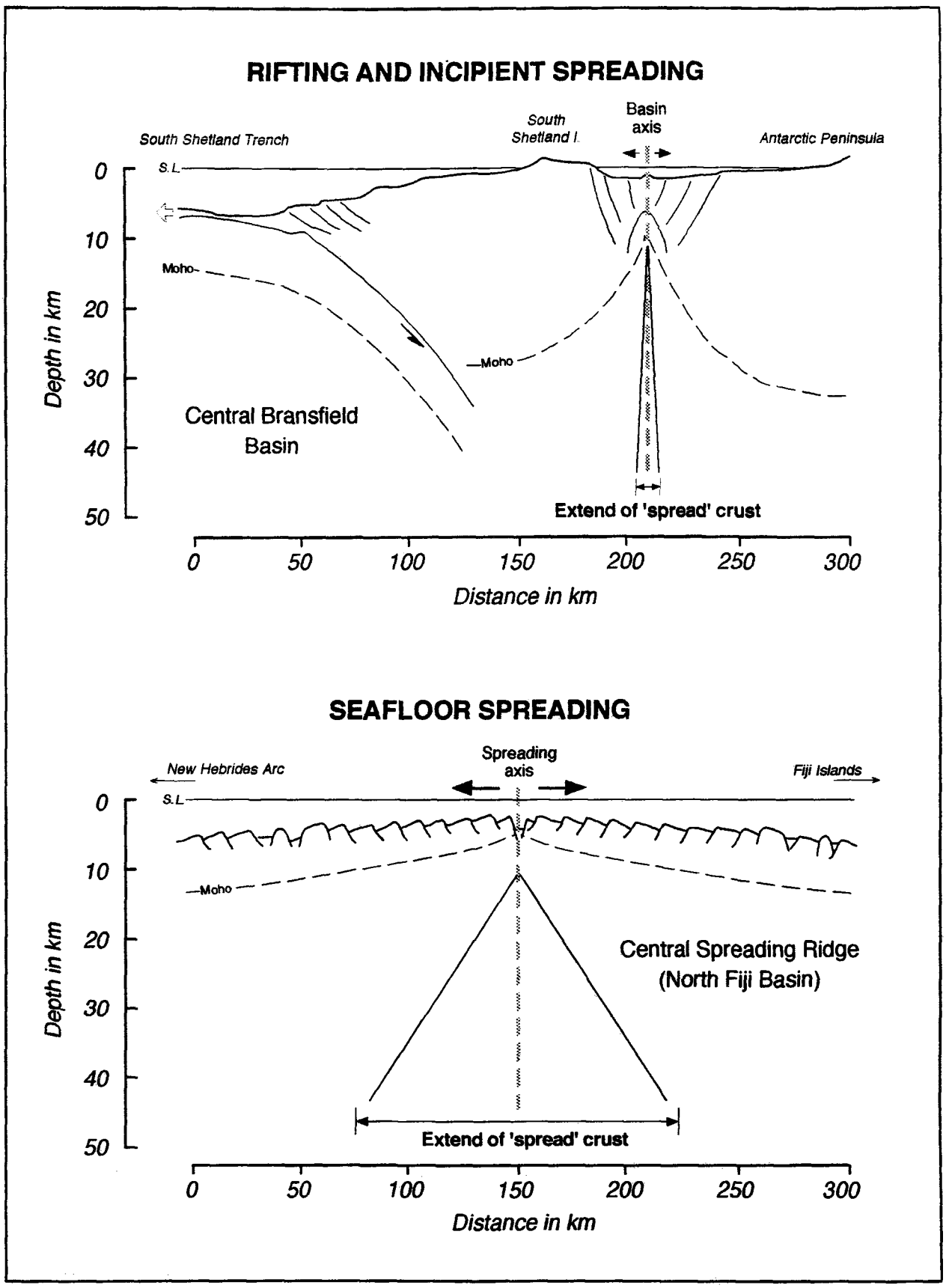

Fig. 9.1. Comparison of models for how backarc extension is accomplished for the Central Bransfield Basin (upper) and for the Central Spreading Ridge (lower). Cross section of the Bransfield Basin is based in Trow and Gamboa (1992), and cross-section of the North Fiji Basin is based in Hussong and Uyeda (1981). Note the different estimates for the width of the crust formed by seafloor spreading ('spread' crust) in the Central Spreading Ridge (150 km) and in the Central Bransfield Basin (less than 10 km).

proximity of the left-lateral plate boundary of the South Scotia Ridge, and the presence of transtensional focal mechanisms north of the Eastern Bransfield Basin (Fig. 9.2) may explain part of this strike-slip motion. Small basins similar to the troughs of the Eastern Bransfield Basin have been observed along the South Scotia Ridge between the northern and southern crests. The troughs have been interpreted as pull-apart basins, as the Hesperides Deep, a rhombohedral trough more than 5000 m deep and fully mapped during the Scotia 92 cruise (Canals et al., 1992; ORCA Group, 1992) (Fig. 9.2). On Figure 9.2, nine focal mechanisms and the main seismic events from the region based on data from Pelayo and Wiens (1989) are also located. Earthquakes along the South Scotia Ridge show normal and strike-slip faulting. Events near Elephant Island show strike-slip, normal and thrust faulting; the normal faulting event is deeper and may indicate tension within a downgoing slab. Normal faulting earthquakes are also associated with rifting in Bransfield Basin (Pelayo and Wiens, 1989).

Numerous small volcanic cones, 50 to 125 m high and 1 to 3 km^2 of basal area, are scattered at the southwestern part of the Eastern Bransfield Basin. They show a disorganized distribution, and only one apparent volcanic lineation (labelled G in Fig. 9.3) forming a neovolcanic ridge may be identified. This abundance of small volcanic edifices can be interpreted either in terms of youth of the volcanism, or/and low magmatic budget in the basin. This kind of volcanism together with the rift graben morphology, and by analogy with other known rifting backarc basins (see next paragraph), indicate that the Eastern Bransfield Basin may be in a pre-spreading rifting stage, that is, backarc rifting prior to true spreading. The basin is then dominated by extensional and strike-slip tectonism and with associated diffused volcanism (Fig. 9.3). Further work based on the petrology, geochemistry, and geochronology of the rocks cropping out in the Eastern Bransfield Basin should be done in order to test this hypothesis.

Similar features are observed in southern Havre Trough (Wright, 1993), and North Mariana between 22°25'N-20°N (Martinez et al., 1995) where pre-spreading rifting also predominates. There, a segmented *en echelon* rift system of deep troughs, of similar size than the Eastern Bransfield Basin, are opening and active backarc rifting propagates progressively towards the north. An extreme example is the Sumisu Rift (Taylor et al., 1991), where a system of troughs rift and develop into the present-day Izu-Bonin volcanic arc (Taylor et al., 1991; Taylor, 1992).

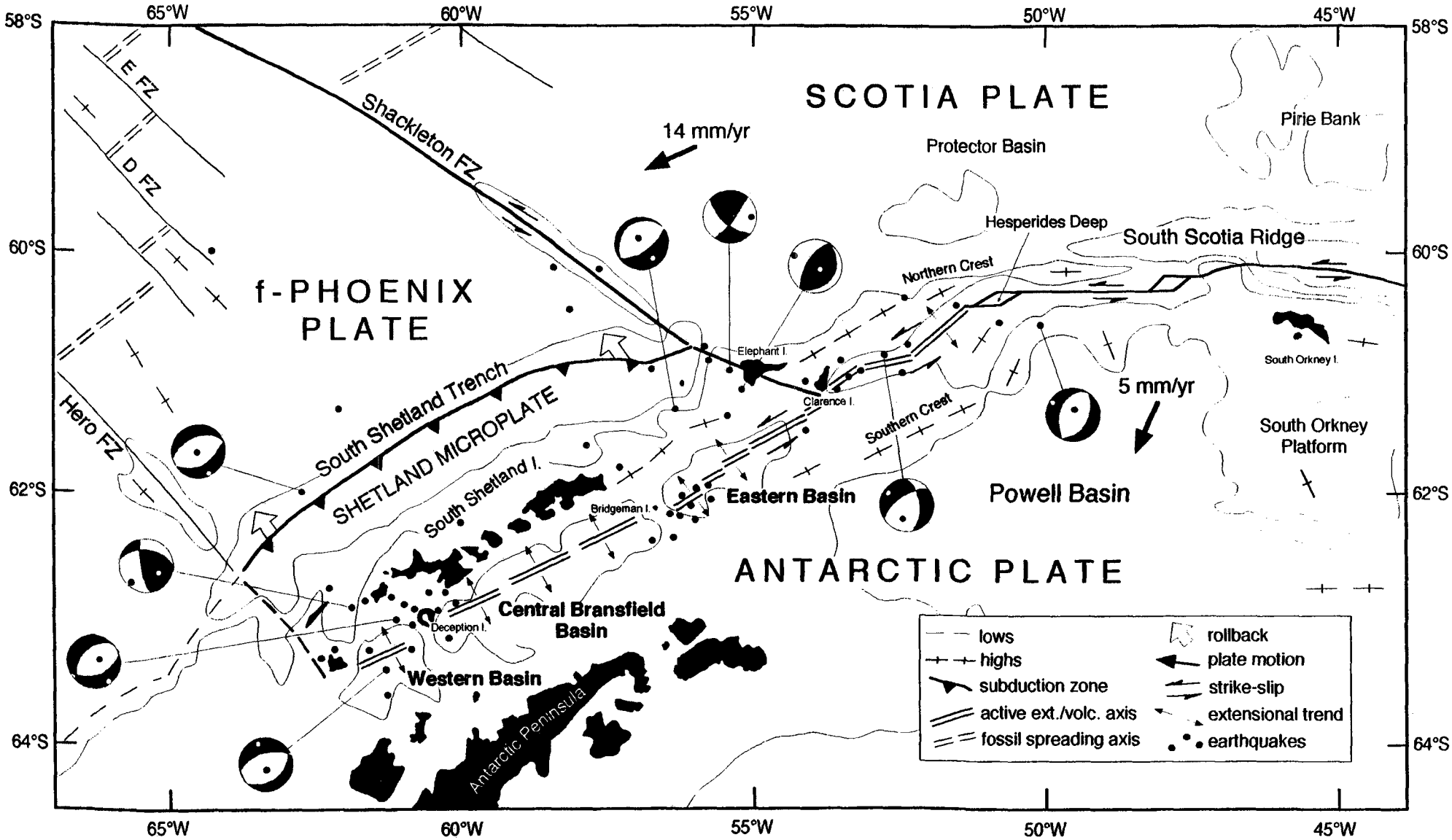

Fig. 9.2. Morphostructural sketch of the northwest Antarctic Peninsula and the South Scotia Ridge region. Shallow earthquakes and focal mechanism in the area are depicted from Pelayo and Wiens (1989). Plate motion and velocities are from Lawver et al. (1995). Feature locations are taken from interpretation of the GEOSAT free-air gravity anomaly map (Fig. 6.15).

The Central Bransfield Basin

The morphology of the Central Bransfield Basin is dominated by six large volcanic edifices aligned with the basin axis that protrude from the sedimented seafloor (Fig. 9.3). Many other smaller, scattered volcanic edifices have also been identified. The thick sedimentary cover (approximately 1 km) observed on the seismic reflection lines prevents the horst and graben basement structure of the basin from cropping out. This progressively deepens towards the northeast up to 2950 m at 57°50'W. The trend of the main structures and the linear arrangement and shape of the large volcanic edifices suggest that a NW-SE extension may be taking place in the Central Bransfield Basin (Fig. 9.3). Even if the amount of extension for both Central and Eastern Bransfield basins is similar and proportional to the amount of subduction caused by the rollback effect (Lawver et al., 1995), some of the differences between them may be due to the strike-slip component affecting the Eastern Bransfield Basin (Figs. 9.2, 9.3).

As a general rule, in the Central Bransfield Basin, the volcanic edifices are larger, 100 to 600 m high, and up to 150 km^2 of basal area, and less numerous than on the Eastern Basin (Fig. 9.3). This may be explained either in terms of maturity of the volcanism or/and higher magmatic supply in the Central Bransfield Basin (see section 9.2 for more details about the evolution of these volcanoes). We interpret the evidence of concentration of extensional faulting along the active and young MORB-type volcanoes (Keller et al., 1991) located at the basin-axis, as the result of incipient seafloor spreading through the continental crust of the Central Bransfield Basin (Fig. 9.1).

In other areas, such as the Red Sea, or in backarc basin setting, as the Okinawa Trough, initial stages of seafloor spreading have also been reported (Bonatti, 1985; Sibuet et al., 1987). The Red Sea may be considered the best example of the transition from continental to oceanic rifting from north to south (Bonatti, 1985; Cochran and Martinez, 1988). The initial breakthrough of oceanic crust and the beginning of organized seafloor spreading occurs in essentially punctiform hot areas located along axial fissures. Axial propagation from each hot point forms linear spreading segments. The Okinawa Trough is a backarc basin formed by extension within the continental lithosphere (like the Bransfield Basin). In the Okinawa Trough three different areas are distinguished: Northern, Middle and Southern Troughs. The crust in the Northern Trough is continental and still at the stage of thinning. On the Southern Trough, the backarc oceanic crust is

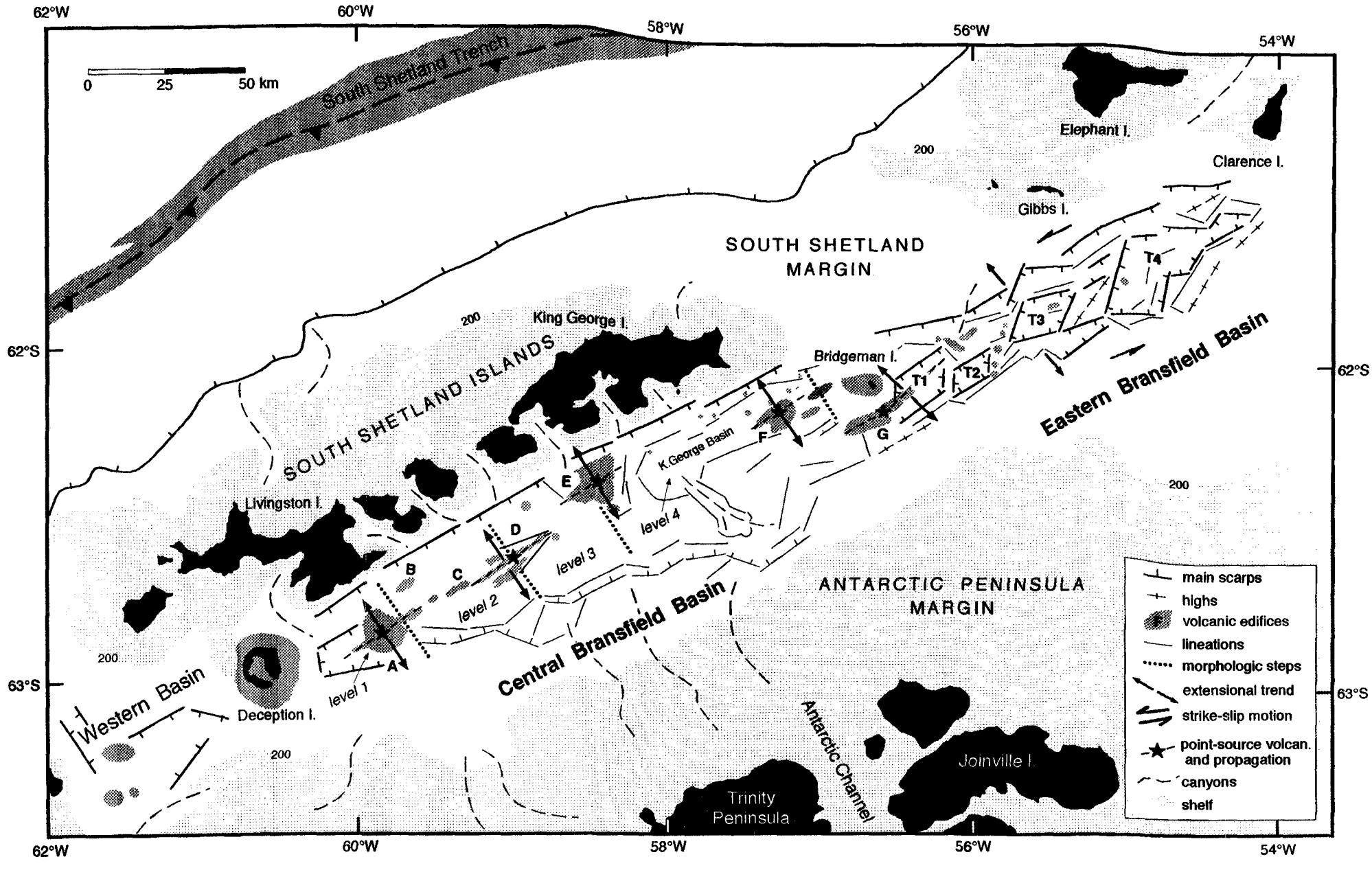

Fig. 9.3. Interpretative geodynamic sketch of the Central and Eastern Bransfield Basins. A to G are the submarine volcanic edifices identified. T1 to T4 are the four troughs identified on the Eastern Bransfield Basin. A NW-SE extension is assumed in the Central Bransfield, whereas a left-lateral strike slip component is suggested for the Eastern Bransfield Basin.

exposed through a series of elongate ridges presenting linear magnetic anomalies associated. Finally, the Middle Trough is in a transitional stage between the last two (Sibuet et al., 1987). There is a gradation from backarc basin localized accretion in the Southern Okinawa Trough to backarc basin diffuse extension on the Northern Trough. This is also similar to what is observed in the Bransfield Basin. The Central Bransfield Basin exhibits more organized and localized volcanism, and the southern Eastern Bransfield Basin displays more diffuse volcanism with small edifices scattered over the seafloor.

Some basic questions

The Bransfield Basin is formed by rifting of the Antarctic Peninsula parallel to the South Shetland Trench. It seems that most of the extension occurring on the Bransfield Basin involves a combination of rifting of the pre-existing thinned continental crust and injection of intrusions and volcanism. Seafloor spreading, defined by Martinez et al. (1995) as extension accommodated primarily by accretion of new backarc crust and lithosphere, may occur only discontinuously along the Central Bransfield Basin. Thus, following the different stages of backarc evolution defined by Martinez et al. (1995) (see section 3.3), we consider that the Eastern Bransfield Basin may be represented by the stage C and the Central Bransfield Basin by a transitional stage between C and D (Fig. 3.6). We suggest that the Bransfield Basin is undergoing a progressive opening and volcanic propagation towards the northeast, with incipient seafloor spreading in the Central Bransfield Basin and pre-spreading backarc rifting in the Eastern Bransfield Basin.

Taking this into account, several points and questions need to be considered:

- What is the timing and what controls the initial rifting?

This is still a point of debate. Barker (1982), Barker and Dalziel (1983), Barker et al., (1991), and Lawver et al. (1995) considered that the present extension in the Bransfield started about 4 Ma ago. This is when accretion at the Antarctic-Phoenix spreading centre stopped, as recorded by the marine magnetic anomalies. In contrast, Birkenmajer (1992) suggested that incipient rifting could have begun between 26 to 22 Ma ago, according to radiometric ages of extensional dykes on King George Island.

Evidence from the Okinawa Trough, also formed by extension within continental lithosphere, indicates an early rifting phase around 13 Ma ago (Sibuet et al., 1995). Hussong and Uyeda (1981) consider that rift propagation along an arc system requires at least 6 Ma, which is in clear contrast with what has been suggested by Barker (1982) and others for the Bransfield Basin. It seems that an intermediate solution between the two age models suggested for the Bransfield opening may better agree with the observed structures in the basin and with the very slow and virtually aseismic subduction along the South Shetland Trench.

- What is the amount of thinning and extension?

The crustal structure of the Bransfield Basin has been modelled by Ashcroft (1972), Guterch et al. (1985 and 1991), and Grad et al. (1993) based on seismic refraction data. All of them agree that the Bransfield Basin is formed by thinned crust underlain by an anomalous mantle upwelling. However, the depth to Moho is very different in these models (ranging between 14 and 30 km), and the exact amount of thinning as well as extension remains to be solved. From bathymetric data, we tentatively suggest maximum values of 60 km of extension for the Central Bransfield Basin and about 40 km for the Eastern Bransfield Basin.

As a reference, in the Okinawa Trough the crustal thickness increases from 10 km in the southern troughs to 30 km in the north and the total amount of extension decreases from 80 km in the southern Okinawa Trough to 74 km in the north (Sibuet et al., 1995).

- How wide is the crust formed by seafloor spreading? At what rate?

We know that the rate of extension in the Bransfield Basin is approximately equivalent to the rate of rollback at the South Shetland Trench. However, the amount of true oceanic crust created is almost non existent in comparison with a mature backarc basin (Fig. 9.1). Roach et al. (1978), Parra et al. (1984 and 1988) and González-Ferrán (1991), from marine magnetic and aeromagnetic data, suggested the start of seafloor spreading between 1.3 Ma and 2 Ma ago, at an average velocity of 2.5 to 9 mm/yr full rate. Nevertheless, unlike Vine-Matthew's reversal sequences, representing complete zones of newly accreted crust, in the Central Bransfield Basin we do not have continuous bands of magnetic lineations. Thus, we suggest that the above calculations are not reliable.

If we consider the young (less than 0.3 Ma; e.g. Keller et al., 1992) seamounts of the Central Bransfield Basin as representative of incipient spreading, the width of crust formed is less than 10 km (Fig. 9.1). When the Bransfield Rift Anomaly is tentatively interpreted as Anomaly 1 (section 6.4), the maximum age of spreading in the Central Bransfield Basin would be 0.71 Ma and the resulting maximum full rate 0.83 mm/yr. As spreading is not well organized and discontinuous, these should be considered maximum values.

9.1.2. THE NORTH FIJI BASIN: YOUNG TO MATURE SEAFLOOR SPREADING

The two areas studied at the north and central parts of the complex 12 Ma-old North Fiji Basin are representative of different degrees of maturity, in terms of organized seafloor spreading (Fig. 9.1). Thus, each of the active spreading ridges (Central Spreading, South Pandora-Tripartite) illustrates at the present-day a particular stage of backarc oceanic accretion, from young to mature.

The Central Spreading Ridge

The Central Spreading Ridge located in the central part of the North Fiji Basin is the best developed, both in structure and magmatism, of all the spreading centres identified in the basin (Fig. 9.1). The variability between superficial and deep structure will be discussed in detail in section 9.4. The Central Spreading Ridge is 3.5 Ma old, as magnetic Anomalies 1 to 2A have been clearly identified (Huchon et al., 1994). Two recent axial reorganizations have been reported, at 3 and 1.5 Ma (Auzende et al., 1995). The full spreading rate, the fastest within the basin, is intermediate and decreases northwards from 82 to 52 mm/yr. A main E-W extensional trend is considered for the N-S segment, changing to NE-SW and NW-SE for the N160 and N15 segments, respectively (see Chapter 7).

The accretion in the central part of the North Fiji Basin is distributed on two synchronous active axes (Auzende et al., 1994b). The Central Spreading Ridge and the West Fiji Ridge (see section 5.3) are propagating in opposite directions, isolating an intermediate plate west of the Fiji Islands. This twin-ridge system can be compared with the Easter (e.g. Naar et al., 1991) and Juan Fernandez (e.g. Francheteau et al., 1987) microplates on the East Pacific Rise, although such a case was not documented before on backarc basins (Auzende et al., 1995b). Moreover, the relationship between the central and northern systems, the Central Spreading Ridge and South Pandora-

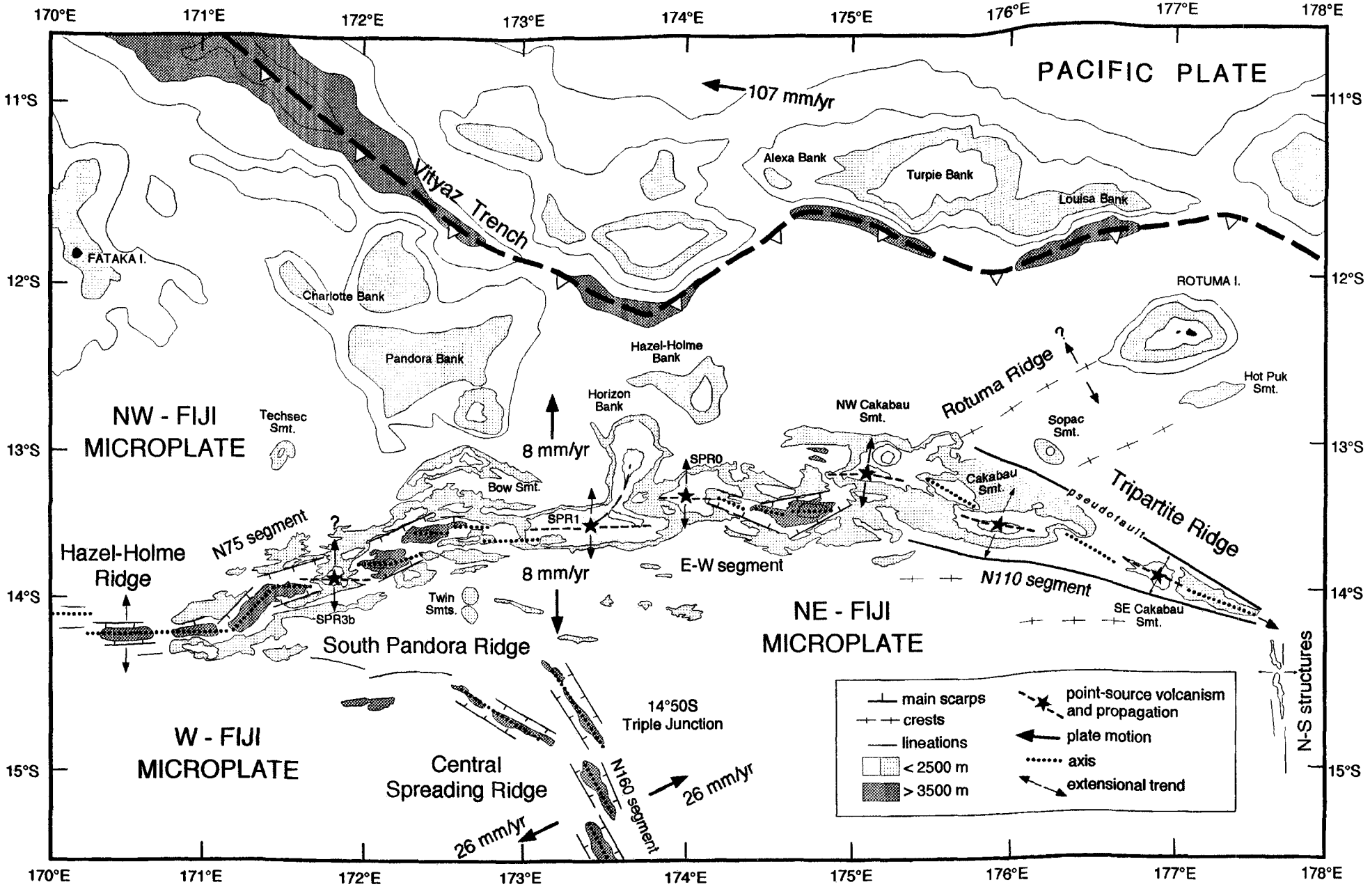

Fig. 9.4. Interpretative geodynamic sketch of the northern part of the North Fiji Basin comprising the South Pandora and Tripartite Ridges and northern part of the N160 segment of the Central Spreading Ridge. Plate motions within the North Fiji Basin are from marine magnetic anomalies (see Chapters 7 and 8), and from hot-spot motion in the Pacific Plate (Doutch, 1986).

Tripartite ridges respectively, is still not clear. Even if they are opening perpendicular to each other, there is no triple junction between the present-day axes (Fig. 9.4).

The South Pandora-Tripartite Ridges

Relatively old crust is present in the northern part of the North Fiji Basin, at the mature South Pandora Ridge. Although Auzende et al. (1988b, 1995c) suggest that spreading stopped at the northern part of the North Fiji Basin sometime between 3 Ma and the present-day (see section 5.4), new data obtained during the NOFI cruise (see section 8.1) along the South Pandora Ridge demonstrates the contrary. We can affirm that oceanic spreading processes have been occurring almost continuously for at least 7 Ma along the South Pandora Ridge, as revealed by the identification of Anomalies 1 to 3A (Lagabrielle et al., 1996). At a regional scale, this mature spreading system shows a relatively stable geometry, as revealed by the well-organized E-W parallel pattern of magnetic lineations suggesting a N-S extension (Fig. 9.4). The magnetic anomalies identified suggest a full spreading rate of 16 mm/yr (see section 8.3), which classifies the South Pandora Ridge as an ultra-slow spreading centre.

The young N110 trending Tripartite Ridge is located at the eastern end of the South Pandora Ridge (see Chapter 8). Magnetic Anomaly 1 is clearly identified (see section 8.3), and in consequence, we may affirm that the Tripartite Ridge is a young spreading centre formed at least 0.71 Ma ago. The structural and magnetic patterns along the Tripartite Ridge indicated a V-shaped structure narrowing towards the southeast. This suggests an axial propagation of the Tripartite Ridge with a propagating tip located at 177°30'E, exactly where the N-S structures appear (Fig. 9.4). The converging V-shaped lineations, named pseudofaults (Hey, 1977; Hey et al., 1980), correspond to the limits between the newly created and the pre-existing lithosphere of the basin, mainly trending E-W. From the magnetic anomalies, the calculate full spreading rate is ultra-slow and decreases from 8.5 mm/yr at 176°15'E to 0 mm/yr at the tip of the pseudofault (177°30'E). In addition, ferrobasalts have been identified about 15-20 km inside the pseudofault (Sinton et al., 1994), a position predicted to be most conducive to eruption in association with propagating rifts, as in the Galapagos Rift (Christie and Sinton, 1981; Sinton et al., 1983). All these points support the interpretation of the Tripartite Ridge as an active and young propagating rift.

Some basic questions

The Central Spreading Ridge and the South Pandora-Tripartite Ridges are both active centres where new oceanic crust is created through organized seafloor spreading. Both systems would be classified as more evolved than stage D (Fig. 3.6), following the four stages of backarc evolution (Martinez et al., 1995) (see section 3.3). The Central Spreading Ridge and the South Pandora-Tripartite Ridges are not the sole locus of seafloor spreading; at least three more active ridges (see section 5.3 and Fig. 5.5) with various positions and orientations form also part of a complex spreading system within the basin. The North Fiji Basin is, then, one of the world's ocean basin having the largest cumulate length of active spreading centres for a given surface of seafloor (Lagabrielle, pers. comm.). It is one of the most evolved backarc basins in the world opening together with the Lau Basin, in the inter-arc region between the opposite verging New Hebrides and Tonga subduction zones (Hamburger and Isacks, 1988).

Concerning the present-day opening in the North Fiji Basin, some fundamental questions appear.

- Is the present-day spreading in the North Fiji Basin subduction-related?

In contrast to the neighbouring Lau Basin (see section 5.1), where opening seems to be caused by the rollback of the Tonga subduction zone hinge (Parson and Hawkins, 1994), the present-day opening in the North Fiji Basin does not seem to be related or parallel to any subduction. Petrologic, geochemical and structural data (Boespsflug, 1990; Eissen et al., 1991; Sinton et al., 1985 and 1993; Bendel, 1993) suggest that the present-day Central Spreading Ridge is independent of the active New Hebrides subduction zone. Moreover, although the general trend of the curved South Pandora Ridge mirrors the fossil Vityaz Trench (Fig. 9.4), the origin of the South Pandora Ridge was not related to subduction along the trench. During the Late Miocene, when the ridge started spreading, the trench was already inactive (e.g. Falvey, 1978). In addition, the geochemistry of the South Pandora Ridge lavas shows a predominance of E-MORB sources along-axis, with no influence of active or fossil subduction zones. Trace element analysis indicate that this enrichment may be due to a mantelic source (Guivel et al., 1995).

- What induces the present opening in the North Fiji Basin?

It is understood that the basin started opening around 12 Ma ago, when the Ontong Java Plateau and associated seamounts collided at the edge of the Australian borderland, the now inactive Solomon-Vityaz subduction system (e.g. Auzende et al., 1988b) (see section 5.4 and Fig. 5.6). However, the causes of the present-day opening are controversial. We recall that the North Fiji Basin is characterized by shallow depths with respect to the Pacific basin, very high heat flow, shallow Moho beneath the spreading axis, low seismic velocities in the crust, low density upper mantle, and local high of the geoid (see Chapter 5) . All these features suggest that the North Fiji Basin development is linked to a regional thermal anomaly (hot mantle plume) responsible for a higher rate of mantle convection that induces rapid crustal production. This inherent process, together with the deformation generated by the dominantly transcurrent motion between the Pacific and Indo-Australian Plates (Hamburger and Isacks, 1988) may explain the current opening in the interarc region.

9.2. Backarc versus mid-ocean ridge spreading: Differences and similarities

Some authors considered that spreading centres in backarc basins are less clearly defined morphologically and geophysically than at mid-ocean ridges (Lawver et al., 1976; Lawver and Hawkins, 1978), and that backarc extension in marginal basins was more diffuse (Lawver and Hawkins, 1978; Tamaki, 1985; Hamburger and Isacks, 1988). However, a series of fundamental geological and geophysical characteristics links the backarc basin and mid-ocean ridge tectonic environments as zones of lithospheric accretion (Karig, 1971; Taylor and Karner, 1983; Weissel, 1981). Both are characterized by relatively shallow seafloor with high heat flow and high seismic attenuation, active crustal seismicity and thin ocean crust. Basement rocks in both environments are commonly composed of tholeiitic basalts. The backarc ridge segmentation pattern is similar to that found at mid-ocean ridges, magnetic lineations are recognizable and parallel to the present-day axis, and the axial zone (rift valley or axial high) is about 10 to 20 km wide (Table 9.I). These common characteristics have led to an obvious tectonic analogy with seafloor spreading at mid-ocean ridges. Lithospheric accretion in backarc basins takes place along discrete spreading centres resembling those of major oceans (Taylor and Karner, 1983; Weissel, 1981; Auzende et al., 1988b).

9.2.1. SEGMENTATION

The initial rifting within the volcanic arc may already pre-determine the future segmentation in backarc spreading ridges, as has been suggested in the Sumisu Rift within the Izu-Bonin Arc (Taylor et al., 1991; Taylor, 1992) and the northern Mariana Trough (Martinez et al., 1995). Thus, the zig-zag pattern of faults limiting the *en echelon* troughs and their dimensions characterizing the present-day Eastern Bransfield Basin geometry may reflect the initial pattern of arc rifting, and may also determine the future segmentation of the basin. In the following stage, during incipient seafloor spreading, the axial volcanic propagation starts from individual hot-points, forming linear proto-spreading segments, as observed in the Northern and Central Red Sea (Cochran and Martinez, 1988). The constant distance between each eruptive centre (about 50 km) suggests regular spacing of the upwelling zones and a segmentation of the rift into compartments (Bonatti, 1985). The spacing between the edifices in the Central Bransfield Basin,

between 25-30 km, agrees with these hypotheses. This model implies that beneath each initial hot point there is a zone of preferential upwelling of upper mantle material.

The recognition that backarc basins have an extensive rifting stage prior to spreading has helped to reconcile some of their initially perceived differences with mid-ocean spreading centres. The study of mature systems such as the North Fiji Basin has confirmed some similarities in backarc spreading parameters (rates, morphotectonics, magnetization, crustal structure and geochemistry) to those of mid-ocean. Nevertheless, although the fundamental accretionary processes may be similar (see section 9.4), differences between backarc and mid-ocean ridge spreading centres occur, and they are especially evident when looking at ridge segmentation hierarchy and axial discontinuities.

The Central Spreading Ridge and the South Pandora-Tripartite Ridges are segmented into three first-order segments named according to their orientation, and between 300 and 125 km long (Table 9.I). This is half of the first-order segmentation observed in mid-ocean ridges (between 600 and 300 km long) (Macdonald et al., 1991; see Table 2.I). In consequence, it appears that the first-order segments in mid-ocean ridge would be at the scale of the whole backarc basin, and that the first-order segment backarc basins correspond to the second-order in mid-ocean ridges.

The longevity of these first-order segments is another point that differentiates backarc from mid-ocean ridges. The Tripartite Ridge dates from at least 0.7 Ma, and the Central Spreading Ridge from 3.5 to 1 Ma. Both backarc ridges are shorter-lived than mid-ocean ridges, where segments of order 1 have a longevity at least 5 Ma (Macdonald et al., 1991; see Table 2.I).

9.2.2. DISCONTINUITIES

The axial discontinuities along the Central Spreading Ridge and South Pandora-Tripartite Ridges (overlapping spreading centres, propagating rifts, offsets and devals) (Table 9.I) are analogous to those described along mid-ocean ridges (Hey, 1977; Hey et al., 1980; Macdonald and Fox, 1983; Macdonald et al., 1988, 1991; Schouten et al., 1985; Whitehead et al., 1984).

The fundamental difference between mid-ocean ridge and backarc axial discontinuities is the lack of large transform faults and fracture zones

SEAFLOOR SPREADING

Area	Age	Spr. rate	1st order segments			2nd order segments			Axis	
	(Ma)	full (mm/yr)	trend	length (km)	discont.	name	length (km)	discont.	morphology	depth (m)
SPR-TR South Pandora and Tripartite Ridges	7	8.5-16 ultra-slow	N75 E-W N110	180 330 300	non transform (NTD) offset	SPR 3-4 SPR 0-1-2 TR 1-2-3	85 90 90	offsets small O.S.C.	rift valley/axial high rift valley/axial high axial seamounts	900 - 4600
CSR Central Spreading Ridge	3.5	50-80 intermed.	N160 N15 N-S	210 165 265	triple junctions propagating rifts	CSR 1-2-3 CSR 4-5 CSR 7-8-9	74.5 84.5 71.2	offsets devals	rift valley axial high axial high	1800 - 4200

RIFTING AND INCIPIENT SPREADING

CBB-EBB Central and Eastern Bransfield Basins	< 4 ?	2.5?-9? ultra-slow	N60 N45	230 150	-	A to G T1-2-3-4	18.5 20	-	axial seamounts troughs	500 - 2600

Table 9.I. Synthesis of the main characteristics of the South Pandora-Tripartite Ridges, Central Spreading Ridge, and Central-Eastern Bransfield Basins.

separating first-order segments in the backarc ridges. Small, short-lived offsets (Table 9.I) showing curved patterns, with no off-axis traces, are the only strike-slip features displacing the axis, like the numerous offsets observed along the N160 segment of the Central Spreading Ridge (Fig. 7.5) and along the N75 segment of the South Pandora Ridge (Fig. 8.6). This might be a general characteristic of backarc accretion, as also observed in the Woodlark Basin (Taylor et al., 1995) and Lau Basin spreading centres (Parson et al., 1990).

Another point is the presence of non-rigid discontinuities characteristic of fast spreading ridges (Macdonald and Fox, 1983; Lonsdale, 1985) along the ultra-slow South Pandora Ridge, like the 173°50'E overlapping spreading centre between SPR1 and SPR0 (Fig. 8.6). This suggests an independence between the spreading rate and the magmatic budget underneath these robust segments, allowing rapid reorganizations along the ridge.

9.2.3. IN SITU OBSERVATIONS

At the scale of submarine observations similarities and differences between backarc and mid-ocean ridges have also been pointed out. Variability of the present-day tectonic, volcanic and hydrothermal activities is reported from diving observations along the Central Spreading Ridge (see section 7.3).

Different axial morphologies are observed between Stations 14 and 19°S, respectively located 20 km apart at the centre and end of CSR7 segment (N-S segment). These may be related with the shape and boundaries of the magma chamber underneath (Ondréas et al., 1993). Small-scale variations have been observed within Stations 4 and 14. These variations show that at this scale (within 1 km), magma erupts randomly in time and space, and tectonic activity takes place in narrow, discrete areas (Gràcia et al., 1994). Submersible studies along mid-ocean ridges, such as the East Pacific Rise at 13°N (Vaslet, 1993), 12°50'N (Gente et al., 1986), and between 17°30'S and 21°30'S (Renard et al., 1985) have also emphasized small-scale along-axis morphologic variations.

The hydrothermal activity observed in Station 4 (N15 segment) may be linked to both nascent magmatism and fissuring, which have been also observed in other oceanic sites (Kappel and Ryan, 1986; Gente et al., 1991; Ishibashi and Urabe, 1995).

9.3. Seamount volcanism on backarc basins: Role in accretionary processes

The formation and growth of seamounts in ocean basins are intimately related to melt production and migration in the mantle and to the evolution of the oceanic lithosphere. The seamounts can be grouped in two main classes: the large volcanoes forming oceanic islands and guyots associated with hot-spots, and the numerous small volcanoes related to spreading centres. The second group of volcanoes is associated with mantle upwelling and lithospheric development along the spreading centre (Scheirer and Macdonald, 1995).

In this section we discuss the on-axis and near-axis seamount volcanism systematically observed along the Bransfield Basin, the South Pandora and Tripartite Ridges, and the Central Spreading Ridge, with the aim of establishing the relationship between this seamount volcanism and backarc basins accretionary processes.

9.3.1. BRANSFIELD BASIN

At first sight, the seven large circular volcanoes and ridges (A to G) exposed on the floor of the Bransfield Basin (Fig. 9.3) might be explained as the result of initial fissure eruptions converging in to single vents. However, rectilinear faults affecting the volcanoes do not support this idea, and a more complex model must be considered. We propose that different morphologies of the largest edifices of the Central Bransfield Basin (edifices E, A, and D) may illustrate three successive volcano-tectonic stages (Fig. 9.5).

- 1. Point-source circular volcanoes form at the intersection of two sets of orthogonal trending faults that define the overall basin structure (see Chapter 6). This stage is represented by small scattered circular volcanoes and also by edifice E (Fig. 9.5a).

- 2. Extension occurs, which causes the splitting of the circular edifices by normal faults, and leads to the formation of neovolcanic ridges elongated from the initial point-source. The propagation of the volcanism follows the main N55-N60 direction as in edifice A (Fig. 9.5b), although it may locally follow a N145 normal direction, as in one ridge of edifice F.

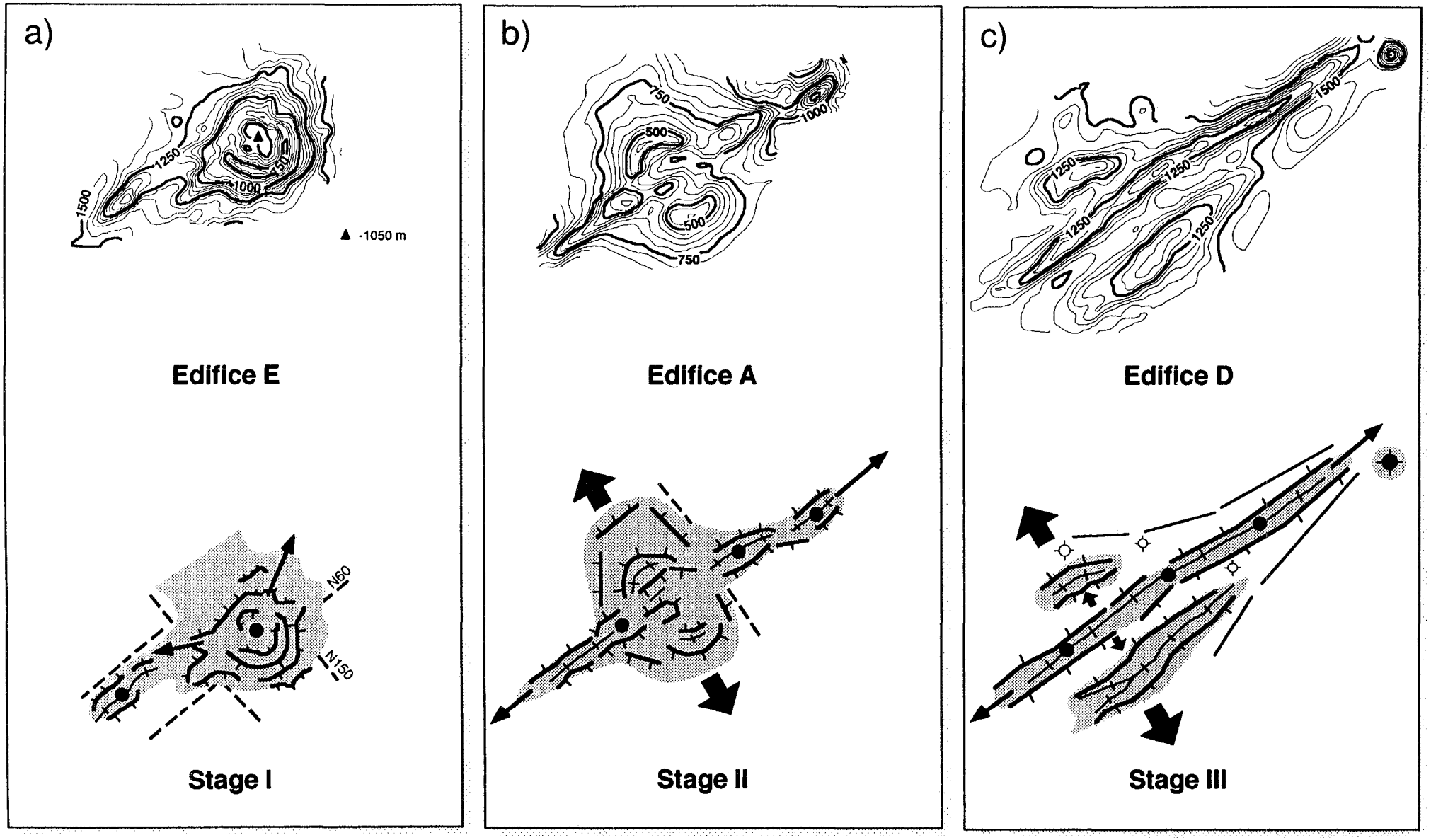

Fig. 9.5. Morphostructural sketch derived from interpretation of the swath bathymetry map depicting the three volcano-tectonic stages in the evolution of Central Bransfield Basin. Thick short arrows: direction of extension. Thin elongated arrows: direction of volcanic propagation.

• 3. Finally, continued extension results in the development of a single neovolcanic ridge, inactivity of the half-volcanoes on both sides and, consequently, their disfigurement. This situation is best illustrated by edifice D (Fig. 9.5c).

There is a significant along-axis variation in seamount basalt chemistry in the Central Bransfield Basin (Keller et al., 1991). Lawver et al. (1995) proposed that as the Bransfield Basin rift develops and deepens, the volcanoes become more MORB-like. The most similar to Normal-Mid Ocean Ridge Basalt (N-MORB) of any sample recovered so far from the Central Bransfield Basin comes from edifice D, which we interpret as characteristic of the maturest stage. Younger, 100,000 year old, backarc type tholeiitic-calc-alkaline basalts have been sampled in edifice F (Fisk, 1990), which is also morphologically less evolved. This significant along-axis variation in seamount basalt chemistry correlates with our interpretation of the distinct seamount morphologies being consistent with the idea of transitional nature of the Central Bransfield Basin from rifting to spreading regimes.

Role of seamounts in axial construction

Seamount volcanism plays a fundamental role in axial construction on slow spreading ridges, as has been suggested by their abundance on the Mid-Atlantic Ridge floor between 24°N and 30°N (Smith and Cann, 1992), 23°25'N and 22°45'N (Bryan et al., 1994), and the Reykjanes Ridge (Murton and Parson, 1993; Smith et al., 1995). A detailed analysis of seamount population made on the axes of Mid-Atlantic Ridge (24°N-30°N) and Reykjanes Ridge shows that seamounts higher than 150 m comprise 15% of the population and they are densely distributed (Smith and Cann, 1992; Smith et al., 1995). In comparison, in the Bransfield Basin up to 37% of the edifices are over 150 m high (see section 4.2.3) and they are more widely-spaced than those usually found at the slow-spreading ridges. Both differences may result from a wider spacing of the fracturing of the basin. This style is probably related to the continental nature of the crust and results in a concentration at the same preferential areas of both volcanism and extension.

Moreover, large split axial volcanoes with a diameter of 10 to 15 km, similar dimensions to those cropping out at the Central Bransfield Basin, are

observed along the Mid-Atlantic Ridge between 37°N and 39°N, near the Azores Islands platform (Ondréas et al., 1995). In this area, the ridge axis shoals to less than 1500 m depth, and the deep axial rift valley that characterizes the Mid-Atlantic Ridge in much of the North Atlantic disappears. These anomalous features are strongly influenced by the presence of the Azores hot spot (Detrick et al., 1995). Another example of large ridge-axis seamounts is the 12 km diameter Axial Volcano located in the central segment of the intermediate Juan de Fuca Ridge (Embley et al., 1990). Currently both volcanically and hydrothermally active, this feature lies at the intersection of the Cobb-Eickelberg seamount chain and the Juan de Fuca Ridge. In consequence, the formation of the Axial Volcano is directly associated with the seamount chain and, at the same time, affected by normal seafloor spreading processes (Embley et al., 1990; Johnson and Embley, 1990).

9.3.2. THE SOUTH PANDORA AND TRIPARTITE RIDGES

South Pandora Ridge

The broad, complex arched E-W trending South Pandora Ridge is characterized by both axial and off-axis seamounts. The axial topography of the South Pandora Ridge is represented by a contrast between segments formed by large volcanic edifices and highly tectonized rift-valleys (see Chapter 8). The axial seamounts are large features located either at the central part of second-order segments (as SPR3b), at the segment end (as SPR0), or occupying the whole segment (as SPR1) (Fig. 8.6). These features seem to form by point source volcanism that propagates following the main structural trends (Fig. 9.4).

The SPR3b seamount protrudes within the N75 trending rift valley but several E-W faults and fractures cut the edifice and the bordering troughs obliquely (Fig. 8.6). We consider that the present-day extensional trend is N-S, normal to the axis-parallel faulting (Fig. 9.4). However, if spreading is orthogonal to the main N75 segment trend, then oblique spreading trending N160-170 will occur, as in the Reykjanes Ridge (Murton and Parson, 1993). Determination of the exact direction of plate separation is essential to the assessment of whether there is oblique spreading along the SPR3 segment (Fig. 8.6). The SPR1 segment is a large, shallow volcanic high composed of several elongated edifices following the main E-W trend (Fig. 9.4). An individualized seamount is located at the central part of the segment (Fig. 8.6), suggesting point-source volcanism. The SPR0 seamount is formed by

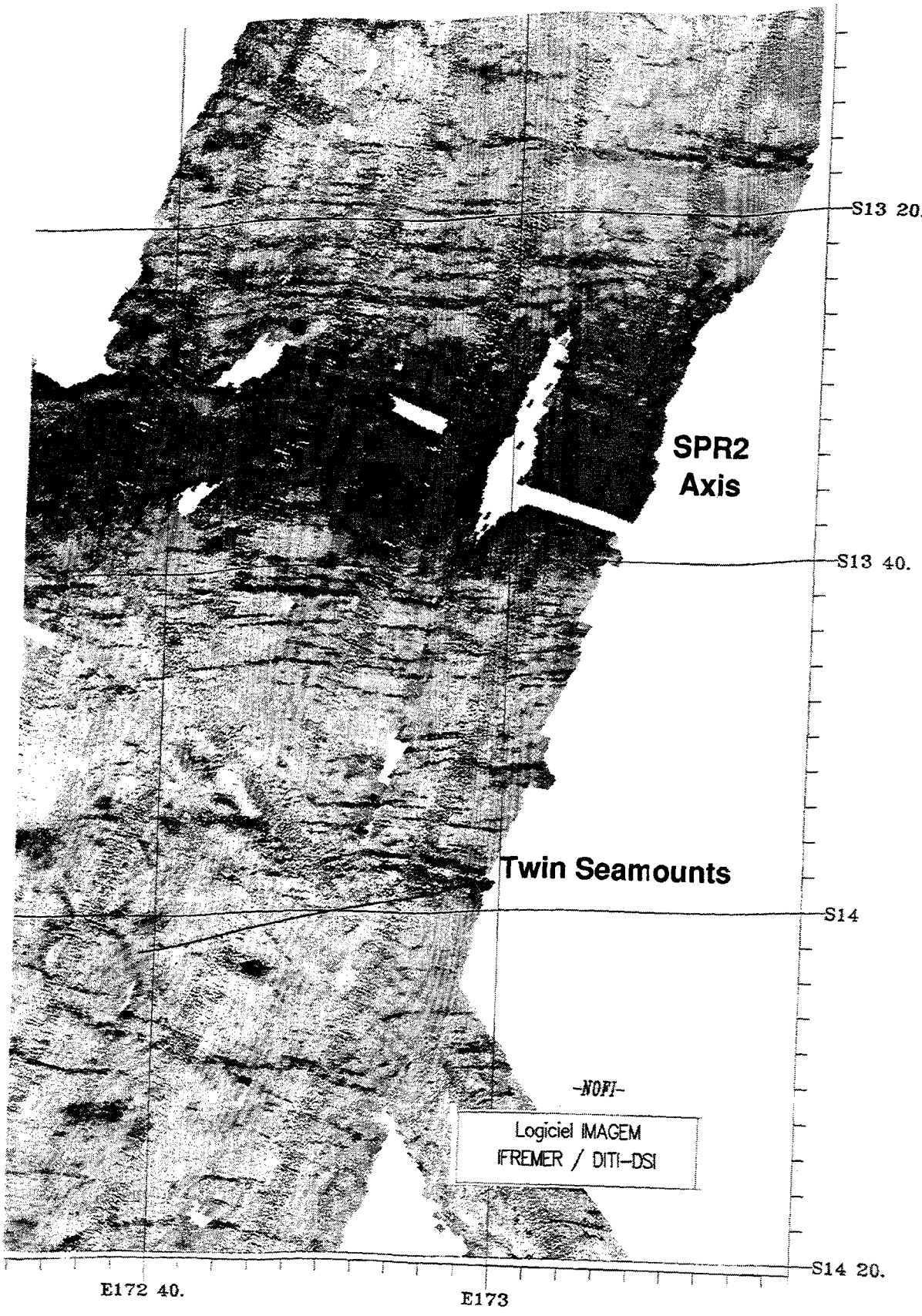

Fig. 9.6. Example of the EM-12 imagery data recorded during the NOFI cruise. The axial zone, characterized by active tectonized region, recently emplaced lavas, and weak sedimentary cover, corresponds to the black areas. Off-axis, the ridge parallel fabric as well as the Twin Seamounts (10 km diameter each) are clearly outlined (Lagabrielle et al., 1995).

two elongated edifices trending N110-120, which seem to result from the split of a previous single seamount centred at 174°E. The southern half, which overlaps with SPR1 (Figs. 8.5, 8.6 and 9.4) seems to propagate towards the west, where small volcanic cones cover the seafloor.

Two types of off-axis seamount are observed along the South Pandora Ridge system: large seamounts and banks, and small volcanic cones.

Two large seamounts are located about 40 km off-axis in the SPR2 segment and symmetrically distributed at either side of 172°36'E: the Bow (north flank), and Twin (south flank) seamounts (see section 8.2 and Fig. 8.5). The centre of the E-W trending Bow Seamount is wide (15 km) and narrows considerably towards its tips, to less than 4 km wide. The Bow Seamount shows a rectilinear and faulted inward facing flank whereas the outward is irregular and curved. This suggest that the Bow Seamount was formed and split at the axis, with an original elliptic shape. These bow forms are also recognized along the Juan de Fuca Ridge (Kappel and Ryan, 1986). The Twin Seamounts are two perfectly round-shaped symmetric volcanoes. The rocks samples recovered by dredging on the southern Twin Seamount are similar to other seamounts dredged in the North Fiji Basin (Price et al., 1990; Price and Kroenke, 1991; Eissen et al., 1994; Lagabrielle et al., 1994a). However, the low reflectivity response of the Twin Seamounts in the imagery map (Fig. 9.6), probably due to a thick sediment cover, suggests that they may not be active at present. The near-axis Horizon Bank, mainly formed by vesicular and porphyric fresh lavas (Lagabrielle et al., 1994b), is directly linked with the northern flank of SPR1 through a narrow sharp ridge (Figs. 8.5, 8.6, and 9.4). Its formation may be related to SPR1, the most robust segment of the entire South Pandora Ridge. Large off-axis seamounts and chains are often related to the wide, shallow, magmatically robust spreading segments, as along the East Pacific Rise, north of Orozco Fracture Zone (16°N) (Macdonald et al., 1992a).

A high concentration of small volcanic cones, 1.5 to 3 km in diameter are observed off-axis in the SPR3 and SPR4 segments (Figs. 8.5 and 8.6). They appear scattered over a 3000 m deep flat plateau. The imagery shows low reflectivity over these cones in relation to a fairly thick sedimentary cover (Fig. 9.6).

Tripartite Ridge

The axial morphology of the Tripartite Ridge is dominated by the NW Cakabau, Cakabau, and SE Cakabau seamounts centred within TR3, TR2 and TR1 segments, respectively (see section 8.2.1). The size and volume of these seamounts tends to decrease towards the southeast according to the direction of ridge propagation (see section 9.1). In consequence, a progressive decrease in the age of the seamounts towards the propagating tip should be considered (Fig. 9.4).

As for the Bransfield Basin, the morphologies of the Tripartite Ridge axial seamounts may also illustrate the volcano-tectonic stages defined above (Fig. 9.5). Point source circular volcanoes form in the central part of the segment protruding into the deep axial grabens. An along-axis volcanic propagation occurs following the N110 trending axial fissures from the initial point source (Fig. 9.4). This is illustrated by the SE Cakabau Seamount, which propagates to the northwest, as well as by the Cakabau Seamount propagating in both directions. Continued extension split the circular edifices by normal faults leading to the formation of a small new axial graben, like that observed within the NW Cakabau Seamount. Asymmetrically, one of the volcanic halves may develop into a propagating neovolcanic ridge. At the tip of the ridge, dozens of small seamounts (2 km basal diameter) mark the present-day axial volcanic propagation of the NW Cakabau Seamount towards the west.

No considerable off-axis volcanism has been observed associated with the Tripartite Ridge due to the limited multibeam coverage, and the youth of this structure.

9.3.3. THE CENTRAL SPREADING RIDGE

Unlike the Bransfield Basin or the South Pandora-Tripartite Ridges where seamounts play a major role in the axial neovolcanism, the axis of the Central Spreading Ridge is devoid of large seamounts. Small (1.5 km diameter) and scattered axial volcanic cones are observed only near the volcanic massif of the 16°50'S triple junction, at the southern CSR3 and northern CSR4 segments (Fig. 7.5). Punctiform volcanism is not observed, perhaps because it is covered by low-relief flows which are the primary products of axial fissural constructional volcanism. However, well developed seamount chains and large volcanoes, about five times larger than the cones described on axis, are abundant within a few tens of

kilometres of the N-S segment axis. They are mainly concentrated along of the CSR7 second-order segment (Figs. 7.6 and 7.7).

Near-axis seamount chains

As described in section 7.2.3, at least 14 seamount chains more than 15 km long have been observed. The chains are composed of two or more seamounts showing different shapes and sizes (Table 7.I). Some of the circular seamounts, like those in E or M (Fig. 7.7), show central depressions up to 1-2 km diameter that are interpreted as caldera collapses, suggesting magmatic chambers underneath (Batiza and Vanko, 1983). The most plausible hypothesis for explaining the origin of these circular seamount chains is that as the central part of the N-S segment is magmatically very robust, chains located within 25 to 30 km of the ridge axis may be associated with the upwelling system beneath the ridge axis. This is similar to the East Pacific Rise, where the largest seamount chains occur adjacent to the ridge axes which are among the shallowest and broadest of their respective segments (Scheirer and Macdonald, 1995). However, a mini hot-spot hypothesis (Shen et al., 1993) has been put forward for the formation of the isolated seamounts located 61 and 92 km off-axis respectively (see Fig. 7.6, 7.7). In contrast, rectangular seamounts, like the ones forming the east-west trending F chain, are delimited by linear and faulted flanks. This N-S faulting pattern parallel to the axis suggests that these seamounts were formed on axis, although this process no longer seems to occur.

Another point to discuss are the ages of the seamount chains. The relative ages of seamounts within a chain are often thought to mimic the age progression of hot-spot volcanoes, becoming older in the direction of absolute plate motion (Scheirer and Macdonald, 1995). Datation of near-axis seamount chains on the Juan de Fuca Ridge (e.g. Desonie and Duncan, 1990) confirms such an age progression decreasing towards the spreading axis. If we apply this hypothesis to the seamount chains of the Central Spreading Ridge, we can affirm that most of the youngest seamounts are located within a distance of 6 to 12.5 km from the axis. Taking an average spreading rate of 80 mm/yr 20°S for the CSR7 segment, these seamounts appear to form in very narrow zones on either side of the ridge axis on crust ranging in age from 0.1 to 0.3 Ma.

9.4. Variability of the superficial and deep structure along the Central Spreading Ridge

As has been explained in section 2.1, there is a strong dependence of axial morphology on the spreading rate (e.g. Menard, 1967; Macdonald, 1982). Axial valleys are considered dynamically stable features (Atwater and Mudie, 1973; Macdonald, 1982), and several steady-state models have been proposed to explain their presence at slow-spreading centres (Sleep, 1969; Lachenbruch, 1973; Anderson and Noltimier, 1973; Tapponnier and Francheteau, 1978; Phipps Morgan et al., 1987; Chen and Morgan, 1990b). However, recent studies reveal a wide variety of ridge morphologic features at slow and intermediate rates instead of an ubiquitous axial depression. Changes from a volcanic dome to a rift valley have been proposed from segments of the Juan de Fuca Ridge (Kappel and Ryan, 1986), Mid-Atlantic Ridge (Fox et al., 1991), Australian-Antarctic Discordance (Palmer et al., 1993), and Pacific-Antarctic Ridge (Marks and Stock, 1994). This morphological variability suggests that, in addition to spreading rate, other parameters such as magma supply and/or crustal thickness exert morphological control.

While maintaining an intermediate spreading rate (50-83 mm/yr), the Central Spreading Ridge is characterized by axial morphologic and gravimetric variability, both in space (along-strike) and time (across-strike). In this section, the along-axis variations in morphology and gravity structure, described in Chapter 7, are related to different thermal regimes. The non steady-state thermal model of Tisseau and Tonnerre (1995) is applied in order to explain the observed variations.

9.4.1. BATHYMETRIC AND GRAVIMETRIC VARIABILITY

Two types of spreading centre can be assumed based on their magmatic budget: a "cold"-type spreading centre, which corresponds to the northern part of the Central Spreading Ridge, and a "hot"-type for the southern part.

The "cold" spreading centres show an axial morphology characterized by a deep rift-valley (N160 segment) or an axial graben (N15 segment), similar to those observed at the Mid-Atlantic Ridge (Fig. 9.7). The roughness of the on- and off-axis topography is very pronounced. The morphology described in section 7.2, and the presence of an interrupted neovolcanic ridge indicate

that magmatism is discontinuous along-axis (non steady-state) and restricted to this area, with no evidence of off-axis volcanic activity.

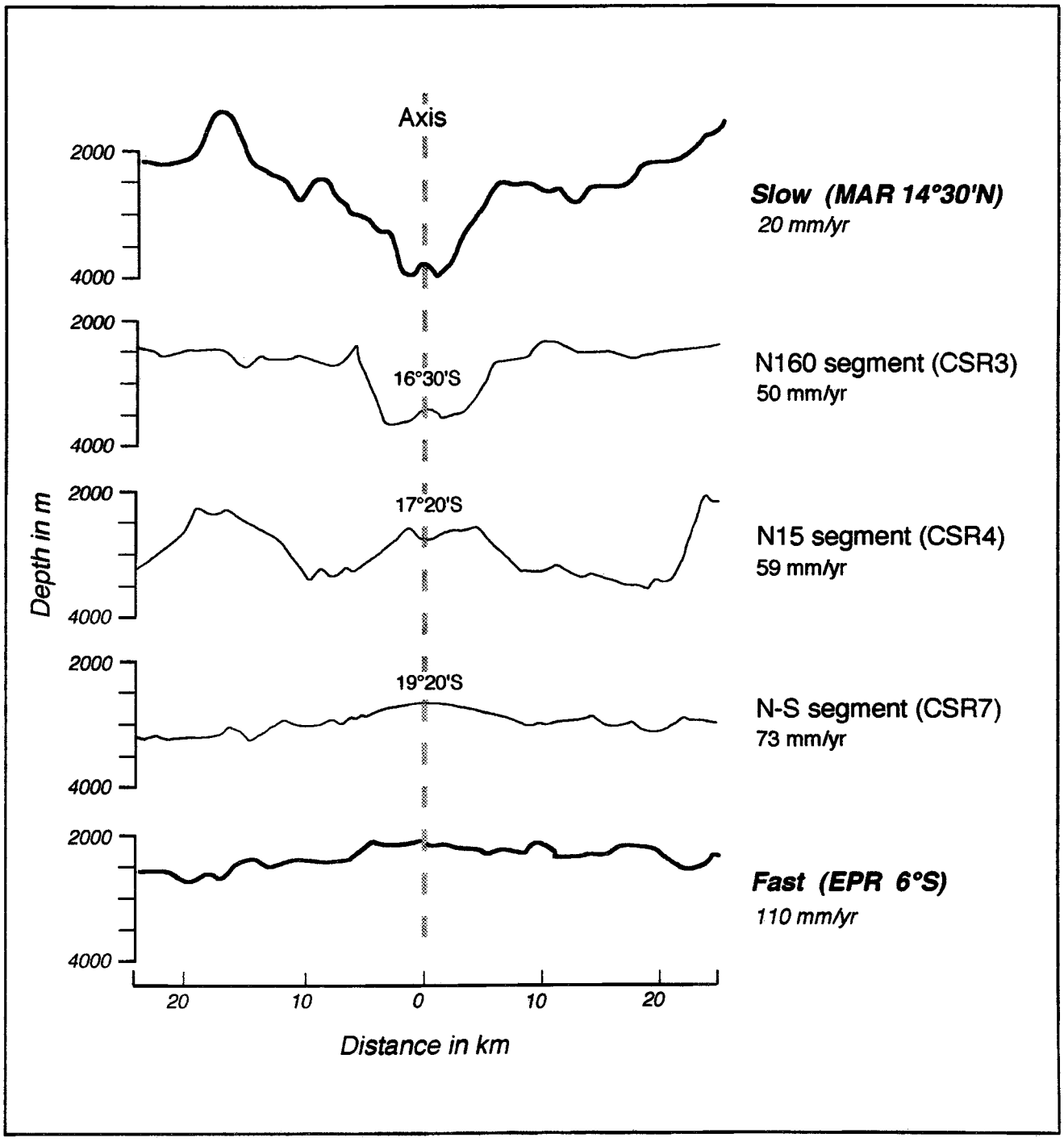

Fig. 9.7. Across-axis bathymetric profiles along the Central Spreading Ridge. Note the dramatic change in axial morphology between the different segments, while the whole spreading rate ranges only between 50 to 73 mm/yr. Compare with the across axis profiles from the slow spreading Mid-Atlantic Ridge and intermediate East Pacific Rise (Fox et al., 1991). Vertical Exaggeration: 5.

In contrast, the "hot" spreading centre represented by the N-S segment has an axial topography similar to that of the East Pacific Rise (Fig. 9.7): a wide volcanic dome, locally with an axial summit caldera. The axial morphology suggest near steady-state magmatism along axis. The off-axis topography is in general smooth and it is only disturbed by the seamount-chains that concentrate on the flanks of CSR7, the most magmatically robust segment (for details about the interpretation of these seamount-chains, see section 9.2).

The gravity structure beneath the Central Spreading Ridge also shows strong differences between the northern and southern parts of the Central Spreading Ridge. The N160 and N15 segments ("cold" spreading centres) have strong variations in the mantle Bouguer anomaly, ranging from -55 to -10 mGal. The "bull's-eye"-shaped gravity lows observed in the 16°50'S triple junction and in the middle of segments CSR2 and CSR3 (Fig. 7.16) are similar to the anomalies found between 27°50'N and 30°40'N on the Mid Atlantic Ridge (Lin et al., 1990; Rommevaux et al., 1994a) and also between 31°S and 34°S along the southern Atlantic (Kuo and Forsyth, 1988; Neumann and Forsyth, 1993). As suggested by Lin and Phipps-Morgan (1992) for slow spreading ridges, these negative anomalies are interpreted as discrete mantle upwellings that result in a thickened crust.

The axis of the N-S segment ("hot" type) shows small-amplitude mantle Bouguer anomaly variations (from -10 to 10 mGal), similar to the low gravity gradients observed along the East Pacific Rise between 9°N-13°N by Madsen et al. (1990). This can be interpreted as sheet-like accretion, a constant crustal thickness (Lin and Phipps-Morgan, 1992) and isostatic compensation of the axial topographic high (Madsen et al., 1990).

Both morphologic and gravimetric features suggest two very different behaviours of magmatism: homogeneous and nearly steady-state magmatism along the N-S segment and heterogeneous and non steady-state magmatism along the N15 and N160 segments. Lava petrology supports this assumption. The lavas are predominantly N-MORB on the "hot" N-S segment. Along the N15 segment three magmatic sources coexist: N-MORB, BABB (transitional E-MORB with Nb anomaly) and OIB lavas. Along the N160 segment, the three sources still coexist but the influence of the BABB source increases (Eissen et al., 1994).

9.4.2. UNEQUIVOCAL RELATIONSHIP BETWEEN FEATURE VARIABILITY AND SPREADING RATE?

Chen and Morgan (1990a, b) presented a mechanical model to explain variations in axial topography and gravity with spreading rate. Their model is based on a layered rheology of the oceanic crust, with an upper brittle layer underlain by a ductile zone. The rheology is determined by the crustal thickness and the thermal structure of the lithosphere, and can result in a decoupling zone under the ridge axis (ductile lower crust). If the decoupling region is small or non-existent, as is the case for slow spreading ridges, then a rift valley is produced as a result of a necking process. If the decoupling region is large, as suggested for the fast spreading ridges, a rise crest high is formed. The critical spreading rate for the formation of a rift-valley or a ridge morphology suggested by both topographic and gravity data is around 70 mm/yr.

A more evolved model is presented by Neumann and Forsyth (1993). They present a 3-D thermal model modified from that of Chen and Morgan (1990b) that includes passive mantle flow, hydrothermal circulation, plate boundary geometry, and variable crustal thickness. The dynamic and isostatic loads produced by this model, applied to a moving, thickening plate, produce a median valley with relief and morphology controlled by the thickness of crust, spreading rate, and mantle temperature.

The bathymetric, gravity and magmatic variations observed along-axis can be related to changes in spreading rate and crustal thickness (Phipps Morgan et al., 1987; Chen and Morgan, 1990b; Neumann and Forsyth, 1993). With a critical spreading rate of 70 mm/yr, the changes in the observed morphologies along the Central Spreading Ridge may, in part, be due to the decrease in spreading rate from 83 mm/yr to 50 mm/yr (south and north, respectively). However this progressive change in the spreading rate does not seem to be accompanied by important changes in the seismically-derived crustal thickness (Kisimoto et al., 1994). Spreading rate and crustal thickness can only explain part of the variations in axial morphology and gravity observed. It is necessary to consider an additional explanation for the variability involving differences in the thermal regimes between the northern and southern segments of the Central Spreading Ridge. This alternative hypothesis is tested by using a non steady-state thermal model, which allows us to take into account a variable heat supply beneath the axis.

9.4.3. APPLICATION OF A NON STEADY-STATE THERMAL MODEL

The thermal model used for this test is that from Tisseau and Tonnerre (1995) (Fig. 9.8). The equations, physical parameters, boundary and initial conditions used for constructing this model are fully explained in Tisseau and Tonnerre (1995).

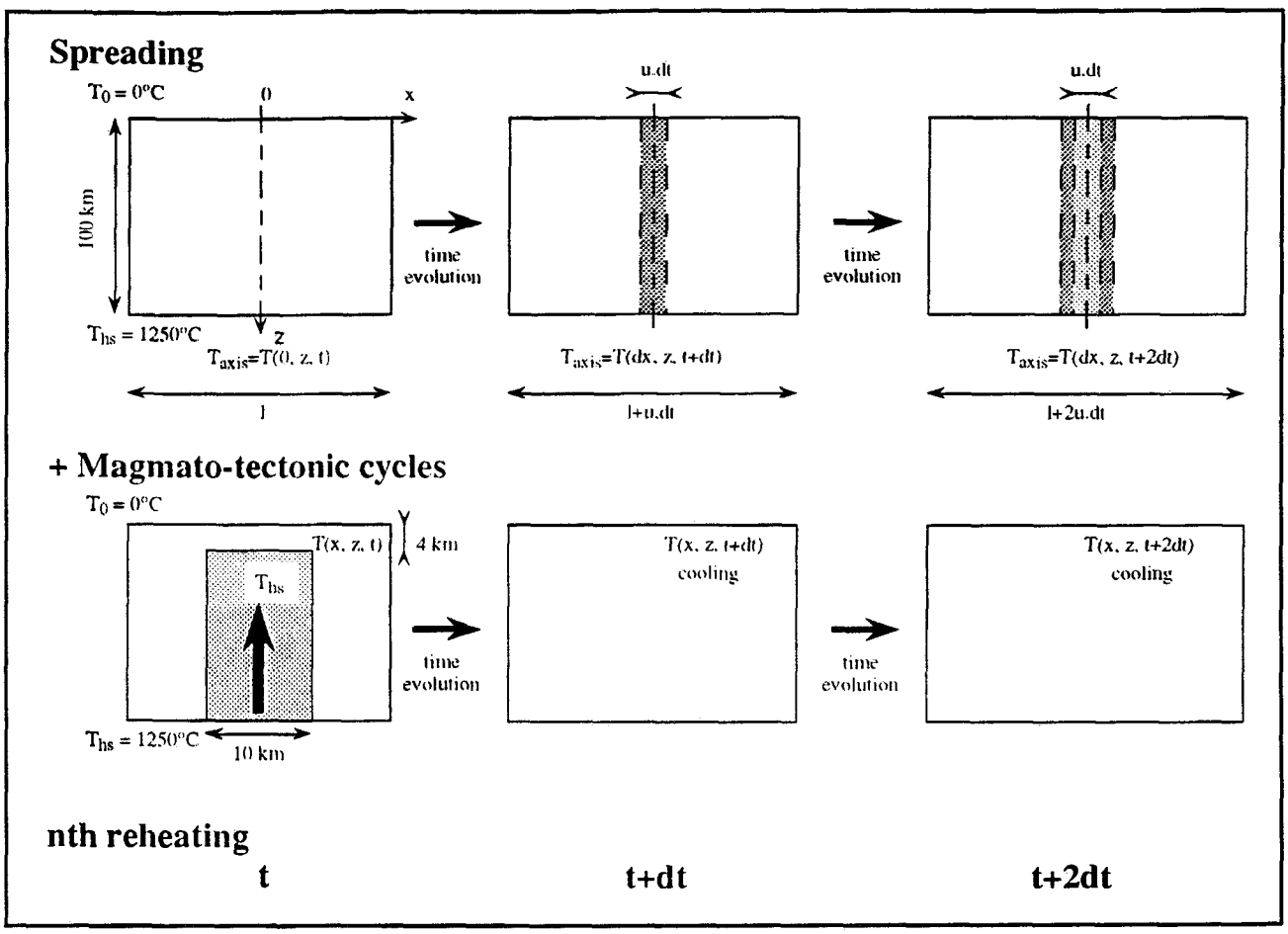

Fig. 9.8. Sketch of the thermal model used (from Tisseau and Tonnerre, 1995). The accretion is viewed as the superposition of the spreading (upper part) and magmato-tectonic cycles (lower part). 0: axis, x: across axis distance, z: depth, t: time, u: full spreading rate, T: temperature, l: full x-dimension of the computed box at t, T_0 and T_{hs}: upper and lower boundary temperatures respectively, T_{axis}: temperature at the axis and in the new created zone.

In this model, the accretion is viewed as the superposition of two processes, spreading with the creation of new oceanic crust, and successive thermal inputs associated with magmato-tectonic cycles. To simulate the spreading, a new two dimensional zone of crust and mantle is accreted at the ridge axis, at regular time intervals (Fig. 9.8). Its width is 1 km and the spreading interval (dt) depends on the spreading rate. At each time step (dt), new axial material is instantaneously emplaced, and its temperature profile

(T_{axis}) is that of the neighbouring zone. Superimposed on spreading are magmato-tectonic cycles that are simulated as thermal inputs (temperature T_{hs}) occurring periodically in a 10 km-wide axial conduit, that extends vertically from 4 km below the seafloor to the bottom of the modelled box (Fig. 9.8). Hot material rises very fast towards the surface (Dick, 1989), and thermal upwelling is modelled to be instantaneous. The periodicity of thermal upwelling events is assumed to be equal to the duration of a magmato-tectonic cycle. Time evolution is a succession of cycles of reheating followed by cooling. Temperature and melt fraction distributions are computed numerically step by step, both in space and time.

Next, the modelling results corresponding to two hypotheses proposed for the Central Spreading Ridge are discussed. To simulate the "cold" northern segment a half-spreading rate of 50 mm/yr is assumed, which corresponds to that calculated at 17°S. A cycle of 200,000 yr reflects the periodicity of topographic lows and highs observed off-axis in the N160 and N15 segments (see section 7.2.3). For the "hot" segments, a spreading rate of 83 mm/yr (calculated at 20°30'S) is used, and a 120,000 yr cycle is considered, which corresponds to the periodicity of the off-axis topography along the N-S segment (see section 7.2.3).

Ridge thermal structure and partial melting

The results of the two Central Spreading Ridge cases modelled are presented in Fig. 9.9, which illustrates the temporal evolution and geometry of the thermal structure and the melting rate for the axial zone of the ridge.

The results for the model of the northern part of the Central Spreading Ridge show progressive cooling in 40,000 year intervals, and after the whole 200,000 yr cycle the isotherms are much more separated and deeper at the axial zone (Fig. 9.9a). This can be translated into thermal subsidence and the existence of a brittle, cold and thick lithosphere that fails by brittle necking, resulting in the formation and development of an axial rift valley. In addition, a strong deepening of the partial melting zone is seen, suggesting temporal variability in the magmatic regime. This corresponds well with the axial morphology observed on the N160 and N15 axes (Figs. 7.8 , 7.9 and 9.7) and with the observed mantle Bouguer anomaly structure (Fig. 7.16).

The model results for the southern Central Spreading Ridge show that, at the end of a 120,000 yr cooling cycle, the isotherms remain grouped close to

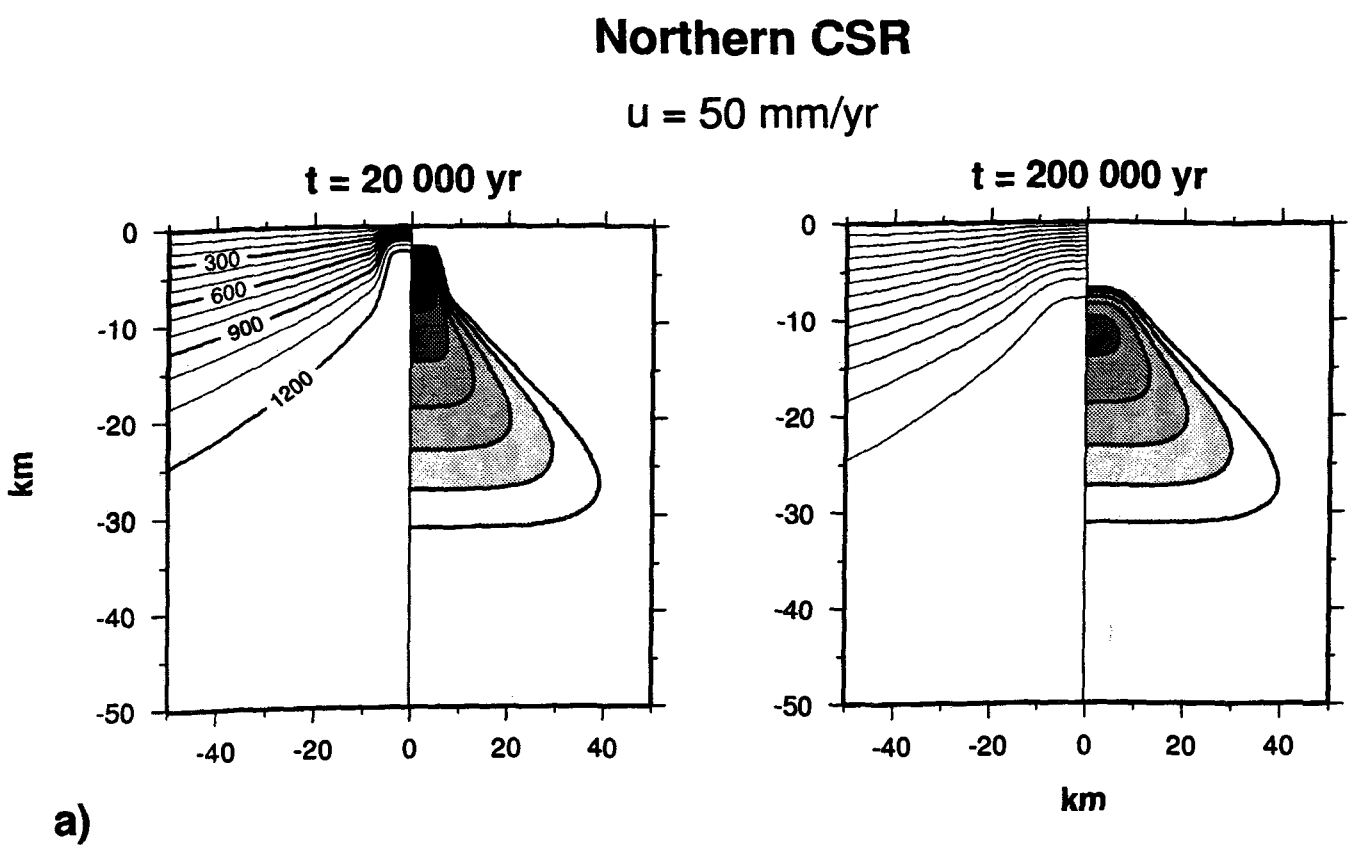

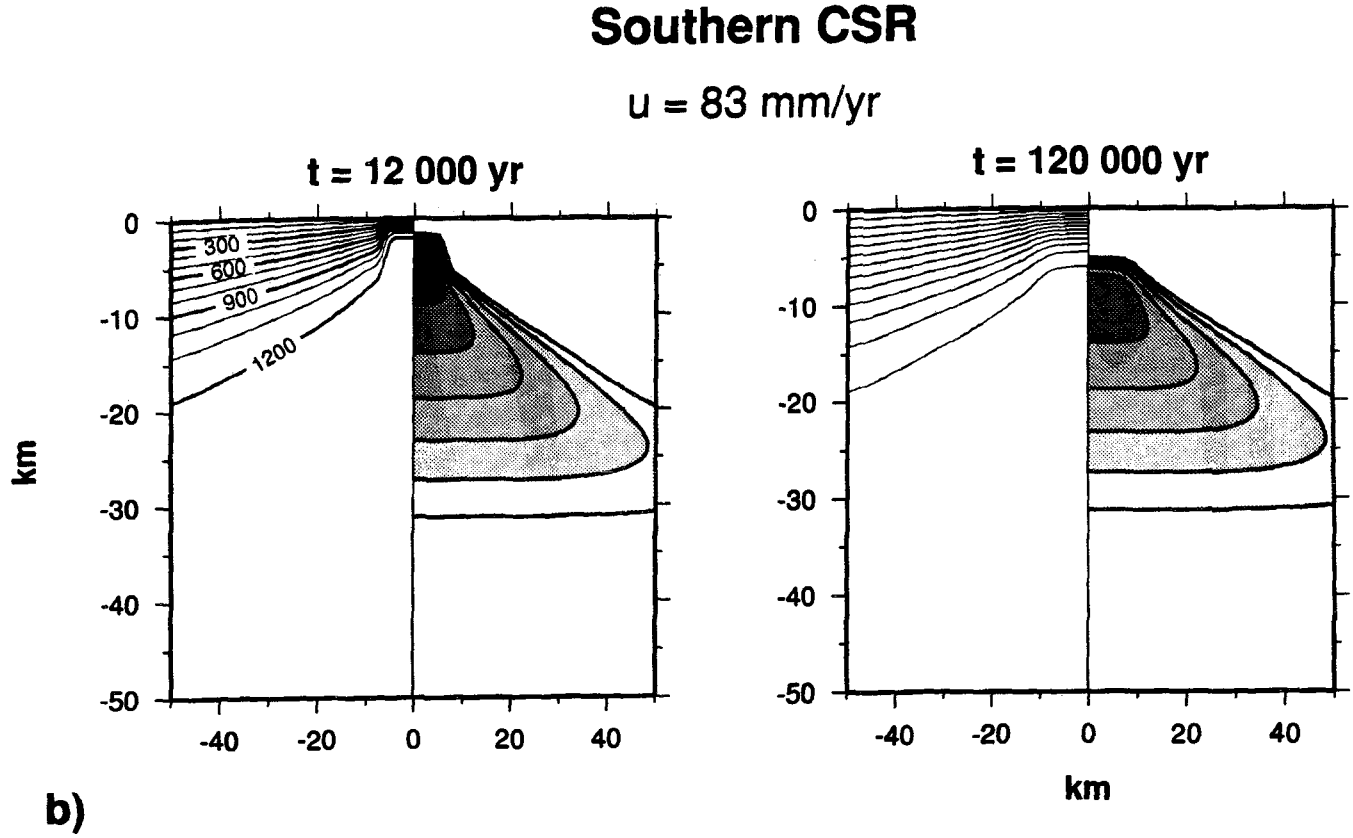

Fig. 9.9. Thermal modelling results for a) the northern (beginning and end of a 200,000 yr cycle with a spreading rate u= 50 mm/yr) and, b) the southern (beginning and end of a 120,000 yr cycle with a spreading rate u= 83 mm/yr) parts of the Central Spreading Ridge. The model domain, centred at the ridge axis, is 100 km wide and 50 km deep . On the left side of each plot the temperature structure is shown, ranging from 0° to 1200°C, with contours at 100°C intervals. The right side corresponds to the melt fraction, ranging from 0% (white) to 22% (black). Scale in km.

the surface at the ridge axis (Fig. 9.9b). The partial melting zone is still shallow and the magma budget is higher and more uniform in time than in the previous case. This thermal structure results in a thin, hot lithosphere with a lower ductile crust that acts as a decoupling zone. This situation is consistent with a fast East Pacific Rise type spreading centre, resulting in a uniform topographic high, as observed along the N-S segment (Fig. 7.9 and 9.7). In addition, this thermal structure is consistent with off-axis volcanism, also present in the N-S segment.

9.4.4. THERMAL PROPAGATION ALONG THE N-S SEGMENT

The boundaries between the "hot" N-S segment and its "cold" bounding segments are the first-order propagating rifts located at 18°10'S and 20°30'S. Heat propagation along the N-S segment at the expense of the adjacent and colder failing segments may explain the rapid spatial changes in the observed morphology and structure between the segments. The hot segment is growing at the expense of the adjacent colder segments, as indicated by the direction of propagation of the segment boundaries (Macdonald et al., 1992a). At the Central Spreading Ridge, the heat propagation southwards and northwards of the N-S segment started at least 1 Ma ago.

This kind of propagation has been proposed in other ridge environments. The dramatic change in axial morphology in the Pacific-Antarctic Ridge may be due to a propagation of the "hot" asthenosphere from a zone north of the Udintsev Fracture Zone towards a relatively "colder" province to the south (Géli et al., 1994; Sahabi et al., in press). Another example is the Reykjanes Ridge, where an important V-shaped ridge structure has been interpreted as an indication of heat-propagation originated at the Iceland hot-spot towards the south (Laughton et al., 1979; Searle and Laughton, 1981).

9.5. Models of backarc oceanic accretion

The observations made on the two backarc basins studied suggest that the superficial morphologic segmentation is also accompanied by a deep segmentation of the gravity structure, as has been pointed out for mid-ocean ridges (e.g. Lin and Phipps Morgan, 1992) (see Chapter 2). From the interpretation of the whole geological and geophysical data set we suggest the following two end-members of backarc crustal accretion and mantle upwelling: focused-type (Fig. 9.10a), and continuous-type accretion (Fig. 9.10b).

9.5.1. FOCUSED-TYPE ACCRETION

The ideal focused-type of accretion (Fig. 9.10a) would be characterized by an extremely contrasted morphology and deep structure along the segments. A focused upwelling of mantle material in the middle of the segment would produce a locally thick crust and point source volcanism. That would be characterized by large amplitude and high gradient circular negative mantle Bouguer anomalies ("bull's eyes") at the centre of the segment. In surface, this would be expressed by large axial volcanoes fed by shallow dykes and with basaltic lavas outcropping. In contrast, the areas not affected by the upwelling would be completely amagmatic with gabbroic and ultramafic rocks exposed at the seafloor surface and related with positive mantle Bouguer gravity anomalies.

The Central Bransfield Basin, the Tripartite Ridge, and the South Pandora Ridge may be characterized by accretionary processes that have trends similar to the focused-type. The point-source volcanism may be installed following sets of orthogonal faults, like edifice C in the Central Bransfield Basin. It is typically located in the central part of the segments as SPR3b (Fig. 9.11a), and the three Cakabau Seamounts. As extension continues, the point source volcanoes split according to an orthogonal extensional trend, like edifices A or D in the Central Bransfield Basin and SPR0, and the NW Cakabau Seamount in the South Pandora and Tripartite Ridges, respectively. This morphologic and structural variability is also correlated to the gravity structure. Large "bull's eye" mantle Bouguer anomalies are obtained centred on the axial seamounts SPR3b and NW Cakabau (TR3), and over the more robust segments of the South Pandora Ridge (as SPR1).

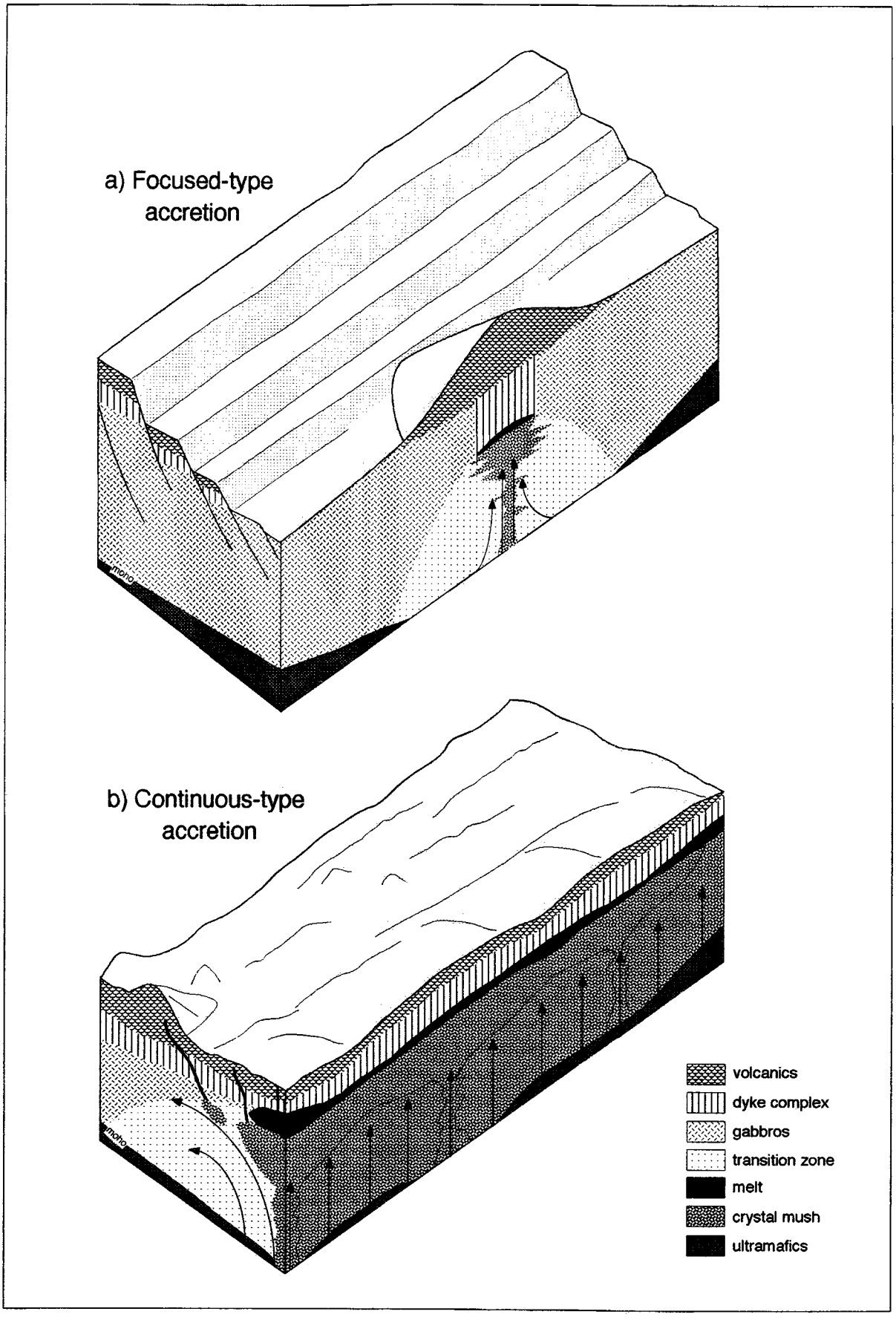

Fig. 9.10. Sketch showing the two end-member models of backarc accretion. In the ideal focused accretion (a) a discrete upwelling of mantle material and crustal construction occur only at the segment centre. In contrast, in the ideal continuous type accretion (b) the magma chamber would be continuous and homogeneous along axis. Solid arrows show mantle flow directions (inspired from draws of Sinton and Detrick, 1992; Lin and Phipps Morgan, 1992; Perfit et al., 1994).

Large point source volcanism, and focused-type accretion may be a common feature reflecting the incipient and young phases of seafloor spreading, as the Bransfield Basin and Tripartite Ridge, respectively. Other young basins also present similar focused volcanism, such as the Red Sea (Bonatti, 1985), the Okinawa Trough (Sibuet et al., 1987), and the Northern Mariana Basin (Martinez et al., 1995), independently of the nature of their crust. However, in mature backarc spreading ridges, as the South Pandora Ridge, focused accretion can result from low, discontinuous, and discrete magma supply beneath the ridge axis, probably related to an ultra-slow spreading rate (less than 20 mm/yr). The Southwest Indian Ridge, that separates Africa from the Antarctic Plate extends from the Bouvet to the Rodriguez triple junctions, and shows similar morphology and gravity anomaly patterns as the South Pandora Ridge. The axial morphology of the Southwest Indian Ridge is characterized by deep rift valleys with large axial seamounts outcropping in the middle correlated with high amplitude large negative gravity anomalies (Rommevaux et al., 1994b). Along the whole length of the ridge (more than 7200 km) the full spreading rate is ultra-slow spreading rate varying only from 13 to 15 mm/yr (Langmuir, 1995)

9.5.2. CONTINUOUS-TYPE ACCRETION

The ideal continuous type of accretion (Fig. 9.10b) would be homogeneous and uninterrupted along the whole length of the ridge. A steady-state magma chamber would produce along-axis permanent upwelling of mantle material and constant crustal thickness. That would be characterized by no significant variations of the along-axis mantle Bouguer anomalies. In surface, that would be expressed by a continuous elevated axial high with extrusive flows and pillow basalts outcropping all along, as result of volcanic construction. The robustness of the axial magmatism would also allow the production of off-axis volcanism (Fig. 9.10b).

The N-S segment of the Central Spreading Ridge of the North Fiji Basin may be characterized by an accretion similar to the continuous type. Along this segment, the axial morphology shows an 8-10 km wide, 70 km long and 200-300 m high axial dome (Fig. 9.11b). Several near-axis volcanic chains are also present. The mantle Bouguer anomalies are almost constant along the N-S segment with anomalies of very small amplitude. The N160 segment of the Central Spreading Ridge although it shows in surface a continuous axial morphology in rift valley, it shows large "bull's eye" mantle Bouguer

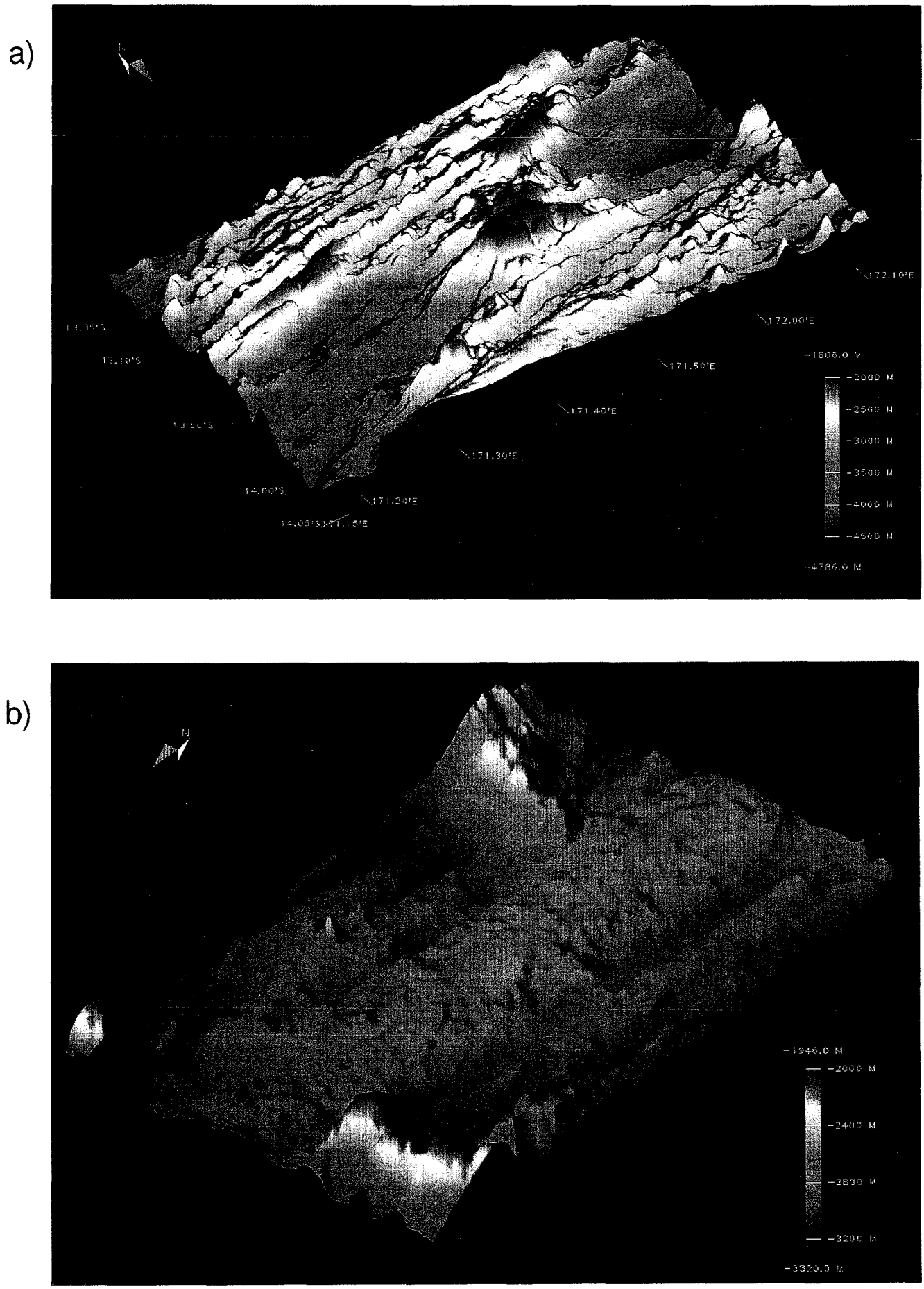

Fig. 9.11. *a) 3-D block of the N75 segment of the South Pandora Ridge, that may be representative of the focused-type accretion. b) 3-D block of the segment CSR7 of the N-S segment of the Central Spreading Ridge, which may illustrate a continuous-type accretion.*

anomalies in the segment centre. This suggests a more focused-like accretion for this segment, which is mainly dominated by tectonic processes.

This backarc accretion type is homogeneous and continuous in time and space. Continuous accretion (Fig. 9.11b), resulting in uniform morphologic features, may be characteristic of mature backarc spreading centres, such as the N-S segment of the Central Spreading Ridge in the North Fiji Basin, the Central Woodlark (Hill et al., 1984), and Central Lau Basin spreading ridges (Parson et al., 1990). These intermediate to fast rate spreading centres are related to a continuous magma supply along a persistent magma chamber, similar to what is observed along the East Pacific Rise (Madsen et al., 1990).

9.5.3. WHAT CONTROLS THE TYPE OF ACCRETION?

The two models presented above are end-members, and there are many gradual variations between them. The essential point is to try to understand what factors control the accretion in backarc spreading centres. Why in some areas do we have focused-like accretion while in others accretion is similar to the continuous-type? We suggest several factors, grouped into internal and external, that may exert control on accretion.

Internal factors

The internal factors are those intrinsically related to the spreading centre and, in consequence, are fundamental to the evolution of the backarc spreading ridge. Some of them are:

- The history and temporal evolution of the spreading centres. As discussed in section 9.1 original rifting of the volcanic arc may determine the compartmentation of the basin and the future ridge segmentation.

- The spreading rate and its along-axis variability. As a general rule, it seems that ultra-slow and slow spreading rates favour a focused-type accretion, whereas intermediate and fast spreading rates support a continuous-type accretion.

- The thermal regime of the ridge and along-axis magmatic budget. This is directly related to the continuity of the magma chamber, which may produce changes in crustal thickness and variations in axial

topography. This is so even if other factors, like the spreading rate, remain constant.

External factors

The external factors are not directly related to the spreading ridge itself, but their presence or proximity may affect and change the evolution of the ridge. Some of these factors are:

- The age, nature, and structure of the surrounding lithosphere where the backarc spreading centre is installed and propagates. One or other accretion type may be favoured depending if the basin is formed by young oceanic crust, pre-existing oceanic crust, or extended and thinned arc or continental crust.

- The proximity of hot-mantle plumes. This exerts a deep influence in the spreading centre and may play a role in changing the type of accretion. Thus, when slow ridges are located near hot-spots, the focused accretion type would be blurred and diluted by a more continuous accretion. The opposite case may occur when a fast spreading ridge is located near a "cold" area.

- The proximity of the subduction zone, velocity and dip angle of the subducting slab may also influence the basin opening rate and the type of accretion.

Chapter 10

CONCLUSIONS

This chapter is subdivided into three sections dealing with local conclusions (one for each of the three areas studied) and a last section including general conclusions. In the local conclusion sections, only the most relevant and new ideas are presented. Apparent unhomogeneity between these sections reflects the marked differences between the areas as well as the stage in our knowledge about them.

10.1. Local conclusions

10.1.1. CENTRAL AND EASTERN BRANSFIELD BASINS

♦ The opening in the Bransfield Basin involves a combination of rifting of the pre-existing crust as well as intrusions and volcanism. The timing of rifting is still a point of debate, with two main tendencies: less than 4 Ma and 26-22 Ma. We suggest that an intermediate value between these age models may better agree with the observed structures and the very slow subduction. The exact amount of thinning and extension still remains to be solved. The Eastern and Central Bransfield Basins are dominated by a NW-SE trending extension, although a strike-slip motion related to the left-lateral South Scotia Ridge would also occur in the Eastern Bransfield Basin.

♦ A progressive opening and volcanic propagation towards the northeast is suggested, with incipient seafloor spreading in the Central Basin and pre-spreading backarc rifting in the Eastern Bransfield Basin. Seafloor spreading occurs only discontinuously along the Central Bransfield Basin and is still not well organized. Inferred from magnetic anomalies, the maximum age of spreading in the Central Bransfield Basin would be 0.71 Ma and the resulting maximum spreading rate, 0.83 mm/yr.

♦ The different morphologies of the largest edifices observed in the Central Bransfield Basin may illustrate three successive volcano-tectonic stages:

formation of circular point-source volcanoes at the intersection of two main sets of faults, extension and along-axis propagation of volcanism. This morphologic evolution correlates well with an along-axis variation in seamount basalt chemistry and age.

10.1.2. CENTRAL SPREADING RIDGE

♦ Two axial morphologies are observed along the mature (3.5 Ma old) Central Spreading Ridge: Mid-Atlantic Ridge type for the N160 segment, and East Pacific Rise type for the N-S segment. In addition, the deep crustal structure, inferred from the mantle Bouguer anomalies, also shows strong differences between the northern and southern parts of the ridge. The spreading rates have intermediate values decreasing northwards only from 83 to 50 mm/yr. This variation in axial morphology and gravity structure can be explained not only by differences in spreading rate and crustal thickness, but also by the thermal regime between segments.

♦ A distinction between a "cold" and a "hot" spreading type is proposed. The "cold" spreading centre corresponds to the northern part of the Central Spreading Ridge (comprising the N160 and N15 segments), and is characterized by weak magmatism related to a low thermal budget, similar to slow-spreading ridges. The "hot" spreading ridge corresponds to the southern part of the Central Spreading Ridge (N-S segment) where a high thermal supply related to a more vigorous volcanic stage is suggested.

♦ The non steady-state thermal model of Tisseau and Tonnerre (1995) is proposed to test the hypothesis of "hot" and "cold" spreading centres. For the "colder" Central Spreading Ridge we have adopted a spreading rate of 50 mm/yr, and a cooling cycle of 200,000 yr. For the "hotter" Central Spreading Ridge the spreading rate is 83 mm/yr and the cooling cycle is 120,000 yr. The thermal and melting structures resulting from the model are consistent with the observed variations along the Central Spreading Ridge. A thermal boundary between the N-S and neighbouring colder segments, and heat propagation along the N-S axis may explain the rapid changes in the axial morphologies and structure in depth between the segments.

10.1.3. SOUTH PANDORA AND TRIPARTITE RIDGES

♦ The South Pandora Ridge is a mature spreading centre that has been expanding continuously since 7 Ma ago with a N-S trending extension. The calculated spreading rate (16 mm/yr) classifies the ridge as an ultra-slow spreading centre. The Tripartite Ridge is a young spreading centre formed at least 0.7 Ma ago that propagates towards the southeast, as suggested by the V-shaped magnetic and structural patterns.

♦ The South Pandora Ridge is characterized for both axial and off-axis seamounts. The axial topography of the South Pandora Ridge is characterized by a strong contrast between segments formed by large seamounts and rift-valleys. The axial seamounts seem to be formed by point source volcanism that propagates along the main structural trends. Two types of off-axis seamounts are observed: large seamounts and small cones.

♦ The axial seamounts along the Tripartite Ridge may also illustrate evolutionary volcano-tectonic stages, as observed along the Central Bransfield Basin. The size and volume of the Tripartite Ridge axial seamounts seems to decrease towards the southeast according to the direction of propagation.

10.2. General conclusions

1. The three areas studied have been classified in terms of backarc evolutive stages. The Central and Eastern Bransfield Basin illustrate the incipient and pre-spreading rifting stages respectively, whereas the areas studied in the North Fiji Basin are representative of well organized seafloor spreading, from young (Tripartite Ridge) to mature spreading (Central Spreading Ridge and South Pandora Ridge).

2. The present-day opening seems to be related to the rollback of the subduction hinge in the Bransfield Basin, whereas it does not seem to be related to any subduction in the North Fiji Basin. We suggest that the current opening in the North Fiji Basin is linked to a regional thermal anomaly, responsible for a higher rate of mantle convection that induces rapid crustal production, together with the transcurrent motion between the Pacific and Indo-Australian Plates.

3. The study of backarc rifting areas, like the Eastern Bransfield Basin, shows that initial rifting of the arc may pre-determine the future segmentation of the basin. The constant distance between each eruptive centre observed in incipient spreading areas, like the Central Bransfield Basin, suggests a regular spacing of the upwellings forming linear proto-segments. Moreover, the study of mature backarc systems as in the North Fiji Basin, shows that the fundamental accretionary processes are similar in backarc and mid-ocean ridges. However, some differences between them have been observed, especially concerning ridge segmentation and axial discontinuities. First-order backarc segmentation is short-lived and about half the length of that in mid-ocean ridges. Axial discontinuities along the Central Spreading Ridge and South Pandora-Tripartite Ridges are analogous to those described in mid-ocean ridges. However, the fundamental difference is the lack of large fracture zones and transform faults separating the backarc segments.

4. Large seamount volcanism may play a fundamental role in backarc axial construction, and may be a common characteristic of slow and ultra-slow mature spreading ridges and incipient spreading centres, as observed along the South Pandora-Tripartite Ridges and the Central Bransfield

Basin, respectively. Different evolutionary volcano-tectonic stages of these seamounts are defined. In contrast, the axis of the intermediate spreading Central Spreading Ridge is devoid of large seamounts. Only near-axis seamount chains are concentrated there, and probably associated with the upwelling system beneath the ridge.

5. Variability of the axial morphology and gravity structure is observed along the Central Spreading Ridge, and cannot be explained only in terms of differences in spreading rate and crustal thickness. We suggest differences in thermal regime between the segments, and we apply a non-steady state thermal model to test this hypothesis. The results obtained are consistent with the variations observed. The limits between the "hot" N-S segment and the "cold" segments are propagating rifts, which may be interpreted as thermal boundaries between segments.

6. Two paradigmatic end-member models of backarc crustal accretion and mantle upwelling are presented, based on the interpretation of the whole geological and geophysical data set: focused-type and continuous-type accretion. The focused-type would be characterized by an extremely contrasted morphology and deep structure along the segments, with punctiform upwellings. Incipient and young phases of seafloor spreading (e.g. Central Bransfield Basin and Tripartite Ridge, respectively) as well as ultra-slow spreading ridges (e.g. South Pandora Ridge) may have trends in common with this accretion type. The continuous-type accretion would be homogeneous and uninterrupted along the ridge, with a persistent magma chamber. Intermediate (e.g. Central Spreading Ridge/N-S segment) and fast spreading mature ridges show processes similar to the continuous accretion. Internal (history and evolution of the ridges, spreading rate, thermal regime) and external factors (age and nature of the surrounding lithosphere, proximity of mantle plumes, and subduction zones) may control the type of accretion.

BIBLIOGRAPHY

Bibliography

Abers, G.A., 1991, Possible seismogenic shallow-dipping normal faults in the Woodlark-D'Entrecasteaux extensional province, Papua New Guinea, *Geology*, **19**, 1205-1208.

Acosta, J., Herranz, P., Sanz, J.L., and Uchupi, E., 1992, Antarctic continental margin: Geologic image of the Bransfield Trough, an incipient oceanic basin, *In:* Poag, C.W., and Graciansky, P.C., (Eds.), *Geological evolution of Atlantic Continental Rises*, Van Nostrand Reinhold, New York, 49-61.

Acosta, J., Canals, M., Alonso, B., and ORCA Group, 1994, *Bathymetry of the Hesperides Deep, Scotia Sea, South Scotia Ridge, Antarctica*, Scale 1:200,000, GRGM (Eds.), University of Barcelona, Barcelona.

Anderson, R.N., and Noltimier, H.C., 1973, A model for the horst and graben structure of mid-ocean ridge crests based on spreading velocities and basalt delivery to the ocean crust, *Geophys. J. R. Astron. Soc.*, **34**, 137-149.

Anderson, R.N., McKenzie, D., and Sclater, J.G., 1973, Gravity, bathymetry and convection in the Earth, *Earth Planet. Sci. Lett.*, **18**, 391-407.

Andrews, D.J., and Sleep, N.H., 1974, Numerical modelling of tectonic flow behind island arcs, *Geophys. J. R. Astron. Soc.*, **38**, 237-251.

Ashcroft, W.A., 1972, *Crustal structure of the South Shetland Islands and Bransfield Strait*, BAS Scient. Rep., **66**, 43 p.

Atwater, T., and Mudie, J. D., 1973, Detailed near-bottom geophysical study of the Gorda Rise, *J. Geophys. Res.*, **78**, 8665-8686.

Auzende, J.M., and Urabe, T, 1994, The STARMER French-Japanese Joint project, 1987-1992, *Mar. Geol*, **116**, 1-3.

Auzende, J.M., Eissen, J.P., Caprais, M.P., Gente, P., Gueneley, S., Harmegnies, F., Lagabrielle, Y., Lapouille, A., Maillet, P., Mazé, J.P., Ondréas, H., Schaaf, A., and Singh, R., 1986a, Accrétion océanique et déformation dans la partie méridionale du bassin Nord-Fidjien: Résultats préliminaires de la campagne océanographique SEAPSO III du N.O. Jean Charcot (Décembre 1985), *C. R. Acad. Sci. Paris*, **303**, 93-98.

Auzende, J.M., Lagabrielle, Y., Schaaf, A., Gente, P., and Eissen, J. P., 1986b, Tectonique intra-océanique décrochante à l'ouest des îles Fidji (Bassin Nord Fidjien), Campagne SEAPSO III du N.O. Jean Charcot, *C. R. Acad. Sci. Paris*, **303**, 241-246.

Auzende, J.M., Eissen, J.P., Lafoy, Y., Gente, P., and Charlou, J.L., 1988a, Seafloor spreading in the North Fiji Basin (Southwest Pacific), *Tectonophysics*, **146**, 317-351.

Auzende, J.M., Lafoy, Y., and Marsset, B., 1988b, Recent geodynamic evolution of the North Fiji Basin (SW Pacific), *Geology*, **16**, 925-929.

Auzende, J.M., Bideau, D., Bonnatti, E., Cannat, M., Honnorez, J., Lagabrielle, Y., Malavieille, J., Mamaloukas-Frangoulis, V., and Mével, C., 1989, Direct observation through slow-spreading oceanic crust, *Nature*, **337**, 726-729.

Auzende, J. M., Honza, E., and the STARMER Group, 1990a, Bathymetric map of the North Fiji Basin Ridge between 16°10'S and 21°40'S, Scale 1: 200000, IFREMER and STA Pub., Six colour sheets, BEICIP Eds., Paris.

Auzende, J. M., Honza, E., Boespflug, X., Deo, S., Eissen, J. P., Hashimoto, J., Huchon, P., Ishibashi, J., Iwabuchi, Y., Jarvis, P., Joshima, M., Kisimoto, K., Kiuwahara, Y., Lafoy, Y., Matsumoto, T., Maze, J.P., Mitsuzava, K., Momma, H., Naganuma, T., Nojiri, Y., Ohta, S., Otsuka, K., Okuda, Y., Ondreas, H., Otsuki, A., Ruellan, E., Sibuet, M., Tanahashi, M., Tanaka, T., and Urabe, T., 1990b, Active spreading and

hydrothermalism in North Fiji Basin (SW Pacific): Results of Japanese-French cruise Kaiyo 87, *Mar. Geophys. Res.*, **12**, 269-283.

Auzende, J.M., Urabe, T., Bendel, V., Deplus, C., Eissen, J.P., Grimaud, D., Huchon, P., Ishibashi, J., Joshima, M., Lagabrielle, Y., Mevel, C., Naka, J., Ruellan, E., Tanaka, T., and Tanahashi, M., 1991, In situ geological and geochemical study of an hydrothermal site on the North Fiji Basin ridge, *Mar. Geol.*, 98 259-269.

Auzende, J.M., Hey, R., Pelletier, B., and Lafoy, Y., 1993, Propagation d'une zone d'accretion a l'est de la dorsale du Bassin Nord-Fidjien (SW Pacific), *C. R. Acad. Sci. Paris*, **317**, 671-678.

Auzende, J.M., Gràcia Mont, E., Bendel, V., Huchon, P., Lafoy, Y., Lagabrielle, Y., De Alteriis, G., and Tanahashi, M., 1994a, A possible triple junction at 14°50'S on the North Fiji Basin Ridge (Southwest Pacific)?, *Mar. Geol.*, **116**, 25-37.

Auzende, J.M., Pelletier, B., and Lafoy, 1994b, Twin active spreading ridges in the North Fiji Basin (southwest Pacific), *Geology*, **22**, 63-66.

Auzende, J.M., Halbach, P., Allspach, A., Becker, K., Blum, N., Bonnier, O., van Gerven, M., Halbach, M., Koschinsky, A., Lange, D., Madureira, M.J., Manoutsoglou, E., Mrazek, J., Münch, U., Pratt, C., Rahders, E., van Reusel, A., Richter, S., Seifert, T., Spangenberg, T., Stenzler, J., Thiermann, F., Türkay, M., and, Windoffer, R., 1995a, Activité tectonique, magmatique et hydrothermale autour des triples jonctions de 16°50'S-173°30'E et de 16°30'S-176°10'E dans le Bassin Nord Fidjien (SW Pacifique): Campagne HYFIFLUX, *C. R. Acad. Sci. Paris*, **321**, 239-246.

Auzende, J.M., Hey, R.N., Pelletier, B., Rouland, D., Lafoy, Y., Gràcia, E., and Huchon, P., 1995b, Propagating rift west of the Fiji Archipelago (North Fiji Basin, SW Pacific), *J. Geophys. Res.*, **100**, 17823-17835.

Auzende, J.M., Pelletier, B., and Eissen, J.P., 1995c, The North Fiji Basin: Geology, structure and geodynamic evolution, *In:* Taylor, B., (Ed.), *Back-arc basins: Tectonics and magmatism*, Plenum Publ. Corp., New York, 139-170.

Ballard, R.D., and Moore, J.G., 1977, *Photographic Atlas of the Mid-Atlantic Ridge*, Springer, New York, 114 pp.

Ballard, R.D., Holcomb, R.T., and Van Andel, T.H., 1979, The Galapagos Rift at 86°W: 3. Sheet flows, collapse pits, and lava lakes of the rift valley, *J. Geophys. Res.*, **84**, 5407-5422.

Barazangi, M., and Isacks, B., 1971, Lateral variations of seismic wave attenuation in the upper mantle above the inclined earthquake zone of the Tonga island arc: deep anomaly in the upper mantle, *J. Geophys. Res.*, **76**, 8493-8516.

Barazangi, M., Pennington, W., and Isacks, B., 1975, Global study of seismic wave attenuation in the upper mantle behind island arcs using P waves, *J. Geophys. Res.*, **80**, 1079-1092.

Barker, D.H.N., and Austin Jr, J.A., 1994, Crustal diapirism in Bransfield Strait, West Antarctica: Evidence for distributed extension in marginal-basin formation, *Geology*, **22**, 657-660.

Barker, P.F., 1970, Plate tectonics of the Scotia Sea region, *Nature*, **228**, 1293-1296.

Barker, P.F., 1972, Magnetic lineations in the Scotia Sea, *In:* Adie, R.J., (Ed.), *Antarctic Geology and Geophysics-Symposium on Antarctic geology and solid earth geophysics*, Universitetforlaget, Oslo, 17-26.

Barker, P.F., 1982, The Cenozoic subduction history of the Pacific margin of the Pacific margin of the Antarctic Peninsula: Ridge crest-trench interactions, *Geol. Soc. London J.*, **139**, 787-801.

Barker, P.F., 1995, Tectonic framework of the East Scotia Sea, *In:* Taylor, B., (Ed.), *Backarc basins: Tectonics and magmatism*, Plenum Publ. Corp., New York, 281-314.

Barker, P.F., and Burrell, J., 1977, The opening of Drake Passage, *Mar. Geol.*, **25**, 15-34.

Barker, P.F., and Hill, I.A., 1981, Back-arc extension in the Scotia Sea, *Phil. Trans. R. Soc. Lond.*, **300**, 249-262.

Barker, P.F., and Dalziel, I.W.D., 1983, Progress in geodynamics of the Scotia Arc region, *In:* Cabré, R. (Ed.), *Geodynamics of the Eastern Pacific region, Caribbean and Scotia Arcs*, Geodyn. Ser., **9**, AGU, Washington D.C., 137-170.

Barker, P.F., Barber, P.L., and King, E.C., 1984, An Early Miocene ridge crest-trench collision on the South Scotia Ridge near 36°W, *Tectonophysics*, **102**, 315-332.

Barker, P.F., Dalziel, I.W.D., and Storey, B.C., 1991, Tectonic development of the Scotia Arc region, *In:* Tingey, R.J. (Ed.), *Antarctic Geology*, Oxford University Press, Oxford, 215-248.

Batiza, R., 1982, Abundances, distribution and sizes of volcanoes in the Pacific Ocean and implications for the origin of non-hotspot volcanoes, *Earth Planet. Sci. Lett.*, **60**, 195-206.

Batiza, R., and Vanko, D., 1983, Volcanic development of small oceanic central volcanoes on the flanks of the East Pacific Rise inferred from narrow-beam echosounder surveys, *Mar. Geol.*, **54**, 53-90.

Bendel, V., 1993, *Cadre géologique et composition des minéralisations hydrothermales en contexte arrière-arc: Exemple de la dorsale du Bassin Nord Fidjien*, Thèse nouveau régime, Univ. Bretagne Occidentale, Brest, 259 p.

Bendel, V., Fouquet, Y., Auzende, J.M., Lagabrielle, Y., Grimaud, D., and Urabe, T., 1993, The White Lady hydrothermal field, North Fiji back-arc Basin, Southwest Pacific, *Economic Geol.*, **88**, 2237-2249.

Benes, V., Scott, S.D., and Binns, R.A., 1994, Tectonics of rift propagation into a continental margin: Western Woodlark Basin, Papua New Guinea, *J. Geophys. Res.*, **99**, 4439-4455.

Bibee, L.D., Shor, G.G.Jr., and Lu, R.S., 1980, Inter-arc spreading in the Mariana Trough, *Mar. Geol.*, **35**, 183-197, 1980.

Binns, R.A., and Scott. S.D., 1993, Actively forming polymetallic sulfide deposits associated with felsic volcanic rocks in the Eastern Manus backarc basins, Papua New Guinea, *Econ. Geol.*, **88**, 2226-2236.

Binns, R.A., Scott, S.D., Bodganov, Y.A., Lisitzin, A.P., Gordeev, V.V., Gurvich, E.G., Finlayson, E.J., Boyd, T., Dotter, L.E., Wheller, G.E., and Muravyev, K.G., 1993, Hydrothermal oxide and gold-riche sulfate deposits of Franklin seamount, Western Woodlark Basin, Papua New Guinea, *Econ. Geol.*, **88**, 2122-2153.

Birkenmajer, K., 1992, Evolution of the Bransfield Basin and Rift, West Antarctica, *In*: Yoshida, Y. et al., (Eds.), *Recent progress in Antarctica, Earth Science*, Terra Scientific Publ. Co., Tokyo, 405-410.

Birkenmajer, K., 1994, Evolution of the Pacific margin of the northern Antarctic Peninsula: an overview, *Geol. Rundsch*, **83**, 309-321.

Birkenmajer, K., and Keller, R.A., 1990, Pleistocene age of the Melville Peak volcano, King George Island, West Antarctica, by K-Ar dating, *Bull. Polish Acad. Sci., Earth Sci.*, **38**, 17-24.

Boespflug, X., 1990, *Evolution géodynamique et géochimique des bassins arrière-arc. Exemple des bassins d'Okinawa, de Lau et Nord-Fidjien*, Thèse nouveau régime, Univ. Bretagne Occidentale, Brest, 354 p.

Bonatti, E., 1985, Punctiform initiation of seafloor spreading in the Red Sea during transition from a continental to an oceanic rift, *Nature*, **316**, 33-37.

Both, R.A.,Crook, K., Taylor, B., Brogan, S., Chappell, B., Frankel, E., Liu, L., Sinton, J., and Tiffin, D., 1986, Hydrothermal chimneys and associated fauna in the Manus back-arc basin, Papua New Guinea, *EOS, Trans. AGU*, **67**, 489-490.

British Antartic Survey, 1985, Tectonic map of the Scotia Arc, Scale 1:300.000, Misc 3, B.A.S., Cambridge, UK.

Brocher, T.M., 1985, On the formation of the Vitiaz Trench lineament and North Fiji Basin, *In:* Brocher, T.M., (Ed.), *Investigations of the Northern Melanesian Borderland,* Circum-Pacific Council for Energy and Mineral Resources, Earth Science Ser. **3,** Houston, Texas, 13-34.

Brocher, T.M., and Holmes, R., 1985, Tectonic and geochemical framework of the northern Melanesian borderland: An overview of the KK820316 Leg 2 objectives and results, *In:* Brocher, T.M., (Ed.), *Investigations of the Northern Melanesian Borderland,* Circum-Pacific Council for Energy and Mineral Resources, Earth Science Ser. **3,** Houston, Texas, 1-11.

Bryan, W.B., Humphris, S.E., Thompson, G., and Casey, J.F., 1994, Comparative volcanology of small axial eruptive centers in the MARK area, *J. Geophys. Res.,* **99,** 2973-2984.

Canals, M., Acosta, J., Gràcia, E., Escartín, J, and Grupo O.R.C.A., 1992, Caracterización geológica de la región de enlace entre la Cuenca de Bransfield y la Dorsal Sur de Scotia (Antártida), *Acta Geol. Hisp.,* **27,** 89-110.

Canals, M., Acosta, J., Baraza, J., Bart, P., Calafat, A.M., Casamor, J.L., De Batist, M., Ercilla, G., Farrán, M., Francés, G., Gràcia, E., Ramos-Guerrero, E., Sanz, J.L., Sorribas, J., and Tassone, A., 1994, La Cuenca Central de Bransfield (NW de la Península Antártica): primeros resultados de la campaña GEBRA 93, *Geogaceta,* **16,** 132-135.

Cannat, M., 1990, *Mecanismes de l'accretion et mise à l'affleurement de peridotites et de gabbros à l'axe des dorsales océaniques,* Thèse d'Habilitation à Diriger des Recherches, Univ. Bretagne Occidentale, Brest, 206 p.

Carbotte, S.M., and Macdonald, K.C., 1990, Causes of variation in fault facing direction on the ocean floor, *Geology,* **18,** 749-752.

Carbotte, S.M., and Macdonald, K.C., 1994, Comparison of seafloor tectonic fabric at intermediate, fast and superfast spreading ridges: Influence of spreading rate, plate motions, and ridge segmentation on fault patterns, *J. Geophys. Res.,* **99,** 13609-13631.

Carlson, R.L., and Melia, P.J., 1984, Subduction hinge migration, *Tectonophysics,* **102,** 399-411.

Carney, J.N., and Macfarlane, A., 1982, Geological evidence bearing on the Miocene to Recent structural evolution of the New Hebrides Arc, *Tectonophysics,* **87,** 147-175.

Cochran, J.R., 1979, An analysis of isostasy in the world's oceans. 2. Mid-ocean ridge crests, *J. Geophys. Res.,* **84,** 4713-4729.

Cochran, J.R., and Martinez, F., 1988, Evidence from the northern Red Sea on the transition from continental to oceanic rifting, *Tectonophysics,* **153,** 25-53.

Coleman, P. J., and Packham, G. H., 1976, The Melanesian Borderlands and India-Pacific plates boundary, *Earth Sci. Rev.,* **12,** 197-233.

Collette, B.J., Verhoef, J., and de Mulder, A.F.J., 1980, Gravity and a model of the median rift valley, *J. Geophys.,* **47,** 91-98.

Colley, H., and Hindle, W.H., 1984, Volcanotectonic evolution of Fiji and adjoining arginal basins, *In:* Kokelaar, B.P., and Howells, M.F., (Eds.), *Marginal Basin Geology,* Blackwell, London, 151-162.

Collier, J.S., and Sinha, M.C., 1990, Seismic images of a magma chamber beneath the Lau Basin back-arc spreading centre, *Nature,* **346,** 646-648.

Collier, J.S., and Sinha, M.C., 1992, Seismic mapping of a magma chamber beneath the Valu Fa Ridge, Lau Basin, *J. Geophys. Res.,* **97,** 14031-14053.

Cooper, P., and Kroenke, L.W., 1993, Deep seismicity in the North Fiji Basin, *In:* Kroenke, L.W., and Eade, J.V., (Eds.), *Basin formation, ridge crest processes, and metallogenesis in the North Fiji Basin,* Circum-Pacific Council for Energy and Mineral Resources, Earth Science Ser. **15,** Springer-Verlag, New York, 33-39.

Craig, H., Craig, V.K., and Kim, K.R., 1987a, PAPATUA Expedition 1: Hydrothermal vent surveys in back-arc basins: The Lau, North Fiji, Woodlark, and Manus basins and Havre Trough, *EOS, Trans. AGU*, **68**, 100.

Craig, H., Horibe, Y., Farley, K.A., Welhan, J.A., Kim, K.R., and Hey, R.N., 1987b, Hydrothermal vents in the Mariana Trough: Results of the first Alvin dives, *EOS, Trans. AGU*, **68**, 1531.

Crook, K.A.W., Exon, N.F., Coleman, P.J., 1991, A decade of growth in the South Pacific marine geoscience data base, *Mar. Geol.*, **98**, 155-165.

Chase, C.G., 1971, Tectonic history of the Fiji plateau, *Geol. Soc. Am. Bull.*, **82**, 3087-3110.

Chase, C.G., 1978, Plate Kinematics: The America, East Africa, and the rest of the world, *Earth Planet. Sci. Lett.*, **37**, 355-368.

Chen, Y., and Morgan, W.J., 1990a, Rift valley/No rift valley transition at Mid-Ocean Ridges, *J. Geophys. Res.*, **95**, 17571-17581.

Chen, Y., and Morgan, W.J., 1990b, A nonlinear rheology model for the Mid-Ocean Ridge axis topography, *J. Geophys. Res.*, **95**, 17583-17604.

Cherkis, N.Z., 1980, Aeromagnetic invetigations and seafloor spreading history in the Lau Basin and northern Fiji Plateau, U.N. ESCAP, *CCOP/SOPAC Techn. Bull.*, **3**, 37-45.

Christie, D.M., and Sinton, J.M., 1981, Evolution of abyssal lavas along propagating segments of the Galapagos spreading center, *Earth Planet. Sci. Lett.*, **56**, 321-335.

Dalziel, I.W.D., 1984, The tectonic evolution of a fore-arc terrane, southern Scotia Ridge, Antarctica, *Geol. Soc. Am. Spec. Pap.*, **200**, 32 p.

Dalziel, I.W.D., 1989, *Tectonics of the Scotia Arc, Antarctica*, Field Trip Guidebook T180, 28th Int. Geol. Congress, AGU, Washington D.C., 206 p.

Dalziel, I.W.D., Dott, R.H., Winn Jr, R.D., and Bruhn, R.L., 1975, Tectonic relations of South Georgia to the southernmost Andes, *Geol. Soc. Am. Bull*, **86**, 1034-1040.

Davis, E.E., and Lister, C.R.B., 1974, Fundamentals of ridge crest topography, *Earth Planet. Sci. Lett.*, **21**, 405-413.

Davis, E.E., Currie, R.G., Sawyer, B.S., and Kosalos, J.G., 1986, The use of swath bathymetric and acoustic image mapping tools in marine geoscience, *Mar. Technol. Soc. J.*, **20**, 17-27.

De Alteriis, G., Ruellan, E, Auzende, J.M., Ondréas, H., Bendel, V., Gràcia Mont, E., Huchon, P., Lagabrielle, Y., and Tanahashi, M., 1993, Propagating Rifts in the North Fiji Basin (Southwest Pacific), *Geology*, **21**, 533-536.

Desonie, D.L., and Duncan, R.A., 1990, The Cobb-Eikelberg seamount chain: Hotspot volcanism with mid-ocean ridge basalt affinity, *J. Geophys. Res.*, **95**, 12697-12711.

Detrick, R.S., and Humpris, S.E., 1992, RIDGE and Inter-Ridge: Cooperative interdisciplinary studies of mid-ocean ridges, *Acta Geol. Hispanica*, **27** (3-4), 3-11.

Detrick, R.S., Needham, H.D., and Renard, V., 1995, Gravity anomalies and crustal thickness variations along the Mid-Atlantic Ridge between 33°N and 40°N, *J. Geophys. Res.*, **100**, 3767-3787.

Dewey, J.F., 1980, Episodicity, sequence and style at convergent plate boundaries, *In:* Strangeway, D. (Ed.), *The continental crust and its mineral ressources*, Geol. Assoc. Canada, Sp. Rep. **20**, 553-574.

Dick, H.J.B., 1989, Abissal peridotites, very slow spreading ridges and ocean ridge magmatism, *In*: Saunders, A.D., and Norry, M.J., (Eds.), *Magmatism in the ocean basins*, Geol. Soc. Sp. Publ., **42**, 71-105.

Doutch, H.F., 1986, *Plate-tectonic map of the Circum-Pacific Region, southwest quadrant*, Scale :10,000,000, Circum-Pacific Council for energy and Mineral Ressources, AAPG.

Dubois, J., Pascal, G., Barazangi, M., Isacks, B.L. and Oliver, J., 1973, Travel times of seismic waves between the new hebrides and Fiji Islands: A zone of low velocity beneath the Fiji Plateau, *J. Geophys. Res.*, **78**, 3431-3436.

Dubois, J., Launay J., Récy, J. and Marshall, J., 1977, New Hebrides trench: subduction rate from associated lithospheric bulge, *Can. J. Earth Sci.*, **14**, 250-255.

Dvorkin, J., Nur, A., Mavko, G., and Ben-Avraham, Z., 1993, Narrow subducting slabs and the origin of backarc basins, *Tectonophysics*, **227**, 63-79.

Dyment, J., Lagabrielle, Y., Ruellan, E., Pelletier, B., Goslin, J. and the NOFI cruise scientific party, 1995, Magnetic anomalies on the South Pandora active spreading center, North Fiji Basin, *Terra Nova*, **7**, 149 (abstract).

Eade, J.V., and Gregory, M.R., 1993, Sediments of the Norh Fiji Basin, *In:* Kroenke, L.W., and Eade, J.V., (Eds.), *Basin formation, ridge crest processes, and metallogenesis in the North Fiji Basin*, Circum-Pacific Council for Energy and Mineral Resources, Earth Science Ser. **15**, Springer-Verlag, New York, 75-98.

Eissen, J. P., Lefèvre, C., Maillet, P., Morvan, G., and Nohara, M., 1991, Petrology and geochemistry of the central North Fiji Basin spreading centre (Southwest Pacific) between 16°S and 22°S, *Mar. Geol.*, **98**, 201-239.

Eissen, J. P., Nohara, M., and Cotten, J., 1994, North Fiji Basin basalts and their magma sources: Part I. Incompatible elements constraints, *Mar. Geol*, **116**, 153-179.

Embley, R.W., Murphy, K.M., and Fox, C.G., 1990, High-resolution studies of the summit of Axial Volcano, *J. Geophys. Res.*, **95**, 12785-12812.

Falvey, D.A., 1975, Arc reversals, and a tectonic model for the North Fiji Basin, *Austr. Soc. of Explor. Geophys. Bull.*, **6**, 47-49.

Falvey, D.A., 1978, Analysis of paleomagnetic data from the New Hebrides, *Bull. Aust. Soc. Explor. Geophys.*, **9** (3), 117-123.

Fisk, M.R., 1990, Volcanism in the Bransfield Strait, Antarctica. *J. South Am. Earth Sci.*, **3**, 91-101.

Forsyth, D.W., 1975, Fault plane soultions and tectonics of the South Atlantic and Scotia Sea, *J. Geophys. Res.*, **80**, 1424-1443.

Fouquet, Y., Von Stackelberg, U., Charlou, J.L., Erzinger, J., Foucher, J.P., Herzig, P., Mühe, R., Soakai, S., Wiedicke, M., and Whitechurch, H., 1991, Hydrothermal activity and metallogenesis in the Lau backarc basin, *Nature*, **349**, 778-781.

Fowler, C.M.R., 1990, *The Solid Earth: An introduction to global geophysics*, Cambridge University Press, Cambridge (UK), 472 p.

Fox, P.J., Grindlay, N.R., and Macdonald, K.C., 1991, The Mid-Atlantic Ridge (31°S-34°30'S): Temporal and spatial variations of accretionary processes, *Mar. Geophys. Res.*, **13**, 1-20.

Francheteau, J., Needham, H.D., Choukroune, P. Juteau, T., Ségret, M., Ballard, R.D., Fox, P.J., Normark, W., Carranza, A., Cordova, D., Guerrero, J., Rangin, C., Bougault, H., Cambon, P., and Hekinian, R., 1979, Massive deep-sea sulfide ore deposits discovered on the East Pacific Rise, *Nature*, **277**, 523-528.

Francheteau, J.A., Yelles-Chaouche, and Craig, H., 1987, The Juan Fernandez microplate north of the Nazca-Pacific-Antarctic plate junction at 35°S, *Earth Planet. Sci. Lett.*, **86**, 253-286.

Gamboa, L.A.P., and Maldonado, P.R., 1990, Geophysical investigations in the Bransfield Strait and in the Bellingshausen Sea-Antarctica, *In:* St. John, B., (Ed.), *Antarctica as an Exploration Frontier: Hydrocarbon potential, Geology and Hazards*, Am. Assoc. Petrol. Geol., Studies in Geology 31, 127-141.

Garrett, S.W., 1990, Interpretation of reconnaissance gravity and aeromagnetic surveys of the Antarctic Peninsula, *J. Geophys. Res.*, **95**, 6759-6777.

Géli, L., Ondréas, H., Olivet, J.L., Sahabi, M., Aslanian, D., and Gilg-Capar, L., 1994, Thermal structure vs. spreading rate at intermediate spreading rates: The example of the Pacific-Antarctic Ridge between 55°S and 63°S, *EOS Trans. AGU*, **7**, 330.

Gente, P., 1987, *Etude morphostructurale comparative de dorsales océaniques à taux d'expansion variés*, Thèse de doctorat, Univ. Bretagne Occidentale, Brest, 371 p.

Gente, P., Auzende, J.M., Renard, V., Fouquet, Y., and Bideau, D., 1986, Detailed geological mapping by submersible of the East Pacific Rise axial graben near 13°N, *Earth Planet. Sci. Lett.*, **78**, 224-236.

Gente, P., Mevel, C., Auzende, J.-M., Karson, J.A., and Fouquet, Y., 1991, An example of a recent accretion on the Mid-Atlantic Ridge: The Snake Pit neovolcanic ridge (MARK area, 23°22'N), *Tectonophysics*, **190**, 1-29.

Gilg-Capar, L ,1994, *Etude des anomalies du Geoïde a moyennes longueurs d'onde: Implications sur les mecanismes de l'accrétion et l'origine du volcanisme intraplaque*, Thèse nouveau régime, Univ. Bretagne Occidentale, Brest, 273 p.

Gill, J.B., and Gorton, M., 1973, A proposed geological and geochemical history of eastern Melanesia, *In:* P.J. Coleman, (Ed.), *The Western Pacific: Island Arcs, Marginal Seas and Geochemistry*, University of Western Australia Press, 543-566.

Gill, J.B., Stork, A.L., and Whelan, P.M., 1984, Volcanism accompanying backarc basin development in the southwest Pacific, *Tectonophysics*, **102**, 207-224.

González-Ferrán, O., 1985, Volcanic and tectonic evolution of the Northern Antarctic Peninsula- Late Cenozoic to Recent, *Tectonophysics*, **114** 389-409.

González-Ferrán, O., 1991, The Bransfield rift and its active volcanism, *In*: Thomson, R.A., Crame, J.A., and Thomson, J.W., (Eds.), *Geological evolution of Antarctica*, Cambridge, Cambridge University Press, 505-509.

Goslin, J., Lagabrielle, Y., Ruellan, E., Pelletier, B., Maia, M., Dyment, J. and the NOFI cruise scientific party, 1995, A gravity survey of an active spreading ridge in a back-arc environment: The South Pandora Ridge in the North Fiji Basin, *Terra Nova*, **7**, 149 (abstract).

Gràcia, E., 1992, *El segment N160 de la Conca Nord-Fijiana (Pacífic sud-oest): Morfoestructura d'un eix d'acreció d'edat quaternària dins una conca marginal*, Tesi de licenciatura, Facultat de Geologia, Universitat de Barcelona, 145 p.

Gràcia, E., Auzende, J.M., and Canals, M., 1992, Estructura y evolución del segmento N160 de la dorsal de la Cuenca Nor-Fidjiana (Pacífico suroeste), Sp. Issue "Dorsales Oceànicas", Canals, M., and Gràcia, E., (Eds.), *Acta Geol. Hisp.*, **27** (3-4), 79-89.

Gràcia, E., Ondréas, H., Bendel, V., and STARMER group, 1994, Multi-scale morphologic variability of the North Fiji Basin ridge (SouthWest Pacific), *Mar. Geol*, **116**, 133-153.

Gràcia, E., Canals, M., Farran, M., Prieto. M.J., Sorribas, J., and GEBRA Team, 1996a, Morphostructure and evolution of the Central and Eastern Bransfield Basins (NW Antarctic Peninsula), *Mar. Geophys. Res.*, **18**, 1-3.

Gràcia, E., Tisseau, C., Maia, M., Tonnerre, T., Auzende, J.M., and Lagabrielle, Y., 1996b, Variability of the gravity structure along the Central Spreading Ridge (North Fiji Basin): Evidence for contrasting thermal regimes, *Mar. Geophys. Res.*, **18**, 1-3.

Grad, M., Guterch, A., and Sroda, P., 1992, Upper crustal structure of Deception Island area, Bransfield Strait, West Antarctica, *Ant. Sci.*, **4**, 469-476.

Grad, M., Guterch, A., and Janik, T., 1993, Seismic structure of the lithosphere across the zone of subducted Drake plate under the Antarctic plate, West Antarctica, *Geophys. J. Int.*, 115, 586-600.

Green, D., and Cullen, D.J., 1973, The tectonic evolution of the Fiji region, *In:* Coleman, P.J., (Ed.), *The Western Pacific: Island Arcs, Marginals Seas and Geochemistry,* University of Australia Press, Nedlands, 127-145.

Grindlay, N.R., Fox, P.J., and Vogt, P.R., 1992, Morphology and tectonics of the Mid-Atlantic Ridge (25°-27°30S) from Sea Beam and magnetic data, *J. Geophys. Res.*, **97**, 6983-7010.

Guivel, C., Eissen, J.P., Lagabrielle, Y., and Dosso, L., 1995, Basaltes enrichis en zone d'accretion arrière-arc: Les rides Sud-Pandora et Tripartite du Bassin Nord-Fidjien, *Congrès Soc. Geol. Fr.*, espécial "Lithosphere Océanique", Brest.

Guterch, A., Grad, M., Janik, T., Perchuc, E., and Pajchel, J., 1985, Seismic studies of the crustal structure in West Antarctica 1979-1980. Preliminary results, *Tectonophysics*, **114**, 411-429.

Guterch, A., Grad, M., Janik, T., and Perchuc, E., 1991, Tectonophysical models of the crust between the Antarctic Peninsula and the South Shetland trench, *In*: Thomson, R.A., Crame, J.A., and Thomson, J.W., (Eds.), *Geological evolution of Antarctica,* Cambridge, Cambridge University Press, 499-504.

Halunen, A.J.Jr., 1979, *Tectonic history of the Fiji Plateau,* Ph. D. Thesis, Univ. of Hawaii, Honolulu, 127p.

Hamburger, M.W., and Isacks, B.L., 1987, Deep earthquakes in the southwest Pacific : A tectonic interpretation, *J. Geophys. Res.*, **92**, 13841-13854.

Hamburger, M.W., and Isacks, B.L., 1988, Diffuse back-arc deformation in the southwestern Pacific, *Nature*, **332**, 599-604.

Hamburger, M.W., Everingham, I.B., Isacks, B.L., and Barazangi, M., 1988, Active tectonism within the Fiji Platform, southwest Pacific, *Geology*, **16**, 237-241.

Hamburger, M.W., Everingham, I.B., Isacks, B.L., and Barazangi, M., 1990, Seismicity and crustal structure of the Fiji Platform, Southwest Pacific, *J. Geophys. Res.*, **95**, 2553-2573.

Harland, W.B., Armstrong, R.L., Cox, A.V., Craig, L.E., Smith, A.G., and Smith, D.G., 1990, *A geologic time scale 1989*, Cambridge Univ. Press, 263 pp.

Hawkes, D.D., 1981, Tectonic segmentation of the northern Antarctic Peninsula, *Geology*, **9**, 220-224.

Hawkins, J.W., 1976, Petrology and geochemistry of basaltic rocks of the Lau Basin, *Earth Planet. Sci. Lett.*, **28**, 283-297.

Hawkins, J.W., 1994, Petrologic synthesis: The Lau Basin transect (Leg 135), *In:* Hawkins, J.W., Parson, L.M., Allan, J., et al., (Eds.), *Proc. ODP, Sci. Results*, **135**, College Station, TX., 879-905.

Hawkins, J.W., 1995, The Geology of the Lau Basin, *In:* Taylor, B., (Ed.), *Backarc basins: Tectonics and magmatism*, Plenum Press, New York, 63-129.

Hawkins, J.W., and Batiza, R., 1975, Tholeitic basalt from an active spreading center on the North Fiji plateau near 15°30'S - 173°30'E, *EOS Trans AGU*, **56**, p. 1078, abstract.

Hawkins, J.W., and Helu, S., 1986, Polymetallic sulfide deposits from "black smoker" chimney, Lau Basin, *EOS, Trans. AGU*, **67**, 378.

Haxby, W.F., and Weissel, J.K., 1986, Evidence of small-scale convection from Seasat altimeter data, *J. Geophys. Res.*, **91**, 3507-3520.

Heirtzler, J.R., Dickson, G.O., Herron, E.M., Pitman, W.C., and Le Pichon, X., 1968, Marine magnetic anomalies, geomagnetic field reversals, and motions of the ocean floor and continents, *J. Geophys. Res.*, **73**, 2119-2136.

Henriet, J.P., Meissner, R., Miller, H., and G.R.A.P.E. Team, 1992, Active margin processes along the Antarctic Peninsula, *Tectonophysics*, **201**, 1-25.

Hey, R.N., 1977, A new class of pseudofaults and their bearing on plate tectonics: A propagating rift model *Earth Planet. Sci. Lett.*, **37**, 321-325.

Hey, R., Duennebier, F.K., and Morgan, W.J., 1980, Propagating rifts on Mid-Ocean Ridges, *J. Geophys. Res.*, **85**, 3647-3658.

Hey, R.N., Kleinrock, M.C., Miller, S.P., Atwater, T.M., and Searle, R.C., 1986, Sea Beam/Deep-Tow investigation of an active oceanic propagating rift system, Galapagos 95.5°W, *J. Geophys. Res.*, **91**, 3369-3393.

Hill, I.A., and Barker, P.F., 1980, Evidence for Miocene back-arc spreading in the Central Scotia Sea, *Geophys. J. R. Astron. Soc.*, **63**, 427-440.

Hill, P.A., Reid, R., and Buleka, J., 1984, *Marine geophysical survey of the western Woodlark Basin*, M.V. "Tapini" cruise report, record 1984/32, Bureau Mineral Resources, Canberra.

Hsu, S.K., 1995, XCORR: A cross-over technique to adjust track data, *Computers and Geosciences*, **21**, 259-271.

Huchon, P., Gràcia, E., Ruellan, E., Joshima, M., and Auzende, J. M., 1994, Kinematics of active spreading in the central North Fiji Basin (SW Pacific), *Mar. Geol*, **116**, 69-89.

Hughes Clarke, J.E., Jarvis, P., Tiffin, D.L., Price, R., and Kroenke, L., 1993, Tectonic activity and plate boundaries along the northern flank of the Fiji Platform, *Geo-Mar. Lett.*, **13**, 98-106.

Hussong, D.M., and Uyeda, S., 1981, Tectonic processes and the history of the Mariana Arc: A synthesis of Deep Sea Drilling Leg 60, *In:* Hussong et al., (eds.), *Init. Repts. DSDP 60*, Washington DC, US Gov. Printing Office, 909-929.

Inoue, H., 1986, A least-square smooth fitting for irregularly spaced data: finite-element approach using the cubic B-spline basis, *Geophysics*, **51**, 2051-2061.

Isacks, B.L., and Barazangi, M., 1977, Geometry of the Benioff zones: Lateral segmentation and downward bending of the subducted lithosphere, *In:* Talwani, M., and Pitman, W.C.III, (Eds.), *Island Arcs, Deep Sea Trenches and Back-arc Basins*, Maurice Ewing Series I, AGU, 99-114.

Isacks, B.L., Sykes, L.R., and Oliver, J., 1969, Focal mechanisms of deep and shallow earthquakes in the Tonga-Kermadec region and the tectonics of island arc, *Geol. Soc. Amer. Bull.*, **80**, 1443-1470.

Isacks, B.L., Cardwell, R.K., Chatelain, J.L., Barazangi, M., Marthelot, J.M., Chinn, D., and Louat, R., 1981, Seismicity and tectonics of the central New Hebrides island arc, *In:* Simpson, D.W., and Richards, P.G. (Eds.), *Earthquake prediction, An international Review*, Maurice Ewing Ser., 4, AGU, Washington, 93-116.

Isezaki, N., 1986, A new shipboard three-component magnetometer, *Geophysics*, **51**, 1992-1998.

Ishibashi, J.I., and Urabe, T., 1995, Hydrothermal activity related to arc-backarc magmatism in the western Pacific, *In:* Taylor, B. (Ed.), *Backarc basins: Tectonics and magmatism*, Plenum Press, New York, 451-495.

Jarvis, P., and Kroenke, L., 1993, Structural development of the central North-Fiji Basin triple junction, *Geo-Mar. Lett.*, **13**, 133-138.

Jarvis, P., Hughes-Clarke, J., Tanahashi, M., Tiffin, D., and Kroenke, L., 1994, The western Fiji Transform Fault and its role in the dismemberment of the Fiji Platform, *Mar. Geol.*, **116**, 57-68.

Jeffers, J.D., and Anderson, J.B., 1990, Sequence stratigraphy of the Bransfield Basin, Antarctica: Implications for tectonic history and hidrocarbon potential, *In:* St. John, B. (Ed.), *Antarctica as an Exploration Frontier: Hydrocarbon potential, Geology and Hazards*, Am. Assoc. Petrol. Geol., Studies in Geology 31, 13-30.

Jeffers, J.D., Anderson, J.B., and Lawver, L.A., 1991, Evolution of the Bransfield Basin, Antarctic Peninsula. Thomson, R.A., Crame, J.A., and Thomson, J.W., (Eds.), *Geological evolution of Antarctica*, Cambridge, Cambridge University Press, 481-485.

Johnson, H.P., and Embley, R.W., 1990, Axial Seamount: An active ridge axis volcano on the Central Juan de Fuca Ridge, *J. Geophys. Res.*, **95**, 12689-12696.

Jolivet, L., and Tamaki, K., 1992, Neogene kinematics in the Japan Sea region and volcanic activity of the NE-Japan arc, *In:* Tamaki, K., Suyehiro, K., Allan, J., McWilliams, M., et al., (Eds.), *Proc. ODP, Sci. Results*, **127/128**, College Station, TX., 1311-1331.

Jollivet, D., Hashimoto, J., Auzende, J.M., Honza, E., Ruellan, E., Dutt, S., Iwabushi, Y., Jarvis, P., Joshima, M., Kawai, T., Kawamoto, T., Kisimoto, K., Lafoy, Y., Matsumoto, T., Mitsuzawa, K., Naganuma, T., Naka, J., Otsuka, K., Otsuki, A., Rao, B., Tanahashi, M., Tanaka, T., Temakon, J.S., Urabe, T., Veivau, T. and Yokokura, T., 1989, Premières observations de communautés animales associées à l'hydrothermalisme arrière-arc du Bassin Nord-Fidjien, *C. R. Acad. Sci. Paris*, **309**, 301-308.

Kappel, E. S., and Ryan, W. B.F., 1986, Volcanic episodicity and a non steady-state rift valley along the Northeast Pacific Spreading Centers: Evidence from Sea-Marc I, *J. Geophys. Res.*, **91**, 13925-13940.

Karig, D.E., 1970, Ridges and basins of the Tonga-Kermadec island arc system, *J. Geophys. Res.*, **75**, 1443-1470.

Karig, D.E., 1971, Origin and development of marginal basins in the Western Pacific, *J. Geophys. Res.*, **76**, 239-254.

Karig, D.E., 1974, Evolution of arc systems in the western Pacific, *Ann. Rev. Earth Planet. Sci.*, **2**, 51-75.

Kearey, P., and Vine F.J., 1990, *Global Tectonics*, Blackwell Sci. Pub., Oxford, 302 p.

Keller, R., and Fisk, M.R., 1992, Quaternary marginal basin volcanism in the Bransfield strait as a modern analogue of the southern Chilean ophiolites, *In:* Parson, L.M., Murton, B.J., and Browning, P., (Eds.), *Ophiolites and their Modern Oceanic Analogues*, Geol. Soc. Sp. Publ., **60**, 155-169.

Keller, R.A., Fisk, M.R., White, W.M., and Birkenmajer, K., 199?, Isotopic and trace element constraints on mixing and melting models of marginal basin volcanism, Bransfield Strait, Antarctica, *Earth Planet. Sci. Lett.*, **111**, 287-303.

Keller, R.A., Strelin, J.A., Lawver, L.A., and Fisk, M.R., 1994, Dredging young volcanic rocks in Bransfield Strait, *Antarctic J. U. S.*, **XXVIII** (1993 review issue), 98-100.

Kim, Y., Chung, T.W., and Nam, S.H., 1992, Marine magnetic anomalies in the Bransfield Strait, Antarctica, *In:* Y. Yoshida et al. (Ed.), *Recent Progress in Antarctic Earth Science*. Terra Sci. Pub. Company (TERRAPUB), Tokyo, 431-437.

King, E.C., and Barker, P.F., 1988, The margins of the South Orkney continent, *J. Geol. Soc. London*, **145**, 317-331.

Kisimoto, K., Tanahashi, M., and Auzende, J.M., 1994, Crustal structure variation along the central rift-ridge axis in the North-Fiji Basin: Implications from seismic reflection and refraction data, *Mar. Geol*, **116**, 101-111.

Kleinrock, M.C., and Hey, R.N., 1989, Detailed tectonics near the tip of the Galapagos 95.5°W propagator: How the lithosphere tears and a spreading axis develop, *J. Geophys. Res.*, **94**, 13801-13838.

Klepeis, K.A., and Lawver, L.A., 1994, Bathymetry of the Bransfield Strait, southeastern Shackleton fracture zone and South Shetland Trench, *Antarctic J. U. S.*, **XXVIII**, 103-104.

Klitgord, K.D., 1976, Sea-floor spreading: The central anomaly magnetization high, *Earth Planet. Sci. Lett.*, **29**, 201-209.

Klitgord. K.D., and Mudie, J.D., 1974, The Galapagos spreading center: A near bottom geophysical survey, *Geophys. J. R. Astron. Soc.*, **38**, 563-586.

Kogan, M.G., 1976, Gravity anomalies and main tectonic units of the southwest Pacific, *J. Geophys. Res.*, **81**, 5240-5248.

Kroenke, L.W., 1984, *Cenozoic Tectonic Development of the Southwest Pacific*, UN ESCAP, CCOP/SOPAC Tech. Bull., 6, 122 p.

Kroenke, L.W., Jouannic, C., Woodward, P., 1983, Bathymetry of the southwest Pacific. Chart 1 of the Geophysical Atlas of the Southwest Pacific, scale 1:6442192 at 0°, Mercator Projection, 2 sheets, *UN ESCAP, CCOP/SOPAC Techn. Secr.*

Kroenke, L.W., Eade, J.V., and Scientific party, 1993a, Overview and principal results of the second leg of the firts joint CCOP/SOPAC-Tripartite cruise of the R/V Kana-Keoki: North Fiji Basin survey (KK820316 leg 03), *In:* Kroenke, L.W., and Eade, J.V., (Eds.), *Basin formation, ridge crest processes, and metallogenesis in the North Fiji Basin*, Circum-Pacific Council for Energy and Mineral Resources, Earth Science Ser. **15**, Springer-Verlag, New York, 1-10.

Kroenke, L.W., Smith, R., and Nemoto, K., 1993b, Morphology and structure of the seafloor in the northern part of the North Fiji Basin, *In:* Kroenke, L.W., and Eade, J.V., (Eds.), *Basin formation, ridge crest processes, and metallogenesis in the North Fiji Basin*, Circum-Pacific Council for Energy and Mineral Resources, Earth Science Ser. **15**, Springer-Verlag, New York, 11-19.

Kuo, B. and Forsyth, D., 1988, Gravity anomalies of the ridge-transform system in the South Atlantic between 31° and 34.5°S: upwelling centers and variations in crustal thickness, *Mar. Geophys. Res.*, **10**, 205-232.

Lachenbruch, A., 1973, A simple mechanical model for oceanic spreading centers, *J. Geophys. Res.*, **78**, 3395-3417.

Lafoy, Y., 1989, *Evolution géodynamique des bassins marginaux Nord Fidjien et de Lau (Sud-Ouest Pacifique)*, Thèse nouveau régime, Univ. Bretagne Occidentale, Brest, 261p.

Lafoy, Y., Auzende, J.M., Ruellan, E., Huchon, P., and Honza, E., 1990, The 16°40'S triple junction in the North Fiji Basin (SW Pacific), *Mar. Geophys. Res.*, **12**, 285-296.

Lagabrielle, Y., Auzende, J.M., Eissen, J.P., Janin, M.C., and Cotten, J., 1994a, Geology and geochemistry of a 800 m continuous section through young upper oceanic crust in the North Fiji Basin, *Mar. Geol.*, **116**, 113-132.

Lagabrielle, Y., Ruellan, E., Tanahashi, M., Pelletier, B., Bourgois, J., Buffet, G., de Alteriis, G., Dyment, J., Goslin, J., Gràcia, E., Iwabuchi, I., Jarvis, P., Joshima, M., Karpoff, A.M., Matsumoto, T., Ondréas, H., and Sardou, O., 1994b, Active spreading along the South Pandora Ridge in the North Fiji Basin (SW Pacific): First results of the NOFI cruise (French-Japanese New Starmer program), *EOS, Trans. AGU*, **75**, 673.

Lagabrielle, Y., Ruellan, E., Tanahashi, M., and the NOFI scientific team, 1995, An 800 km survey of the active spreading axis in the northern North Fiji Basin: Results of the NOFI cruise of the R/V L'Atalante over the South Pandora and Tripartite Ridges (August-September 1994), *InterRIDGE News*, **4** (1), 29-36.

Lagabrielle, Y., Ruellan, E., Tanahashi, M., Bourgois, J., Buffet, G., de Alteriis, G., Dyment, J., Goslin, J., Gràcia, E., Iwabuchi, I., Jarvis, P., Joshima, M., Karpoff, A.M., Matsumoto, T., Ondréas, H., Pelletier, B., and Sardou, O., 1996, Active oceanic spreading in the northern North Fiji basin. Results of the NOFI cruise of the R/V L'Atalante, *Mar. Geophys. Res.*, **16**, 1-3.

Langmuir, C., 1995, *InterRIDGE investigation of the Southwest Indian Ridge: A Project Plan*, InterRIDGE Steering Comitee Meeting, GEOMAR, Kiel (Germany), 11-12 September 1995.

Langmuir, C.H., Bender, J.F., and Batiza, R., 1986, Petrologic and tectonic segmentation of the East Pacific Rise, 5°30'-14°30'N, *Nature*, **322**, 422-429.

Lapouille, A., 1986, Present-day opening of the northwestern part of the North Fiji Basin (Southwest Pacific), *South Pacific Marine Geol. Notes, Tech. Sec.*, CCOP/SOPAC, **12**, 285-296.

Larter, R.D., and Barker, P.F., 1989, Seismic stratigraphy of the Antarctic Peninsula Pacific margin: A record of Pliocene-Pleistocene ice volume and paleoclimate, *Geology*, **17**, 731-734.

Larter, R.D., and Barker, P.F., 1991, Effects of ridge crest-trench interaction on Antarctic-Phoenix spreading: Forces on a young subducting plate, *J. Geophys. Res.*, **96**, 19583-19607.

Larue, B.M., Pontoise, B., Malahoff, A., Lapouille, A., and, Latham, G.V., 1982, Bassins marginaux actifs du Sud-Ouest Pacifique: Plateau Nord-Fidjien, bassin de Lau, *In:* Equipe Géologie-Géophysique ORSTOM Noumea, (Eds.), *Contribution à l'étude géodynamique du Sud-Oest Pacifique*, Travaux et Documents ORSTOM, **147**, 363-406.

LaTraille, S.L., and Hussong, D.M., 1980, Crustal structure across the Mariana Island arc, *In:* Hayes, D.E., (Ed.), *The Tectonic and geologic evolution of southeast Asian Seas and Islands*, Geophys. Monogr. Ser., AGU, **23**, 209-222.

Laughton, A.S., Searle, R.C., and Roberts, D.G., 1979, The Reykjanes Ridge crest and the transition between its rifted and non-rifted regions, *Tectonophysics*, **55**, 173-177.

Lawver, L.A., and Hawkins, J.W., 1978, Diffuse magnetic anomalies in marginal basins: Their possible tectonic and petrologic significance, *Tectonophysics*, **45**, 323-339.

Lawver, L.A., Hawkins, J.W., and Sclater, J.G., 1976, Magnetic anomalies and crustal dilation in the Lau Basin, *Earth Planet. Sci. Lett.*, **33**, 27-35.

Lawver, L.A., Sclater, J.G., and Meinke, L., 1985, Mesozoic and Cenozoic reconstructions of the South Atlantic, *Tectonophysics*, **114**, 233-254.

Lawver, L.A., Keller, R.A., Fisk, M.R., and Strelin, J., 1995, Bransfield Strait, Antarctic peninsula: Active extension behind a dead arc, *In:* Taylor, B., (Ed.), *Back-Arc basins: Tectonics and magmatism*, Plenum Publ. Corp., New York, 315-342.

Le Douaran, S., and Francheteau, J., 1981, Axial depth anomalies from 10°N to 50°N along the Mid-Atlantic Ridge: Correlation with other mantle properties, *Earth Planet. Sci. Lett.*, **54**, 29-47.

Lewis, B.T.R., 1979, Periodicities in volcanism and longitudinal magma flow on the East Pacific Rise at 23°N, *Geophys. Res. Lett.*, **6**, 753-756.

Lewis, B.T.R., 1981, Isostasy, magma chambers and plate driving forces on the east Pacific Rise, *J. Geophys. Res.*, **86**, 4868-4880.

Lin, J., and Parmentier, E.M., 1989, Mechanisms of lithospheric extension at mid-ocean ridges, *Geophys. J.*, **96**, 1-22.

Lin, J., and Phipps-Morgan, J., 1992, The spreading rate dependence of three-dimensional mid-ocean ridge gravity structure, *Geophys. Res. Lett.*, **19**, 13-16.

Lin, J., Purdy, G.M., Schouten, H., Sempere, J.C., and Zervas, C., 1990, Evidence from gravity data for focused magmatic accretion along the Mid-Atlantic Ridge, *Nature*, **344**, 627-632.

Livermore, R., Mc Adoo, D., and Marks, K., 1994, Scotia Sea tectonic from high-resolution satellite gravity, *Earth Planet. Sci. Lett.*, **123**, 255-268.

Lonsdale, P., 1985, Nontransform offsets of the Pacific-Cocos plate boundary and their traces on the rise flank, *Geol. Soc. Am. Bull.*, **96**, 313-327.

Louat, R., and Pelletier, B., 1989, Seismotectonics and present-day relative plate motion in the New Hebrides Arc-North Fiji Basin region, *Tectonophysics*, **167**, 41-55.

Louat, R., Daniel, J., and Isacks, B., 1982, Sismicité de l'Arc des Nouvelles Hebrides, *In:* Equipe Géologie-Géophysique ORSTOM Noumea, (Eds.), *Contribution à l'étude géodynamique du Sud-Oest Pacifique*, Travaux et Documents ORSTOM, **147**, 111-148.

Ludwig, W.J., and Rabinowitz, P.D., 1982, The collision complex of the North Scotia Ridge, *J. Geophys. Res.*, **87**, 3731-3740.

Luyendyk, B.P., Bryan, W.B., and Jezek, P.A., 1974, Shallow structure of the New Hebrides island arc, *Geol. Soc. Am. Bull.*, **85**, 1287-1300.

Macdonald, K.C., 1982, Mid-Ocean Ridges: Fine scale tectonic, volcanic and hydrothermal processes within the plate boundary zone, *Ann. Rev. Earth Planet. Sci.*, **10**, 155-190.

Macdonald, K.C., 1986, The crest of the Mid-Atlantic Ridge: Models for crustal generation and tectonics, *In* : Vogt, P.R., and Tucholke, B.E., (Eds.), *The Geology of North-America, The Western North Atlantic Region*, Geol. Soc. Amer., vol. M, 51-68.

Macdonald, K.C., and Fox, P.J., 1983, Overlapping spreading centers: A new kind of accretion geometry on the East Pacific Rise, *J. Geophys. Res.*, **88**, 9393-9406.

Macdonald, K.C., and Fox, P.J., 1988, The Axial Summit Graben and cross-sectional shape of the East Pacific Rise as indicators of axial magma chambers and recent volcanic eruptions, *Earth Planet. Sci. Lett.*, **88**, 119-131.

Macdonald, K.C., and Fox, P.J., 1990, The mid-ocean ridge, *Scient. Am.*, **262**, 72-79.

Macdonald, K.C., Luyendyk, B.P., and Von Herzen, R.P., 1973, Heat flow and plate boundaries in Melanesia, *J. Geophys. Res.*, **78**, 2537-2546.

Macdonald, K.C., Sempere, J.C., and Fox, P.J., 1984, East Pacific Rise from Siqueiros to Orozco Fracture Zones: Along-strike continuity of the axial neovolcanic zone and structure and evolution of overlapping spreading centers, *J. Geophys. Res.*, **89**, 6044-6069.

Macdonald, K.C., Sempere, J.C., Fox, P.J. and Tyce, R., 1987, Tectonic evolution of ridge-axis discontinuities by the meeting, linking, or self-decapitation of neighboring ridge segments, *Geology*, **15**, 993-997.

Macdonald, K.C., Fox, P.J., Perram, L.J., Eisen, M.F., Haymon, R.M., Miller, S.P., Carbotte, S.M., Cormier, M.H., and Shor, A.N., 1988, A new view of the mid-ocean ridge from the behavior of ridge-axis discontinuities, *Nature*, **335**, 217-225.

Macdonald, K.C., Scheirer, D.S., and Carbotte, S., 1991, Mid-ocean ridges: Discontinuities, segments and giant cracks, *Science*, **253**, 986-994.

Macdonald, K.C., Fox, P.J., Miller, S., Carbotte, S., Edwards, M.H., Eisen, M., Fornari, D.J., Perram, L., Pockalny, R., Scheirer, D., Tighe, S., Weiland, C., and Wilson, D., 1992a, The East Pacific Rise and its flanks 8°-18°N: History of segmentation, propagation and spreading direction based on SeaMarc II and SeaBeam studies, *Mar. Geophys. Res.*, **14**, 299-344.

Macdonald, K.C., Scheirer, D.S., Carbotte, S., and Fox, P.J., 1992b, Recent advances in the understanding of mid-ocean ridge tectonics and volcanism using swath-mapping tools, *Acta Geol. Hispanica*, **27** (3-4), 13-32.

Madsen, J.A., Forsyth, D.W., and Detrick, R.S., 1984, A new isostatic model for the East Pacific Rise, *J. Geophys. Res.*, **89**, 9997-10015.

Madsen, J.A., Detrick, R.S., Mutter, J.C., Buhl, P., and Orcutt, J.A., 1990, A two- and three-dimensional analysis of gravity anomalies associated with the East Pacific Rise at 9°N and 13°N, *J. Geophys. Res.*, **95**, 4967-4987.

Maillet, P., Eissen, J.P., Lapouille, A., Monzier, M., Baleivuanala, V., Butscher, J., Gallois, F., and Lardy, M., 1986, La dorsale active du bassin Nord Fidjien entre 20°00S et 20°53S: Signature magnétique et morphologique, *C. R. Acad. Sci. Paris*, **302**, 135-140.

Malahoff, A., Feden, R.H., and Fleming, H.S., 1982a, Magnetic anomalies and tectonic fabric of marginal basins north of the New Zealand, *J. Geophys. Res.*, **87**, 4109-4125.

Malahoff, A., Hammond, S.R., Naughton, J.J., Keeling, D.L., and Richmond, R.N., 1982b, Geophysical evidence for post-Miocene rotation of the islands of Viti Levu, Fiji, and its

relationship to the tectonic development of the North Fiji Basin, *Earth Planet. Sci. Lett.*, 57, 398-414.

Malahoff, A., Kroenke, L.W., Cherkis, N., and Brozena, J., 1993, Magnetic and tectonic fabric of the North Fiji and Lau Basins, *In:* Kroenke, L.W., and Eade, J.V., (Eds.), *Basin formation, ridge crest processes, and metallogenesis in the North Fiji Basin,* Circum-Pacific Council for Energy and Mineral Resources, Earth Science Ser. **15**, Springer-Verlag, New York, 67-82.

Maldonado, A., Larter, R.D., and Aldaya, F., 1994, Forearc tectonic evolution of the South Shetland Margin, Antarctic Peninsula, *Tectonics*, **13**, 1345-1370.

Malinverno, A., 1993, Transition between a valley and a high at the axis of mid-ocean ridges, *Geology*, **21**, 639-642.

Malinverno, A., and Pockalny, R.A., 1990, Abyssal hill topography as an indicator of episodicity in crustal accretion and deformation, *Earth Planet. Sci. Lett.*, **99**, 154-169.

Marks, K.M., and Sailor, R.V., 1986, Comparison of Geos-3 and Seasat altimeter resolution capabilities, *Geophys. Res. Lett.*, **13**, 697-700.

Marks, K.M., and Stock, J.M., 1994, Variations in ridge morphology and depth age relationships on the Pacific-Antarctic Ridge, *J. Geophys. Res.*, **99**, 531-541.

Martinez, F., Naar, D.F., Reed IV, T.B., and Hey, R.N., 1991, Three-dimensional SeaMarc II, gravity, and magnetics study of large-offset rift propagation at the Pito Rift, Easter Microplate, *Mar. Geophys. Res.*, **13** (4), 255-287.

Martinez, F., Fryer, P., Baker, N.A., and Yamazaki, T., 1995, Evolution of backarc rifting: Mariana Trough 20°-24°N, *J. Geophys. Res.*, **100**, 3807-3827.

McAdoo, D.C., and Marks, K.M.,1992, Gravity fields of the Southern Ocean from GEOSAT data, *J. Geophys. Res.*, **97**, 3247-3260.

McKenzie, D., and Morgan, W.J., 1969, Evolution of triple junctions, *Nature*, **224**, 125-133.

McKenzie, D., and Bowin, M.J., 1976, The relationship between bathymetry and gravity in the Atlantic Ocean, *J. Geophys. Res.*, **81**, 1903-1915.

Menard, H.W., 1967, Seafloor spreading, topography, and the second layer, *Science*, **157**, 923-924.

Miller, S.P., and Hey, R., 1986, Three dimensional magnetic modelling of a propagating rift, Galapagos 95°30'W, *J. Geophys. Res.*, **91**, 3395-3406.

Minster, J.B., and Jordan, T.H., 1978, Present-day plate motions, *J. Geophys. Res.*, **83**, 5331-5354.

Molnar, P., and Atwater, T., 1978, Inter-arc spreading and Cordilleran tectonics as alternatives related to the age of subducted oceanic lithosphere, *Earth Planet. Sci. Lett.*, **41**, 330-340.

Morris, E., and Detrick, R.S., 1991, Three-dimensional analysis of gravity anomalies in the MARK area, Mid-Atlantic Ridge 23°N, *J. Geophys. Res.*, **96**, 4355-4366.

Murton, B.J., and Parson, L.M., 1993, Segmentation, volcanism and deformation of oblique spreading centres: A quantitative study of the Reykjanes Ridge, *Tectonophysics*, **222**, 237-257.

Naar, D.F., Martinez, F., Hey, R.N., Reed, T.B., and Stein, S., 1991, Pito Rift: How a large offset rift propagates, *Mar. Geophys. Res.*, **13**, 287-309.

Nagihara, S., and Lawver, L.A., 1989, Heat flow measurements in the King George Basin, Bransfield Basin, *Ant. J. Sci*, **23**, 123-125.

Neff, D.B., and Wyatt, S.B., 1986, Noise suppression by the radial amplitude-slope rejection method, *Geophysics*, **51** (3), 844-850.

Neumann, G., and Forsyth, D., 1993, The paradox of the axial profile: Isostatic compensation along the axis of the Mid-Atlantic Ridge?, *J. Geophys. Res.*, **98**, 17891-17910.

Nilsson, K., Florendo, F., and Hawkins, J.W., 1989, Petrology of a nascent triple junction, northeastern Lau Basin, *EOS Trans. AGU*, **73**, 1389.

NOAA/NGDC, 1992, GEODAS Marine Geophysical Data, 2 CD-ROM.

Nojiri, Y., Ishibashi, J.I., Kawai, T., Otsuki, A. and Sakai, H., 1990, Hydrothermal plumes along the North Fiji Basin spreading axis, *Nature*, **342**, 667-670.

O.R.C.A. Group, 1992, Resultados preliminares de la campaña de geología marina Scotia-92. Estudio geológico y geofísico de la dorsal sur del Arco de Scotia, *In:* J.L. Martínez (Ed.), *Geología de la Antártida Occidental.*, III Congreso Geológico de España, Salamanca, 203-212.

Oliver, J., Isacks, B., Barazangi, M., and Mitronovas, 1973, Dynamics of the downgoing lithosphere, *Tectonophysics*, **19**, 133-147.

Ondréas, H., Ruellan, E., Auzende, J.M., Bendel, V., De Alteriis, G., Gràcia-Mont, E., Lagabrielle, Y., and Tanahashi, M., 1993, Variabilité morphostructurale à l'échelle kilométrique de la dorsale du Bassin Nord Fidjien: Exploration in situ du segment compris entre 18°50'S et 19°S, *C. R. Acad.Sci. Paris*, **316**, 115-122.

Ondréas, H., Fouquet, Y., Charlou, J.L., Costa, T., Donval, J.P., Knoery, J., Lourenço, N., Pellé, H., Segonzac, M., and Tivey, M.K., 1995, Diva 1 cruise: In situ observation of the limit between effusive and explosive submarine volcanism on the Menez Gwen and 38°20'N segments of the Mid-Atlantic Ridge, *Terra Nova*, **7**, 209 (abstract).

Packham, G.H., and Falvey, D.A., 1971, An hypothesis for the formation of marginal seas in the western Pacific, *Tectonophysics*, **11**, 79-109.

Palmer, J., Sempéré, J.C., Christie, D.M., and Phipps Morgan, J., 1993, Morphology and tectonics of the Australian-Antarctic discordance between 123°E and 128°E, *Mar. Geophys. Res.*, **15**, 121-152.

Parker, R., 1972, The rapid calculation of potential anomalies, *Geophys. J. R. Astr. Soc.*, **31**, 447-455.

Parmentier, E.M., and Phipps Morgan, J., 1990, Spreading-rate dependence of three-dimensional structure in oceanic spreading centers, *Nature*, **348**, 325-328.

Parra, J.C., González-Ferrán, O., and Bannister, J., 1984, Aeromagnetic survey over the South Shetland Islands, Bransfield Strait and part of the Antarctic Peninsula, *Rev. Geol. Chile*, **23**, 3-20.

Parra, J.C., Yañez, G., and USAC Working Group, 1988, Aeromagnetic survey of the Antarctic Peninsula and surrounding seas: Integration of the data obtained at different altitudes, *Ser. Cient. Inst. Ant. Chileno*, **38**, 118-131.

Parson, L.M, Pearce, J.A., Murton, B.J., and RRS Charles Darwin Scientific party, 1990, Role of ridge jumps and ridge propagation in the tectonic evolution of the Lau back-arc basin, SW Pacific, *Geology*, **18**, 470-473.

Parson, L.M., and Hawkins, J.W., 1994, Two-stage ridge propagation and the geological history of the Lau backarc basin, *In:* Parson, L.M., Hawkins, J.W., Allan, J.F., et al., (Eds.), *Proc. ODP, Sci. Results*, **135**, College Station, TX (Ocean Drilling Program), 819-828.

Pelayo, A.M., and Wiens, D.A., 1989, Seismotectonics and relative plate motions in the Scotia Sea region, *J. Geophys. Res.*, **94**, 7293-7320.

Pelletier, B., and Louat, R., 1989, Sismotectonics and present day relative plate motion in the Tonga-Lau and Kermadec-Havre region, *Tectonophysics*, **165**, 237-250.

Pelletier, B., and Auzende, J.M., 1994, Geometry and structure of the Vityaz Trench Lineament, *Seafloor mapping in the west and south-west Pacific: Results and applications*, Nouméa, 4-9 November, SOPAC Misc. Rep. 184 (abstract), p. 55.

Pelletier, B., Charvis, P., Daniel., J., Hello, Y., Jamet, F., Louat, R., Nanau, P., and Rigolot, P., 1988, Structure et linéations magnétiques dans le coin nord-ouest du bassin Nord-Fidjien: résultats préliminaires de la campagne EVA 14 (août 1987), *C. R. Acad. Sci. Paris*, **306**, 1247-1254.

Pelletier, B., Lafoy, Y., and Missegue, F., 1993, Morphostructure and magnetic fabric of the Northwestern North Fiji Basin, *Geophys. Res. Lett.*, **20** (12), 1151-1154.

Perfit, M.R., Fornari, D.J., Smith, M.C., Bender, J.F., Langmuir, C.H., and Haymon, R.M., 1994, Small-scale spatial and temporal variations in mid-ocean ridge crest magmatic processes, *Geology*, **22**, 375-379.

Phipps-Morgan, J., and Forsyth, D.W., 1988, 3-D flow and temperature perturbations due to a transform offset: Effects on oceanic crustal and upper mantle structure, *J. Geophys. Res.*, **93**, 2955-2966.

Phipps-Morgan, J., Parmentier, E.M., and Lin, J., 1987, Mechanisms for the origin of Mid-Ocean Ridge Axial Topography: Implications for the thermal and mechanical structure of accreting plate boundaries, *J. Geophys. Res.*, **92**, 12823-12836.

Pitman, W.C.III, and Heirtzler, J.R., 1966, Magnetic anomalies over the Pacific-Antarctic Ridge, *Science*, **154**, 1164-1171.

Price, R.C., and Kroenke, L.W., 1991, Tectonics and magma genesis in the northern North Fiji Basin, *Mar. Geol.*, **98**, 241-258.

Price, R.C., Johnson, L.E., and Crawford, A.J., 1990, Basalts of the North Fiji Basin: The generation of backarc basin magmas by mixing of depleted and enriched mantle sources, *Contrib. Mineral. Petrol.*, **105**, 106-121.

Prieto, M.J., 1996, *Sismoestratigrafía de las Cuencas Central y Oriental de Bransfield (Peninsula Antarctica)*, Tesi de licenciatura, Facultat de Geologia, Universitat de Barcelona, in prep.

Prieto, M.J., Gràcia, E., Canals, M., Ercilla, G., and De Batist, 1995, Recent sedimentary history of the Bransfield Basin, *VII ISAES*, Siena (Italy).

Prieto, M.J., Gràcia, E., Canals, M., Ercilla, G., and De Batist, in press, Sedimentary history of the Central Bransfield Basin, VII ISAES Proceedings, *Terra Antarctica*.

Prince, R. and Forsyth, D., 1988, Horizontal extent of anomalously thin crust near the Vema Fracture Zone from the three dimensional analysis of gravity anomalies, *J. Geophys. Res.*, **93**, 8051-8063.

Purdy, G.M., Sempéré, J.C., Schouten, H., Dubois, D.L., and Goldsmith, R., 1990, Bathymetry of the Mid-Atlantic Ridge, 24-31N: A map series, *Mar. Geophys. Res.*, **12**, 247-252.

Renard, V., Hekinian, R., Francheteau, J., Ballard, R.D., and Backer, H., 1985, Submersible observations at the axis of the ultra-fast-spreading East Pacific Rise (17°30' to 21°30'S), *Earth Planet. Sci. Lett.*, **75**, 339-353.

Renard, V., Voisset, M., and Needham, H.D., 1991, The research vessel L'Atalante's mapping system: The EM12 dual echo-sounder. Evaluation of its performance for mid-oceanic ridge bathymetric investigations, *EOS Trans. AGU*, **72**, 470.

Renner, R.G.B., Sturgeon, L.J.S., and Garrett, S.W., 1985, *Reconnaissance gravity and aeromagnetic surveys of the Antarctic Peninsula*, BAS, Sci. Rep., **110**, 50 p.

Roach, P.J., 1978, The nature of back-arc extension in Bransfield Strait. *Geophys. J. Res. Astron. Soc.*, **53**, 165.

Rodda, P., and Kroenke, L.W., 1984, Fiji: A fragmented arc, *In:* Kroenke, L.W. (Ed.), *Cenozoic tectonic development of the southwest Pacific*, UN ESCAP CCOP/SOPAC, Tech. Bull., **6**, 87-109.

Rommevaux, C., Deplus, C., Patriat, P., and Sempéré, J.C., 1994a, Three-dimensional gravity study of the Mid-Atlantic Ridge: Evolution of the segmentation between 28° and 29°N during the last 10 m.y., *J. Geophys. Res.*, **99**, 3015-3029.

Rommevaux, C., Patriat, P., Munschy, M., Sauter, D., and Mendel, V., 1994b, Crustal production of an ultra-slow spreading ridge: 3D gravity study of the Southwest Indian Ridge between Melville FZ and the triple junction. Comparison with the Central Mid-Atlantic Ridge, *EOS Trans. AGU,* **75** (44), 654.

Rona, P., and Gray, D., 1980, Structural behaviour of fracture zones symmetric and asymmetric about a spreading axis: Mid-Atlantic Ridge (latitude 23°N to 27°N), *Geol. Soc. Amer. Bull.*, **91**, 485-494.

Ruellan, E., Huchon, P., Auzende, J. M., and Gràcia, E., 1994, Propagating rifts and overlapping spreading centers in the North Fiji Basin, *Mar. Geol.*, **116**, 37-57.

Sahabi, M., Géli, L., Olivet, J.L., Gilg-Capar, L., Roult, G., Ondréas, H., Beuzart, P., and Aslanian, D., in press, Morphological reorganization within the Pacific-Antarctic Discordance, *Earth Planet. Sci. Lett.*

Sandwell, D.T., 1984, A detailed view of the South Pacific geoid from satellite altimetry, *J. Geophys. Res.*, **89**, 1089-1104.

Sandwell, D.T., 1992, Antarctic marine gravity field from high-density satellite altimetry, *Geophys. J. Int.*, **109**, 437-448.

Sandwell, D.T., and McAdoo, D.C., 1988, Marine gravity of the Southern Ocean and Antarctic Margin from Geosat, *J. Geophys. Res.*, **93**, 10389-10396.

Sandwell, D.T., and McAdoo, D.C., 1990, High-accuracy, high-resolution gravity profiles from 2 years of the Geosat Exact Repeat Mission, *J. Geophys. Res.*, **95**, 3049-3060.

Sandwell, D.T., and Smith, W.H.F., 1992, Global marine gravity from ERS-1, Geosat and Seasat reveals new tectonic fabric, *EOS Trans. AGU*, **73**, 133.

Sandwell, D.T., Yale, M.M., and Smith, W.H.F., 1994, ERS-1 Geodetic Mission reveals detailed tectonic structures, *EOS Trans. AGU*, **75**, 155.

Saunders, A.D., and Tarney, J., 1984, Geochemical characteristics of basaltic volcanism within back-arc basins, *In:* Kokelaar, B.P., and Howells, M.F., (Eds.), *Marginal basin geology: Volcanic and associated sedimentary and tectonic processes in modern and ancient marginal basins,* Geol. Soc. Sp. Pub., **16**, 59-76.

Sclater, J.G., 1972, Heat flow and elevation of the marginal basins of the western Pacific, *J. Geophys. Res.*, **77**, 5705-5719.

Sclater, J.G., and Menard H.W., 1967, Topography and heat flow of the Fiji Plateau, *Nature*, **216**, 991-993.

Sclater, J.G., and Francheteau, J., 1970, The implications of terrestrial heat-flow observations on current tectonic and geochemical models of the crust and upper mantle of the earth, *Geophys. J. R. Astr. Soc.*, **20**, 509-542.

Sclater, J.G., Karig, D., Lawver, L.A., and Louden, K., 1976, Heat flow, depth and crustal thickness of the marginal basins of the Philippine Sea, *J. Geophys. Res.*, **81**, 309-318.

Sclater, J.G., Ritter, U.G., and Dixon, F.S., 1972, Heat flow in the Southwestern Pacific, *J. Geophys. Res.*, **77**, 5697-5704.

Scotese, C.R., Gahagan, L.M., and Larson, R.L., 1988, Plate tectonic reconstructions of the Cretaceous and Cenozoic ocean basins, *Tectonophysics*, **155**, 27-48.

Scott, S.D., and Binns, R.A., 1995, Hydrothermal processes and contrasting styles of mineralization in the western Woodlark and eastern Manus basins of the western Pacific, *In:* Parson, L.M., Walker, C.L., and Dixon, D.R., (Eds.), *Hydrothermal vents and processes,* Geol. Soc. Sp. Pub., **87**, 191-205.

Scheirer, D.S., and Macdonald, K.C., 1993, Variation in cross-sectional area of the axial ridge along the East Pacific Rise: Evidence for the magmatic budget of a fast spreading center, *J. Geophys. Res.*, **98**, 7871-7885.

Scheirer, D.S., and Macdonald, K.C., 1995, Near-axis seamounts on the flanks of the East Pacific Rise, 8°N to 17°N, *J. Geophys. Res.*, **100**, 2239-2259.

Schlosser, P., Suess, E., Bayer, R., and Rhein, M., 1988, ^{3}He in the Bransfield Strait waters: Indication for local injection from backarc rifting, *Deep Sea Res.*, **35** (12), 1919-1935.

Schouten, H., and McCamy, K., 1972, Filtering marine magnetic anomalies, *J. Geophys. Res*, **77**, 7089-7099.

Schouten, H., Klitgord, K.D., and Whitehead, J.A., 1985, Segmentation of mid-ocean ridges, *Nature*, **317**, 225-229.

Searle, R.C., and Laughton, A.S., 1981, Fine scale sonar study of tectonics and volcanism on the Reykjanes Ridge, *Oceanol. Acta*, **4**, 5-18.

Sempere, J.C., Purdy, G.M., and Schouten, H., 1990, Segmentation of the Mid-Atlantic Ridge between 24°N and 30°40'N, *Nature*, **344**, 427-431.

Shen, Y., Forsyth, D.W., Scheirer, D., and Macdonald, K.C., 1993, Two forms of volcanism: Implications for mantle flow and off-axis crustal production on the west flank of the southern East Pacific Rise, *J. Geophys. Res.*, **98**, 17875-17889.

Sibuet, J.C., Letouzey, J., Barbier, F., Charvet, J., Foucher, J.P., Hilde, T.W.C., Kimura, M., Ling-Yun, C., Marsset, B., Muller, C., and Stéphan, J.F., 1987, Back-arc extension in the Okinawa Trough, *J. Geophys. Res.*, **92**, 14041-14063.

Sibuet, J.C., Hsu, S.K., Shyu, C.T., and Liu, C.S., 1995, Structural and kinematic evolutions of the Okinawa Trough backarc basin, *In:* Taylor, B., (Ed.), *Back-arc basins: Tectonics and magmatism*, Plenum Publ. Corp., New York, 343-379.

Sinton, J.M., and Detrick, R.S., 1992, Mid-ocean ridge magma chambers, *J. Geophys. Res.*, **97**, 197-216.

Sinton, J.M., Wilson, D.G., Christie, D.M., Hey, R.N., and Delaney, J.R., 1983, Petrologic consequences of rift propagation on oceanic spreading ridges, *Earth Planet. Sci. Lett.*, **62**, 193-207.

Sinton, J.M., Johnson, KT.M., and Price, R.C., 1985, Petrology and geochemistry of volcanic rocks from the Northern Melanesian Borderland, *In:* Brocher, T.M., (Ed.), *Investigations of the Northern Melanesian Borderland*, Circum-Pacific Council for Energy and Mineral Resources, Earth Science Series **3**, Houston, Texas, 135-66.

Sinton, J.M., Price, R.C., Johnson, K.M., Staudigel, H., and Zindler, A., 1993, Petrology and geochemistry of submarine lavas from the Lau and North Fiji backarc basins, *In:* Kroenke, L.W., and Eade, J.V., (Eds.), *Basin formation, ridge crest processes, and metallogenesis in the North Fiji Basin*, Circum-Pacific Council for Energy and Mineral Resources, Earth Science Ser. **15**, Springer-Verlag, New York, 119-135.

Sleep, N., 1969, Sensivity of heat-flow and gravity to the mechanism of seafloor spreading, *J. Geophys. Res.*, **74**, 542-549.

Smellie, J.L., 1987, Geochemistry and tectonic setting of alkaline volcanic rocks in the Antarctic Peninsula: A review, *J. Volc. Geoth. Res.*, **32**, 269-285.

Smellie, J.L., 1990, Graham Land and South Shetland Islands, *In:* LeMasurier,W.E., and Thomson, J.W., (Eds.), *Volcanoes of the Antarctic Plate and Southern Oceans*, Ant. Res. Ser., AGU, Washington D.C., **48**, 302-359.

Smellie, J.L., Liesa, M., Muñoz, J.A., Sàbat, F., Pallàs, R., and Willan, R.C.R., 1995, Lithostratigraphy of volcanic and sedimentary sequences in central Livingston Island, South Shetland Islands, *Ant. Sci.*, **7** (1), 99-113.

Smith, D.K., 1992, Illuminating the seafloor, *Oceanus*, **35** (4), 74-81.

Smith, D.K., and Cann, J.R., 1992, The role of seamount volcanism in crustal construction at the Mid-Atlantic Ridge (24°-30°N), *J. Geophys. Res.*, **97**, 1645-1658.

Smith, D.K., Humphris, S.E., and Bryan, W.B., 1995, A comparison of volcanic edifices at the Reykjanes Ridge and the Mid Atlantic Ridge at 24°-30°N, *J. Geophys. Res.*, **100**, 22485-22498.

Solomon, S.C., and Toomey, D.R., 1992, The structure of mid-ocean ridges, *Ann. Rev. Earth. Planet. Sci.*, **20**, 329-364.

Sorribas, J., Farran, M., Canals, M., and Díaz, J.I., 1995, Large vs. small scale multibeam mapping in deep areas, *Oceans 95 MTS/IEEE Proceedings*, **3**, 1928-1934.

Spiess, F.N., and Tyce, R.C., 1973, Marine physical laboratory deep tow instrumentation system, *Scripps Inst. Ocean.*, Ref. 73-4, 73 p.

Steckler, M.S., and ten Brink, U.S., 1986, Lithospheric strengh variations as a control on new plate boundaries: Examples from the northern Red Sea region, *Earth Planet. Sci. Lett.*, **79**, 120-132.

Suess, E., Fisk, M., and Kadko, D., 1988, Thermal interaction between backarc volcanism and basin sediments in the Bransfield Strait, Antarctica, *Ant. J. U. S.*, **22** (5), 46-49.

Tamaki, K., 1985, Two modes of back-arc spreading, *Geology*, **13**, 475-478.

Tamaki, K., 1995, Opening tectonics of the Japan Sea, *In:* Taylor, B., (Ed.), *Back-arc basins: Tectonics and magmatism*, Plenum Publ. Corp., New York, 407-420.

Tamaki, K., and Honza, E., 1992, Global tectonics and formation of marginal basins: Role of the western Pacific, *Episodes*, **14**, 224-230.

Tanahashi, M., Kisimoto, K., Joshima, M., Jarvis, P., Iwabuchi, Y., Ruellan, E., and Auzende, J.M., 1994, 800 km long N-S spreading system of the North Fiji Basin, *Mar. Geol.*, **116**, 10-24.

Tapley, B.D., Born, G.H., and Parke, M.E., 1982, The SEASAT altimeter data and its accuracy assesment, *J. Geophys. Res.*, **87**, 3179-3188.

Tapponnier, P., and Francheteau, J., 1978, Necking of the lithosphere and the mechanics of slowly accreting plate boundaries, *J. Geophys. Res.*, **83**, 3955-3970.

Tatsumi, Y., Maruyama, S., and Nohda, S., 1990, Mechanism of backarc opening in the Japan Sea: Role of astenospheric injection, *Tectonophysics*, **181**, 299-306.

Taylor, B. (Ed.), 1995, *Backarc basins: Tectonics and magmatism*, Plenum Press, New York, 524 p.

Taylor, B., 1979, Bismarck Sea: Evolution of a back-arc basin, *Geology*, **7**, 171-174.

Taylor, B., 1987, A geophysical survey of the Woodlark-Solomons region. *In:* Taylor, B.R, and Exon, N.F., (Eds.), *Marine Geology, Geophysics, and Geochemistry of the Woodlark - Solomon Islands*, Circum-Pacific Council for Energy and Mineral Resources, Earth Science Series, Houston, Texas, 25-48.

Taylor, B., 1992, Rifting and the volcanic-tectonic evolution of the Izu-Bonin-Mariana Arc, *In:* Taylor, B., Fujioka, K., et al., (Eds.), *Proc. ODP, Sci. Results*, **126**, College Station, TX., 627-651.

Taylor, B., and Karner, G.D., 1983, On the evolution of marginal basins, *Rev. Geophys. Space Phys.*, **21** (18), 1727-1741.

Taylor, B., Klaus, A., Brown, G.R., Moore, G.F., Okamura, Y., and Murakami, Y., 1991, Structural development of the Sumisu Rift, Izu-Bonin Arc, *J. Geophys. Res.*, **96**, 16113-16129.

Taylor, B., Crook, K., and Sinton, J., 1994, Extensional transform zones and oblique spreading centers, *J. Geophys. Res.*, **99**, 19707-19718.

Taylor, B., Goodliffe, A., Martinez, F., and Hey, R., 1995, Continental rifting and initial sea-floor spreading in the Woodlark Basin, *Nature*, **374**, 534-537.

Tiffin, D.L., 1993a, GLORIA surveys in frontier areas of the southwest Pacific, *Geo-Mar. Lett.*, **13**, 65-70.

Tiffin, D.L., 1993b, Tectonic and structural features of the Pacific/Indo-Australian plate boundary in the North Fiji-Lau Basin regions, southwest Pacific, *Geo-Mar. Lett.*, **13**, 126-131.

Tisseau, C., and Tonnerre, T., 1995, Non steady-state thermal model of spreading ridges: Implications for melt generation and mantle outcrops. *In:* Vissers, R.L.M., and Nicolas, A., (Eds.), *Mantle and lower crust exposed in oceanic ridges and in ophiolites*, Kluwer Academic Pub., Nederlands, 181-214.

Tivey, M.A., and Johnson, H.P., 1987, The Central Anomaly Magnetic High: Implications for Ocean Crust Construction and Evolution, *J. Geophys. Res.*, **92**, 12685-12694.

Tokarski, A.K., 1991, Late Cretaeous-Cenozoic structural history of King George Island, South Shetland Islands, and its plate-tectonic setting, *In:* Thomson, R.A., Crame, J.A., and Thomson, J.W., (Eds.), *Geological evolution of Antarctica*, Cambridge, Cambridge University Press, 493-497.

Toksöz, M.N., and Bird, P., 1977, Formation and evolution of marginal basins and continental plateaus, *In:* Talwani, M., and Pitman, W.C.III, (Eds.), *Island Arcs, Deep Sea Trenches and Back-arc Basins*, Maurice Ewing Series I, AGU, 379-393.

Toksöz, M.N., and Hsui, A.T., 1978, Numerical studies of back-arc convection and the formation of marginal basins, *Tectonophysics*, **50**, 177-196.

Trouw, R.A.J., and Gamboa, L.A.P., 1992, Geotransect Drake Passage-Weddell Sea, Antarctica, *In:* Y. Yoshida et al. (Ed.), *Recent Progress in Antarctic Earth Science*. Terra Sci. Pub. Company (TERRAPUB), Tokyo, 417-422.

Urabe, T., Auzende, J.M., et al., 1992, Bathymetric map of the central part of the North Fiji Basin, southwest Pacific between 14°20S and 21°50S, 2 colored map, scale 1/500000, Sp. Coord. Promoting Sci. Tech. Pub., Japan.

Uyeda, S., 1977, Some basic problems in the trench-arc-back-arc systems, *In:* Talwani, M., and Pitman, W.C.III, (Eds.), *Island Arcs, Deep Sea Trenches and Back-arc Basins*, Maurice Ewing Series I, AGU, 1-14.

Uyeda, S., and Kanamori, H., 1979, Back-arc opening and the mode of subduction, *J. Geophys. Res.*, **84**, 1049-1062.

Vaslet, N, 1993, *Apport des images du sonar latéral SAR à l'étude de la structure fine des dorsales rapides: Application sur les relations entre tectonisme-magmatisme-hydrothermalisme (exemple de la dorsale Est Pacifique entre 13°20'N et 11°50'N)*, Thèse nouveau régime, Univ. Bretagne Occidentale, Brest, 336 p.

Vine, F.J., 1966, Spreading of the ocean floor: New evidence, *Science*, **154**, 1405-1415.

Vine, F.J., and Matthews, D.H., 1963, Magnetic anomalies over oceanic ridges, *Nature*, **199**, 947-949.

Vogt, P.R., 1979, Global magmatic episodes: New evidence for the steady-state mid-oceanic ridge, *Geology*, **7**, 93-98.

Vogt, P.R., 1986, Magnetic anomalies and crustal magnetization, *In* : Vogt, P.R., and Tucholke, B.E., (Eds.), *The Geology of North-America, The Western North Atlantic Region*, Geol. Soc. Amer., vol. M, 229-256.

Watanabe, T., Langseth, M.G., and, Anderson, R.N., 1977, Heat flow in back-arc basins of the Western Pacific, *In:* Talwani, M., and Pitman, W.C.III, (Eds.), *Island Arcs, Deep Sea Trenches and Back-arc Basins*, Maurice Ewing Series I, AGU, 137-161.

Weaver, S.D., Saunders, A.D., Pankhurst, R.J., and Tarney, J., 1979, A geochemical study of magmatism associated with the initial stages of back-arc spreading: the Quaternary volcanics of Bransfield Strait from South Shetland Islands, *Contr. Miner. Petrol.*, **68**, 151-169.

Weissel, J.K., 1981, Magnetic lineations in marginal basins of the west Pacific, *Philos. Trans. R. Soc. London,* Ser. A, **300**, 223-247.

Weissel, J.K., and Watts, A.B., 1979, Tectonic evolution of the Coral Sea Basin, *J. Geophys. Res.*, **84**, 4572-4582.

Whitehead, J.A., Dick, H.J.B., and Schouten, H., 1984, A mechanism for magmatic accretion under spreading centres, *Nature*, **312**, 146-148.

Whiticar, M.J., Suess, E., and Wehner, H., 1985, Thermogenic hydrocarbons in surface sediments of the Bransfield Strait, Antarctic Peninsula, *Nature*, **314**, 87-90.

Wilson, D.S., 1990, Kinematics of overlapping rift propagation with cyclic rift failure, *Earth Planet. Sci. Lett.*, **96**, 384-392.

Wilson, J.T., 1965, A new class of faults and their bearing on continental drift, *Nature*, **207**, 343-347.

Woodhall, D., 1987, Geology of Rotuma, *Miner. Res. Dept. Fiji Bull.*, 8, 40 p.

Wright, I.C., 1993, Pre-spread rifting and heterogeneous volcanism in the southern Havre Trough back-arc basin, *Mar. Geol.*, **113**, 179-200.

Yan, C.Y., and Kroenke, L.W., 1993, A plate tectonic reconstruction of the southwest Pacific, 0-100 Ma, *In:* Berger, W.H., Kroenke, L.W., Mayer, L.A., et al., (Eds.), *Proceedings of the Ocean Drilling Program, Scientific Results*, **130**, 697-709.

APPENDIX

Appendix

In this section we present a list of articles and abstracts in which the author contributed. A copy of the most important papers(*) is presented in the next pages.

A) List of articles:

Auzende J.M., Eissen J.P., Okuda Y., Bendel V., Ciabrini J.P., **Gràcia Mont E.**, Hirose K., Iwabuchi Y., Joshima M., Kisimoto K., Lafoy Y., Lagabrielle Y., Maillet P., Marumo K., Momma H., Naka J., Ruellan E., Tanahashi M., et Yamaguchi K., (1991): Propagation "en échelon" de la dorsale du Bassin Nord-Fidjien entre 16°40S et 14°50S (Yokosuka 90-Starmer). *C. R. Acad. Sci. Paris*, t. 312, série II, p. 1531-1538.

Auzende J.M., Honza E., Mazé J.P., Bendel V., Eissen J.P., **Gràcia Mont E.**, Huchon P., Lafoy Y., Lagabrielle Y., Ruellan E., Iwabuchi Y., Nojiri Y., Otsuka K., Tanahashi M., Tanaka T., and Urabe T., (1992): Comments on the SeaBeam map of the North Fiji Basin ridge between 16°10S and 21°40S. *Ofioliti*, 17 (1), p. 43-53.

Auzende J.M., Tanahashi M., Bendel V., Geistdoerfer P., **Gràcia Mont E.**, et Pratt C., (1992): Resultats preliminaires des plongées du "Shinkai 6500" sur la dorsale du Bassin Nord-Fidjien (SW Pacifique)-Programme STARMER *C. R. Acad. Sci. Paris*, t. 314, série II, p. 491-498.

Auzende J.M., Urabe T., Tanahashi M., Ruellan E., Bendel V., Fiala A., Fujikura K., Geistdoerfer P., **Gràcia Mont E.**, Grimaud D., Ishibashi J.I., Joshima M., Kisimoto K., Kojima S., Maillet P., Matsumoto T., Mitsuzawa K., Murai M., Naka J., Nargeolet P.H., Nojiri Y., Ohta S., Pranal V., and Pratt C., (1992): Japanese Submersible Explores the North Fiji Basin. *EOS, Transactions of AGU*, 73, (11), p. 116-117.

*Auzende J.M., Collot J.Y., Lafoy Y., **Gràcia E.**, Géli L., Ondréas H., Eissen J.P., Larue M.B., Olisukulu C., Tolia D., and Biliki, N. (1994): Evidence for sinistral strike-slip deformation in the Solomon Island Arc. *Geo-Marine Letters*, 14, p. 232-237.

*Auzende J.M., **Gràcia E.**, Bendel, V., Huchon P., Lafoy Y., Lagabrielle Y., De Alteriis G., and Tanahashi M., (1994): A possible triple junction at 14°50S on the North Fiji Basin ridge? (SW Pacific). *Mar. Geol.*, 116, p. 25-35.

*Auzende J.M., Hey R.N., Pelletier B., Rouland D., Lafoy Y., and **Gràcia E.** (1995): Propagating rift west of the Fiji archipelago (North Fiji Basin). *J. Geophys. Res.*, 100 (B9), p. 17823-17835.

Canals M. y **Gràcia E.** eds, (1992): Mid-Ocean Ridges / Dorsales Oceànicas. *Acta Geologica Hispanica*, Sp. Issue, 27 (3-4), 125 p.

Canals M., Acosta J., **Gràcia E.**, Escartín J., y Grupo ORCA (1992): Estudio del sector occidental del a Dorsal Sur de Scotia y su relación con la Cuenca de Bransfield (Antàrtida): Resultados de la campaña Scotia 92. *Acta Geologica Hispanica*, Sp. Issue: "Dorsales Oceànicas", M. Canals y E. Gràcia eds., 27 (3-4), p. 89-111.

Canals M., Acosta J., Baraza J., Bart P., Calafat A.M., Casamor J.L., De Batist M., Ercilla G., Farràn M., Francés G., **Gràcia E.**, Ramos E., Sanz J.L., Sorribas J., y Tassone A., (1994): La Cuenca Central de Bransfield (NW de la Peninsula Antàrtica): primeros resultados de la campaña GEBRA 93. *Geogaceta*, 10, p. 132-135.

Canals M., **Gràcia E.**, Farràn M., Prieto, M.J., Sorribas J., Parson L.M. and GEBRA group (in press): The very early stages of seafloor spreading: Bransfield Basin, Western Antartica. *Proceedings VII ISAES.*

*De Alteriis G., Ruellan E., Auzende J.M., Ondréas H., Bendel V., **Gràcia Mont E.**, Lagabrielle Y., Huchon P., and Tanahashi M., (1993): Propagating rifts in the North Fiji Basin (southwest Pacific) *Geology*, 21, p. 583-586.

Gràcia E., Auzende J.M., y Canals M. (1992): Estructura y evolución del segmento N160 de la dorsal de la Cuenca Nor-Fidjiana (Pacífico suroeste). *Acta Geologica Hispanica*, Sp. Issue: "Dorsales Oceànicas", M. Canals y E. Gràcia eds., 27 (3-4), p. 79-89.

***Gràcia E.**, Ondréas H., Bendel V., and Starmer group, (1994): Multi-scale morphologic variability of the North Fiji Basin ridge (SW Pacific). *Mar. Geol.*, 116, p. 133-151.

Gràcia E., Canals M., Farrán M., Prieto, M.J., Sorribas J., and GEBRA Team (1996): Morphostructure and evolution of the Bransfield back-arc basin (NW Antarctic Peninsula), *Mar. Geophys. Res.*, 18 (1-3).

Gràcia E., Tisseau C., Maia M., Tonnerre T., Auzende J.M., and Lagabrielle Y., (1996): Variability of the axial morphology and gravity structure of the Central Spreading Ridge (North Fiji Basin): Application of a non-steady state thermal model. *Mar. Geophys. Res.*, 18 (1-3).

Grupo O.R.C.A: Acosta J., de Andrés J.R., Argullós J., Calafat A., Canals M., Casamor J.L., Davies T., Escartín J., **Gràcia E.**, Herranz P., Mateu G., Rey J., Sanz J.L., Soler M., Somoza L. y Sorribas J., (1992): Resultados preliminares de la campaña de geologia marina "Scotia 92". Estudio geológico y geofísico de la dorsal sur del arco de Scotia. *Geología de la Antàrtida Occidental.* J.López-Martínez (Ed). Simposios T 3, p. 203-212. III Congreso Geológico de España y VII Congreso Latinoamericano de Geología. Salamanca, España, 1992.

Grupo O.R.C.A: Acosta J., Argullós J., Calafat A., Canals M., Casamor J.L., Escartín J., **Gràcia E.**, Herranz P., Sanz J.L., y Sorribas J., (1994): Bathymetry of the Hesperides Deep (Scotia Sea-South Scotia Ridge-Antarctica). Map scale 1:200.000. Grup de Recerca Geociències Marines (Universitat de Barcelona).

*Huchon P., **Gràcia E.**, Ruellan E., Joshima M., and Auzende J.M., (1994): Kinematics of active spreading in the central North Fiji Basin (SW Pacific). *Mar. Geol.*, 116, p. 69-87.

Lagabrielle, Y., Ruellan, E., Tanahashi, M., Bourgois, J., Buffet, G., De Alteriis, G., Goslin, J., **Gràcia-Mont, E.**, Iwabushi, Y., Jarvis, P., Joshima, M., Karpoff, A.M., Lui, T., Matsumoto, T., Ondréas, H., Pelletier, B., and Sardou, O. (1995): A 800 km survey of the active spreading axis in the northern North Fiji Basin. Reults of the NOFI cruise of the RV L'Atalante over the South Pandora and Tripartite ridges (August-September 1994). *InterRidge News*, 4 (1), p. 29-36.

Lagabrielle, Y., Ruellan, E., Tanahashi, M., Bourgois, J., Buffet, G., De Alteriis, G., Goslin, J., **Gràcia-Mont, E.**, Iwabushi, Y., Jarvis, P., Joshima, M., Karpoff, A.M., Lui, T., Matsumoto, T., Ondréas, H., Pelletier, B., Sardou, O. and Tupua, E., (1995): Segmentation d'une dorsale océanique en domaine arrière-arc: l'axe d'accrétion Sud-Pandora-Tripartite (Bassin Nord Fidjien). Résultats de la campagne NOFI de L'Atalante. *C. R. Acad. Sci. Paris*, 321, p. 393-400.

Lagabrielle, Y., Ruellan, E., Tanahashi, M., Bourgois, J., Buffet, G., De Alteriis, G., Dyment, J., Goslin, J., **Gràcia-Mont, E.**, Iwabushi, Y., Jarvis, P., Joshima, M., Karpoff, A.M., Lui, T., Matsumoto, T., Ondréas, H., Pelletier, B., Sardou, O. (1996): Active oceanic spreading in the northern North-Fiji Basin. Results of the NOFI cruise of the R/V L'Atalante. *Mar. Geophys. Res.*, 18 (1-3).

Ondréas H., Ruellan E., Auzende J.M., Bendel V., De Alteriis G., **Gràcia-Mont E.**, et Tanahashi M., (1993): Variabilité morphostructurale à l'échelle kilométrique de la dorsale du Bassin Nord-Fidjien: Exploration *in situ* du segment compris entre 18°50S et 19°S. *C. R. Acad. Sci. Paris*, t. 316, série II, p. 115-122.

*Ruellan E., Huchon P., Auzende J.M., and **Gràcia E.**, (1994): Propagating rifts and overlapping spreading center in the North Fiji Basin. *Mar. Geol.*, **116**, p. 37-56.

B) Abstracts and congress participations:

Auzende J.M., Bendel V., **Gràcia Mont E.**, Tisseau C., Lagabrielle Y., Brenon I., and De Alteriis G., (1992): Magmatic-amagmatic alternation at intermediate spreading ridge (North Fiji Basin). *American Geophysical Union (A.G.U.)* Spring meeting, Montreal (Canada) (May 14-16), p. 285, T31-B8.

Auzende J.M., **Gràcia Mont E.**, Bendel V., Lafoy Y., Lagabrielle Y., Okuda Y., and Ruellan E., (1992): Morphologic variations at an intermediate spreading ridge (North Fiji Basin). *29th International Geological Congress (I.G.C.)*, Kyoto (Japan), 24 August-3 September 1992. Abstract C-7, O-1, 4070, p. 34.

Canals M., Acosta J., Baraza J., Bart P., Calafat A., Casamor J.L., De Batist M., Ercilla G., Farran M., **Gràcia E.**, Ramos E., Sanz J.L., Sorribas J., and Tassone A., (1994): Morphostructure and recent evolution of the Bransfield Strait (NW Antarctic Peninsula). *XIX European Geophysical Society (E.G.S.)* , Grenoble (France) (April 25-29).

Canals M., Acosta J., Baraza J., Farran M., **Gràcia E.**, Sorribas J., and GEBRA and ORCA Teams, (1994): Swath bathymetry gives new highligths on the geodynamics of the South Scotia Ridge and Bransfield Basin, Western Antarctica. *European Conference on Grand Challenges in Ocean and Polar Sciences*, Bremen (Germany) (12-16 September).

Canals M., **Gràcia E.**, Acosta J., and ORCA group (1994): The Transform plate-boundary between Scotia and Antarctic plates. *Seafloor mapping in the West and Southwest Pacific. Results and Applications.* Lifou-Nouméa (New Caledonia) (4-9 November 1994).

Gràcia E., Auzende J.M., Tisseau C., and Huchon P., (1993): Recent evolution of the North Fiji Basin Spreading Ridge from bathymetric and magnetic data: thermal outcomes. *European Union of Geosciences (EUG VII)*, Strasbourg (France) 4 to 8 April 1993. Terra Abstracts, vol.5, B-5, p. 109.

Gràcia E., Canals M., Ferran M., Sorribas J., and GEBRA group (1994): The Bransfield Back-Arc Basin (NW Antarctic Peninsula): The initial stage of seafloor spreading. *Seafloor mapping in the West and Southwest Pacific. Results and Applications.* Lifou-Nouméa (New Caledonia) (4-9 November 1994).

Gràcia E., Tisseau C., Maia M., Tonnerre T., Auzende J.M., and Ruellan E. (1994): Thermal modeling of axial morphologic and gravimetric variations along the Central Spreading Ridge (North Fiji Basin). *Seafloor mapping in the West and Southwest Pacific. Results and Applications.* Lifou-Nouméa (New Caledonia) (4-9 November 1994).

Gràcia E., Lagabrielle, Y., Ondréas, H., Ruellan, E., Auzende, J.M., Canals, M., Urgelés, R., and Tanahashi, M., (1995): Faulting and volcanism in backarc basins: Mutual control at various spreading centers. *4th RIDGE Theoretical Institution*, Lake Tahoe, California (USA) (9-11 June 1995).

Gràcia E., Canals M., Prieto M.J., Sorribas J., and Farràn, M., (1995): Early seafloor spreading and rifting in the Bransfield Basin, *VII International Symposium on Antarctic Earth Sciences*, Siena (Italy), 10-15 September 1995, p. 165, Abstract.

Huchon P., Ruellan E., **Gràcia E.**, and Auzende J.M., (1992): Kinematics of active oceanic spreading in the North Fiji basin from magnetic and structural data. *29th International Geological Congress (I.G.C.)*, Kyoto (Japan), 24 August-3 September 1992. Abstract C-7, O-5, 6028, p. 35.

Lagabrielle Y., Tanahashi M., Ruellan E., Pelletier B., Auzende J.M., Bourgois J., Buffet G., De Alteriis G., Goslin J., **Gràcia E.**, Iwabushi I., Jarvis P., Joshima M., Karpoff A.M., Matsumoto T., Ondréas H., and Sardou O., (1994): Active spreading axis in the northern region of the North Fiji Basin: Preliminary results of the NOFI cruise (R/V L'Atalante) New-Starmer project. *Seafloor mapping in the West and Southwest Pacific. Results and Applications.* Lifou-Nouméa (New Caledonia) (4-9 November 1994).

Lagabrielle Y., Ruellan E., Tanahashi M., Pelletier B., Bourgois J., Buffet G., De Alteriis G., Dyment J., Goslin J., **Gràcia E.**, Iwabushi I., Jarvis P., Joshima M., Karpoff A.M., Matsumoto T., Ondréas H., and Sardou O., (1994): Active spreading along the South Pandora Ridge in the northern North Fiji Basin (SW Pacific): first results of the NOFI cruise (French-Japanese New-Starmer program). *American Geophysical Union (A.G.U.)* Fall meeting, San Francisco, California (December 5-9)

Ondréas H., **Gràcia E.**, Bendel V., Auzende J.M., and Ruellan E., (1993): Kilometric variability in accretionary processes along the North Fiji Basin Ridge: *in situ* observations. *European Union of Geosciences (EUG VII)*, Strasbourg (France), 4 to 8 April 1993. Terra Abstracts, vol. 5, D-11, p. 464.

Prieto M.J., **Gràcia E.**, Canals M., Ercilla G., and De Batist, (1995): Recent sedimentary history of the Bransfield Basin, *VII International Symposium on Antarctic Earth Sciences*, Siena (Italy), 10-15 September 1995, p. 315, Abstract.

Tisseau C., Auzende J.M., Brenon I., and **Gràcia Mont E.**, (1992): Profondeur du plancher océanique à age zero dans le Bassin Nord-Fidjien (SW Pac): Essais de modelisation. *14ème Reunion de Sciences de la Terre*, Toulouse 13-15 Avril, Soc. Géol. Fr.